DISSERTATION

NEAR-BANK PROCESSES, BIOENGINEERING, AND THE DORMANT WILLOW POST METHOD

Submitted by

Gregory V. Wilkerson

Civil Engineering Department

In partial fulfillment of the requirements

for the Degree of Doctor of Philosophy

Colorado State University

Fort Collins, Colorado

Spring 1999

UMI Number: 9941570

UMI
300 North Zeeb Road
Ann Arbor, MI 48103

COLORADO STATE UNIVERSITY

March 23, 1999

WE HEREBY RECOMMEND THAT THE DISSERTATION PREPARED UNDER OUR SUPERVISION BY GREGORY V. WILKERSON ENTITLED NEAR-BANK PROCESSES, BIOENGINEERING, AND THE DORMANT WILLOW POST METHOD BE ACCEPTED AS FULFILLING IN PART REQUIREMENTS FOR THE DEGREE OF DOCTOR OF PHILOSOPHY.

Committee on Graduate Work

____

____

____

____
Co-advisor

____
Advisor

____
Department Head

ABSTRACT OF DISSERTATION

NEAR-BANK PROCESSES, BIOENGINEERING, AND

THE DORMANT WILLOW POST METHOD

Bioengineered systems were constructed along Harland Creek, Mississippi, using the dormant willow post method. The systems were constructed using live posts harvested from sections of the trunks of native black willows (*Salix nigra*). The posts were planted vertically along the banks in a 1 m by 1 m rectangular grid. Rows in the grid were aligned parallel to the edge of water, and three to five rows of willow posts were planted. In time, willow posts develop roots, stems, branches, and leaves; features that enhance the ability of willow posts to stabilize streambanks and reduce erosion.

The objectives of this research were to study near-bank processes and the influence of planted black willow posts on those processes. It is hypothesized that willow posts planted along an eroding bank will thrive only if the posts are able to induce net sediment deposition. Soil samples derived from the banks of Harland Creek were analyzed but no indication that the willow posts are inducing deposition was found.

Three study reaches were established. Planted willow posts were present in two of the reaches; the third reach was a control reach in which no manmade bank stabilization was present. Vegetation density data were collected at each study reach in August 1997, January 1998, and March 1998 using a horizontal point frame. Vegetation density was found to be as much as 44% greater for the reaches with willow posts than for the control

reach. This observation suggests that willow posts help create a suitable environment for the establishment of volunteer vegetation.

Physical model test results revealed that willow posts significantly change flow patterns atop the bank. Depth-averaged velocities amid the simulated willow posts were reduced by more than 50% in the model. It was determined that computed Manning's roughness coefficients (*n*-values) did not correlate with the configuration of the simulated willow posts.

An analytical model for predicting flow through emergent vegetation in trapezoidal channels is presented. The model predicted depth-averaged velocities behind the dowels to within 2%, on average, of velocities computed from the model study data.

Gregory V. Wilkerson
Civil Engineering Department
Colorado State University
Fort Collins, CO 80523
Spring 1999

ACKNOWLEDGEMENTS

I want to thank everyone who has contributed to this research. To my advisor, Dr. Chester C. Watson, I am most grateful. Because of his patience, insight, support, and, most of all, his pleasant demeanor, I will remember negotiating this effort with fondness. I also thank the other members of my academic committee (Drs. Steven R. Abt, Ralph L. Dix, Neil S. Grigg, and James L. Smith) for their guidance and friendship. Their unwavering support is a continuous source of inspiration for me.

Dr. David S. Beidenharn and Dr. Phil G. Combs of the U.S. Army Engineer Waterways Experiment Station (WES) provided an opportunity for me to perform research at WES that was paramount for this study. I am truly grateful for having had that opportunity. Thanks to Ms. Deborah W. Cooper, Mr. David L. Derrick, Dr. Craig J. Fischenich, Mr. James R. Leech, Mr. Kevin Pigg, and Ms. Kendall Smith for making my visit to WES memorable.

Numerous students and several staff members at Colorado State University helped in the fieldwork, laboratory testing, and data analysis. I thank each of these individuals because without their help I would still be writing Chapter 1. I would like to thank Mr. David Mooney, Mr. Peter Marxhausen, and especially Mr. Daniel Armstrong for their help in analyzing data. Thanks to Ms. Gloria Garza, Mary Casey, and Mr. Christopher I. Thornton for their day-to-day assistance and friendship.

The U.S. Army Waterways Experiment Station and the National Science Foundation provided funding for this research.

DEDICATION

To my parents—Johnnie, Edward, Bettye, and Oscar.

TABLE OF CONTENTS

LIST OF TABLES

LIST OF FIGURES

LIST OF SYMBOLS

Symbol	Description
A	channel cross-section area
A_i	representative area
b	representative width
b	width of the point frame
$b_{1/2}$	distance from the wake centerline to the point at which the velocity defect is equal to $(u_{n,j})_{\max}/2$
C_d	drag coefficient
d	cylinder diameter
d	flow depth at a point
d_{50}	median grain-size of sediment
$d_{50,\mathrm{bed}}$	median grain-size of bed material
$d_{50,\mathrm{bank}}$	median grain-size of bank material
d_g	geometric mean grain-size of sediment
d_i	grain-size used to characterize sediment
d_i	flow depth a location j
d_{max}	maximum channel depth
D	depth of flow
D	hydraulic depth
$D(z)$	depth at any point, z, across the width of the channel

Symbol	Description
F_d	drag force on vegetation
Fr	Froude number
g	gravitational constant
G	soil gradation coefficient
h	height from the ground to the highest point at which vegetation was observed
h_{50}	median height of vegetation
h_i	the length of the ith cylinder that is submerged in water
h_f	friction head loss
h_{mean}	mean height of vegetation
H_a	alternative hypothesis
H_i'	head at section i
H_i''	head at section i
H_o	null hypothesis
$k(\Delta x)$	coefficient for computing $U_{\infty}(x,z)$
K	cotangent of side slope
l_x	longitudinal spacing between vegetation
l_y	lateral spacing between vegetation
L	characteristic channel length
L	characteristic length of pin used to measure vegetation density
M_D	median value
n	Manning's roughness coefficient
n	number of samples

Symbol	Description
n-value	Manning's roughness coefficient
P	wetted perimeter
Q_{bank}	flow rate over the bank of the flume
Q_{bed}	flow rate over the bed of the flume
Q_{calc}	discharge calculated from the depth-averaged velocities
r	perpendicular distance from toe of slope to point of interest
$r(z)$	perpendicular distance from toe of slope to point of interest
$r_{X,Y}$	correlation coefficient
$r^2_{X\|Y}$	multiple-partial coefficient of determination
R	hydraulic radius
Re	Reynolds number
s_x	sample standard deviation
$s_{x,y}$	sample covariance
s_y	sample standard deviation
$S_{f,avg}$	friction slope
$S_{f,i}$	friction slope
S_0	channel-bed slope
$T_{n:\alpha}$	tabulated value used to perform Wilcoxon matched-pairs signed-rank test
T_+	computed test statistic for Wilcoxon matched-pairs signed-rank test
T_-	computed test statistic for Wilcoxon matched-pairs signed-rank test
$u_{\max}$	velocity defect at center of wake
$(u_{n,i})_{\max}$	velocity defect at center of wake

Symbol	Description
$u_{n,i}(\Delta x_i, \Delta z_i)$	velocity defect at arbitrary point *n* due to the *i*th cylinder
$u_{n,i}(\Delta x, \Delta z)$	velocity defect at arbitrary point *n* due to the *i*th cylinder
$u_{total}(x, z)$	total velocity defect at a point in a flow field
u_x	longitudinal component of velocity at a point
u_y	vertical component of velocity at a point
u_z	transverse component of velocity at a point
$\vec{u}_{xz}$	horizontal velocity vector
U_0	cross-section averaged velocity
U_{0i}	approach velocity to the *i*th cylinder
U_x	depth-averaged velocity
$U_x(x, z)$	depth-averaged velocity
$U_x(z)$	depth-averaged velocity
$U_\infty(x)$	reference free stream velocity
$U_\infty(x, z)$	reference free stream velocity
Veg_d	vegetation density index
$VDI(h_{mean})$	vegetation density index
$VDI(h_{50})$	vegetation density index
V_i	cross-section averaged velocity
W	channel width
x	longitudinal coordinate in channel
x_i	variable values

Symbol	Description
$\bar{x}$	sample mean
Δx	longitudinal distance between two points
X	variable names
y	vertical distance from datum
y_i	variable values
$\bar{y}$	sample mean
y_{act}	measured water surface elevation
y_{est}	computed water surface elevation
Y	flow depth over the channel bed (nominal flow depth)
Y	variable name
z	lateral coordinate in channel
z_{toe}	lateral coordinate of toe of slope
Δz	lateral distance between two points
α	level of significance
β_0	coefficient
β_1	coefficient
γ	skewness of sediment grain-size
μ	dynamic viscosity
τ_{xy}	shear stress
ν	kinematic viscosity
ρ	fluid density
$\rho_{X,Y}$	correlation coefficient

Symbol	Description
σ	standard deviation
σ_g	geometric standard deviation of sediment grain-size

1. Introduction

Erosion is a common occurrence along many kilometers of streams and rivers throughout the United States. Erosion of streams causes deterioration of agricultural lands, sediment pollution, reservoir filling, and water table lowering. The cost of removing sediment, the loss of prime meadow and agricultural lands, and damage to physical property adjacent to eroding streams is valued at millions of dollars annually. The U.S. Army Corps of Engineers (USACE) estimated 229,000 km (142,000 mi) of waterways in the U.S. are in need of erosion protection at an annual cost of $1 billion (USACE, 1981). The National Research Council (1992) indicated that even if 600,000 km (363,000 mi) of river and stream segments in the U.S. are protected and restored within the next 20 years as recommended by the President's Commission on Americans Outdoors (1986), this would amount to less than 1.3% of the total length of streams potentially requiring treatment (Brookes and Shields, 1996). Thus, because of cost, many watersheds experiencing substantial erosion cannot be repaired or maintained using conventional practices (i.e., riprap, gabions, concrete surfacing, etc.). The need to develop less costly stabilization techniques is apparent from the figures cited above. Also driving the need to develop new bank stabilization techniques are issues related to ecology, the environment, and aesthetics.

The primary objective of this research is to study near-bank processes (i.e., the interactions between mechanical operatives, modulating reactions, and constituent variables that directly influence the bank along a river or stream). Emphasis is placed on the influence of black willow (*Salix nigra*) cuttings that were planted in 1994 as part of an experimental bank stabilization project. The insight gained from this study will be used to make recommendations for improving the effective use of planted vegetation for bank stabilization, or bioengineering. Bioengineering offers an alternative to conventional bank stabilization practices that is less costly (Schiechtl and Stern, 1997; Watson et al., 1997) and provides ecological, environmental and aesthetic benefits.

Presented in the following section is background information about the field site for this study and events that led to willow cuttings being planting at the field site. The main objectives of this study are presented in Section 1.2. A review of literature reporting on relevant theories and observations is presented in Chapter 2. The test and sampling procedures followed are described in Chapter 3. Data derived over the course of this study is presented in Chapter 4 and an analysis of the data is presented in Chapter 5. An assessment of the findings and a summary of conclusions are presented in Chapters 6 and 7, respectively.

1.1 Background

Since 1984, through a federally funded program called the Demonstration Erosion Control (DEC) Project, ongoing research has been sponsored to address problems associated with watershed instability, i.e., erosion, sedimentation, flooding, and environmental degradation (Wang et al., 1997). DEC Project activities encompass 16 watersheds comprising 6,000 km^2 (2,300 mi^2) within the Yazoo River watershed in north central Mississippi. Developing and demonstrating systems' approaches for restoring watershed stability are among the primary objectives of the project. Evaluation of stabilization projects includes consideration of cost effectiveness, reliability, ecological value, and environmental benefits. The research reported herein was performed in conjunction with the DEC Project.

1.1.1 Harland Creek - The Study Site

The study site for the research proposed herein is Harland Creek. It is located in Holmes County, Mississippi in the Upper Yazoo Basin (Figure 1.1). The 2-year

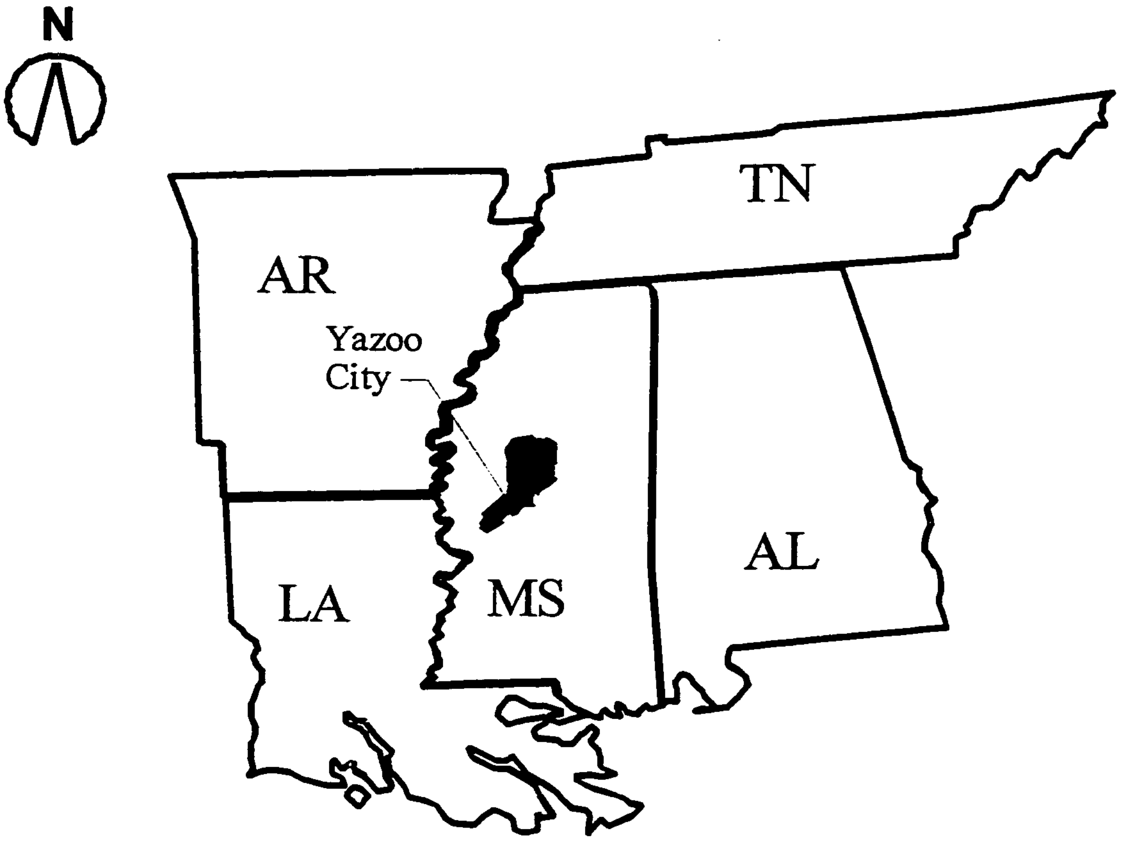

Figure 1.1 – Map showing Upper Yazoo Basin.

recurrence interval discharge is approximately 106 m^3/s (3,750 cfs). At the 2-year recurrence interval discharge, the average flow width of Harland Creek is approximately 29 m (95 ft) and the average depth is approximately 1.8 m (6 ft), however, these dimensions vary significantly along the reach (Watson et al., 1995). There is significant sand and gravel transport through the study area. The sediment transport rate is estimated to be 7.8 million kg (8,700 tons) per day at the 2-year discharge. The median bed sediment size (d_{50}) is 0.5 mm (0.020 in.) and gravel up to approximately 4 cm (1.5 in.) in diameter is common.

Harland Creek has been an extremely active meandering channel (Watson et al., 1995). By comparing bank-lines in four sets of aerial photographs (taken between 1955 and 1991) Watson et al. estimated that the average bank migration rate is 4.3 m (14 ft) per year or about 15% of the bendway channel width annually. To the landowner, this translates to movement of a full channel width in less than 7 years and a land loss of approximately 300 ha per km (12 acres per mi) of stream in the same period.

1.1.2 Willow Post (Bioengineered) Systems along Harland Creek

DEC Project watershed stabilization efforts have resulted in the construction of numerous bed and bank stabilization structures. For one class of stabilization techniques, live plants are used as building material in contrast to conventional practices that use inert materials exclusively. Terms used to describe these techniques include biotechnology, soil bioengineering, biogeotechnology and bioengineering. Herein, the term bioengineering is used.

Bioengineered systems are mainly constructed using live unrooted cuttings from suitable shrub and tree species and are planted in the ground by various means and in various configurations (Wu, 1995). The plant cuttings take root and become established on the slope. Bioengineering systems and construction methods have been described by Schiechtl (1980), Gray and Leiser (1982), Coppin and Richards (1990), and Schiechtl and Stern (1997) among others. Based on function, Schiechtl (1973) developed a classification scheme for bioengineering techniques comprised of four classes: soil protection techniques, ground stabilization techniques, combined construction techniques, and supplementary construction techniques. The specific functions of each class of techniques are presented in Table 1.1

Table 1.1 – Classification of Bioengineering Techniques by Function (adapted from Schiechtl and Stern, 1997)

Soil/surface protection techniques protect the soil, by virtue of their dense surface cover, from sheet erosion and degradation. These techniques improve the soil-water regime and soil temperature, thereby increasing the biological processes in the soil. Mulch cover affords the soil protection from raindrop action even before the sown grasses, herbs and woody species become established. Soil protection techniques consist of turf establishment, grass seeding, direct seeding of shrubs and trees, erosion control netting, seed mats, precast concrete cellular blocks, and live brush mats.
Ground/soil stabilization techniques modify or completely eliminate the mechanical forces active in the soil: these techniques stabilize and protect lake shorelines, river banks, canal banks and natural slopes through the binding action of the root systems and increased evapotranspiration. The techniques are comprised of linear or single point systems of bushes and trees, or branches, which are capable of vegetative propagation, and are usually supplemented by the provision of a dense ground cover to guard against erosion. Ground stabilization techniques include live cuttings, wattle fence and wattles, hedge and/or brush layer construction.
Combined construction techniques support and stabilize unstable lake shorelines, river and canal banks, in combination with solid structures (stone, wood, concrete, steel, plastics, etc.), resulting in increased effectiveness and prolonged lifespan. Combined construction techniques consist of live and inert materials and thus are immediately effective. The effectiveness of the planted vegetation increases with its advancing age and size.
Supplementary construction techniques, i.e., seeding and planting, undertaken to bring a project to its final shape and appearance. These techniques help to diversify the originally established vegetative cover and to safeguard its continued existence.

At Harland Creek, a bioengineering technique referred to as the dormant willow post method was implemented in February, 1994. The willow post systems were constructed using live posts harvested from sections of the trunks of native black willows (*Salix nigra*; Derrick, 1997; Watson et al., 1997). The willow post method is fundamentally different from other bioengineering methods because the posts are installed vertically (Figure 1.2), whereas most methods call for horizontal layering (Watson et al., 1994). Although bioengineering practitioners have historically used similar techniques, Mr. Don Roseboom of the Illinois State Water Survey is considered the originator of the modern willow post technique. The method is described in Roseboom (1992). Abraham and Derrick (1993) have also utilized this technique.

Acceptable willow posts for Harland Creek willow post systems were 3 to 4 m (10 to 14 ft) in length and 8 to 15 cm (3 to 6 in.) in diameter at the butt end (Figure 1.3). The posts were planted vertically in holes that were 2 to 3 m (6 to 10 ft) deep and spaced 1 m (3 ft) apart forming a rectangular grid. The rows of the grid were aligned parallel to the edge of water during base flow and the first row of willows were positioned 30 cm (1 ft) landward of the edge of water (Figure 1.2). The holes were formed using a 20-cm (8-in.) diameter auger and up to 1.2 m (4 ft) of the post protruded above the ground.

In time, planted willow posts develop root systems, stems, branches, and leaves (Figure 1.4). Each of these features enhance the capability of willow posts to stabilize streambanks.

1.1.3 Mississippi Climate

Climate is an important factor in the successful use of bioengineered systems. The climate in Mississippi is described by Blackmarr (1995, p. 40) as follows:

> "Mississippi has a humid climate. The annual temperature for the state is approximately 65° F, ranging from an average of 62° in the northeast to 68° in the southwest. The annual precipitation ranges from about 50 inches in the northern part of the state to about 68 inches near the gulf coast in southeastern Mississippi. The principal source of moisture is the Gulf of Mexico from which tropical airmasses bring moisture inland from the gulf, particularly during summer and fall. Occasionally, moisture from the eastern Pacific Ocean reaches Mississippi. In general, precipitation is the result of convective showers from surface heating of moist air or the frontal lifting of moist air over polar continental airmasses moving into the state from the north. Precipitation resulting from frontal systems occur as general, widespread rain associated with warm fronts and as intense showers, squall lines, thunderstorms, and severe weather associated with rapid convergence of cold fronts with moist, tropical airmasses. Frontal systems are most common in late winter and spring (U.S. Geological Survey, 1991; Testa and Lago, 1994)."

Figure 1.2 – Planted willow posts along Harland Creek, Mississippi.

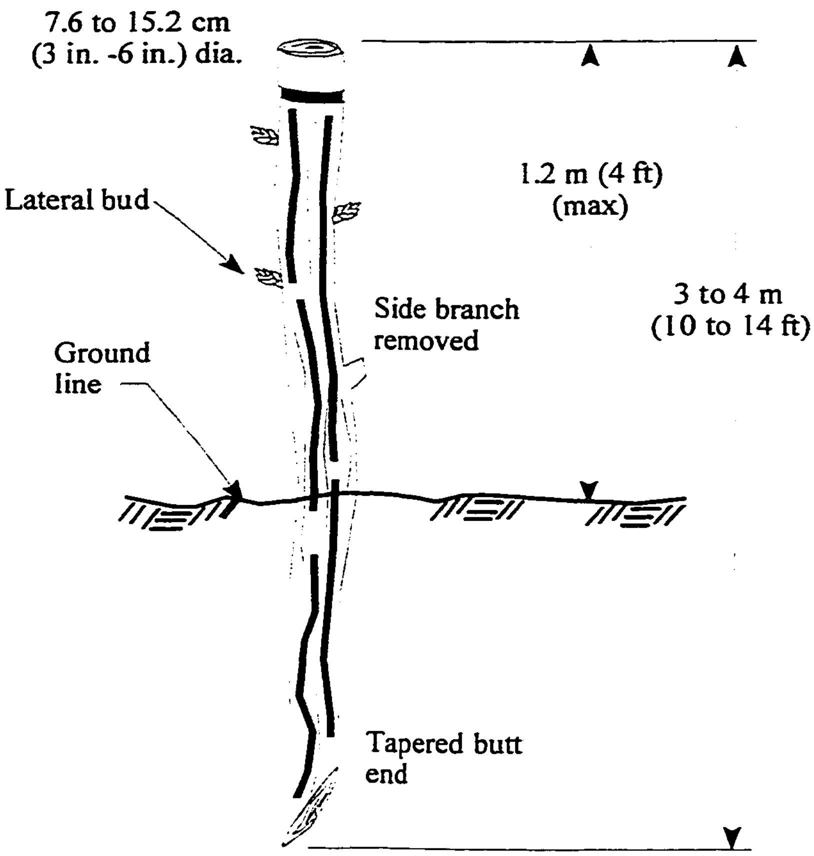

Figure 1.3 – Sketch of dormant willow post.

Figure 1.4 – Close-up of planted willow post showing stems, branches, and leaves.

1.2 Research Objectives

The principal objectives of this study are:

(1) to study near-bank processes, i.e., sediment scour and deposition, vegetative growth, and depth-averaged velocity distributions;

(2) to interpret the influence of planted willow posts on near-bank processes;

(3) to perform a physical model study in which the effects of different simulated willow post systems would be assessed and compared;

(4) to assess the utility of available analytical models for predicting the impact of planted willow posts on flow velocities;

(5) to develop an analytical model for predicting the velocity distribution in a stream or channel with planted willow posts; and

(6) to make recommendations for improving the design of willow post bank stabilization systems.

To achieve the stated objectives, the following working hypothesis will be evaluated in this study: willow posts planted along an eroding bank will thrive only if the posts are able to induce net sediment deposition (that is, more sediment must be deposited on the bank annually than is eroded).

2. Literature Review

Processes that govern stream behavior stem from interactions between many parameters, i.e., watershed attributes, discharge, bed and bank material properties, vegetal characteristics, etc. Near-bank processes are the subject of this research thus parameters deemed important to those processes are evaluated. In this chapter, studies are reviewed that report on near-bank processes and techniques for measuring relevant variables.

2.1 Bank Erosion/Deposition Gages and Maximum Scour Depth Gages

To facilitate monitoring changes in channel cross-sectional form, during and as a result of flood events, simple gages (erosion pins and maximum scour depth gages) were placed along the surveyed cross-sections. In the reports reviewed, similar techniques were used.

While studying bank erosion along Watts Branch, a channel in Montgomery County, Maryland, Wolman (1959) began using what he termed the pin method. Steel pins, 30 cm (1 ft) long and 6.4 mm (1/4 in.) in diameter, were driven horizontally into a river bank, approximately 30 cm (1 ft) below the flood plain and at intervals of 1.5 m (5 ft) measured parallel to the top of bank. Wolman determined the amount of bank erosion that occurred between field visits by comparing the initial and final protruding distance of each erosion pin.

Hooke (1979) used horizontally driven erosion pins to measure erosion on sections of river banks in Devon, England and reported that these functioned well, especially on larger rivers of 30 to 700 km^2 (12 to 270 mi^2) drainage areas, where most of the banks are composed of silty alluvial material.

In a manuscript describing scour and fill in sand-bed streams, Colby (1964) described a number of methods for determining scour and fill (i.e., photography, mechanical or sonic soundings, stage-discharge relations, probing with a steel rod or soil tube, plastic ribbons, and log chains). Of particular interest are the log chains used to gage maximum depths of scour. Each chain is attached to a ring, which is then slipped over the top of a steel angle that is driven into the streambed beforehand. A pin keeps the ring from coming off the top of the angle, but the ring is free to slide down the angle easily if scour removes sand from below the ring and chain.

It is noted that none of the reviewed studies consider erosion and deposition (or scour and fill) on sloping banks. Wolman (1959) and Hooke (1979) used horizontal pins to monitor banklines, and the log chains described by Colby (1964) were used in streambeds. Similar instruments could be placed on sloping banks to monitor scour and fill thereon.

2.2 Soils

The distinctive characteristics and behavior of bank sediments have long been recognized (Church and Rood, 1983) and the influence of bank properties on channel geometry have been clearly demonstrated (Schumm, 1960, 1971; Ferguson, 1973; Thorne et al., 1988). Even though most engineers and scientists accept that bank material properties do influence hydraulic geometry, there is no consensus of opinion on the linkage between bank characteristics, bank processes, and stable channel geometry (Thorne and Osman, 1988; Thorne, 1990).

2.2.1 Soil Texture

The relative proportions of sand, silt, and clay in a soil determines the soil class, textural class, textural grade, or texture (Black, 1968). For every soil textural class there is a corresponding descriptive name. Presented in Figure 2.1 is the textural classification

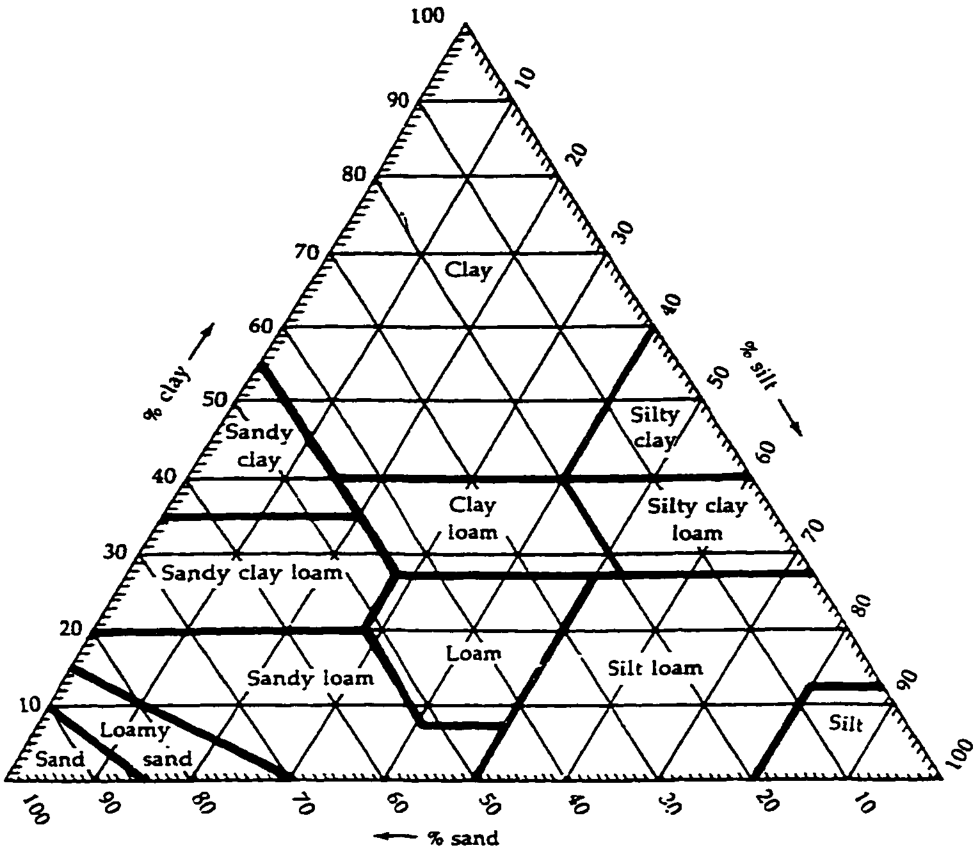

Figure 2.1 – Relationship between soil particle size distribution and soil texture classes (from Soil Survey Staff, 1960).

used currently (1999) by the United States Department of Agriculture; given the results of a particle-size analysis the figure is used to determine the name to apply to the soil.

Soil texture as such is not of direct importance for most purposes (Black, 1968). Where use is made of soil classifications based on texture, one is usually interested in the information about other properties that may be provided by knowledge of texture together with supplementary information on the relationships between texture and the properties of interest. Experience has shown that many important soil properties vary with texture but none of the relationships applies under all circumstances. Consequently, texture does not provide an entirely suitable basis for making inferences about other properties.

A thorough assessment of the suitability of a soil to serve as a substrate for plant growth requires consideration of the physical and chemical characteristics of the soil but such analyses are beyond the scope of this research. There is a correspondence between texture and several physical soil properties related to suitability (i.e., water-holding capacity, water-release character, and drainage capacity); for general applications, then, soil texture can be used as a surrogate for predicting soil suitability for plant growth as shown in Figure 2.2.

As with suitability, texture is not the only variable that must be considered to completely determine soil erodibility but texture does have an important bearing on erosivity (Ayres, 1936). Grissinger et al. (1981), for example, performed several physical and chemical tests on fine-grained materials of low cohesion. The tests were correlated with measured particle, or aggregate, erosion rates and it was determined that the clay content of the samples was the most significant variable for predicting erodibility. A guide for assessing the erodibility of soil based on texture is presented in Figure 2.3.

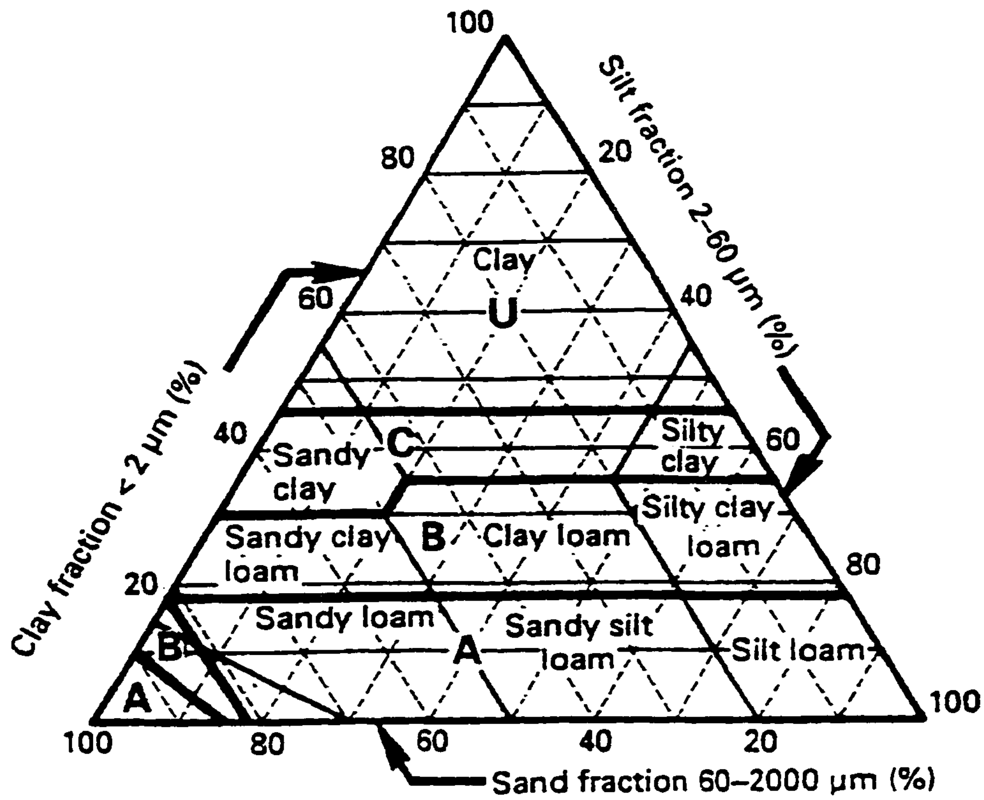

Figure 2.2 – Relationship between soil particle size distribution and soil suitability (A - least suitable, B - moderately suitable, C - just suitable, U - unsuitable). From Coppin and Richards, 1990, p. 94. Reprinted with permission from CIRIA/Butterworths.

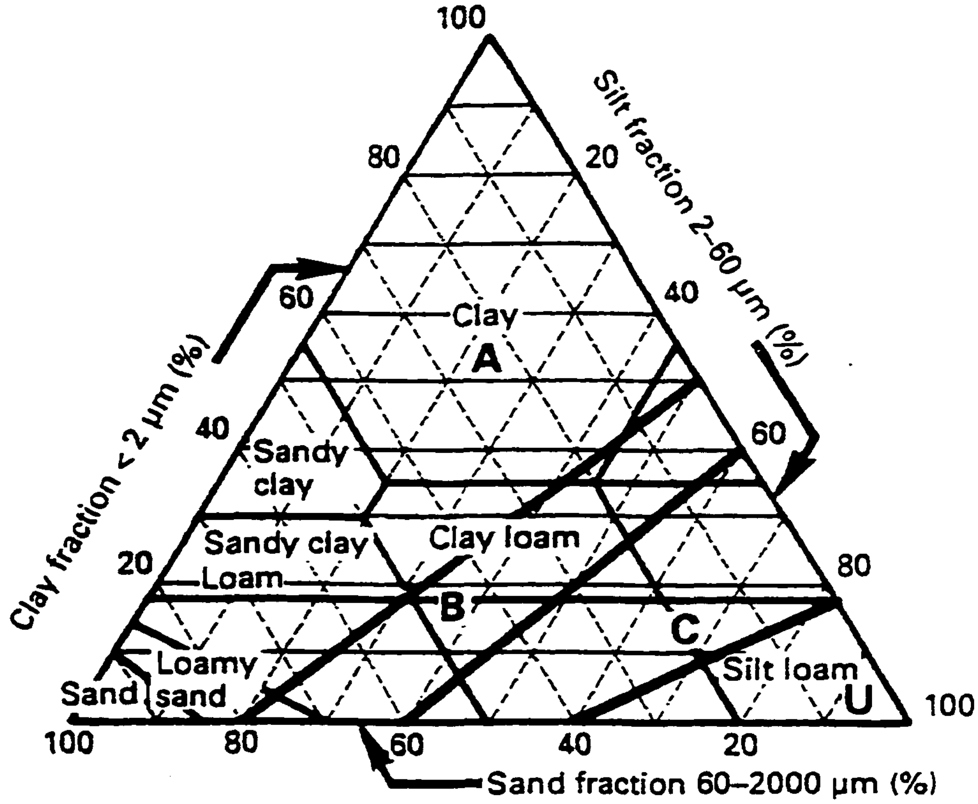

Figure 2.3 – Relationship between soil particle size distribution and soil erodibility (A - least susceptible, B - moderately susceptible, C - most susceptible, U - unsuitable). From Coppin and Richards, 1990, p. 94. Reprinted with permission from CIRIA/Butterworths.

2.2.2 Soil Particle-Size Statistics

Characterization of the particle-size distribution of a soil is often accomplished by selecting the grain size for which a predetermined percentage of the soil, by weight, is finer. One frequently used characteristic particle-size is the median grain size, d_{50}, i.e., the size for which 50% of the material is finer. Other particle sizes used to characterize soil include d_{16}, d_{25}, d_{30}, d_{75}, d_{84}, and d_{90}.

The most frequently used statistics for characterizing the particle-size distribution of a soil are derived under the assumption that the logarithms of the grain sizes are normally distributed (Vanoni, 1975). That is, the particle size distribution is assumed to be log-normal. In practice, particle-size statistics are calculated in the same manner when the size distribution is not log-normal. The equations used in practice for estimating the geometric mean size (d_g), the geometric standard deviation (σ_g), and the skewness (γ) of sediment are

$$d_g = \sqrt{d_{84} d_{16}} \tag{2.1}$$

$$\sigma_g = \sqrt{d_{84} / d_{16}} \tag{2.2}$$

$$\gamma = \log\left(\frac{d_g}{d_{50}}\right) \Big/ \log \sigma_g \tag{2.3}$$

Another term commonly used to describe the distribution of particle sizes is the gradation coefficient, defined as (Yang, 1996)

$$G = \frac{1}{2}\left(\frac{d_{84}}{d_{50}} + \frac{d_{50}}{d_{16}}\right) \tag{2.4}$$

2.3 Vegetation

The presence of vegetation in a channel, on the banks of a channel, or in the floodplain can significantly complicate the evaluation of flow conditions. There is variable flow resistance and momentum exchange between the channel, the channel banks, and the floodplain, and there are impacts upon turbulence. Flow through and over woody vegetation is further complicated by the fact that several thresholds exist at which the resistance components (form and shear drag) change because of vegetal response.

Whether or not vegetation is beneficial, with regards to near-bank processes, is debatable. Detrimental effects ascribed to vegetation include reduction of channel conveyance, impairment of revetment visibility for inspection, hindrance of flood-fighting activities, and adverse effects on revetment and levee durability (Shields, 1991). Conversely, healthy riparian vegetation provides shade that prevents excessive water temperature fluctuations, performs a vital role in nutrient cycling and water quality, improves the aesthetic and recreational value of a site, and is immensely productive as wildlife habitat (Fischenich, 1997).

Simon and Hupp (1987) studied several stream channels in the Obion-Forked Deer River basin in west Tennessee that have been modified (dredged and straightened) periodically since the turn of the century. Hupp and Simon demonstrated that patterns of riparian species distribution are strongly associated with the channel geomorphic stage of adjustment to modification. They concluded that patterns of species distribution could be used to infer ambient bank stability. Thorne et al. (1988) used Chang's method (Chang, 1980) to predict the hydraulic geometry of gravel-bed rivers and found that differences between measured and predicted hydraulic geometry could be significantly reduced by taking into account the type and density of streambank vegetation.

Shields (1991) performed an empirical study on the effects of woody vegetation on riprap stability. In his study, damage rates for revetments along the Sacramento River with and without woody vegetation were compared. It was found that damage rates among the former were substantially less than the latter for revetments of the same age and located on banks of similar curvature.

Although it is difficult, if not impossible, to set apart the stabilizing influence of vegetation from other variables that affect near-bank processes, published observations supporting the benefits of healthy riparian vegetation abound. Happ et al. (1940), for example, noted that the banks of Tobitubby and Hurricane Creeks in Lafayette County, Mississippi, are generally well protected by vegetation and are fairly stable except in areas that had been artificially cleared.

The recognition of vegetation as an influential factor in channel behavior leads hydraulic engineers, fluvial geomorphologists and others interested in characterizing river channels to develop qualitative and quantitative procedures for describing vegetation in channels and floodplains. These procedures are often employed in channel assessment surveys and in estimating flow resistance due to vegetation. Techniques for estimating flow resistance in vegetated floodways (e.g., Manning's n) can be grouped into three general categories (Fischenich, 1996; Flippin-Dudley, 1997): direct measurement, handbook methods, and analytical approaches. Following is a review of techniques and parameters used to estimate flow resistance in vegetated channels.

2.3.1 Direct Measurement

Direct measurement of flow resistance requires channel cross-section geometry data and stage versus velocity data from several locations along a channel. The direct measurement of flow resistance is a time consuming and cumbersome process. Equipment and recommendations for measurement of open-channel flow are described in the National Handbook of Recommended Methods for Water Conservation (U.S. Geological Survey, 1977).

2.3.2 Handbook Methods

Handbook methods involve the use of tables or photographs for estimating flow resistance (Flippin-Dudley, 1997). These methods rely on individual judgement and ability to compare the characteristics of the channel (and vegetation) under investigation with those presented in the handbook. Chow (1959), Barnes (1967), and Hicks and Mason (1991), among others, present photographs of channels of known resistance accompanied by qualitative descriptions of the channel.

2.3.3 Analytical Models for Predicting Vegetal Effects

Several analytical methods for predicting vegetal flow resistance have been developed and most use physical plant characteristics and foliage distribution as variables in the computation of flow resistance (Flippin-Dudley, 1997). Fenzl and Davis (1964), Gwinn and Ree (1980), and Temple (1991), among others, related flow resistance to the number of plant stems per unit area. An equation developed by Rahmeyer (1994) uses the effective height (the total height of a plant minus the height of the plant stem), stem diameter, and stem density of vegetation to predict flow resistance. Kouwen and Unny (1973) proposed using the ratio of the total cross-sectional area of flow to the area blocked by vegetation as a parameter for predicting flow resistance. Kouwen (1988) recommended using biomechanical (stiffness) properties to predict flow resistance for submerged grasses. Fisher (1995) developed an equation for predicting resistance due to a specific type of vegetation (*Ranunculus*) as a function of the flow velocity, hydraulic radius, and the vegetation surface area ratio.

Petryk and Bosmajian (1975), Fischenich (1996), and Flippin-Dudley (1997) used Veg_d to predict flow resistance in vegetated channels; Lopez and Garcia (1997) used Veg_d and the deflection angle of the vegetation. The variable Veg_d is defined as

$$Veg_d = \frac{\sum A_i}{bhL} \tag{2.5}$$

where A_i is the area of the ith plant normal to the principal direction of flow, b is the width of the channel or representative measurement area, h is the height of the vegetation or measurement area, and L is the length of channel over which the vegetation has been characterized.

2.3.4 Channel Flow in the Presence of Willow Posts

A literature review was performed to find an analytical model that would facilitate evaluating the impact of newly planted willow post systems on channel flow. For evaluating the suitability of potential models, a planted willow post system is regarded herein as a collection of rigid cylinders placed along a sloping streambank. Further, it is assumed that no other vegetation is present in significant quantities on the stream bank, i.e., the bank has been severely eroded or recently regraded.

Petryk (1969) studied drag forces on individual cylinders in different multi-cylinder arrangements under a variety of open-channel flow conditions. A model was developed for predicting the mean velocity distribution across a channel, the drag on each cylinder, and the resistance to flow of a given cylinder arrangement. Experimental tests were performed for several cylinder patterns to verify results from his model. For some arrangements the cylinders were distributed across the width of the channel, while in other cases the cylinders were placed along one side of the channel (simulating floodplain flow conditions). Results from Petryk's model were found to be within an accuracy of about 30 percent.

Yano (1966) developed a model similar to the model developed by Petryk (1969). The principle difference between the two models is the theoretical underpinnings from which each was developed. Yano's model uses linear superposition of momentum defects whereas Petryk's model uses linear superposition of velocity defects.

Nepf (1998) developed a physically based model for evaluating the impact of emergent vegetation on drag, turbulence, and diffusion. Wooden dowels were used in laboratory experiments performed by Nepf to simulate rigid cylindrical vegetation. Laboratory observations followed a trend that was consistent with predicted values of the bulk drag coefficient. Field measurements of diffusion were made in stands of smooth cordgrass (*Spartina alterniflora*) at the Great Sippewisset Marsh, Cape Cod, Maine. Nepf also measured diffusion rates in the laboratory; both sets of data were consistent with predictions from her model.

Lopez and Garcia (1997) used a two-equation turbulence model based on the k-ε closure scheme to study open-channel flow and turbulence through nonemergent (i.e., fully submerged) vegetation. Lopez and Garcia's model was used to evaluate the effects of flow parameters, sediment properties, and plant structure on the suspended sediment transport capacity of open-channels in which there is vegetation.

Fischenich (1997) developed a model for describing vertical velocity profiles and the shear stress distribution inside and above vegetation canopies along densely vegetated floodways. Fischenich's model uses empirical and theoretical concepts from boundary layer meteorology. In his model, flow resistance is related to measurable characteristics of the channel, vegetation, and flow.

The model developed by Petryk (1969) has been adopted for this study. Following is a summary of the reasons why the other models were not selected:

- Petryk (1969) compared predictions from his model and the model developed by Yano (1966) with measurements recorded from laboratory tests. From the comparison, Petryk noted that his method is generally better for flow situations where the cylinders are distributed only along one side of the channel, as is generally the case for the planted willow post systems at Harland Creek.
- The model developed by Nepf (1998) was developed for conditions encountered in wetlands thus some of the assumptions underlying the model are not valid for willow posts systems, i.e., the willow posts are not sparsely

distributed. Also, it is expected that there is a great difference in the range of velocities modeled by Nepf versus what would be encountered during a flood event on the order of bankfull flow conditions at Harland Creek.

- The model developed by Lopez and Garcia (1997) was not selected because it was developed for evaluating flow through nonemergent vegetation. Although it is reasonable that the willow posts would be completely submerged during bankfull flow conditions, the willows would not be submerged for the majority of flow conditions encountered. Modeling the willow post systems as emergent vegetation, thus, will yield the most relevant results.
- Planted willow posts systems, as envisioned for this study, are constructed on sloping streambanks where little if any woody vegetation is present immediately after construction. This condition is deemed the most critical for survival of the willow posts. The model developed by Fischenich (1997) was derived and evaluated for conditions of dense vegetation. Fischenich's model, therefore, was not deemed suitable for evaluating the effects of newly planted willow posts on open-channel flow.

Details about the theory, assumptions, and implementation of the model developed by Petryk (1969) follow.

2.4 Petryk's Model for Predicting Flow Through Vegetation

Wake superposition refers to combining the effects of two or more wake producing bodies (Petryk, 1969). That is, it is a procedure by which the effects of upstream wake producing objects are coupled to predict the downstream flow field. From Reichardt's differential equation for calculating the distribution of momentum in a two-dimensional wake (Reichardt, 1943), Petryk was able to show that the total velocity defect at a point in a flow field, $u_{total}(x,z)$, could be described by summing the velocity defects contributed by individual wake producing objects (linear superposition) or

$$
\begin{aligned}
u_{total}(x,z) &= u_{n,1}(\Delta x_1,\Delta z_1)+u_{n,2}(\Delta x_2,\Delta z_2)+\cdots+u_{n,m}(\Delta x_m,\Delta z_m) \\
&= \sum_{i=1}^{m} u_{n,i}(\Delta x_i,\Delta z_i) \\
&= \sum_{i=1}^{m} u_{n,i}(\Delta x,\Delta z)
\end{aligned} \tag{2. 6}
$$

where $u_{n,1}(\Delta x_1,\Delta z_1)$, $u_{n,2}(\Delta x_2,\Delta z_2)$, ... , and $u_{n,m}(\Delta x_m,\Delta z_m)$ are velocity defects contributed by individual objects, m is the number of wakes affecting the flow at a given point n with coordinates (x, z), and Δx_i and Δz_i are longitudinal and transverse distances, respectively, from the ith wake producing object to the point n.

In a flow field containing wakes, the depth-averaged velocity, $U_x(x,z)$, at any point (x,z) is given by

$$U_x(x,z) = U_\infty(x,z) + u_{total}(x,z) \tag{2.7}$$

where $U_\infty(x,z)$ is the reference free stream velocity at the point of interest in the channel. Figure 2.4 defines the terms above diagrammatically (all velocities are averaged over the depth of flow).

From limited experimental results and based on approximate agreement with Eskinazi's data (Eskinazi, 1959), Petryk (1969) chose the following equations to describe the wake of an infinite cylinder in a two-dimensional fully developed turbulent viscous layer:

$$u_{n,i}(\Delta x,\Delta z) = \frac{(u_{n,i})_{\max}}{2}\left[1+\cos\left(\frac{\pi\Delta z}{2b_{1/2}}\right)\right] \tag{2.8}$$

$$\frac{(u_{n,i})_{\max}}{U_{0i}} = \frac{u_{n,i}(\Delta x,0)}{U_{0i}} = -0.90\left(\frac{\Delta x}{C_d d}\right)^{-0.7} \tag{2.9}$$

$$\frac{2b_{1/2}}{C_d d} = 0.48\left(\frac{\Delta x}{C_d d}\right)^{0.59} \tag{2.10}$$

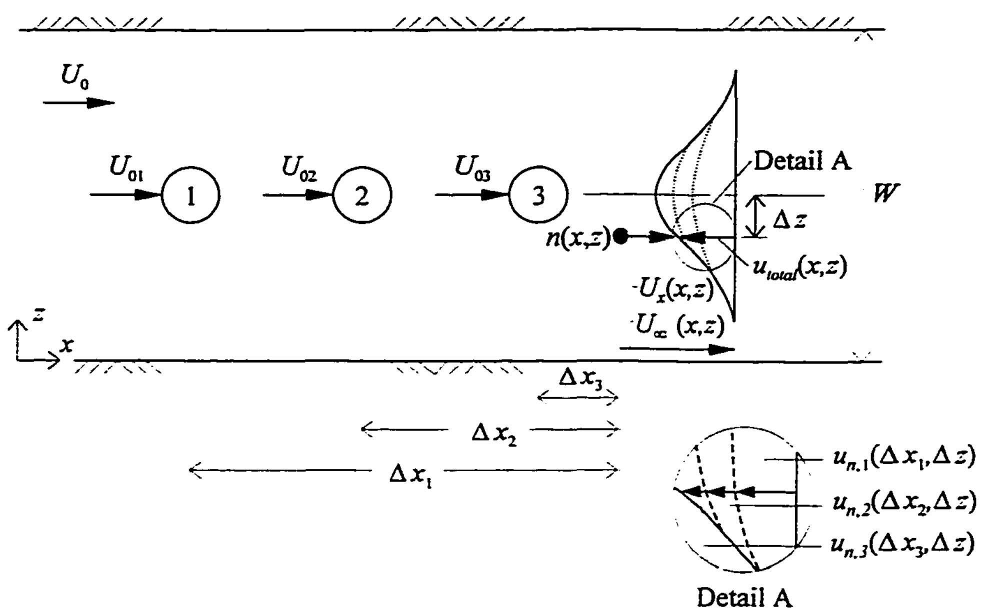

Figure 2.4 – Wake behind a single row of cylinders in a rectangular channel (plan view).

in which, as indicated in Figure 2.4, $u_{n,i}(\Delta x, \Delta z)$ is the velocity defect at an arbitrary point n due to the ith cylinder; $(u_{n,i})_{\max}$ is the velocity defect at the center of the wake; Δx and Δz are longitudinal and transverse distances, respectively, from the center of the ith cylinder to the point n; U_{0i} is the approach velocity to the ith cylinder; C_d is the drag coefficient at the ith cylinder; d is the diameter of the ith cylinder; and $b_{1/2}$ is the distance from the wake centerline to the point at which the velocity defect is equal to $(u_{n,i})_{\max}/2$.

For approximately zero bed-slope conditions (2.8), (2.9), and (2.10) can be used to estimate the wake and spread characteristics behind a cylinder. If the channel slope is relatively large, however, a correction for the effect of slope on the decay of wakes is necessary. Petryk reasoned that for open-channel flow, the effect of slope is to reduce the velocity defect, while the effect of channel slope on the wake width is small. Using equations developed by Hill et al. (1963), Petryk deduced the following equation for predicting $(u_{n,i})_{\max}$ for sloping channels:

$$\frac{(u_{n,i})_{\max}}{U_{0i}} = -0.90\left(\frac{\Delta x}{C_d d}\right)^{-0.7}\left(\frac{1}{1-\dfrac{g\Delta x S_0}{U_{0i}^2\,2}}\right)^{3/2} \tag{2.11}$$

in which g is the gravitational constant and S_0 is the channel bottom slope. Petryk neglected the effect of slope on wake width. Equations (2.8), (2.10), and (2.11) completely describe the mean velocity distribution for a wake in an open-channel flow with a sloping bed.

2.4.1 Velocity Profiles Behind Cylinders

The use of (2.7) with (2.8) through (2.11) for predicting velocity profiles across a channel in the wake of a single cylinder or a given multi-cylinder distribution is described below.

2.4.1.1 Single Cylinder in Rectangular Channel

With reference to (2.7), the velocity distribution in the wake of a single cylinder is described by

$$U_x(x,z) = U_\infty(x,z) + u_{n,1}(\Delta x, \Delta z) \tag{2.12}$$

where $u_{n,1}(\Delta x, \Delta z)$ is the velocity defect and $U_\infty(x,z)$ is the reference free stream velocity at the point n, as shown in Figure 2.5. For a rectangular channel the reference free stream velocity can be assumed constant across the width of the channel thus $U_\infty(x,z) = U_\infty(x)$. An expression for $U_\infty(x)$ can be derived from the continuity equation as follows (Li and Shen, 1973):

$$\begin{aligned} Q = U_0 WD &= D\int_W U_x(x,z)dz \\ &= D\int_W \left[U_\infty(x) + u_{n,1}(\Delta x, \Delta z)\right]dz \\ &= DU_\infty(x)\,W + D\int_W u_{n,1}(\Delta x, \Delta z)dz \end{aligned} \tag{2.13}$$

which, after rearrangement yields

$$U_\infty(x) = U_0 - \frac{1}{W}\int_W u_{n,1}(\Delta x, \Delta z)dz \tag{2.14}$$

where D is the depth of flow, W is the channel width, and U_0 is the mean velocity based on flow area. From (2.8), (2.12), and (2.14) the velocity distribution across a rectangular channel in the wake of a single cylinder can be computed.

2.4.1.2 Multi-Cylinder Distributions in Rectangular Channel

In this section an algorithm is presented by which the approach velocity to individual cylinders can be predicted when there are multiple cylinders in a rectangular channel. To begin, the approach velocity to the first cylinder, U_{01}, is simply taken to be

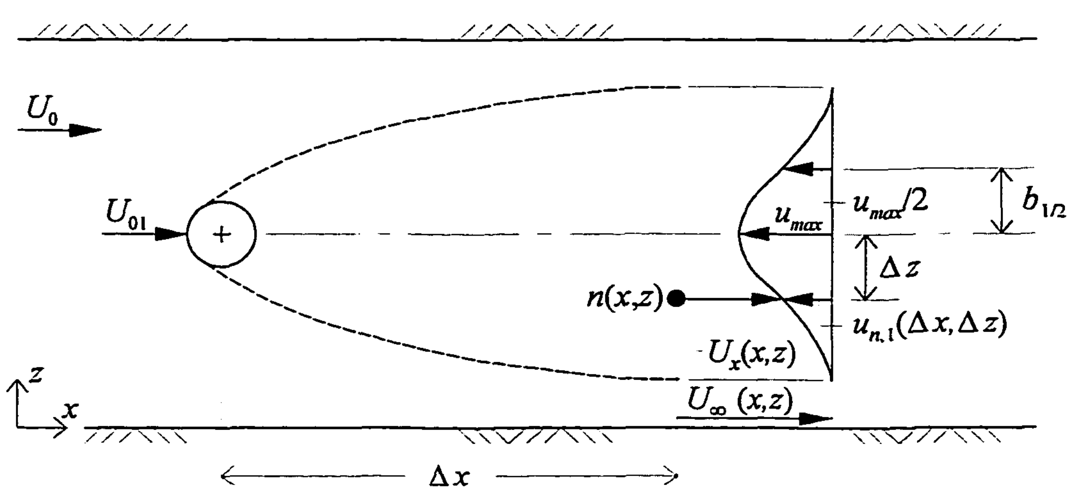

Figure 2.5 – Wake behind a single cylinder in a rectangular channel (plan view).

equal to the cross-section averaged velocity in the channel, U_0, that is $U_{01} = U_0$ (Figure 2.6). From (2.7), the approach velocity to the second cylinder, U_{02}, is

$$\begin{aligned} U_{02} &= U_x(x_2, z_2) \\ &= U_\infty(x_2) + u_{2,1}(\Delta x, \Delta z) \\ &= U_\infty(x_2) + u_{2,1}(x_2 - x_1, z_2 - z_1) \end{aligned} \tag{2.15}$$

where $u_{2,1}(x_2 - x_1, z_2 - z_1)$ is the velocity defect at cylinder 2 due to the wake produced by cylinder 1. Also, following the derivation of (2.14),

$$U_\infty(x_2) = U_0 - \frac{1}{W}\int_W u_{2,1}(\Delta x, \Delta z)dz \tag{2.16}$$

The integral in (2.16) can be expanded based on (2.8) to yield

$$\begin{aligned} \int_W u_{2,1}(\Delta x, \Delta z)dz &= \int_W \frac{(u_{2,1})_{\max}}{2}\left[1 + \cos\left(\frac{\pi(\Delta z}{2b_{1/2}}\right)\right]dz \\ &= \frac{1}{2}u_{2,1}(\Delta x, 0)\int_W 1 + \cos\left(\frac{\pi(\Delta z)}{2b_{1/2}}\right)dz \end{aligned} \tag{2.17}$$

The width of the wake behind cylinder 1 and the channel width must be considered in evaluating (2.17). For the case where the wake width does not extend to either wall in a channel, the integration limits for (2.17) are from $-2b_{1/2}$ to $2b_{1/2}$. If the width of the wake does extend to one or both walls in a channel then the wake is constricted and the integration limits must be adjusted accordingly. The width of the wake can be determined from (2.10).

With reference to Figure 2.4 and Figure 2.6, the approach velocity to cylinder 3 can be expressed as

$$\begin{aligned} U_{03} &= U_x(x_3, z_3) \\ &= U_\infty(x_3) + \sum_{i=1}^{2} u_{3,i}(\Delta x, \Delta z) \\ &= U_\infty(x_3) + u_{3,1}(\Delta x, \Delta z) + u_{3,2}(\Delta x, \Delta z) \end{aligned} \tag{2.18}$$

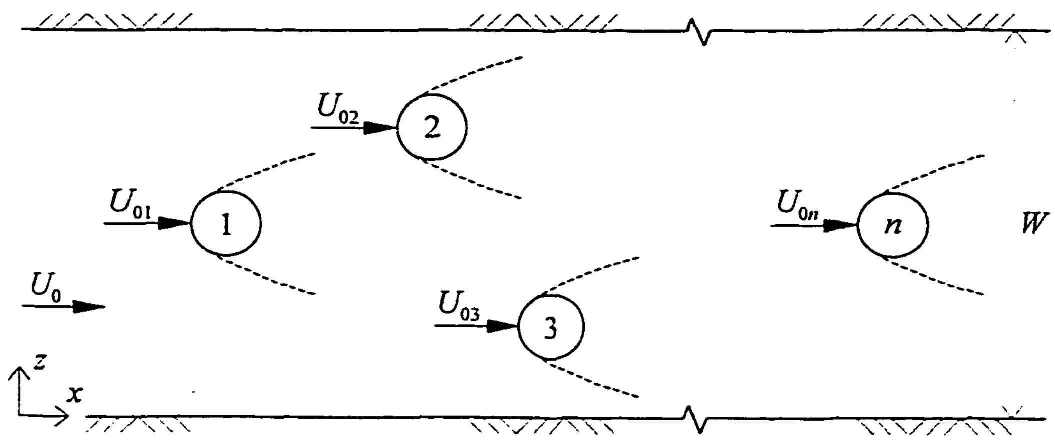

Figure 2.6 – Multi-cylinder distribution in a rectangular channel (plan view).

where $u_{3,1}(x_3 - x_1, z_3 - z_1)$ is the velocity defect due to the first cylinder and $u_{3,2}(x_3 - x_2, z_3 - z_2)$ is due to the second cylinder. The reference free stream velocity at cylinder 3 is

$$
\begin{aligned}
U_\infty(x_3) &= U_0 - \frac{1}{W}\sum_{i=1}^{2}\int_W u_{3,i}(\Delta x, \Delta z)dz \\
&= U_0 - \frac{1}{W}\int_W u_{3,1}(\Delta x, \Delta z)dz - \frac{1}{W}\int_W u_{3,2}(\Delta x, \Delta z)dz
\end{aligned}
\tag{2.19}
$$

To compute the value of U_{03} use (2.8) and (2.19).

The approach velocity to the *n*th cylinder (Figure 2.6) is calculated using

$$
\begin{aligned}
U_{0n} &= U_x(x_n, z_n) \\
&= U_\infty(x_n) + \sum_{i=1}^{m} u_{n,i}(\Delta x, \Delta z)
\end{aligned}
\tag{2.20}
$$

and

$$
U_\infty(x_n) = U_0 - \frac{1}{W}\sum_{i=1}^{m}\int_W u_{n,i}(\Delta x, \Delta z)dz \tag{2.21}
$$

where m is the number of cylinders which have influence on the *n*th cylinder. For the *n*th cylinder, when $(u_{n,i})_{\max}/U_{0i} < 0.02$, Petryk (1969) and Li and Shen (1973) arbitrarily assumed that the wake effect due to the *i*th cylinder was completely dissipated.

2.4.2 Assumptions and Limitations for Petryk's Model

The assumptions and limitations of Petryk's model are summarized below. Details regarding the selection of drag coefficients and the discontinuance of wakes are also presented.

2.4.2.1 General Assumptions

General assumptions and limitations for using Petryk's model are as follows:

1. Flow in the channel is uniform.

2. The slope of the channel bed is constant.
3. Each wake decays independently of the downstream or upstream distribution of cylinders (this assumption was critical in the derivation of the superposition of wakes concept).
4. Flow approaching the cylinder is fully developed open-channel flow.
5. The flow around each cylinder is such that free surface effects are small (depth-to-diameter ratio greater than 4) and aeration does not affect the drag coefficient (Froude number based on cylinder size is less than or equal to unity).
6. The spacing between cylinders is at least 6 diameters in the downstream direction and 3 diameters in the crosswise direction.
7. Each cylindrical element protrudes above the water surface.
8. When $(u_{n,i})_{max}/U_{0i} < 0.02$, the wake effect due to the ith cylinder has been completely dissipated.

2.4.2.2 Drag Coefficients

The drag coefficient in an idealized two-dimensional flow is about 1.2 for a cylinder Reynolds number, $Re = U_0 d/\nu$ (U_0 is the approach velocity to the cylinder, d is the cylinder diameter, and ν is the fluid kinematic viscosity), range of 8×10^3 to 2×10^5 as reported in Schlichting (1979) and other standard texts. Flow around a vertical cylinder in an open-channel, though, has many characteristics that could change the drag magnitude from the idealized two-dimensional case. Nonetheless, Petryk (1969)—using the experimental results of Hsieh (1964), Isaacs (1965), and from his own tests—concluded that if there is no aeration behind a cylinder and free surface effects are not significant, then the best estimate of the drag coefficient is the two-dimensional value of 1.2.

Whereas Petryk (1969) assumed a constant drag coefficient of 1.2 in his analyses, herein a drag coefficient was determined for each cylinder based on the calculated approach velocity to the cylinder. For $Re \geq 8\text{x}10^3$ the drag coefficient, C_d, was set equal to 1.2. For $1 < Re \leq 8\text{x}10^3$, C_d was estimated using (White, 1991):

$$C_d = 1 + 10.0Re^{-2/3} \tag{2.22}$$

The principle reason for using (2.22) is that flow conditions were considered herein for which $Re < 8\text{x}10^3$. Petryk implied that his analysis only considered conditions for which $Re \geq 8\text{x}10^3$.

2.4.2.3 Wake Discontinuance

When a wake spreads to the edge of a channel, the wall constricts it. This must be taken into consideration in using equations presented in this section where integration over the width of a wake is performed. If the wake is not constricted, the integration limits are from $-2b_{1/2}$ to $2b_{1/2}$. If a wall constricts the wake width then the integration limits must be adjusted accordingly.

Wake decay is described in Petryk's model with power equations and consequently, predicted velocity defects never reach zero. Petryk (1969) and Li and Shen (1973) addressed this matter by arbitrarily assuming the wake to be completely dissipated when the maximum defect caused by the ith cylinder, $u_{\max}$, became less than 2% of the approach velocity to the ith cylinder, U_{0i}, or

$$\frac{u_{\max}}{U_{0i}} \leq 0.02 \tag{2.23}$$

This criterion was used herein in the application of Petryk's model.

3. Approach and Methodology

Several means of approach were taken to collect data for this study. In broad terms, field, laboratory, and analytical techniques were employed. In this chapter, the data collection techniques are described in detail.

3.1 Selection of Study Reaches and Transects

Stabilization and habitat improvement works were constructed along the banks of a 14-segment, 3,750-m (11,705-ft) reach of Harland Creek between the years 1993 and 1994 (Derrick, 1997). A total of five treatments were applied to the banks: willow posts, bendway weirs, bendway weirs and willow posts, bendway weirs and longitudinal peaked stone toe (LPST), and willow posts and LPST. Figure 3.1 illustrates each segment (reach) and lists the applied treatments. Five segments are treated with bendway weirs, three are treated using willow posts, and two are treated with willow posts and a single bendway weir. In two segments there are willow posts planted behind LPST, in another segment there are bendway weirs and LPST, and one segment incorporates all three of the protection methods. For this study, two improved segments and one unimproved segment of Harland Creek were selected for monitoring. Within each of the selected study reaches at least four belt transects were established and subjected to detailed inspection. General descriptions of the study reaches follow.

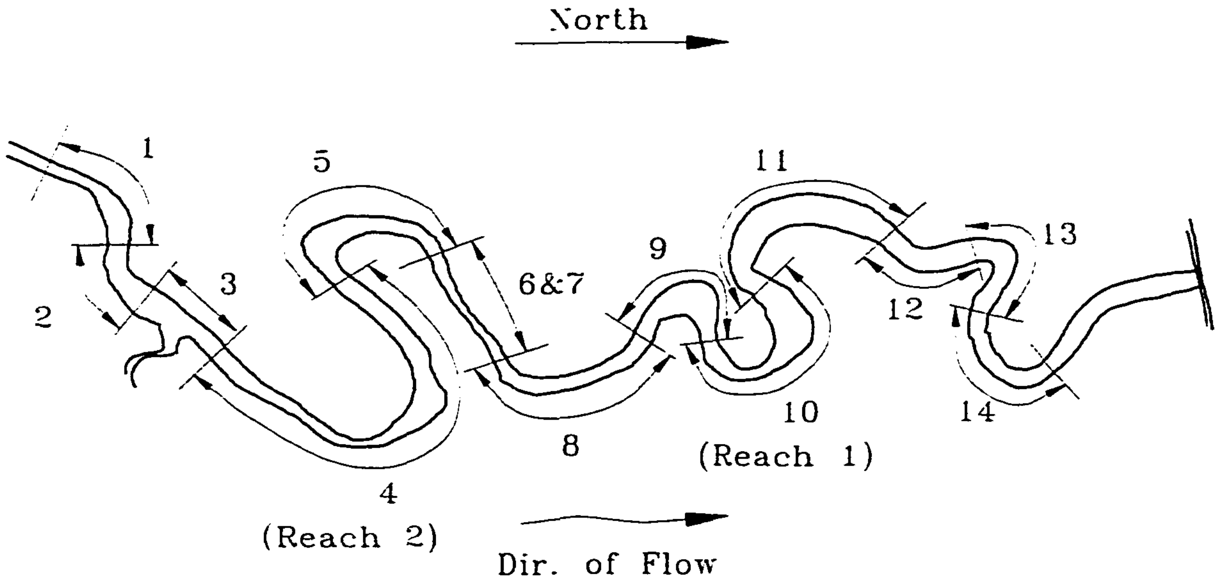

Segment	Treatment
1	Bendway weirs
2	Bendway weirs
3	Bendway weirs
4	One bendway weir and willow posts (3 rows/5 rows around bend)
5	Bendway weirs and willow posts (2 rows) and LPST*
6	Willow posts (3 rows)
7	Willow posts (3 rows)
8	Willow posts (5 rows)
9	Bendway weirs and LPST*
10	Bendway weirs and willow posts (5 rows)
11	Bendway weirs
12	Bendway weirs
13	Willow posts (4 rows/5 rows around bend) and LPST*
14	Willow posts (2 rows), LPST*

*LPST = Longitudinal peaked stone toe dike with tiebacks

Figure 3.1 – Harland Creek 14-segment improvement plan.

3.1.1 Study Reaches with Willow Posts

In establishing objectives for this study, a decision was made to focus on the performance of solitary willow post systems constructed to protect actively eroding banks. Therefore, all segments of Harland Creek with either LPST (segments 5, 9, 13, and 14) or multiple bendway weirs (segments 1, 2, 3, 5, 9, 11, and 12) were not considered as potential study reaches.

Also eliminated from consideration were three segments with solitary willow post systems (segments 6, 7, and 8). Each segment was straight, uniform in width, and had alternate bars present. The morphology of the segments indicates relative stability (Shen et al., 1981) thus segments 6, 7, and 8 were deemed inappropriate for critically evaluating the performance of the willow post systems. The remaining two segments (segments 4 and 10), are treated with willow posts and a single bendway weir, and each is located along a meander bend. It was reasoned that as long as the area influenced by the bendway weirs was avoided, the two segments could be treated as if only willow posts were present. A part of each segment was selected as a study reach; these are referred to herein as Reach 1 and Reach 2 (Figure 3.1). Reach 2 begins about 1.2 km (4,000 ft) upstream of Reach 1.

Within Reaches 1 and 2, rectangular areas spanning across the width of the channel and about 3 m (10 ft) along the length of channel (belt transects) were established approximately 30 m (100 ft) apart. Five belt transects were established in Reach 1 and four were established in Reach 2. Within each belt transect a cross-section survey was performed, soil samples were collected, erosion pins were placed, and vegetation density measurements were recorded.

3.1.2 Control Study Reach

A third reach (Reach 3) was established to serve as a control reach. Data derived from Reach 3 serves as control data for assessing the influence of planted willow posts on Reaches 1 and 2. Reach 3 was located about 5 km (3 mi) upstream of Reach 2. The five belt transects established in Reach 3 were located in an area that has never been subjected to man-made bank stabilization. The first four belt transects in Reach 3 were about 30 m (100 ft) apart and the fifth transect was about 0.91 km (3,000 ft) upstream of the nearest belt transect. As with Reaches 1 and 2, surveys of the belt transects in Reach 3 were performed, soil samples were collected, erosion pins were placed, and vegetation density measurements were recorded.

3.2 Stream Channel Cross-Sectional Form

A cross-section survey was performed within each belt transect using an electronic total station. Data from the surveys (Appendix A) were used to calculate a number of channel form (shape and size) parameters. Channel size parameters evaluated herein include cross-sectional area (A), width (W), hydraulic depth ($D = A/W$), maximum depth (d_{max}), wetted perimeter (P), and hydraulic radius ($R = A/P$). Channel shape parameters include the width-depth ratio (W/D), W/d_{max}, and d_{max}/D. The channel form parameters evaluated herein were calculated for the estimated bankfull stage, which was chosen because it is assumed to have morphologic significance. Procedures followed for estimating the bankfull stage are presented in Section 3.2.1.

To facilitate monitoring changes in channel cross-section form, during and as a result of flood events, simple gages (erosion pins and maximum scour depth gages) were placed along the surveyed cross-sections.

3.2.1 Estimation of Bankfull Stage

Based on observations, the active floodplain was initially considered to be equal to the bankfull level for Reaches 1 and 2. The active floodplain is defined herein as a strip of relatively smooth land that is overflowed in times of high water (Rice, 1949) and formed by a combination of deposition on the inside of river curves and deposition from overbank flows (Wolman and Leopold, 1957). In Reach 3 no active floodplain was observed at any of the established belt transects so the valley flat (floodplain) was initially considered the bankfull level.

To refine the estimated bankfull levels, the following procedures, described by Williams (1978), were evaluated:

- the elevation at which W/D becomes a minimum;
- the stage corresponding to the first maximum of the bench index, as defined by Riley (1972); and
- the stage corresponding to a change in the relation of A to W.

It was noted by Williams (1978) that if an investigator thinks of bankfull in relation to a particular overflow surface (i.e., the valley flat; active floodplain; low, middle or most prominent bench; average elevation of highest surface of the channel bars), these three methods can be applied only locally. That is, to just the overflow surface predetermined in the field to represent bankfull. As suggested by Williams, the three methods used to estimate the bankfull stage were applied locally, that is, in the vicinity of the initially assumed bankfull level.

3.2.2 Bank Erosion and Deposition Gages

Horizontal erosion pins were used to detect bank erosion and vertically driven pins were used to monitor changes in the cross-section ground line. All the erosion pins were 90-cm- (3-ft-) long, 9.5-mm- (3/8-in.-) diameter steel rebar. Hooke (1979) recommended that pins of at least 80 cm (2.6 ft) in length be used on all actively eroding banks. One horizontal erosion pin and five vertical pins were placed in each transect, in line with the surveyed cross-section. The horizontal pin was placed about 0.6 m (2 ft) below the floodplain on the outer (concave) bank; about 15 cm (6 in.) of the pin was left protruding from the bank. Of the five vertical pins, three were placed along the outer bank—on the lower, middle, and upper part of the bank; one was placed on the left floodplain, and one was placed on the right floodplain. The vertical pins were left protruding about 46 cm (18 in.) above the ground. The relative locations of the erosion pins are shown in Figure 3.2.

The coordinates and ground elevation of each erosion pin was surveyed in August 1997 using an electronic total station. The initial protruding length of each pin was determined by calculating the difference between the ground and top elevation of each erosion pin. Erosion and accretion along each cross-section was monitored by measuring the protruding length of the erosion pins during field visits made in December/January 1997-98, March 1998, and August 1998.

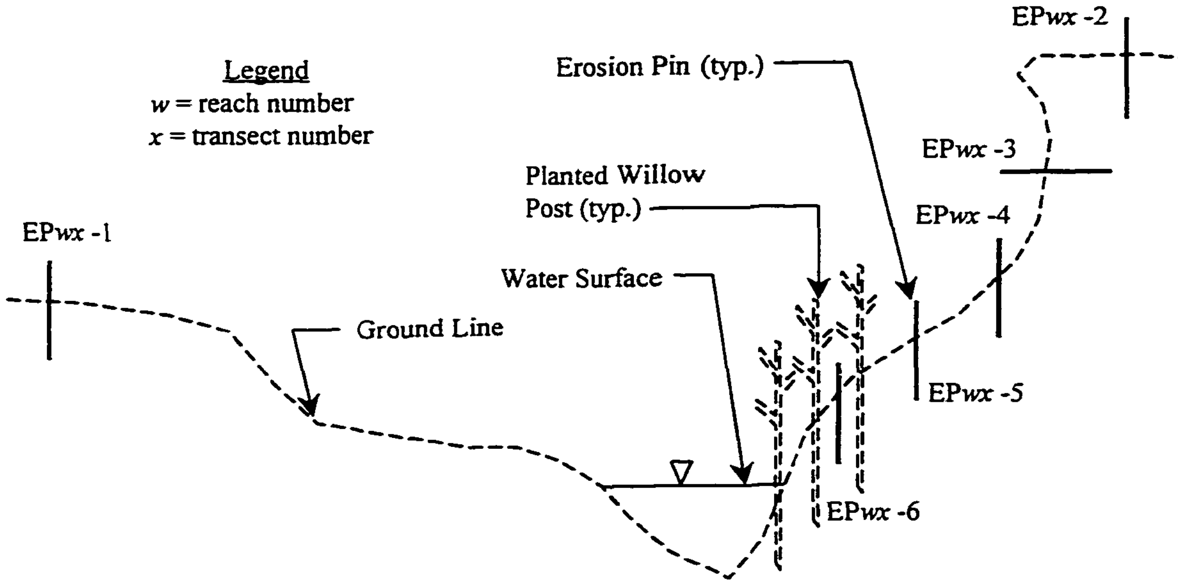

Figure 3.2 – Typical erosion pin (EP) locations and corresponding pin numbers (not to scale).

3.2.3 Maximum Scour Depth Gage

For the purpose of detecting the maximum scour depths on the banks, washers were placed over the vertical erosion pins at selected transects. Assuming the washers fall as the ground beneath is scoured, the maximum scour depth attained at gaged erosion pins can be determined by measuring changes in the distance from the top of the erosion pin to the washer. The maximum scour depth gages were checked whenever the protruding lengths of the erosion pins were measured.

3.3 Soils

Soil samples were collected from within each belt transect. Described in the following sections are the procedures used to derive soil samples in the field, the process by which soil samples were analyzed in the laboratory, and the statistical test that was performed to assess spatial patterns in the soil characteristics.

3.3.1 Soil Sampling Methodology

Within each belt transect, soil samples were taken from along the banks, the bed, and the bar, approximately 3 m (10 ft) downstream of the surveyed cross-sections. The relative locations from which soil samples were taken are shown in Figure 3.3. The ground elevation and the coordinates of all points chosen for soil sampling were surveyed using an electronic total station.

Each soil sample derived in the field was designated as SS*wx-yz* where SS means soil sample, *w* is the reach number, *x* is the transect number, *y* indicates the point number assigned to the sampling location in the transect, and *z* indicates the depth increment from which the sample was taken (Figure 3.3). Soil samples designated as SS*wx*-2*z*, SS*wx*-4*z*,

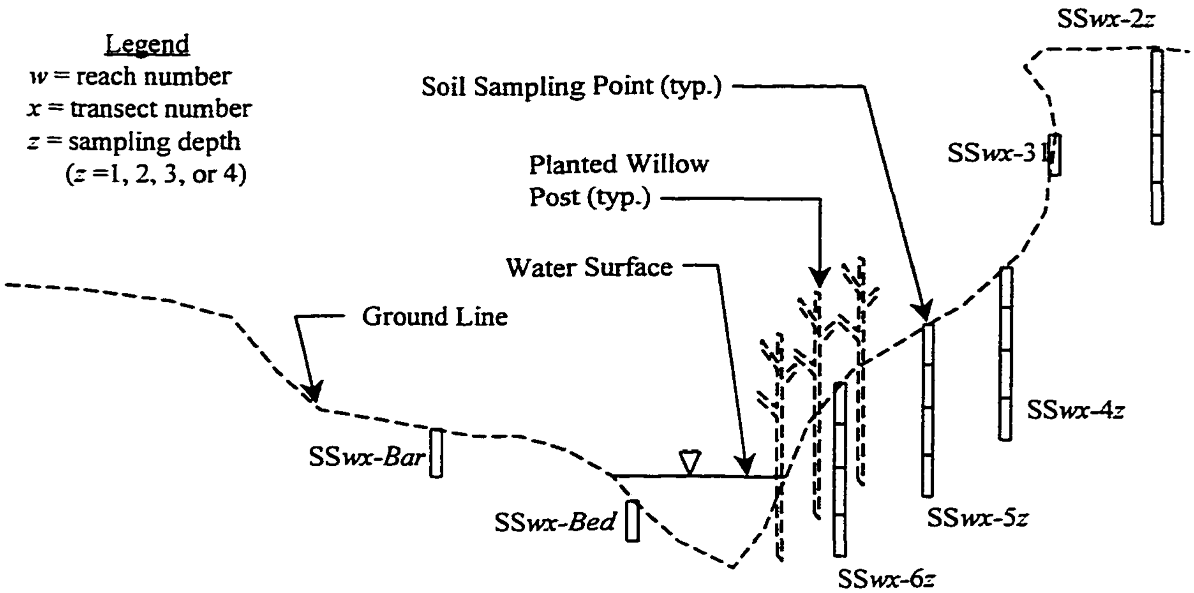

Figure 3.3 – Relative locations of soil sampling points (SS) and designated point numbers (not to scale).

SS*wx-5z*, and SS*wx-6z* were collected using a bucket auger with a 7.1-cm- (2.8-in.-) diameter bucket. The bucket is open at the top and partially closed at the bottom with an open cutting edge for drilling and retaining soil (Figure 3.4).

It was desired that soil samples be derived from several depth increments and due to the dimensions of the bucket it was convenient to extract samples at depth increments of 0-18 cm (0-7 in.), 18-36 cm (7-14 in.), 36-53 cm (14-21 in.), and 53-71 cm (21-28 in.). Based on results from an exploratory study in which bank material from two depth increments were analyzed to detect changes in soil texture as a function of depth (Wilkerson, 1998), it was concluded that 18 cm (7 in.) depth increments would yield a reasonable indication of the vertical soil gradient.

Soil samples designated as SS*wx-31* are comprised of material collected from the vertical face of the bank as shown in Figure 3.3, and were removed using a hand trowel. Sediment from the bed of the stream, SS*wx-Bed*, was gathered with the assistance of a five-gallon plastic bucket after removing the top lid and bottom of the bucket. The bucket was placed over the area of the bed being sampled to isolate it from the flowing water and only shallow sections of the bed were chosen for sampling so that the bucket was not submerged. After placing the bucket on the bed, sediment from the bed was removed slowly by hand to minimize the loss of fines and other material. A soil sample was removed from the point bar in each transect using a hand trowel. Samples derived from the point bars were designated SS*wx-Bar*.

All soil samples derived in the field were placed in sealable plastic bags and transported for analysis to the sediment laboratory at Colorado State University, Engineering Research Center.

Figure 3.4 – Photograph of bucket auger used to collect soil samples.

3.3.2 Analysis of Soil Samples

Grain-size analysis is a process by which the proportion of each grain-size present in a given soil, grain-size distribution, is determined (USACE, 1970). The grain-size distribution of coarse-grained soils is determined directly by sieve analysis, while that of fine-grained soils is determined indirectly by hydrometer analysis. Guidance in performing sieve and hydrometer analysis was taken from the American Society for Testing and Materials (ASTM, 1993), USACE (1970), and Bowles (1992).

The principal value of the hydrometer analysis is to determine the silt and clay size distribution of soil particles, i.e., particle sizes smaller than the No. 200 (0.075 mm or 0.0030 in.) sieve. Data derived from the analysis are transformed into particle size and frequency values using equations derived from Stokes law. Stokes law gives the relationship among the fall velocity of a sphere in a fluid, the diameter of the sphere, the specific weight of the sphere and of the fluid, and the fluid viscosity. A complete description of Stokes law and hydrometer analysis can be found in reports on the measurement of soil properties (i.e., ASTM, 1993; USACE, 1970; and Bowles, 1992).

The specific gravity of the soils tested was assumed to be 2.65. This assumption seems reasonable given that the specific gravity of silica is 2.66 and for clay minerals ranges from 2.2 to 2.6 (Sowers, 1979). The sensitivity of Stokes law to different values of specific gravity was evaluated to assess the implications of using an assumed value. Using values of specific gravity ranging from 2.65 to 2.85 resulted in only small variations in the calculated particle size and frequency (less than 3% and 4%, respectively). Further, Sowers (1979) notes that a small change in specific gravity does not influence other soil properties and that an estimate of the actual specific gravity is adequate for many computations.

3.3.3 Statistical Analysis of Soil Grain-size Data

Soil samples were collected and soil grain-size analyses were performed to facilitate the evaluation of variations in bank material grain-size as a function of depth below the surface of the bank. Soil samples were derived from four depth increments at several points along the bank, as described in Section 3.3.1. The results of the grain-size analyses are presented in Chapter 5. The Wilcoxon matched-pairs signed-ranks test was used to analyze trends in the bank material grain-size and is described below.

The Wilcoxon matched-pairs signed-ranks test is a nonparametric hypothesis testing procedure for data from two related samples (Daniel, 1990) and is an alternative to the t-test for dependent (correlated) samples (Statsoft, 1995). Related samples can arise from "before and after" or "pre- and post-test" experiments in which measurements are taken on the same objects both before and after some intervening treatment or experimental manipulation. The nonparametric Wilcoxon matched-pairs signed-ranks test is chosen over the t-test for dependent samples because there is no evidence to indicate that paired differences between the soil samples are normally distributed.

The variable of interest in the analysis of two related samples is the difference between two measurements within pairs (Daniel, 1990). If the measurements within sample pairs are sufficiently disparate, it can be concluded that the two treatments have different effects or that one treatment is more effective than another or no treatment, as the case may be.

A sample of the calculations required to perform the Wilcoxon matched-pairs signed-ranks test is presented in Table 3.1 using the median grain-size of soil samples from Reach 1; sampling points 4, 5, and 6; and depth increments 1 and 2. After calculating the signed difference between the depth increment 1 and 2 samples, the magnitude of the differences are ranked in ascending order and then the sign of the difference is assigned to the rank. From the rank values T_+ and T_- are computed where (Daniel, 1990)

T_+ = the sum of the ranks with positive signs

T_- = the sum of the ranks with negative signs

T_+ or T_- is the test statistic depending on the alternative hypothesis.

Regarding the soil samples, the question of interest: "Is the surface soil finer than the subsurface soil along Harland Creek in the vicinity of the willow posts?" The hypotheses for evaluating the question are:

H_0: $M_D \geq 0$

H_a: $M_D < 0$

where M_D is the median value of the population of differences. Sufficiently small values of T_+ will cause rejection of H_0 and provide evidence for H_a that the surface soil is finer than the subsurface soil. If the computed value of T_+ is less than or equal to tabulated $T_{n:\alpha}$, where n is number of measurement pairs and α = 0.05 is the level of significance, then H_0, will be rejected. Details of the Wilcoxon matched-pairs signed-ranks test are presented in texts on nonparametric statistical procedures, i.e., Daniel (1990).

Table 3.1 – Calculations Required for Performing Wilcoxon Matched-Pairs Signed-Ranks Test

Reach No.	Soil Sampling Pt. No.	Transect No.	d_{50} [mm] Depth Increment 1	2	Difference	Rank
1	4	2	0.0459	0.0318	0.0142	8
		3	0.0415	0.0851	-0.0437	-10
		4	0.0271	0.0262	0.0009	2
	5	1	0.0788	0.0338	0.0451	11
		2	0.0376	0.0444	-0.0068	-5
		3	0.0572	0.0497	0.0075	6
		4	0.1466	0.0285	0.1181	12
		5	0.0179	0.0194	-0.0014	-3
	6	1	0.0375	0.0273	0.0102	7
		2	0.0298	0.0268	0.0031	4
		3	0.0746	0.0322	0.0424	9
		4	0.0321	0.0327	-0.0007	-1
		5	0.2006	0.0255	0.1751	13
$T_+ = 72$			$T_{n=13:\alpha=0.05} = 21$			

Conclusion: Since $T_+ \geq T_{n\alpha}$, fail to reject H_0 and conclude that there is no evidence to support H_a, that the d_{50} of the surface soil is smaller than the d_{50} of the subsurface material.

3.4 Vegetation Density

To quantitatively characterize the density of vegetation along the banks of Harland Creek, the horizontal point frame (Figure 3.5), was used. The horizontal point frame measures the frontal area of vegetation projected onto a plane perpendicular to the ground. In addition to developing the instrument, Flippin-Dudley (1997) compared it to existing methods for estimating vegetation density (i.e., the board method and the camera method) and demonstrated that the horizontal point frame technique was rapid and more objective than other methods for evaluating vegetation density.

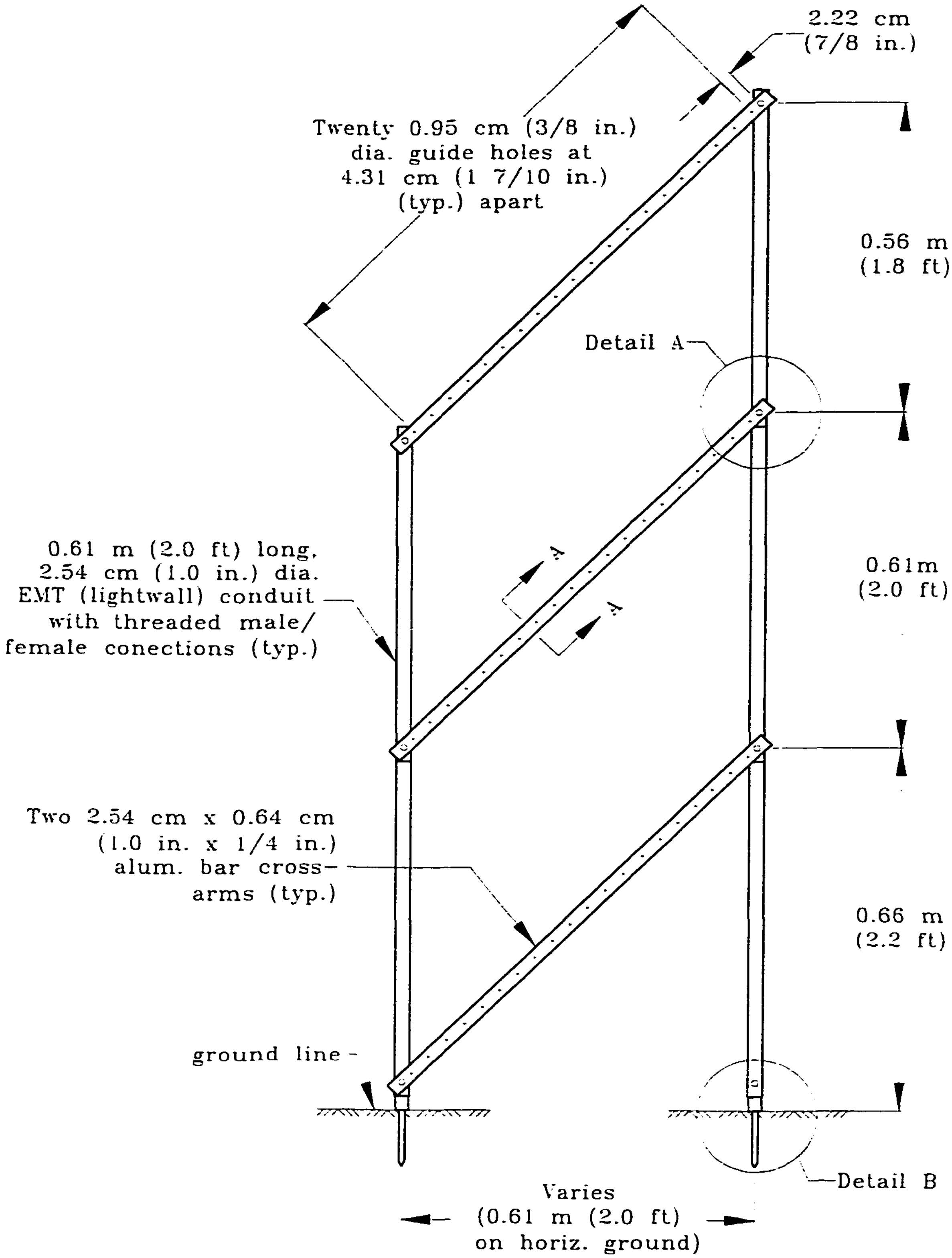

Figure 3.5 – Horizontal point frame.

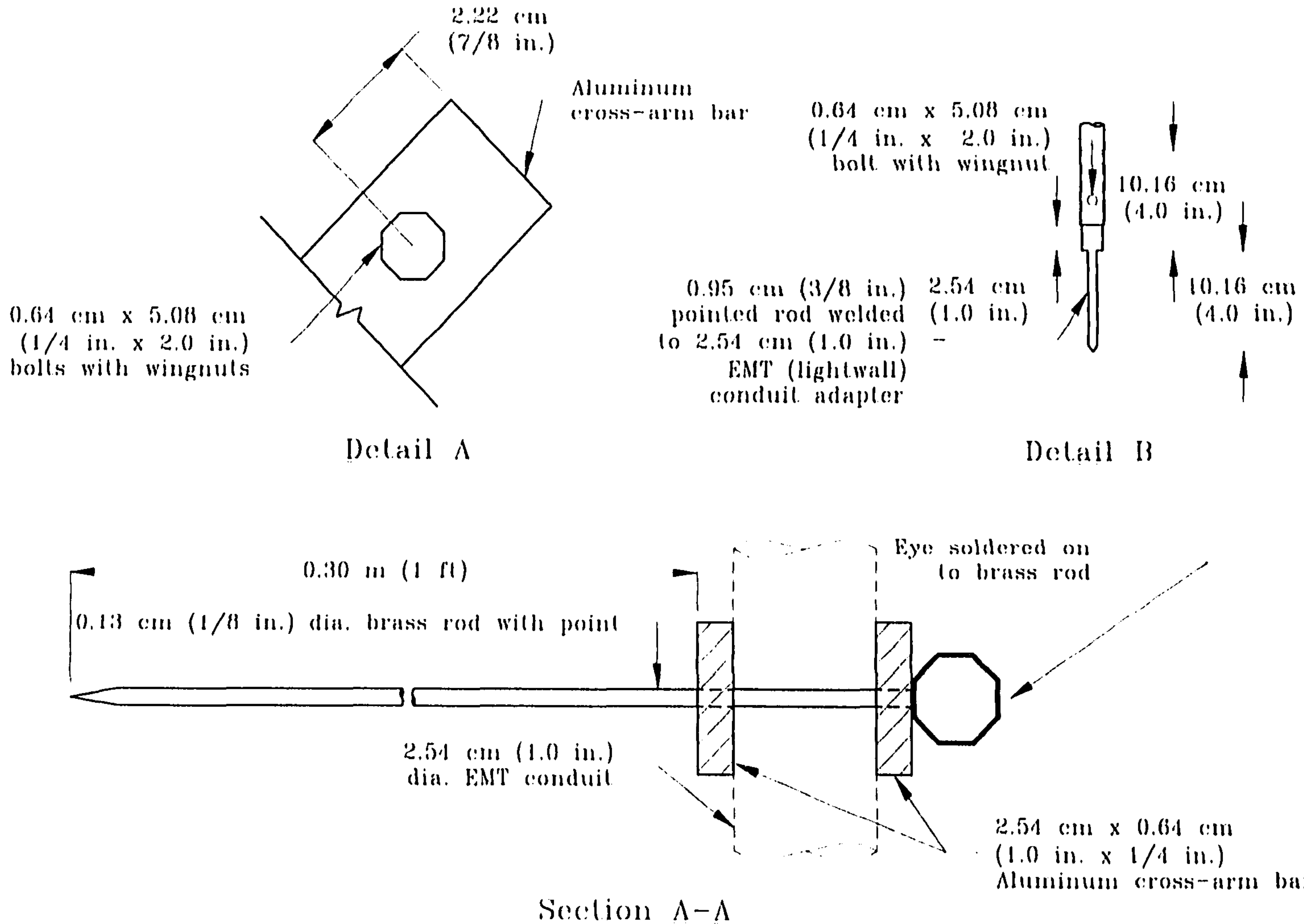

Figure 3.5 – (cont.)

The horizontal point frame is comprised of two vertical poles that are connected by several inclined bars (cross-arms). A slender pin of known length is inserted through equally spaced guide holes in the cross-arms while the operator counts the number of times that the tip of the pin intersects vegetation. A hit is recorded each time the pin encounters vegetation while being pushed through a guide hole.

A detailed description of the horizontal point frame and how it was used in this study follows. The principle reason for recording measurements of vegetation density was to establish a quantitative basis for comparing the vegetal characteristics of the three study reaches.

3.4.1 Horizontal Point Frame Dimensions

The horizontal point frame used (Figure 3.5) can sample vegetation density from the ground up to 1.8 m (6 ft) above the ground by changing the number of 0.6-m- (2-ft-) long poles and cross-arms joined together. The cross-arms are 1 m (3 ft) in length and are inclined to allow for sampling variability in the horizontal and vertical directions. The horizontal width of the point frame varies depending on the slope of the ground and the orientation of the frame but on level ground the width of the frame is 61 cm (2.0 ft). The number of hits was derived using a brass pin that extends 0.3 m (1 ft) beyond the point frame when fully inserted through a guide hole (Figure 3.5 and Figure 3.6).

There are 20 guide holes in each cross-arm that are equally spaced over a length of 82 cm (2.7 ft) and three cross arms were used. The holes in the cross-arms are numbered from 1 (at the top) to 60 (at the ground) to facilitate recording the number of hits observed for each guide hole.

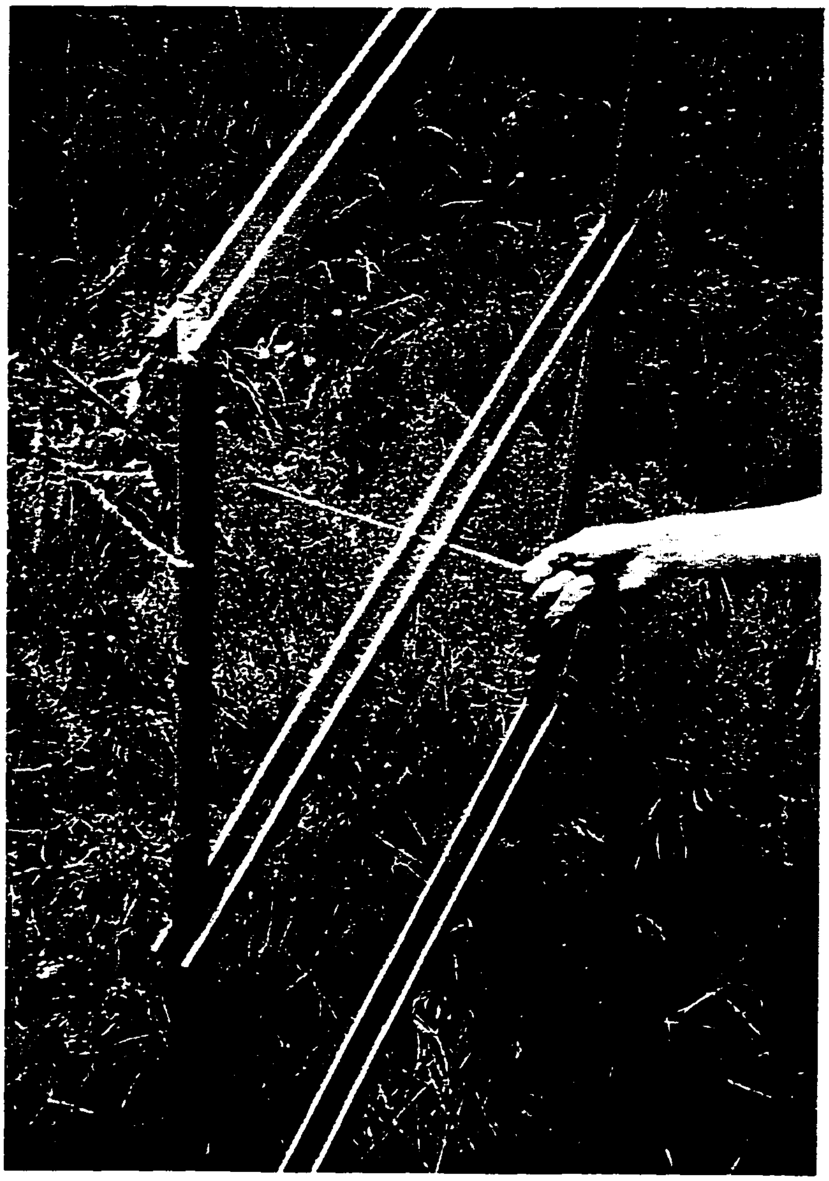

Figure 3.6 – Horizontal point frame in use.

3.4.2 Use of the Horizontal Point Frame

Vegetation density measurements were taken in each transect only on the outer (concave) bank. According to Flippin-Dudley (1997) about one hundred hits are required to reduce sampling error to about 10% of the mean. Sufficient measurements were made in each transect, therefore, to attain a minimum of 100 hits.

To achieve the desired number of hits, the horizontal point frame had to be setup in multiple locations. At least four locations were established in each transect and that was generally sufficient to attain 100 hits. Setting up the point frame consists of placing the frame stakes into the ground at the chosen location. To avoid bias, setup locations were selected randomly within each transect except that at least one setup was on the floodplain. For each setup, the frame was aligned so that it formed a plane normal to the direction of flow in the stream. In using the horizontal point frame, the number of hits and corresponding hole numbers were noted by one operator and recorded by a second operator.

3.4.3 Vegetation Density Indices

Three vegetation density indices (VDI's) have been established herein from data derived using the horizontal point frame. The first VDI is

$$Veg_d = \frac{No.\ of\ Hits}{No.\ of\ Points \cdot Pin\ Length} \tag{3.1}$$

where *No. of Hits* is the total number of hits observed for the setup; *No. of Points* was determined by counting the number of pin holes leading up to the pin hole where 100% of the vegetation was at or below; and *Pin Length* is the protruding length of the pin used to count hits, when fully inserted into a guide hole. Equation (3.1) was proposed by Flippin-Dudley (1997). By definition (3.1) is equivalent to

$$Veg_d = \frac{\sum A_i}{bhL} \tag{2.5}$$

when b is the width of the point frame, h is the height from the ground to the highest guide hole for which hits were recorded, and L is the protruding length of the fully inserted pin. The other VDI's that were calculated are

$$VDI(h_{50}) = Veg_d \cdot h_{50} \tag{3.2}$$

and

$$VDI(h_{mean}) = Veg_d \cdot h_{mean} \tag{3.3}$$

where h_{50} is the median height of the vegetation (or the height of the lowest guide hole for which 50% of the vegetation was at or below) and h_{mean} is the mean height of the vegetation. Mean height was calculated using

$$h_{mean} = \frac{\sum_{i=m}^{n} \left[(No.\, Hits)_i \cdot (Hgt.\, of\ Guide\ Hole)_i \right]}{\sum_{i=m}^{n} (No.\, Hits)_i} \tag{3.4}$$

where m corresponds to the number of the guide hole closest to the ground and n is the number of the guide hole highest above the ground for which a hit was recorded.

3.4.4 Seasonality

Vegetation density measurements were recorded during three periods: August 1997, January 1998, and March 1998. In each season the same procedures were used.

3.5 Dimensional Analysis of Flow Through Vegetation

For analyzing model studies and for correlating the results of experimental research, it is essential that researchers employ dimensionless parameters (Roberson and Crowe, 1985). The basic objective in dimensional analysis is to reduce the number of separate variables involved in a problem to a smaller number of independent dimensionless groups. In the process of combining variables to form dimensionless groups, the number of independent groups thus obtained is less than the number of original variables.

Dimensionless parameters can be determined by performing dimensional analysis on the variables involved in the process under consideration. Buckingham (1915) showed that the number of independent dimensionless groups of variables (dimensionless parameters) needed to correlate the variables in a given process is equal to $n - m$, where n is the number of variables involved and m is the number of basic dimensions included among the variables. Buckingham's Π theorem is used in this section to investigate the functional relationship between variables affecting open-channel flow with emergent cylindrical elements.

The first step in applying the Buckingham Π theorem is to identify those variables that are significant to the problem. The following variables are deemed most relevant for flow through vegetation:

F_D	drag force on vegetation [F]
ρ	fluid density [M/L^3]
μ	fluid viscosity [M/LT]
g	gravitational constant [L/T^2]

d	diameter of vegetation [L]
U_x	depth-averaged velocity [L/T]
U_0	cross-section averaged velocity [L/T]
h_i	submerged height of vegetation [L]
l_x	longitudinal spacing between vegetation [L]
l_y	lateral spacing between vegetation [L]
$d_{50.bed}$	median grain-size of bed material [L]
$d_{50.bank}$	median grain-size of bank material [L]
S_0	channel-bed slope
K	cotangent of channel side slope

The variable U_x is related to U_0 through Q_{calc}, that is, $Q_{calc} = f(U_x)$ and $U_0 = f(Q_{calc}, A)$. Since U_x and U_0 are not independent variables, only U_0 will be used from hereon in the development of dimensionless parameters.

Using d, U_0, and ρ as repeating variables for applying the Buckingham Π theorem yields the following functional relationship between the variables listed above:

$$\frac{F_D}{\rho U_0^2 d^2} = f\left(\frac{\rho U_0 d}{\mu}, \frac{U_0}{\sqrt{gd}}, \frac{h_i}{d}, \frac{l_x}{d}, \frac{l_y}{d}, \frac{d_{50,bed}}{d}, \frac{d_{50,bank}}{d}, S_0, K\right) \tag{3.5}$$

Recognizing that several of the terms in (3.5) are common dimensionless parameters, it can be rewritten as

$$C_d = f\left(Re, Fr, \frac{h_i}{d}, \frac{l_x}{d}, \frac{l_y}{d}, \frac{d_{50,bed}}{d}, \frac{d_{50,bank}}{d}, S_0, K\right) \tag{3.6}$$

where Re is the Reynolds number and Fr is the Froude number based on the diameter of the vegetation. The parameters in (3.6) will be used to provide guidance in the physical and analytical model studies described in Section 3.6 and Section 3.7, respectively.

3.6 Physical Model Flume Study

A study of the willow post systems constructed along Harland Creek was performed using a 12:1 physical-scale model (based on the diameter and spacing of the simulated willow posts). The objective of the study was to investigate the influence of willow post systems on near-bank flow processes. Willow post configurations different from that constructed along Harland Creek were also modeled. Descriptions of the model, the tests that were performed, and the data derived from the model are presented in the following sections.

3.6.1 Flume and Test Section Geometry

A 4.88-m- (16.0-ft-) long test section was constructed in a 1.52-m- (5.0-ft-) wide, rectangular Plexiglass flume (Figure 3.7). One-half of a trapezoid was formed in the test section of the flume. The bank in the flume had a width of 76.2 cm (2.5 ft) and 2H:1V side slopes. The bed of the flume was 76.2 cm (2.5 ft) wide. The bank was comprised of a uniform sand with a median grain size of 0.33 mm (0.013 in.). The bed was lined with a uniform gravel, d_{50} = 19 mm (0.75 in.), and was formed with a longitudinal slope of zero. Grain-size distribution curves for the bed and bank materials are plotted in Figure 3.8.

Based on the diameter of the wooden dowels used to simulate the willow posts, the physical-scale ratio of the model is 12:1. That is, the willow posts at Harland

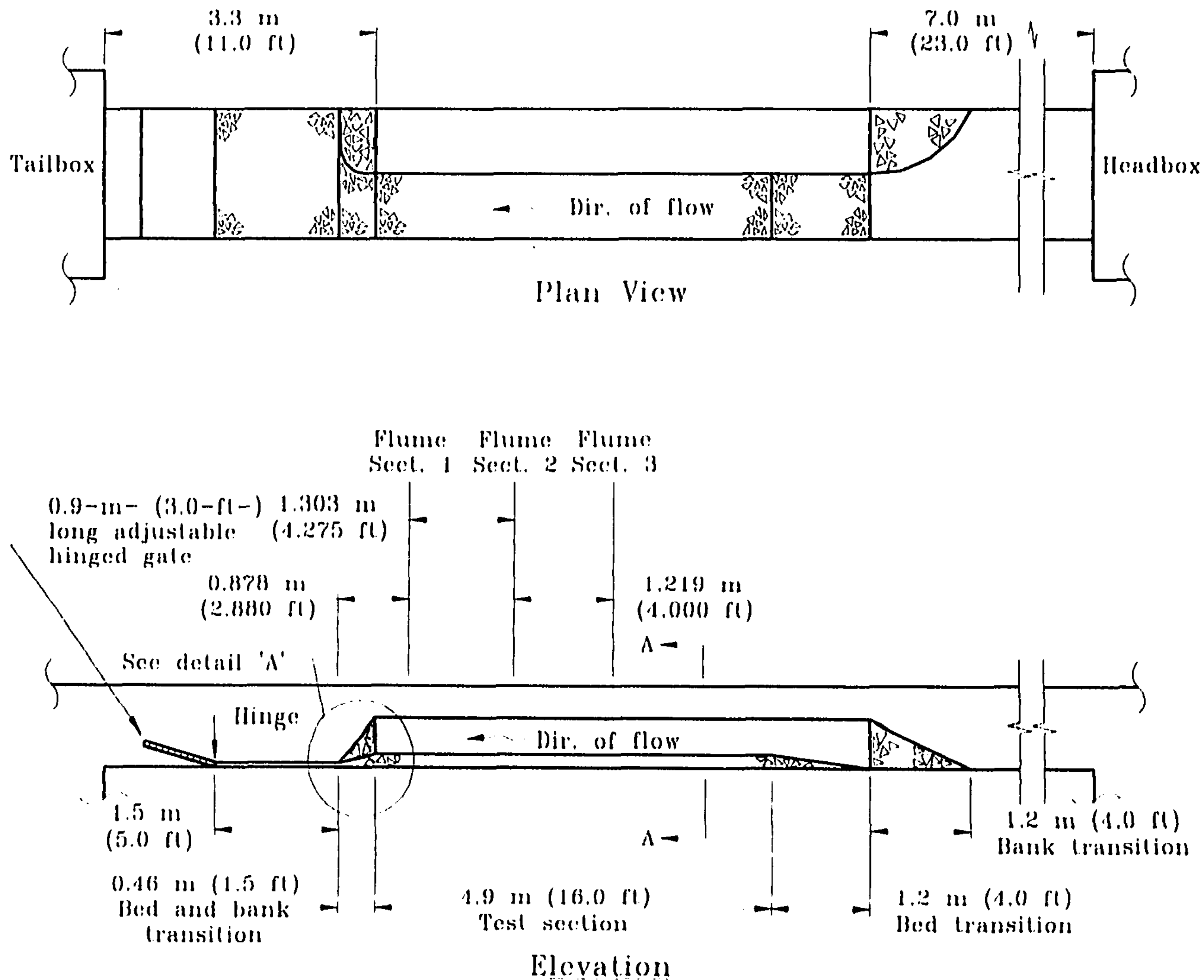

Figure 3.7 – Flume used for model study.

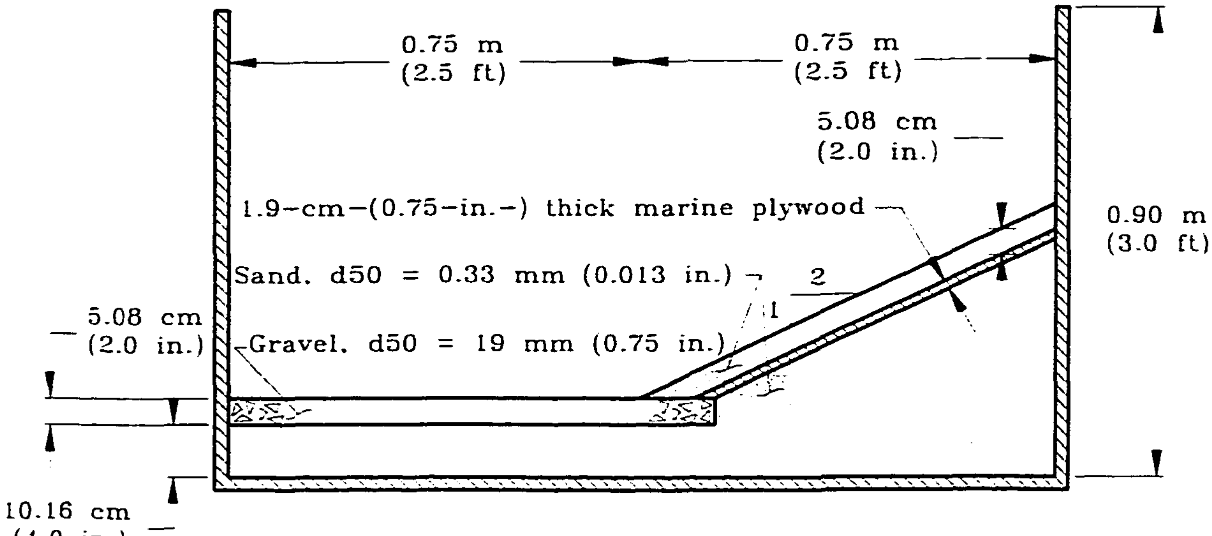

Section A-A

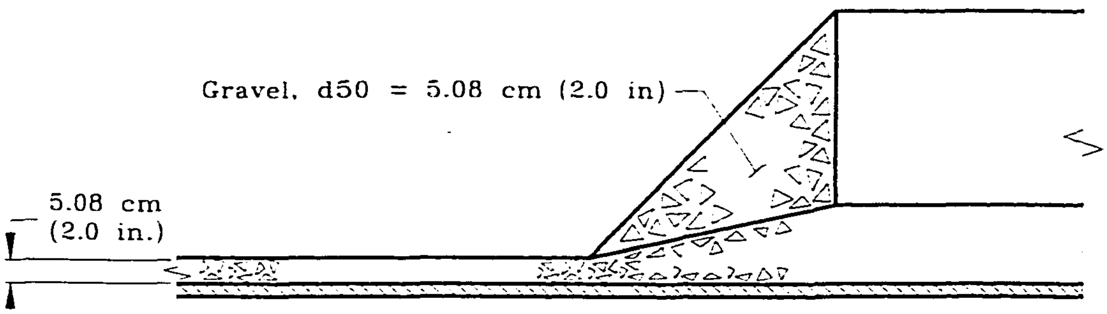

Detail 'A'

Figure 3.7 – (cont.)

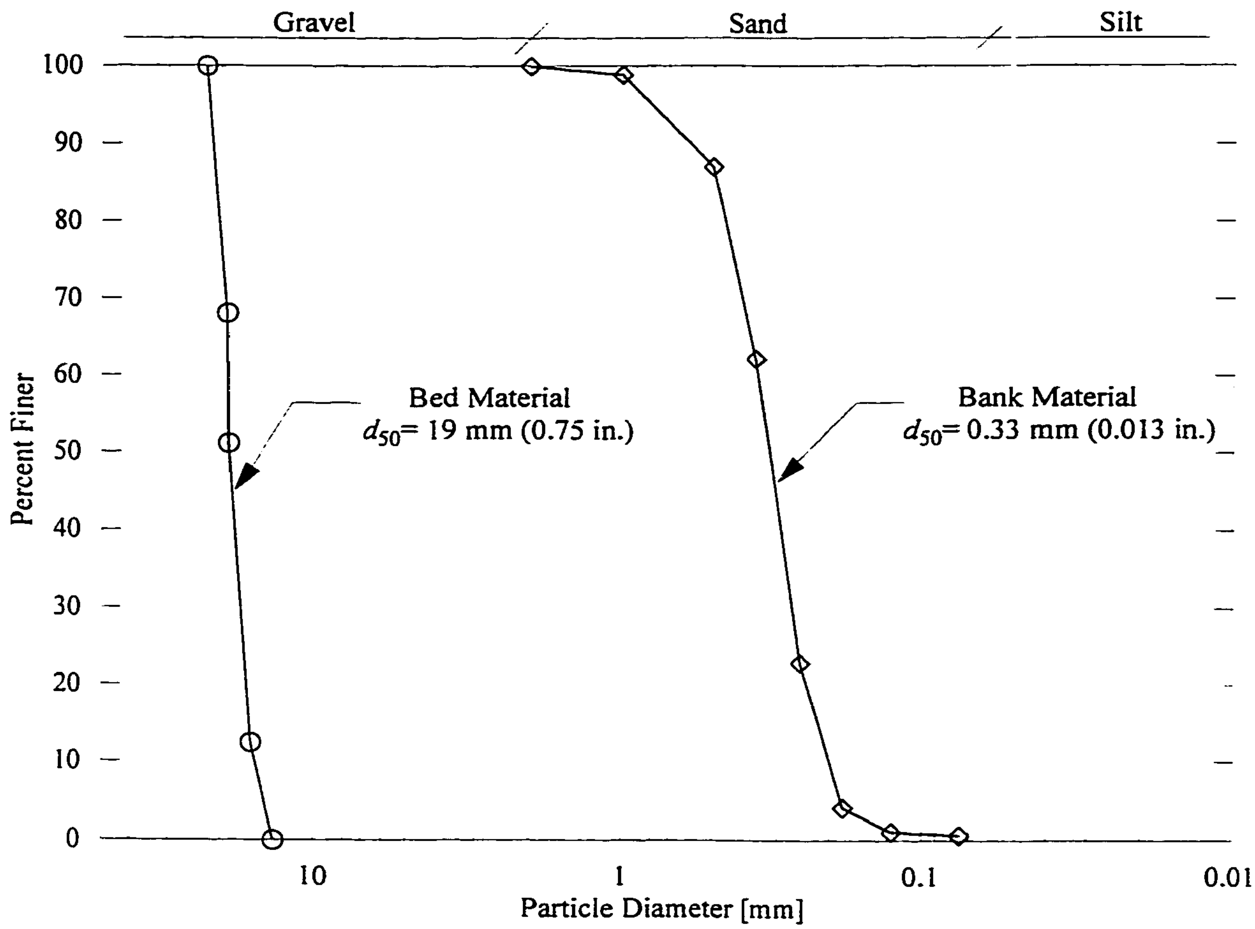

Figure 3.8 – Plot showing grain-size distribution of flume bed and bank material.

Creek were approximated to have a mean diameter of 7.6 cm (3.0 in.) and were simulated in the flume by wooden dowels with a diameter of 6.4 mm (0.25 in.). The dowels were anchored in 19-mm- (0.75-in.-) thick marine plywood with pre-drilled holes. The plywood was overlain by 5.1 cm (2.0 in.) of sand and the surface of the plywood was roughened to promote unity with the sand.

3.6.2 Flow Control

Flow through the flume was provided by re-circulating water through two variable capacity pumps, each with a discharge capacity of 70 l/s (2.5 cfs). The discharge rate from each conduit leading into the flume was set using a calibrated rating curve from which discharge was determined as a function of the amount of deflection observed in a mercury filled differential manometer. The flow depth in the flume was adjusted by raising or lowering a hinged gate located at the tail end of the flume (Figure 3.7).

3.6.3 Modeled Willow Post Configurations

Prior to running tests with simulated willow posts (dowels), base tests were performed in which water was run through the flume without any dowels along the bank (Configuration 0). Following the base tests, four dowel arrangements were constructed on the bank along the 4.88-m- (16.0-ft-) long test section of the flume. Figure 3.9 shows each dowel configuration diagrammatically.

The first dowel configuration (Configuration 1a) consisted of three rows of dowels placed in a 7.6-cm x 7.6-cm (3.0-in. x 3.0-in.) rectangular grid; the protruding height of each dowel was approximately 24.1 cm (9.5 in.). The second dowel configuration (Configuration 1b) also consists of three rows of dowels in a rectangular

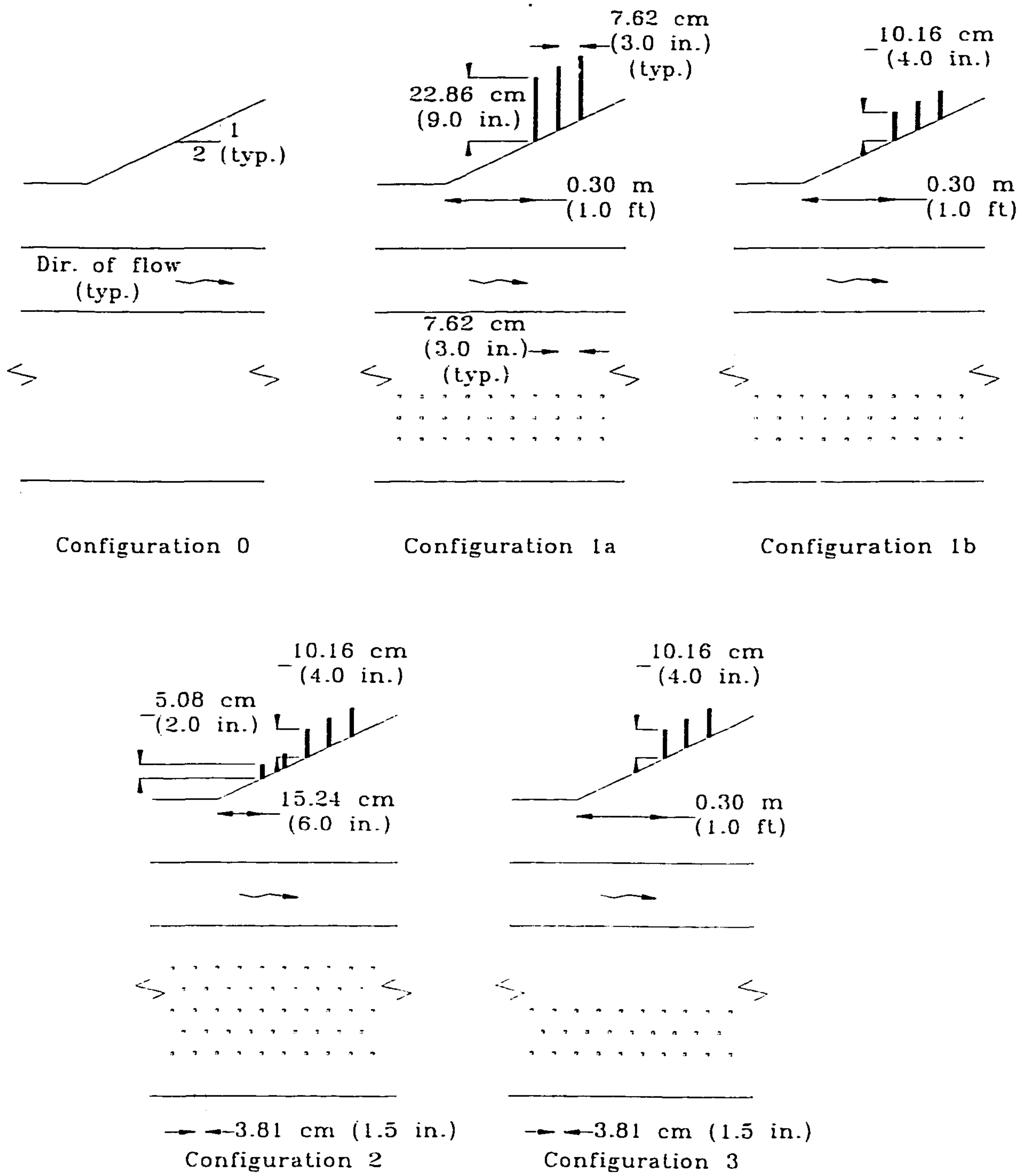

Figure 3.9 – Dowel configurations examined in flume.

grid. Configuration 1b is the same as Configuration 1a except that the protruding height of the dowels is 10.2 cm (4.0 in.). It is noted that Configuration 1b more closely resembles the willow post systems at Harland Creek than any of the other configurations.

The third arrangement (Configuration 2) had five rows of dowels (Figure 3.7). The two rows of dowels closest to the toe of the bank were 5.1 cm (2.0 in.) in height while the three remaining rows of dowels were 10.2 cm (4.0 in.) in height; alternate rows of dowels were staggered. The fourth arrangement (Configuration 3) contained three rows of 10.2-cm- (4.0-in.-) high dowels with the middle row staggered.

3.6.4 Velocity Measurements

Point velocity measurements were made in the flume study with a commercially available three-dimensional acoustic Doppler velocimeter (ADV). The primary advantages of the ADV probe are that it is simple to use and that it takes velocity measurements in a remote sampling volume.

The sampling rate of the ADV was 25 Hz and data were recorded for at least 30 seconds at all points sampled. The average value of the recorded velocities is reported herein as the measured point velocity. The ADV probe was used to gather point velocity data in (1) a vertical plane oriented normal to the direction of flow and (2) in a horizontal plane just below the water surface. Detailed descriptions of the locations at which velocity measurements were recorded follow.

3.6.4.1 Vertical Plane Velocity Measurements

Point velocity measurements were taken along vertical axes in a plane that was oriented normal to the direction of flow (Figure 3.10). Such measurements were recorded

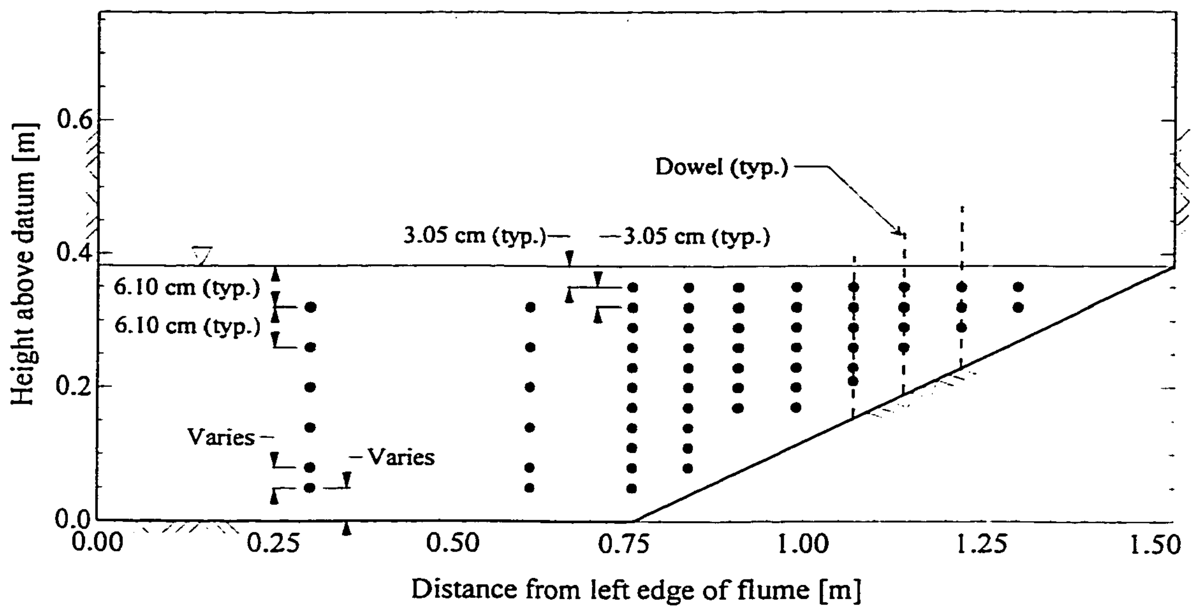

Figure 3.10 – Cross-section (vertical plane) point velocity measurement locations.

for every dowel configuration, flow depth, and discharge rate established in the flume. For each test, point velocity measurements were taken at Flume Sect. 2 (Figure 3.7). For one test, point velocity measurements were also recorded at Flume Sect. 1. Measurements recorded at Flume Sect. 1 were compared with measurements made at Flume Sect. 2 under similar hydraulic conditions.

Atop the bank, the vertical axes along which velocities were measured were spaced 7.62 cm (0.25 ft) apart; the vertical distance between points along each axis was generally 3.05 cm (0.10 ft). Atop the flume bed, vertical lines were established at distances of 0.305 m (1.0 ft) and 0.610 m (2.0 ft) from the left end of the flume bed; measurements were typically taken at vertical increments of 6.10 cm (0.20 ft). Figure 3.10 shows typical point locations at which velocity measurements were recorded.

3.6.4.2 Horizontal Plane Velocity Measurements

For three of the flume tests, velocity measurements were made atop the bank in a horizontal plane located 6.10 cm (0.20 ft) below the water surface. The nominal flow depth in each of the tests was 38.1 cm (1.25 ft). The axes along which velocity measurements were recorded form a grid with a transverse node spacing of 3.05 cm (0.10 ft) and a longitudinal node spacing of 6.10 cm (0.20 ft). The total width of the grid was 36.6 cm (1.2 ft) and the total length was 24.4 cm (0.8 ft). The upstream edge of the plane was located at Flume Sect. 2. Typical points at which velocity measurements were recorded in the horizontal plane are illustrated in Figure 3.11.

The decision to locate the horizontal plane 6.10 cm (20 ft) below the water surface was dictated by a limitation of the ADV probe. The objective was to measure velocities

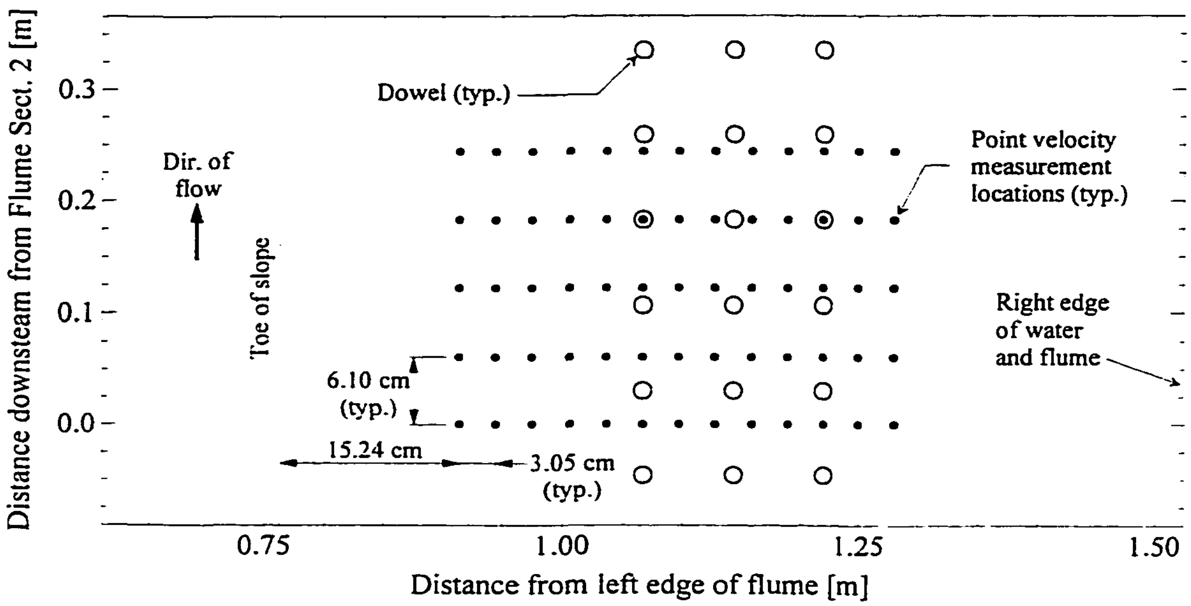

Figure 3.11 – Horizontal plane point velocity measurements.

as near as possible to the edge of water but the ADV probe could not take readings any closer to the water surface than 6.10 cm (0.20 ft).

3.6.5 Targeted Flow Conditions

Three flow conditions, each with a particular discharge and depth, were targeted for use in the flume. The aim in selecting flow conditions was to simulate a range of mean flow velocities likely to occur in Harland Creek; consequently, prototype velocities of 0.30 m/s (1.0 fps), 0.61 m/s (2.0 fps), and 0.91 m/s (3.0 fps) were targeted for simulation in the flume.

Using Froude number criterion and based on the flume being a 12:1 physical-scale model of Harland Creek (Section 3.6.1), the targeted prototype velocities translate to model velocities of 0.09 m/s (0.29 fps), 0.18 m/s (0.58 fps), and 0.26 m/s (0.87 fps). Targeted discharges of 22.9 l/s (0.81 cfs), 61.4 l/s (2.17 cfs), and 115.0 l/s (4.06 cfs) were paired with flow depths of 22.9 cm (0.75 ft), 30.5 cm (1.00 ft), and 38.1 cm (1.25 ft), respectively, to achieve the desired model velocities.

3.6.6 Tested Flow Conditions

Flow rates in the flume were calculated using depth-averaged velocities and then compared to the targeted flow rates described in Section 3.6.5. The procedures used to calculate depth-averaged velocities and flow rates in the flume are described in Appendix B.

A comparison of the target and calculated discharges was made to confirm that the targeted discharges had been attained in the flume. The targeted and calculated flow rates are presented in Table 3.2. It is noted that significant differences in the values were found in several cases, up to a maximum of 23.0%, and insignificant differences were found in other cases. It is concluded from this analysis that the flow rate measuring device in the flume did not perform reliably during testing and that the targeted discharges were not attained for several of the tests. Because of these findings, the calculated discharges will be used herein when reporting flow rates for the flume tests.

Table 3.2 – Targeted Versus Calculated Flume Discharges

Config. No.	Nominal Flow Depth cm (ft)	Targeted Discharge l/s (cfs)	Calculated Discharge** l/s (cfs)	%Difference
0	22.9 (0.75)	22.94 (0.810)	22.96 (0.811)	-0.1%
	30.5 (1.00)	61.45 (2.170)	57.57 (2.033)	6.3%
	38.1 (1.25)	114.97 (4.060)	112.13 (3.960)	2.5%
0*	22.9 (0.75)	22.94 (0.810)	23.22 (0.820)	-1.2%
1a	22.9 (0.75)	22.94 (0.810)	20.30 (0.717)	11.5%
	30.5 (1.00)	61.45 (2.170)	56.24 (1.986)	8.5%
	38.1 (1.25)	114.97 (4.060)	112.96 (3.989)	1.8%
1b	38.1 (1.25)	114.97 (4.060)	88.55 (3.127)	23.0%
2	38.1 (1.25)	114.97 (4.060)	99.93 (3.529)	13.1%
3	38.1 (1.25)	114.97 (4.060)	89.85 (3.173)	21.9%

*Velocity measurements for this test were made at Flume Sect. 1 shown in Figure 3.5.

**The calculated discharges shown here were taken from Table 4.13 through Table 4.22.

3.6.7 Calculation of Roughness Coefficients

During each test conducted in the flume, water surface elevations were measured at three locations along the flume test section (Figure 3.7): Flume Sects. 1, 2, and 3. The water surface elevations were measured using a point gage calibrated to indicate a value of zero when lowered to the flume bed.

The measured water surface elevations, the calculated discharge values, and the channel geometry were used to calculate a Manning's roughness coefficient (*n*-value) for each test. The *n*-value for each test was calculated by performing standard step backwater calculations (Henderson, 1966). In performing the backwater calculations, different *n*-values were used along with estimated water surface elevations, y_{est}. The *n*-value and water surface elevations were computed using an iterative procedure that minimized the combined sum of the squared differences between (1) the measured water surface elevations, y_{act}, and y_{est}; and (2) the total energy H'_{i+1} and H''_{i+1} where

$$H'_{i+1} = (y_{est})_{i+1} + \frac{V_{i+1}^2}{2g} \tag{3.7}$$

and

$$\begin{aligned} H''_{i+1} &= H''_i + h_f \\ &= H''_i + S_{f,avg}\Delta x \\ &= H''_i + \frac{1}{2}\left(S_{f,i} + S_{f,i+1}\right)\Delta x \end{aligned} \tag{3.8}$$

where V_{i+1} is the cross-section averaged velocity based on the flow depth measured at Flume Sect. *i*, and *g* is the gravitational constant. Also, *i* varies from 1 to *m*-1 where *m* is the total number of cross-sections at which water surface elevations were measured, $S_{f,i}$ is the friction slope at the *i*th cross-section (calculated using Manning's equation), and Δx is the distance between the *i*th section and the adjacent upstream section. The total energy at Flume Sect. 1, H'_1 and H''_1, is given by

$$H'_1 = (y_{est})_1 + \frac{V_1^2}{2g} \tag{3.9}$$

and

$$H_1'' = H_1' \tag{3.10}$$

The results of the detailed calculations that were performed in calculating *n*-values are presented in Appendix B.

3.7 Analytical Model of Flow Through Willow Posts

Two analytical models for predicting depth-averaged velocity distributions in trapezoidal channels are introduced in this section. The first model can be used to estimate the velocity distribution in straight trapezoidal channels. The second model can be used to compute velocity profiles in trapezoidal channels with emergent cylindrical elements. Petryk's model (Petryk, 1969; Li and Shen, 1973) for predicting velocities in rectangular channels with emergent cylindrical elements was described in Section 2.4. A modification to Petryk's model is introduced in this section that allows the model to be used for estimating velocity distributions in trapezoidal channels.

3.7.1 Free Stream Velocity Distribution in Trapezoidal Channel

In introducing Petryk's model in Section 2.4, the following equation was introduced for predicting the depth-averaged velocity at any point (x,z) in the channel:

$$U_x(x,z) = U_\infty(x,z) + u_{total}(x,z) \tag{2.7}$$

where $U_\infty(x,z)$ is the reference free stream velocity at the point of interest in the channel, and $u_{total}(x,z)$ is the total velocity defect at the point of interest. A rectangular channel was being discussed in Section 2.4 thus the reference free stream velocity could be assumed constant across the width of the channel, i.e., $U_\infty(x,z) = U_\infty(x)$. A value for $U_\infty(x)$ was derived from the continuity equation and presented in (2.14). For a trapezoidal channel $U_\infty(x,z)$ cannot be assumed constant across the width of the channel. In the following paragraphs, an expression for $U_\infty(x,z)$ is derived for flow in trapezoidal channels.

3.7.1.1 Continuity Equation for a Trapezoidal Channel

The continuity equation for a trapezoidal channel is

$$\begin{aligned} Q &= \int_W D(z) U_x(x,z)\,dz \\ &= \int_W D(z) U_\infty(x,z)\,dz + \sum_{i=1}^{m} \int_W D(z) u_{n,i}(\Delta x, \Delta z)\,dz \end{aligned} \tag{3.11}$$

where $D(z)$ is the flow depth at any point across the width of the channel. Now it is assumed that

$$U_\infty(x,z) = k(\Delta x)\, U_x(z) \tag{3.12}$$

where $k(\Delta x)$ is a coefficient that varies with position along the length of the channel and $U_x(z)$ is the depth-averaged velocity at any point across the width of a trapezoidal channel when no wakes are present in the flow field (Figure 3.12). Substituting equation (3.12) into the continuity equation yields

$$\begin{aligned} Q &= k(\Delta x) \int_W D(z) U_x(z) dz + \sum_{i=1}^{m} \int_W D(z) u_{n,i}(\Delta x, \Delta z) dz \\ &= k(\Delta x) Q + \sum_{i=1}^{m} \int_W D(z) u_{n,i}(\Delta x, \Delta z) dz \end{aligned} \tag{3.13}$$

Solving (3.13) for $k(\Delta x)$ yields

$$k(\Delta x) = 1 - \frac{1}{Q} \sum_{i=1}^{m} \int_W D(z) u_{n,i}(\Delta x, \Delta z) dz \tag{3.14}$$

Now (3.12) becomes

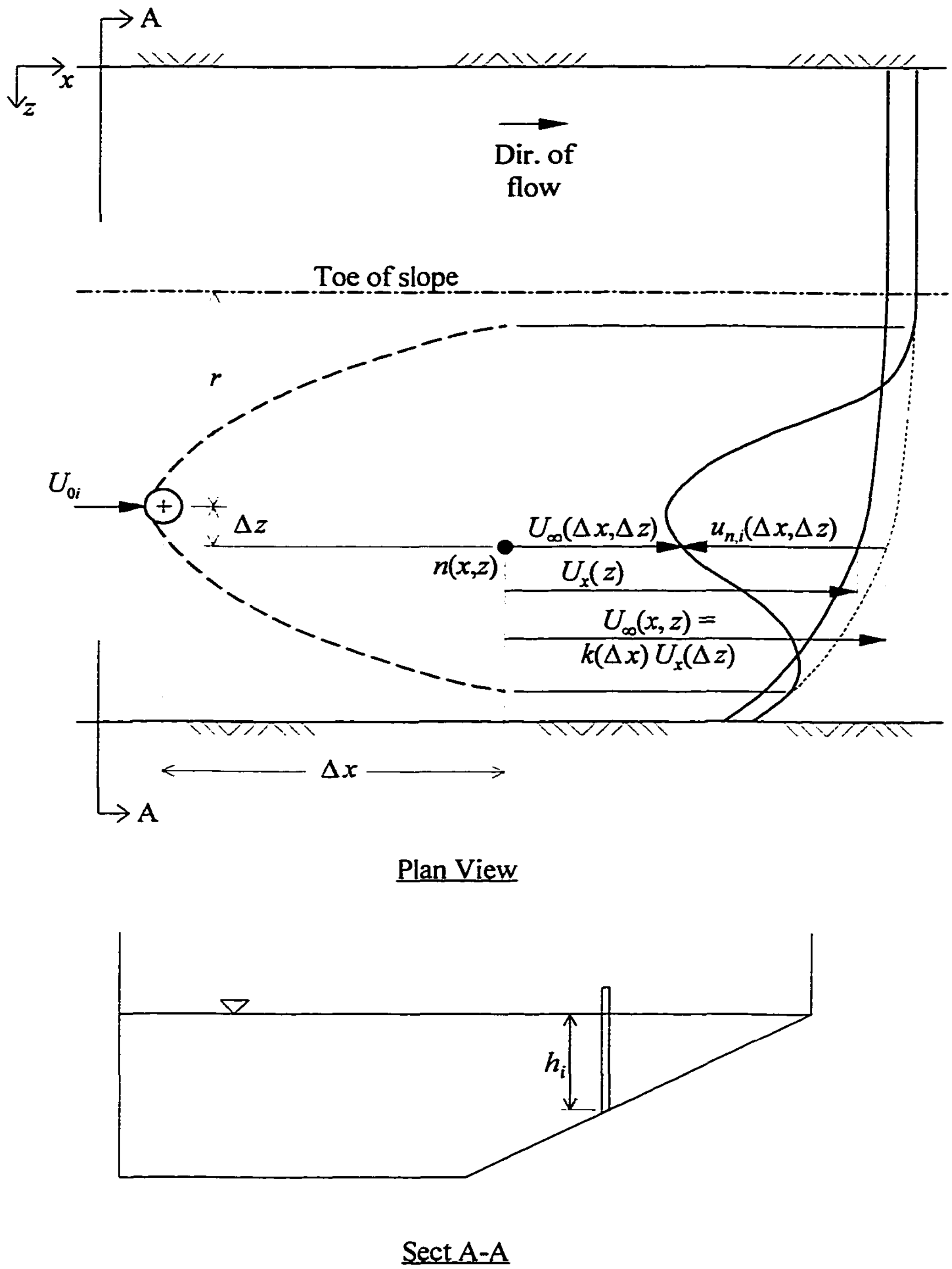

Figure 3.12 – Definition sketch for terms used to derive continuity equation for trapezoidal channel.

$$U_\infty(x,z) = U_x(z) - \frac{U_x(z)}{Q}\sum_{i=1}^{m}\int_W D(z)\,u_{n,i}(\Delta x,\Delta z)\,dz \tag{3.15}$$

Replacing $D(z)$ in (3.15) with the submerged cylinder height, h_i (i.e., the length of the ith cylinder that is immersed in water (Figure 3.12) results in

$$U_\infty(x,z) = U_x(z) - \frac{U_x(z)}{Q}\sum_{i=1}^{m} h_i \int_W u_{n,i}(\Delta x,\Delta z)\,dz \tag{3.16}$$

A relation for predicting $U_x(z)$ must be known to solve (3.16). An empirical relationship for predicting values of $U_x(z)$ is developed in the following section.

3.7.1.2 Depth-Averaged Velocity Distributions in Trapezoidal Channel (Based on Model Study Data)

Data from Maynord (1992) was used to examine depth-averaged velocity distributions in trapezoidal channels (Appendix C). An equation of the form

$$\frac{U_x(r)}{U_0} = \beta_0 + \beta_1 \exp(r/Y) \tag{3.17}$$

was found to suitably fit the data reported by Maynord (U_0 is the cross-section averaged velocity; β_0 and β_1 are coefficients; r is the perpendicular distance from the toe of slope to the vertical line for which the depth-averaged velocity was calculated (Figure 3.12), r is positive atop the bank and negative atop the channel bed; and Y is the channel flow depth atop the bed). Parameters were estimated for (3.17) using the method of least squares and Maynord's data.

Having established a general form for an equation describing the velocity distribution across the width of a trapezoidal channel, a specific equation was sought for the flume study performed for this research. A plot of $U_x(r)/U_0$ versus r/Y for the flume data is presented in Figure 3.13. The equation derived from the data is

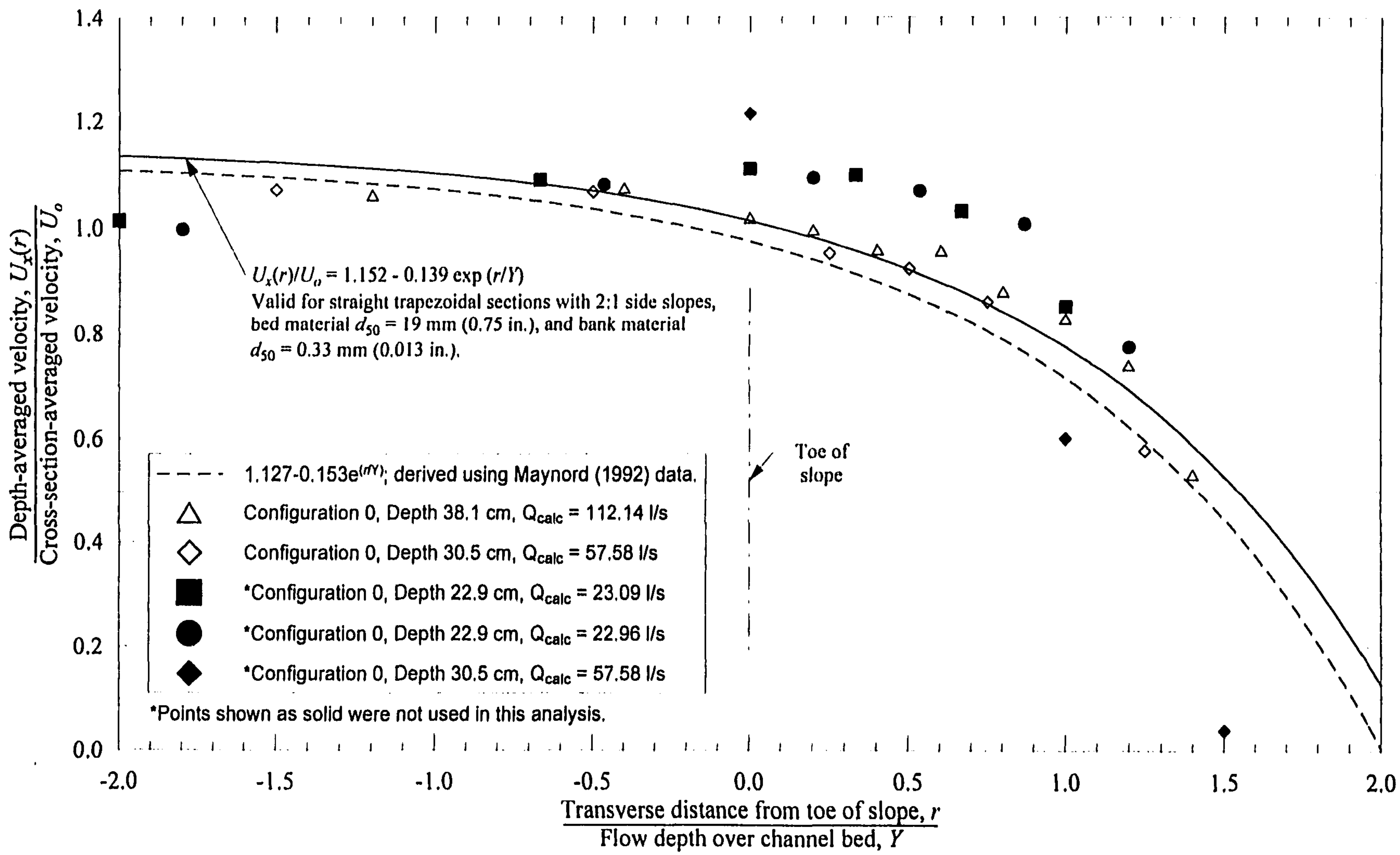

Figure 3.13 – Depth-averaged velocity distribution in trapezoidal channel based on data from flume study.

$$\frac{U_x(r)}{U_0} = 1.152 + 0.139\exp(r/Y) \tag{3.18}$$

Some of the calculated depth-averaged velocities from the flume study data were not deemed to be representative of depth-averaged velocities in a trapezoidal channel, particularly those for tests in which the nominal flow depth was 22.9 cm (0.75 ft), and thus were not used in deriving (3.18). Points that were not used are shown in Figure 3.13 as solid points.

In order to use (3.18) in the models presented herein for predicting flow through vegetation, the variable r must be written as a function of z, i.e.,

$$\frac{U_x(z)}{U_0} = 1.152 + 0.139\exp(r(z)/Y) \tag{3.19}$$

Both $r(z)$ and r are lateral distances from the toe of slope to the point of interest. Since the equations for predicting flow velocities through vegetation are a function of z, the use of $r(z)$ instead of r facilitates solving them. In general $r(z) = \pm|z - z_{toe}|$, where z_{toe} is the z-coordinate of the toe of slope; $r(z)$ must be positive atop the bank and negative over the channel bed.

3.7.2 Modification to Petryk's Model

In Section 2.4 an algorithm was presented for using Petryk's model to predict velocity distributions in rectangular channels with emergent cylindrical elements. The development of (3.19) provides a means for modifying Petryk's model for use in trapezoidal channels. The modifications applied to Petryk's model are described below.

The following equation was given in Section 2.4 for predicting the velocity distribution in the wake of a single cylinder in a rectangular channel:

$$U_x(x,z) = U_\infty(x,z) + u_{n,1}(\Delta x, \Delta z) \tag{2.12}$$

Equation (2.12) is applicable to trapezoidal channels as well but should be used with (3.16) for estimating $U_\infty(x,z)$, the free stream. Equation (3.16) requires an equation for predicting $U_x(z)$ such as (3.19), which was derived for the physical model used in this study.

In Petryk's method the proposed equation for predicting velocity at a point (x_n, z_n) in a multi-cylinder arrangement was:

$$\begin{aligned} U_{0n} &= U_x(x_n, z_n) \\ &= U_\infty(x_n) + \sum_{i=1}^{m} u_{n,i}(\Delta x, \Delta z) \end{aligned} \tag{2.20}$$

For trapezoidal channels, the term $U_\infty(x_n)$ in (2.20) must be replaced with $U_\infty(x_n, z_n)$ as defined in (3.16). Rewriting (2.20) with $U_\infty(x_n, z_n)$ gives

$$\begin{aligned} U_{0n} &= U_x(x_n, z_n) \\ &= U_\infty(x_n, z_n) + \sum_{i=1}^{m} u_{n,i}(\Delta x, \Delta z) \end{aligned} \tag{3.20}$$

In order to evaluate $U_\infty(x_n, z_n)$ an equation similar to (3.19) must be derived for the particular channel being evaluated. Equations (2.8), (2.9), (2.10), and (2.11) were given for evaluating $\sum_{i=1}^{m} u_{n,i}(\Delta x, \Delta z)$ in a rectangular channel; the same relationships should also be used for a trapezoidal channel.

3.7.3 Proposed Model

Using experimental data from the flume study described in Section 3.5, Petryk's model (Section 2.4) was re-evaluated and a new model was developed for predicting velocity distributions amid multi-cylinder arrangements in trapezoidal channels. The new model is similar to Petryk's model but has different coefficients and exponents. Another distinction between Petryk's model and the proposed model is that the former has been modified herein for use in evaluating flow through willow posts in trapezoidal channels whereas the latter was developed specifically for that purpose.

Implementation of the proposed model is the same as for the modified version of Petryk's model except that to solve (2.8) for $u_{n,i}(\Delta x, \Delta z)$, instead of (2.9), (2.10) and (2.11) use the following equations for $(u_{n,i})_{\max}$ and $b_{1/2}$:

$$\frac{2b_{1/2}}{C_d d} = 3.75\left(\frac{\Delta x}{C_d d}\right)^{0.65} \tag{3.21}$$

$$\frac{(u_{n,i})_{\max}}{U_{0i}} = \frac{u_{n,i}(\Delta x, 0)}{U_{0i}} = -2.80\left(\frac{\Delta x}{C_d d}\right)^{-1.1} \tag{3.22}$$

To predict the velocity distribution in the wake of a single cylinder in a trapezoidal channel, $U_x(x,z)$, use (2.12) with (3.16) and (2.8). Solving (3.16) requires an appropriate equation for predicting $U_x(z)$ as discussed in Section 3.7.1.2. To solve (2.8) use (3.21) and (3.22).

For a multi-cylinder distribution, use (3.20) to solve for the depth-averaged velocity, U_{0n}, at any point (x_n, z_n) in the channel. To solve for $U_\infty(x_n, z_n)$ use (3.16) and to solve for $\sum_{i=1}^{m} u_{n,i}(\Delta x, \Delta z)$ use (2.8), (3.21), and (3.22).

3.7.4 Comparison between Petryk's Model and the Proposed Model

The proposed equations for describing wakes, (3.21) and (3.22), have much larger coefficients than the equations presented by Petryk, (2.10) and (2.11). In particular, the coefficient for (3.21) is eight times larger than the coefficient for (2.10) and the coefficient for (3.22) is three times greater than the coefficient for (2.9) and (2.11). Explanations for the observed differences are considered below.

Measurements taken by Petryk (1969) for deriving relations to describe wakes in open-channels were quite limited. All measurements were taken in a 1.2-m- (4-ft-) wide flume with a 4.45-cm- (1.75-in.-) diameter cylinder placed in the center. Flow conditions were held constant throughout. Depth-averaged velocities were computed at points spanning the channel width, at sections 9.5, 18.5, and 27.5 diameters downstream of the cylinder. Data were taken, consequently, to describe the shape of the wake at the three sections.

The spread and decay rate of the wake investigated by Petryk (1969) was compared to data derived by Eskinazi (1959) and found to be in approximate agreement. The relations chosen by Petryk for describing wakes, i.e., (2.9), (2.10), and (2.11), were based on data derived at three points and the consistency of those measurements with data reported by Eskinazi.

The data points derived by Petryk along with plots of (2.10) and (2.9) are presented in Figure 3.14 and Figure 3.15, respectively. A noted difference between the work performed by Petryk (1969) and Eskinazi (1959) is that Petryk's measurements were taken in open-channel flow and Eskinazi's measurements were taken in a wind

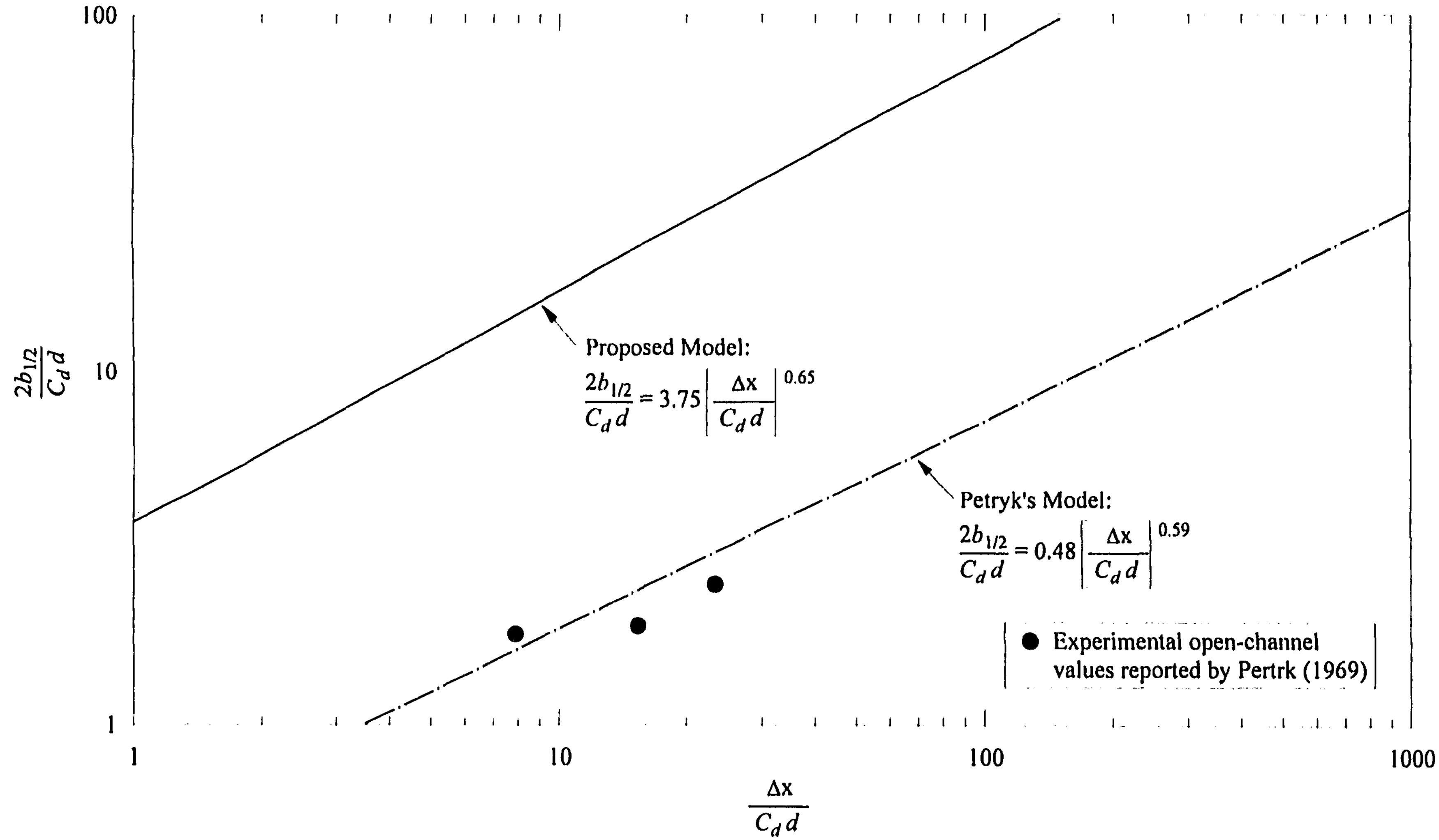

Figure 3.14 – Wake width, $2b_{1/2}$, versus longitudinal distance from wake producing cylinder, Δx. Drag coefficient, $C_d = 1.2$ and cylinder diameter, $d = 4.445$ cm (1.75 in.).

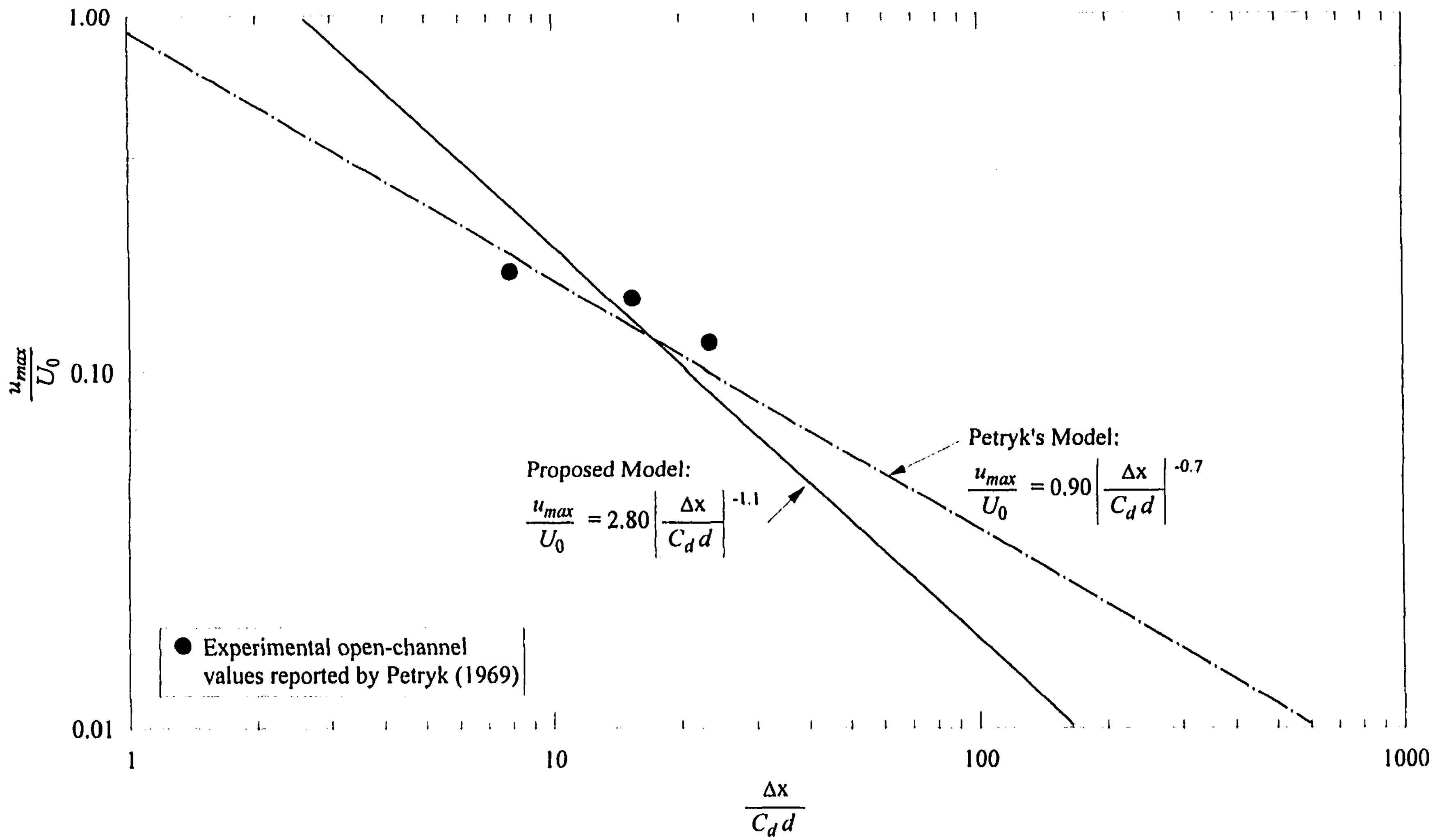

Figure 3.15 – Velocity defect at center of wake, u_{max}, versus longitudinal distance from wake producing cylinder, Δx. Drag coefficient, $C_d = 1.2$ and cylinder diameter, $d = 4.445$ cm (1.75 in.).

tunnel. It is also noted that no adjustments were made to account for differences in the viscous properties of the fluids.

The equation used in the proposed model for predicting wake width, (3.21), is plotted in Figure 3.14. The $\Delta x/C_d d$ values that were reported by Petryk (1969) are 7.9, 15.4, and 22.9. The respective values of Δx are 42.23 cm (16.63 in.), 82.23 cm (32.38 in.), and 122.24 cm (48.13 in.). Also, $C_d = 1.2$; and $d = 4.445$ cm (1.75 in.). Using (3.21), the predicted values of $2b_{1/2}$ are 0.768 m (2.52 ft), 1.19 m (3.89 ft), and 1.53 m (5.03 ft). In contrast, the half-width of the flume used by Petryk was only 0.610 m (2.00 ft). It is implied by (3.21) that the wake observed by Petryk was constricted at the locations where he took measurements.

The relation used in the proposed model for describing wake decay rates, (3.22), is plotted in Figure 3.15. The plotted line for Petryk's model is flatter than the proposed line but both plots are consistent with the measurements taken by Petryk. Again it is proposed that the results obtained by Petryk were affected by constriction of the wake evaluated in his study.

It was noted earlier that Eskinazi's work was performed in a wind tunnel and that Petryk compared his results to Eskinazi's without explicitly accounting for differences in the viscous properties of air and water. Differences in the properties of water and air, and wake constriction are two reasons why the equations proposed herein differ from Petryk's.

3.7.5 Assumptions and Limitations

Assumptions and limitations for Petryk's original model (Section 2.4.2) also apply to the modified version of Petryk's model except there is one additional limitation. Assumptions and limitations for the proposed model are also the same as for Petryk's model except for one of the assumptions and one of the limitations.

The modified version of Petryk's model and the proposed model both require an expression for predicting $U_x(z)$, the depth-averaged velocity at any point across the width of a trapezoidal channel when no dowels are present. Equation (3.19) is used herein with the understanding that the coefficients in the equation were derived for the bed and bank materials used in the model study performed herein. An appropriate equation should be developed for other channels.

In Petryk's original model, for any point in the channel, (x_n, z_n), if it were found that $(u_{n,i})_{\max}/U_{0i} < 0.02$, then it was arbitrarily assumed that the wake effect due to the ith cylinder was completely dissipated (Petryk, 1969; Li and Shen, 1973). This assumption yielded results (predicted values) that occasionally vacillated. The results would vacillate because $(u_{n,i})_{\max}/U_{0i}$ is exclusively a function of the longitudinal distance between ith cylinder and the point (x_n, z_n). Since the criteria prescribed by Petryk, and Li and Shen does not take into consideration the magnitude of velocity defects being eliminated from subsequent computations, on occasion relatively large defects are eliminated from the computations thus leading to abrupt variations in the results. In applying the writer's method it was assumed that the effect due to the ith cylinder at point (x_n, z_n), was completely dissipated when $(u_{n,i})_{\max} < 0.005$.

4. Data

Presented in this chapter are data that will be used to analyze the features of each transect and study reach. Data derived from a physical model study of willow post systems are also presented.

4.1 Bankfull Stage Data

Prior to calculating channel form parameters for the belt transects, an appropriate elevation (level) must be selected. Since the bankfull discharge is assumed to have morphologic significance, the bankfull elevation was estimated herein and then used to calculate channel form parameters for belt transects.

Data for characterizing the cross-sectional form of each transect were derived from the survey that was performed at the beginning of this study. Preliminary estimates of the bankfull stage were set, based on onsite observations of the active floodplain in Reaches 1 and 2. In Reach 3, since no active floodplain was observed, the elevation of the valley flat (floodplain) was considered to be the bankfull stage. To determine the bankfull level more precisely, it was calculated using the following procedures (Williams, 1978):

- the elevation at which W/D becomes a minimum;
- the stage corresponding to the first maximum of the bench index, as defined by Riley (1972); and
- and the stage corresponding to a change in the relation of A to W.

The bankfull stages resulting from application of the three definitions are shown in Table 4.1. Each of the definitions yields practically the same elevation. The bankfull elevations derived using the elevation at which W/D becomes a minimum will be used from hereon for consistency.

Table 4.1 – Estimates of Bankfull Elevation Yielded by Different Methods

Reach No.	Transect No.	Method used to estimate bankfull elevation, m (ft)		
		Method 1	Method 2	Method 3
1	1	31.85 (104.49)	31.85 (104.49)	31.94 (104.79)
	2	32.12 (105.39)	32.12 (105.39)	32.34 (106.09)
	3	32.52 (106.68)	32.52 (106.68)	32.58 (106.88)
	4	32.57 (106.87)	32.57 (106.87)	32.57 (106.87)
	5	32.45 (106.46)	32.45 (106.46)	32.51 (106.66)
2	1	32.69 (107.25)	32.66 (107.15)	32.72 (107.35)
	2	32.58 (106.90)	32.55 (106.80)	32.67 (107.20)
	3	32.72 (107.36)	32.72 (107.36)	32.78 (107.56)
	4	33.11 (108.62)	33.11 (108.62)	33.17 (108.82)
3	1	60.74 (199.28)	60.71 (199.18)	60.86 (199.68)
	2	61.08 (200.38)	61.08 (200.38)	61.17 (200.68)
	3	61.34 (201.25)	61.34 (201.25)	61.55 (201.95)
	4	61.03 (200.22)	61.00 (200.12)	61.30 (201.12)
	5	59.96 (196.71)	59.96 (196.71)	60.44 (198.31)

Method 1 – the elevation at which W/D becomes a minimum
Method 2 – the stage corresponding to a change in the relation of A to W
Method 3 – the stage corresponding to the first maximum of the bench index, as defined by Riley (1972)

4.2 Channel Form Data

Channel size and shape parameters corresponding to the bankfull stage were calculated from survey data for use in analyzing channel form. The calculated parameters include the maximum depth (d_{max}), area, top width (W), wetted perimeter (P), hydraulic radius (R), hydraulic depth (D), W/d_{max}, W/D, and d_{max}/D; the computed values are presented in Table 4.2.

Table 4.2 – Channel Size and Shape Parameters at Bankfull Stage

Reach No.	Trans. No.	Max. Depth d_{max} m (ft)	Area A m^2 (ft^2)	Width W m (ft)	Wetted Perim. P m (ft)	Hydr. Radius R m (ft)	Hydr. Depth D m (ft)	W/d_{max}	W/D	d_{max}/D
1	1	3.36 (11.01)	62.6 (674.1)	28.83 (94.59)	30.34 (99.54)	2.06 (6.77)	2.17 (7.13)	8.59	13.27	1.55
	2	3.97 (13.01)	69.6 (749.1)	29.83 (97.86)	31.83 (104.43)	2.19 (7.17)	2.33 (7.65)	7.52	12.79	1.70
	3	3.94 (12.92)	105.3 (1,133.9)	46.28 (151.83)	47.83 (156.93)	2.20 (7.23)	2.28 (7.47)	11.75	20.33	1.73
	4	3.79 (12.43)	80.7 (868.7)	31.85 (104.48)	33.97 (111.45)	2.38 (7.79)	2.53 (8.31)	8.40	12.57	1.50
	5	3.70 (12.14)	81.9 (881.4)	32.28 (105.90)	34.35 (112.69)	2.38 (7.82)	2.54 (8.32)	8.72	12.72	1.46
2	1	3.52 (11.55)	74.6 (803.0)	29.04 (95.26)	30.87 (101.27)	2.42 (7.93)	2.57 (8.43)	8.25	11.30	1.37
	2	3.38 (11.10)	65.8 (707.95)	28.45 (93.33)	30.06 (98.62)	2.19 (7.18)	2.31 (7.59)	8.41	12.30	1.46
	3	3.76 (12.34)	71.6 (770.6)	32.78 (107.54)	34.53 (113.30)	2.07 (6.80)	2.18 (7.17)	8.71	15.01	1.72
	4	4.50 (14.78)	84.9 (914.3)	35.25 (115.66)	37.55 (123.20)	2.26 (7.42)	2.41 (7.91)	7.83	14.63	1.87
3	1	3.91 (12.82)	71.1 (765.5)	29.72 (97.50)	31.43 (103.13)	2.26 (7.42)	2.39 (7.85)	7.61	12.42	1.64
	2	4.09 (13.42)	64.7 (696.3)	25.83 (84.73)	28.16 (92.39)	2.30 (7.54)	2.50 (8.22)	6.32	10.31	1.64
	3	4.44 (14.55)	83.2 (895.2)	27.69 (90.86)	30.12 (98.82)	2.76 (9.06)	3.00 (9.85)	6.24	9.22	1.48
	4	3.59 (11.78)	62.3 (670.3)	29.27 (96.04)	30.57 (100.30)	2.04 (6.68)	2.13 (6.98)	8.15	13.76	1.69
	5	3.65 (11.99)	69.76 (750.89)	28.93 (94.91)	30.69 (100.69)	2.27 (7.46)	2.41 (7.91)	7.92	12.00	1.51

4.3 Erosion Pin Data

The height of the erosion pins placed in each transect was measured up to five times over a one-year period. Presented in Table 4.3 to Table 4.5 are the recorded height measurements and the date on which each measurement was taken.

Table 4.3 – Reach 1 Erosion Pin Height Data [cm]

Transect No.	Point No.	Date				
		7 Aug 97	30 Oct 97	9 Jan 98	8 Mar 98	8 Aug 98
1	1	46.8	48.2	46.0	45.1	46.0
	2	30.4	31.7	30.5	30.8	30.2
	3	15.2	10.7	8.2	8.5	9.1
	4					
	5	30.3	25.9	26.8	26.5	24.4
	6	25.6	28.0	25.3	24.4	22.9
2	1	29.7	29.0	29.3	29.0	30.2
	2	45.9	46.0	45.7	44.8	45.7
	3	15.2	13.7	10.1	11.3	9.1
	4	36.7	37.2	36.6	36.0	37.5
	5	35.3	36.6	35.7	35.4	36.3
	6	29.8	33.5	24.4	34.7	29.0
3	1	46.0	48.2	46.3	45.7	46.3
	2	43.3	42.4	43.0	44.8	44.2
	3	15.2	15.2	11.3	16.5	16.8
	4	41.2	45.7	46.0	45.7	42.4
	5	42.6	42.7	42.7	42.7	41.5
	6	41.5	43.9	Erosion pin missing		
4	1	46.1	45.1	45.7	44.8	45.4
	2	29.5	32.0	32.0	29.0	29.6
	3	15.2	16.5	14.9	12.8	16.8
	4	46.8	49.4	50.0	48.8	48.8
	5	43.3	42.7	41.8	43.3	42.7
	6	40.7	43.9	Erosion pin missing		
5	1	42.1	42.7	42.7	42.4	42.4
	2	45.7	45.7	46.3	46.0	45.1
	3	15.2	16.8	24.7	27.4	25.0
	4					
	5	47.0	44.2	33.5	41.8	
	6	42.8	42.7	25.3	15.2	

Table 4.4 – Reach 2 Erosion Pin Height Data [cm]

Transect No.	Point No.	Date 7 Aug 97	30 Oct 97	9 Jan 98	8 Mar 98	8 Aug 98
1	1	33.5	33.2	32.9	33.5	32.9
	2	41.0	45.7	42.7	42.1	43.0
	3	15.2	12.2	10.7	10.7	7.0
	4	34.1	36.6	36.6	36.9	37.2
	5	44.2	43.9	43.0	43.0	41.1
	6	42.6	43.0	32.6	34.4	31.1
2	1	52.4	52.4	51.8	53.0	51.5
	2	40.9	46.9	46.0	43.9	45.7
	3	15.2	17.7	14.6	14.6	14.9
	4	41.3	40.2	39.6	40.2	39.0
	5	39.6	45.1	46.3	46.6	46.9
	6	40.8	45.1	43.6	38.7	38.7
3	1	43.5	44.2	42.7	44.0	44.2
	2	44.9	45.1	43.6	43.6	45.4
	3	15.2	18.3	12.2	11.9	9.1
	4	22.8	30.5	29.9	30.5	32.9
	5	41.7	43.3	43.9	44.8	44.8
	6	40.5	45.1	39.9	47.5	40.8
4	1	41.5	42.7	42.7	43.3	43.6
	2	66.4	66.4	66.1	63.1	65.2
	3	15.2	15.2	15.8	15.8	15.2
	4	44.7	45.4	45.1	45.7	45.7
	5	43.2	43.3	44.5	46.3	45.7
	6	39.5	43.6	40.5	39.6	38.1

Table 4.5 – Reach 3 Erosion Pin Height Data [cm]

Transect No.	Point No.	Date				
		8 Aug 97	6 Dec 97	8 Jan 98	8 Mar 98	8 Aug 98
1	1	45.4	46.6	46.3	46.0	45.7
	2	46.2	46.3		46.6	46.3
	3					
	4					
	5					
	6					
2	1	46.6	47.2		47.2	47.2
	2	49.6	48.8	49.1	48.8	49.1
	3	15.2	18.3	18.3	18.3	12.5
	4	46.5	44.8	45.7	47.5	46.0
	5	46.2	46.6	46.9	46.9	45.7
	6	48.0	50.0	50.0	51.2	50.0
3	1	43.8	44.5		45.1	44.8
	2	43.5	43.6	43.3	43.9	44.2
	3	15.2	17.7	16.8	15.5	17.4
	4	39.9	42.7	43.0	37.5	42.7
	5	43.1	45.7	45.7	42.1	45.7
	6	40.7	46.9	49.1	45.7	48.8
4	1	42.7	44.2	0.0	44.2	43.9
	2	44.7	44.2	43.9	43.9	44.2
	3	15.2	15.2	17.1	17.1	15.5
	4	38.6	41.1	38.7	43.0	38.7
	5	42.0	43.9	43.3	46.0	42.4
	6	44.9	47.2	45.7	51.2	46.3
5	1			46.0	45.7	45.4
	2			47.9	50.9	47.9
	3			15.2	16.3	15.5
	4			48.2	47.5	47.5
	5			45.7	45.7	46.0
	6			46.0	43.6	43.9

4.4 Soils Data

For each soil sample derived, a grain-size analysis was performed following procedures described by the ASTM (1993), USACE (1970), and Bowles (1992). Cumulative semi-logarithmic size-frequency graphs were plotted using the data derived from the mechanical and hydrometer analyses. The plots provide a visual image of the soil-size distribution. A typical size-frequency plot of soil data from a single point and four depth increments is shown in Figure 4.1. The plot also shows the size-frequency distribution of soil samples taken from the bed and bar of the same transect.

A number of statistics pertaining to the soil samples were estimated using data derived from the grain-size analyses. Several particle diameters were calculated for which a targeted percentage of the soil sample was finer (i.e., d_{16}, d_{25}, d_{50}, d_{75}, and d_{84}). Other statistics derived from the grain-size data include the geometric mean size (d_g), the geometric standard deviation (σ_g), the skewness (γ), and the gradation coefficient (G); estimators of the statistics are presented in Section 2.2.2. Median grain size diameters (d_{50}) for the soil samples analyzed in this study are presented in Table 4.6. The remaining particle size distribution statistics are presented in Appendix D.

4.5 Vegetation Data

The horizontal point frame was used to make quantitative measurements of vegetation along Harland Creek. A description of the horizontal point frame and how it was used is presented in Section 3.4.1 and Section 3.4.2, respectively. Equations for the three vegetation indices established [Veg_d, $VDI(h_{50})$, and $VDI(h_{mean})$] are presented in Section 3.4.3.

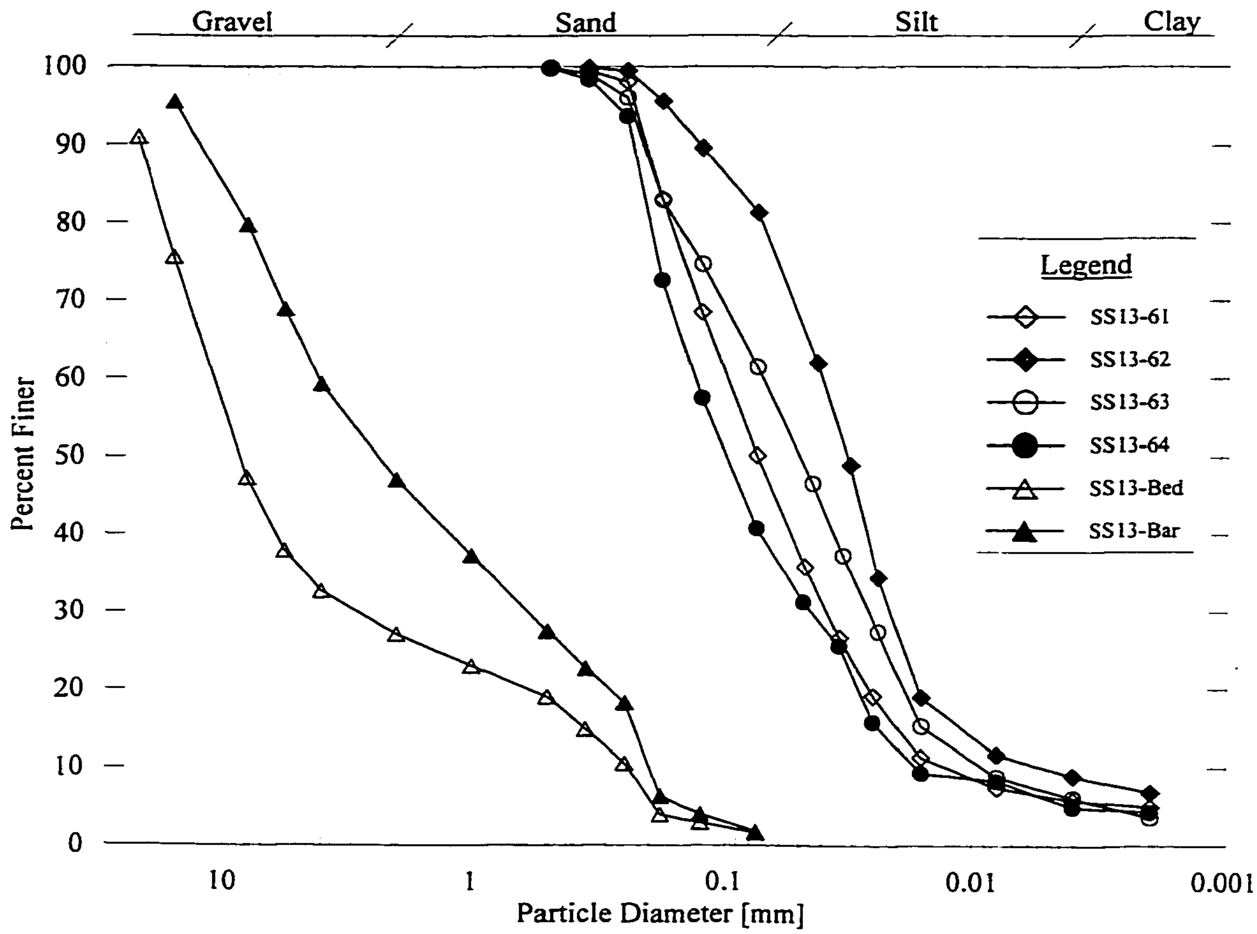

Figure 4.1 – Typical grain size distribution plot.

Table 4.6 – Median Grain Size (d_{50}) of Soil Samples [mm]

Reach No.	Transect No.	Soil Sampling Point Number* 2				3	4				5				6				*Bed*	*Bar*
	Depth Increment*	1	2	3	4	1	1	2	3	4	1	2	3	4	1	2	3	4	1	1
1	1	0.043		0.069		0.043					0.079	0.034	0.030		0.037	0.027	0.029		3.50	16.30
	2	0.040	0.060	0.031	0.020	0.040	0.046	0.032	0.032	0.019	0.038	0.044	0.029	0.028	0.030	0.027	0.021		0.422	0.79
	3	0.042	0.097	0.036	0.031	0.030	0.041	0.085	0.040	0.029	0.057	0.050	0.032	0.079	0.075	0.032	0.050	0.099	8.56	2.36
	4	0.039	0.034	0.027	0.025	0.027	0.027	0.026	0.028	0.022	0.147	0.029	0.029	0.027	0.032	0.033	0.038	0.026	10.90	4.46
	5	0.021	0.016	0.015	0.013	0.022					0.018	0.019			0.201	0.025			23.46	8.66
2	1	0.050	0.101	0.043	0.032	0.048	0.040	0.049	0.037	0.027	0.038	0.028	0.033	0.034	0.052	0.053	0.037	0.037	0.277	2.97
	2	0.042	0.047	0.038	0.027	0.037	0.035	0.064	0.047	0.026	0.034	0.053	0.056	0.041	0.043	0.028	0.026	0.032	1.96	0.62
	3	0.038	0.056	0.027	0.034	0.039	0.031	0.037	0.030	0.032	0.044	0.064	0.036	0.033	0.025	0.025	0.016	0.017	3.92	1.23
	4	0.023	0.020	0.028	0.054	0.046	0.037		0.041	0.021	0.045	0.030	0.026	0.021	0.054	0.056	0.039	0.029	9.85	0.56
3	1	0.036	0.026	0.028	0.034	0.042	0.085	0.029	0.030	0.042									0.051	
	2	0.024	0.021	0.021	0.025	0.023	0.036	0.030	0.029	0.029	0.097	0.070	0.148	0.134	0.112	0.210	0.229	0.098	0.043	5.42
	3	0.026	0.019	0.017	0.016	0.029	0.047	0.023	0.019	0.007	0.034	0.018	0.002		0.013	0.023	0.040		0.191	0.96
	4	0.030	0.021	0.021	0.023	0.021	0.042	0.031	0.030	0.034	0.029	0.055	0.300	0.408	0.030	0.046	2.06	13.37	1.66	0.68
	5	0.029	0.024	0.026	0.023	0.068	0.126	0.087	0.110	0.062	0.132	0.087	0.122	0.053	0.145				0.931	

*See Figure 3.2 for a definition of this term.

Presented in Table 4.7 through Table 4.9 are values of Veg_d, h_{50}, and h_{mean}. These values were calculated from data derived in the field. Values for $VDI(h_{50})$ and $VDI(h_{mean})$ can be derived from these values using (3.2) and (3.3), respectively. Data are presented for each of the three seasons during which vegetation density measurements were recorded. The data used to derive the values shown in Table 4.7 through Table 4.9 (the data recorded in the field) are presented in Appendix E.

4.6 Physical Model Data

Depth-averaged velocities were calculated from point velocity measurements for every flow condition established in the flume. The calculated depth-averaged velocities are presented in Table 4.10 to Table 4.19. At the bottom of each table is the discharge calculated from the depth-averaged velocities (Q_{calc}), the calculated flow rate over the bed of the flume (Q_{bed}), and the flow rate over the bank of the flume (Q_{bank}). The point velocity measurements from which the depth-averaged velocities were calculated are presented in Appendix B.

Presented in Table 4.20 to Table 4.22 are velocity measurements that were recorded for points in a horizontal plane, 6.10 cm (0.2 ft) below the water surface. Table 4.23 shows the calculated n-values, discharge, and nominal flow depth for each of the flume tests. The data used and the calculations performed in order to determine an n-value for each test are presented in Appendix B. The procedure by which the n-values were determined is described in Section 3.6.7.

Table 4.7 – Vegetation Data for Reach 1

Transect No.	Setup No.	August 1997			January 1998			March 1998		
		Veg_d	h_{50}	h_{mean}	Veg_d	h_{50}	h_{mean}	Veg_d	h_{50}	h_{mean}
1	1	0.33	0.92	1.54	1.24	1.22	1.34	1.56	0.52	0.94
	2	2.89	0.82	0.93	0.80	1.72	2.09	5.00	0.42	0.52
	3	0.46	3.42	3.32	1.07	0.62	0.72	0.00	0.00	0.00
	4	2.00	1.82	1.96	0.32	1.22	1.63	0.63	1.32	1.71
	5	-	-	-	-	-	-	0.34	1.22	1.22
2	1	1.08	0.62	0.73	0.26	0.52	1.05	0.82	0.52	0.91
	2	2.71	1.52	1.54	1.00	0.42	0.59	0.47	1.42	2.10
	3	1.62	0.72	1.08	1.14	0.52	0.59	8.33	0.42	0.45
	4	0.40	1.32	1.47	0.63	0.72	0.86	1.70	0.42	0.57
	5	-	-	-	1.14	0.52	0.59	-	-	-
	6	-	-	-	2.83	0.52	0.56	-	-	-
3	1	1.10	2.12	2.07	1.67	0.72	0.79	3.32	1.52	1.84
	2	1.72	2.42	2.69	1.54	1.62	1.56	1.00	0.32	0.38
	3	2.32	1.92	2.16	1.14	1.82	2.18	1.53	0.92	1.11
	4	2.19	1.02	1.24	0.67	1.52	1.89	2.30	1.02	1.41
4	1	4.62	0.92	0.89	0.97	1.32	1.58	0.06	1.82	1.82
	2	3.11	1.12	1.42	0.96	1.82	2.10	1.63	0.82	1.12
	3	1.48	2.02	2.27	0.35	0.62	2.08	0.37	0.92	1.96
	4	1.66	1.82	2.16	0.53	0.82	1.03	1.19	0.92	1.47
5	1	1.31	2.12	2.59	1.00	1.12	1.15	0.76	0.42	0.80
	2	2.83	0.72	0.71	0.33	0.72	0.72	0.51	1.32	1.88
	3	0.35	0.42	1.12	0.56	0.72	1.20	0.00	0.00	0.00
	4	1.62	0.82	1.06	1.00	0.32	0.32	1.28	0.82	1.18
	5	-	-	-	0.57	0.82	1.57	-	-	-
	6	-	-	-	0.70	0.72	0.96	-	-	-

Table 4.8 – Vegetation Data for Reach 2

Transect No.	Setup No.	August 1997			January 1998			March 1998		
		Veg_d	h_{50}	h_{mean}	Veg_d	h_{50}	h_{mean}	Veg_d	h_{50}	h_{mean}
1	1	0.77	2.92	3.10	0.67	1.32	1.60	0.14	2.72	2.95
	2	1.13	1.92	2.42	0.44	3.52	3.22	0.76	1.62	2.00
	3	1.02	4.05	3.30	0.58	1.32	1.83	1.36	1.22	1.79
	4	1.04	3.02	2.92	1.43	0.62	0.90	1.04	0.72	0.97
2	1	2.00	0.92	1.15	1.77	0.82	0.98	0.58	0.52	1.11
	2	1.83	1.82	2.17	0.55	1.02	2.05	0.84	0.82	1.66
	3	1.28	1.02	1.73	0.21	2.62	2.68	0.62	0.52	0.90
	4	0.92	2.42	2.71	0.05	2.12	2.12	0.33	1.52	2.56
	5	-	-	-	4.75	0.42	0.41	-	-	-
3	1	1.50	3.02	2.71	1.13	2.02	1.97	0.48	1.92	2.16
	2	2.03	1.32	1.60	1.63	0.72	0.94	1.40	1.02	1.29
	3	1.40	3.12	3.00	0.75	1.92	1.99	1.73	0.72	1.46
	4	0.61	3.82	3.57	0.98	0.82	1.25	0.33	0.92	1.21
4	1	0.60	2.52	3.08	0.21	1.32	1.70	3.14	1.32	1.58
	2	2.12	2.32	2.25	0.20	5.35	4.97	0.00	0.00	0.00
	3	1.35	3.02	2.93	1.38	1.32	1.74	2.45	1.02	1.19
	4	2.32	1.42	1.59	1.42	1.12	1.38	0.86	1.02	1.88

Table 4.9 – Vegetation Data for Reach 3

Transect No.	Setup No.	August 1997			January 1998			March 1998		
		Veg_d	h_{50}	h_{mean}	Veg_d	h_{50}	h_{mean}	Veg_d	h_{50}	h_{mean}
1	1	0.61	0.82	1.62	0.28	2.02	2.69	0.48	1.02	1.06
	2	0.77	2.92	2.56	0.45	0.52	0.96	0.76	1.42	1.65
	3	1.15	0.62	0.92	0.62	0.62	0.73	0.81	0.92	1.19
	4	0.27	0.42	1.35	0.26	2.52	1.85	0.68	0.82	0.94
	5	-	-	-	0.68	3.32	3.03	0.55	1.32	1.35
	6	-	-	-	0.50	0.32	0.53	-	-	-
	7	-	-	-	0.00	0.00	0.00	-	-	-
	8	-	-	-	0.06	1.92	1.92	-	-	-
2	1	3.11	1.12	1.17	0.35	2.32	2.16	0.63	1.12	1.79
	2	2.47	1.02	0.98	0.04	2.72	4.28	0.46	0.82	1.95
	3	1.27	4.05	3.67	1.67	1.12	1.18	0.57	1.02	1.90
	4	0.48	1.32	1.75	1.43	0.92	1.43	0.65	0.52	0.73
	5	-	-	-	0.58	1.22	1.40	-	-	-
3	1	2.30	0.72	0.73	0.00	0.00	0.00	0.58	2.72	3.07
	2	1.00	2.02	2.24	0.50	0.42	0.42	0.09	3.52	2.92
	3	0.13	5.55	4.30	0.29	0.92	0.92	1.86	2.62	2.38
	4	1.19	1.52	1.24	0.71	1.22	1.25	0.91	1.52	1.62
	5	0.29	1.72	1.88	-	-	-	-	-	-
4	1	2.17	1.12	1.16	0.54	1.92	2.44	1.16	1.02	1.49
	2	1.33	1.02	1.18	1.65	1.02	1.46	1.39	0.62	0.70
	3	1.11	1.12	1.87	0.94	3.72	3.04	0.30	0.82	1.38
	4	0.48	4.05	2.84	0.29	1.42	1.85	0.74	1.32	1.49
5	1	-	-	-	0.24	2.72	3.22	0.73	0.92	1.05
	2	-	-	-	0.45	1.32	1.68	0.70	3.32	3.37
	3	-	-	-	0.61	1.72	1.54	1.26	2.42	2.29
	4	-	-	-	0.15	4.25	4.10	0.31	0.42	0.79
	5	-	-	-	0.31	0.42	0.85	-	-	-
	6	-	-	-	0.33	3.92	3.31	-	-	-

Table 4.10 – Depth-Averaged Velocities, $U_x(z_j)$, and Calculated Discharge based on Physical Model Data (Configuration 0, Nominal Depth 22.9 cm, Flume Sect. 1)

Location No, j	Distance from left edge of flume, z_j [m]	$U_x(z_j)$ [m/s]	$U_x(z_j)/U_o$	$U_x(z_j)/U_x(z_{toe})$	Depth, d_j [m]	$Q_{j-1,j}$ [l/s]
1	0.000	0.103*	1.015	0.915	0.229	
2	0.305	0.103	1.015	0.915	0.229	7.21
3	0.610	0.111	1.089	0.982	0.229	7.47
4	0.762 (toe of slope)	0.113	1.109	1.000	0.229	3.90
5	0.838	0.112	1.098	0.990	0.191	1.80
6	0.914	0.105	1.031	0.929	0.152	1.42
7	0.991	0.087	0.854	0.770	0.114	0.98
8	1.113	0.000*	0.000	0.000	0.053	0.45
9	1.219	0.000*	0.000	0.000	0.000	0.00

Q_{calc} = 23.22 l/s Q_{bed} = 18.58 l/s (80.0% of Q_{calc}) Q_{bank} = 4.64 l/s (20.0% of Q_{calc})

*Interpolated or assumed value

Table 4.11 – Depth-Averaged Velocities, $U_x(z_j)$, and Calculated Discharge based on Physical Model Data (Configuration 0, Nominal Depth 22.9 cm, Flume Sect. 2)

Location No, j	Distance from left edge of flume, z_j [m]	$U_x(z_j)$ [m/s]	$U_x(z_j)/U_o$	$U_x(z_j)/U_x(z_{toe})$	Depth, d_j [m]	$Q_{j-1,j}$ [l/s]
1	0.000	0.101*	0.998	0.917	0.229	
2	0.351	0.101	0.998	0.917	0.229	8.12
3	0.656	0.110	1.080	0.992	0.229	7.34
4	0.762 (toe of slope)	0.110*	1.088	1.000	0.229	2.67
5	0.808	0.111	1.092	1.003	0.206	1.10
6	0.884	0.108	1.069	0.982	0.167	1.56
7	0.960	0.102	1.008	0.926	0.129	1.19
8	1.037	0.078	0.773	0.711	0.091	0.76
9	1.113	0.000	0.000	0.000	0.053	0.22
10	1.219	0.000*	0.000	0.000	0.000	0.00

Q_{calc} = 22.96 l/s Q_{bed} = 18.14 l/s (79.0% of Q_{calc}) Q_{bank} = 4.83 l/s (21.0% of Q_{calc})

*Interpolated or assumed value

Table 4.12 – Depth-Averaged Velocities, $U_x(z_j)$, and Calculated Discharge based on Physical Model Data (Configuration 0, Nominal Depth 30.5 cm)

Location No, j	Distance from left edge of flume, z_j [m]	$U_x(z_j)$ [m/s]	$U_x(z_j)/U_o$	$U_x(z_j)/U_x(z_{toe})$	Depth, d_j [m]	$Q_{j-1,j}$ [l/s]
1	0.000	0.189*	1.070	0.881	0.305	
2	0.305	0.189	1.070	0.881	0.305	17.59
3	0.610	0.189	1.067	0.879	0.305	17.57
4	0.762 (toe of slope)	0.215	1.214	1.000	0.305	9.38
5	0.838	0.169	0.953	0.786	0.267	4.18
6	0.914	0.164	0.926	0.763	0.229	3.14
7	0.991	0.153	0.862	0.710	0.191	2.53
8	1.067	0.106	0.601	0.495	0.152	1.69
9	1.143	0.102	0.578	0.477	0.114	1.06
10	1.219	0.007	0.039	0.032	0.076	0.40
11	1.372	0.007*	0.039	0.032	0.000	0.04

Q_{calc} = 57.58 l/s Q_{bed} = 44.54 l/s (77.4% of Q_{calc}) Q_{bank} = 13.03 l/s (22.6% of Q_{calc})

*Interpolated or assumed value

Table 4.13 – Depth-Averaged Velocities, $U_x(z_j)$, and Calculated Discharge based on Physical Model Data (Configuration 0, Nominal Depth 38.1 cm)

Location No, j	Distance from left edge of flume, z_j [m]	$U_x(z_j)$ [m/s]	$U_x(z_j)/U_o$	$U_x(z_j)/U_x(z_{toe})$	Depth, d_j [m]	$Q_{j-1,j}$ [l/s]
1	0.000	0.273*	1.061	1.041	0.381	
2	0.305	0.273	1.061	1.041	0.381	31.73
3	0.610	0.276	1.073	1.053	0.381	31.92
4	0.762 (toe of slope)	0.262	1.019	1.000	0.381	15.64
5	0.838	0.257	0.997	0.978	0.343	7.16
6	0.914	0.247	0.961	0.943	0.305	6.22
7	0.991	0.247	0.959	0.942	0.267	5.38
8	1.067	0.227	0.882	0.865	0.229	4.47
9	1.143	0.214	0.829	0.814	0.191	3.52
10	1.219	0.190	0.738	0.724	0.152	2.64
11	1.295	0.137	0.534	0.524	0.114	1.66
12	1.524	0.137*	0.534	0.524	0.000	1.80

Q_{calc} = 112.14 l/s Q_{bed} = 79.29 l/s (70.7% of Q_{calc}) Q_{bank} = 32.85 l/s (29.3% of Q_{calc})

*Interpolated or assumed value

Table 4.14 – Depth-Averaged Velocities, $U_x(z_j)$, and Calculated Discharge based on Physical Model Data (Configuration 1a, Nominal Depth 22.9 cm)

Location No, j	Distance from left edge of flume, z_j [m]	$U_x(z_j)$ [m/s]	$U_x(z_j)/U_o$	$U_x(z_j)/U_x(z_{toe})$	Depth, d_j [m]	$Q_{j-1,j}$ [l/s]
1	0.000	0.100*	1.111	1.095	0.229	
2	0.305	0.100	1.111	1.095	0.229	6.94
3	0.610	0.101	1.122	1.106	0.229	6.97
4	0.762 (toe of slope)	0.091	1.014	1.000	0.229	3.33
5	0.838	0.081	0.900	0.887	0.191	1.37
6	0.914	0.047	0.521	0.514	0.152	0.83
7	0.991	0.034	0.379	0.374	0.114	0.41
8	1.219	0.034*	0.379	0.374	0.000	0.44

Q_{calc} = 20.30 l/s Q_{bed} = 17.24 l/s (85.0% of Q_{calc}) Q_{bank} = 3.05 l/s (15.0% of Q_{calc})

*Interpolated or assumed value

Table 4.15 – Depth-Averaged Velocities, $U_x(z_j)$, and Calculated Discharge based on Physical Model Data (Configuration 1a, Nominal Depth 30.5 cm)

Location No, j	Distance from left edge of flume, z_j [m]	$U_x(z_j)$ [m/s]	$U_x(z_j)/U_o$	$U_x(z_j)/U_x(z_{toe})$	Depth, d_j [m]	$Q_{j-1,j}$ [l/s]
1	0.000	0.188*	1.088	0.958	0.305	
2	0.305	0.188	1.088	0.958	0.305	17.48
3	0.610	0.196	1.131	0.996	0.305	17.83
4	0.762 (toe of slope)	0.196	1.136	1.000	0.305	9.11
5	0.838	0.184	1.062	0.935	0.267	4.14
6	0.914	0.168	0.973	0.857	0.229	3.32
7	0.991	0.117	0.678	0.597	0.191	2.28
8	1.067	0.057	0.331	0.292	0.152	1.14
9	1.143	0.035	0.203	0.179	0.114	0.47
10	1.372	0.035*	0.203	0.179	0.000	0.46

Q_{calc} = 56.23 l/s Q_{bed} = 44.42 l/s (79.0% of Q_{calc}) Q_{bank} = 11.81 l/s (21.0% of Q_{calc})

*Interpolated or assumed value

Table 4.16 – Depth-Averaged Velocities, $U_x(z_j)$, and Calculated Discharge based on Physical Model Data (Configuration 1a, Nominal Depth 38.1 cm)

Location No, j	Distance from left edge of flume, z_j [m]	$U_x(z_j)$ [m/s]	$U_x(z_j)/U_o$	$U_x(z_j)/U_x(z_{toe})$	Depth, d_j [m]	$Q_{j-1,j}$ [l/s]
1	0.000	0.292*	1.127	0.966	0.381	
2	0.305	0.292	1.127	0.966	0.381	33.95
3	0.610	0.308	1.186	1.017	0.381	34.84
4	0.762 (toe of slope)	0.303	1.166	1.000	0.381	17.72
5	0.838	0.291	1.121	0.961	0.343	8.18
6	0.914	0.216	0.831	0.712	0.305	6.25
7	0.991	0.163	0.630	0.540	0.267	4.13
8	1.067	0.102	0.395	0.338	0.229	2.51
9	1.143	0.087	0.335	0.287	0.191	1.51
10	1.219	0.110	0.425	0.364	0.152	1.29
11	1.295	0.112	0.432	0.370	0.114	1.13
12	1.524	0.112*	0.432	0.370	0.000	1.46

Q_{calc} = 112.96 l/s Q_{bed} = 86.51 l/s (76.6% of Q_{calc}) Q_{bank} = 26.45 l/s (23.4% of Q_{calc})

*Interpolated or assumed value

Table 4.17 – Depth-Averaged Velocities, $U_x(z_j)$, and Calculated Discharge based on Physical Model Data (Configuration 1b, Nominal Depth 38.1 cm)

Location No, j	Distance from left edge of flume, z_j [m]	$U_x(z_j)$ [m/s]	$U_x(z_j)/U_o$	$U_x(z_j)/U_x(z_{toe})$	Depth, d_j [m]	$Q_{j-1,j}$ [l/s]
1	0.000	0.223*	1.095	1.000	0.381	
2	0.305	0.223*	1.095	1.000	0.381	25.85
3	0.610	0.223*	1.095	1.000	0.381	25.85
4	0.762 (toe of slope)	0.223	1.095	1.000	0.381	12.92
5	0.838	0.224	1.102	1.006	0.343	6.16
6	0.914	0.208	1.024	0.935	0.305	5.33
7	0.991	0.187	0.918	0.838	0.267	4.30
8	1.067	0.131	0.642	0.587	0.229	2.99
9	1.143	0.078	0.386	0.352	0.191	1.67
10	1.219	0.101	0.495	0.452	0.152	1.17
11	1.295	0.098	0.484	0.442	0.114	1.01
12	1.524	0.098*	0.484	0.442	0.000	1.29

Q_{calc} = 88.54 l/s Q_{bed} = 64.62 l/s (73.0% of Q_{calc}) Q_{bank} = 23.92 l/s (27.0% of Q_{calc})

*Interpolated or assumed value

Table 4.18 – Depth-Averaged Velocities, $U_x(z_j)$, and Calculated Discharge based on Physical Model Data (Configuration 2, Nominal Depth 38.1 cm)

Location No, j	Distance from left edge of flume, z_j [m]	$U_x(z_j)$ [m/s]	$U_x(z_j)/U_o$	$U_x(z_j)/U_x(z_{toe})$	Depth, d_j [m]	$Q_{j-1,j}$ [l/s]
1	0.000	0.270*	1.177	1.145	0.381	
2	0.305	0.270	1.177	1.145	0.381	31.38
3	0.610	0.265	1.153	1.121	0.381	31.06
4	0.762 (toe of slope)	0.236	1.028	1.000	0.381	14.53
5	0.838	0.223	0.971	0.944	0.343	6.33
6	0.914	0.190	0.830	0.807	0.305	5.10
7	0.991	0.161	0.701	0.681	0.267	3.82
8	1.067	0.112	0.487	0.473	0.229	2.57
9	1.143	0.084	0.365	0.355	0.191	1.56
10	1.219	0.088	0.384	0.373	0.152	1.12
11	1.295	0.112	0.486	0.473	0.114	1.01
12	1.372	0.112*	0.486	0.473	0.076	0.81
13	1.524	0.112*	0.486	0.473	0.000	0.65

Q_{calc} = 99.95 l/s Q_{bed} = 76.97 l/s (77.0% of Q_{calc}) Q_{bank} = 22.98 l/s (23.0% of Q_{calc})

*Interpolated or assumed value

Table 4.19 – Depth-Averaged Velocities, $U_x(z_j)$, and Calculated Discharge based on Physical Model Data (Configuration 3, Nominal Depth 38.1 cm)

Location No, j	Distance from left edge of flume, z_j [m]	$U_x(z_j)$ [m/s]	$U_x(z_j)/U_o$	$U_x(z_j)/U_x(z_{toe})$	Depth, d_j [m]	$Q_{j-1,j}$ [l/s]
1	0.000	0.227*	1.101	1.000	0.381	
2	0.305	0.227*	1.101	1.000	0.381	26.38
3	0.610	0.227*	1.101	1.000	0.381	26.38
4	0.762 (toe of slope)	0.227	1.101	1.000	0.381	13.19
5	0.838	0.218	1.054	0.957	0.343	6.13
6	0.914	0.197	0.955	0.867	0.305	5.11
7	0.991	0.173	0.839	0.762	0.267	4.03
8	1.067	0.115	0.560	0.508	0.229	2.72
9	1.143	0.096	0.464	0.421	0.191	1.69
10	1.219	0.099	0.479	0.435	0.152	1.27
11	1.295	0.135	0.656	0.595	0.114	1.19
12	1.524	0.135*	0.656	0.595	0.000	1.77

Q_{calc} = 89.87 l/s Q_{bed} = 65.95 l/s (73.4% of Q_{calc}) Q_{bank} = 23.91 l/s (26.6% of Q_{calc})

*Interpolated or assumed value

Table 4.20 – Horizontal Plane Point Velocity Data (Configuration 1a, Nominal Flow Depth = 3.81 cm, $Q_{calc.}$ = 112.98 l/s)

Distance from left edge of flume	Longitudinal distance from Flume Sect. 2									
	x = 0.00 m		x = 0.06 m		x = 0.12 m		x = 0.18 m		x = 0.24 m	
z [m]	u_x [m/s]	u_z [m/s]	u_x [m/s]	u_z [m/s]	u_x [m/s]	u_z [m/s]	u_x [m/s]	u_z [m/s]	u_x [m/s]	u_z [m/s]
0.91	0.2776	-0.0041	0.2776	-0.0041	0.2776	-0.0041	0.2975	-0.0062	0.2559	-0.0002
0.94	0.2553	-0.0028	0.2553	-0.0028	0.2553	-0.0028	0.2367	-0.0012	0.2337	0.0005
0.98	0.2138	0.0010	0.2138	0.0010	0.2138	0.0010	0.2124	0.0017	0.2158	0.0011
1.01	0.1775	0.0010	0.1701	0.0027	0.1772	0.0024	0.1736	0.0047	0.1722	0.0057
1.04	0.1514	-0.0061	0.1339	0.0091	0.1283	-0.0039	0.1199	0.0074	0.1555	-0.0083
1.07	0.1266	0.0032	0.1120	0.0020	0.1225	0.0048	0.1191	0.0036	0.1284	0.0058
1.10	0.1090	0.0033	0.1074	0.0044	0.1120	0.0025	0.1047	0.0040	0.1111	0.0020
1.13	0.0877	0.0046	0.0911	-0.0016	0.1024	0.0101	0.0905	0.0065	0.0743	0.0181
1.16	0.1199	0.0017	0.1264	0.0007	0.1239	0.0011	0.1278	0.0021	0.1220	0.0019
1.19	0.1208	-0.0020	0.1140	0.0108	0.1181	-0.0069	0.1162	0.0031	0.1344	-0.0079
1.22	0.1497	0.0065	0.1592	0.0024	0.1662	0.0117	0.1589	0.0099	0.1615	0.0064
1.25	0.1769	0.0109	0.1911	0.0145	0.1826	0.0106	0.1856	0.0104	0.1822	0.0080
1.28	0.0984	0.0388	0.1523	0.0084	0.1209	-0.0052	0.1515	-0.0078	0.1680	0.0067

Table 4.21 – Horizontal Plane Point Velocity Data (Configuration 1b, Nominal Flow Depth = 3.81 cm, Discharge, $Q_{calc.}$ = 88.63 l/s)

Distance from left edge of flume	Longitudinal distance from Flume Sect. 2									
	x = 0.00 m		x = 0.06 m		x = 0.12 m		x = 0.18 m		x = 0.24 m	
z [m]	u_x [m/s]	u_z [m/s]	u_x [m/s]	u_z [m/s]	u_x [m/s]	u_z [m/s]	u_x [m/s]	u_z [m/s]	u_x [m/s]	u_z [m/s]
0.91	0.2764	-0.0011	0.2894	-0.0026	0.2843	-0.0045	0.2877	-0.0029	0.2859	-0.0059
0.94	0.2570	-0.0009	0.2506	0.0008	0.2647	0.0016	0.2757	-0.0076	0.2635	-0.0034
0.98	0.2446	-0.0012	0.2570	-0.0028	0.2642	-0.0044	0.2641	0.0005	0.2556	0.0000
1.01	0.2242	-0.0041	0.2458	-0.0049	0.2484	0.0009	0.2290	-0.0001	0.2123	-0.0020
1.04	0.2117	-0.0002	0.1866	0.0020	0.2026	-0.0014	0.2164	-0.0021	0.2068	-0.0021
1.07	0.1662	0.0049	0.1677	0.0055	0.1737	0.0011	0.1799	0.0038	0.1556	0.0027
1.10	0.1737	0.0010	0.1377	0.0068	0.1446	0.0006	0.1310	0.0072	0.1312	0.0029
1.13	0.1426	0.0022	0.0941	-0.0202	0.0802	0.0110	0.0925	-0.0014	0.0813	0.0163
1.16	0.0966	0.0048	0.1009	0.0024	0.0913	0.0021	0.1075	0.0006	0.1307	0.0017
1.19	0.1113	0.0007	0.0961	0.0124	0.0823	-0.0065	0.0798	0.0029	0.1022	0.0042
1.22	0.0854	0.0007	0.1282	0.0000	0.1278	0.0071	0.1198	0.0017	0.0725	0.0252
1.25	0.1358	0.0065	0.1659	0.0082	0.1583	0.0073	0.1573	0.0080	0.1498	0.0038
1.28	0.1528	0.0064	0.1475	-0.0054	0.0289	0.0005	0.0262	-0.0012	0.0232	-0.0020

Table 4.22 – Horizontal Plane Point Velocity Data (Configuration 3, Nominal Flow Depth = 3.81 cm, Discharge, $Q_{calc.}$ = 89.76 l/s)

Distance from left edge of flume	Longitudinal distance from Flume Sect. 2									
	x = 0.00 m		x = 0.06 m		x = 0.12 m		x = 0.18 m		x = 0.24 m	
z [m]	u_x [m/s]	u_z [m/s]	u_x [m/s]	u_z [m/s]	u_x [m/s]	u_z [m/s]	u_x [m/s]	u_z [m/s]	u_x [m/s]	u_z [m/s]
0.91	0.2704	-0.0033	0.2637	-0.0008	0.2639	0.0003	0.2755	-0.0037	0.2701	-0.0045
0.98	0.2250	0.0041	0.2456	-0.0029	0.2493	-0.0014	0.2504	-0.0034	0.2450	-0.0024
1.04	0.2023	0.0000	0.1793	0.0011	0.2106	0.0010	0.2318	-0.0043	0.1956	0.0012
1.07	0.1883	0.0015	0.1591	0.0046	0.1890	0.0024	0.1698	0.0072	0.1676	0.0038
1.10	0.1397	0.0066	0.1457	0.0003	0.1257	0.0069	0.1351	0.0064	0.1340	0.0046
1.13	0.1015	-0.0135	0.1066	0.0046	0.1017	0.0007	0.1045	0.0141	0.0946	0.0029
1.16	0.1044	-0.0005	0.1153	0.0002	0.1079	-0.0042	0.1091	0.0003	0.1103	0.0002
1.19	0.0987	-0.0010	0.0953	0.0121	0.1142	-0.0033	0.0910	0.0009	0.1112	0.0067
1.22	0.1343	0.0013	0.1403	-0.0027	0.1309	0.0031	0.1399	0.0038	0.1291	-0.0009
1.25	0.1820	0.0018	0.1859	0.0019	0.1754	0.0024	0.1642	0.0033	0.1693	0.0038
1.28	0.1831	-0.0050	0.0346	-0.0020	0.1794	-0.0012	0.1596	0.0182	0.1513	-0.0110

Table 4.23 – Calculated n-values From Flume Tests

Config. No.	Nominal Flow Depth, Y cm (ft)	Calculated Discharge, Q_{calc} l/s (cfs)	Flow Area, A m^2 (sf)	Cross-Sect. Avg'd Vel., U_0 m/s (fps)	Calculated n-values
0	22.9 (0.75)	22.94 (0.81)	0.226 (2.44)	0.10 (0.33)	0.120
	30.5 (1.00)	57.48 (2.03)	0.325 (3.50)	0.18 (0.58)	0.075
	38.1 (1.25)	112.13 (3.96)	0.455 (4.69)	0.26 (0.84)	0.065
1a	22.9 (0.75)	20.39 (0.72)	0.226 (2.44)	0.09 (0.30)	0.130
	30.5 (1.00)	56.35 (1.99)	0.325 (3.50)	0.17 (0.57)	0.077
	38.1 (1.25)	112.98 (3.99)	0.455 (4.69)	0.26 (0.85)	0.062
1b	38.1 (1.25)	89.76 (3.17)	0.455 (4.69)	0.21 (0.68)	0.074
2	38.1 (1.25)	99.96 (3.53)	0.455 (4.69)	0.23 (0.75)	0.068
3	38.1 (1.25)	89.76 (3.17)	0.455 (4.69)	0.21 (0.68)	0.075

5. Results and Analysis

The data presented in Chapter 4 are evaluated in this chapter. Findings from each data set are presented in separate sections. Comparative analyses between the physical model data, and two analytical models for predicting flow through vegetation (Petryk's model and Wilkerson's model) are also presented.

5.1 Analysis of Bankfull Channel Form Data

Channel size and shape parameters corresponding to the bankfull stage were presented in Table 4.1. The data in Table 4.1 are used to make comparisons between Reach 1, Reach 2, and Reach 3.

It is noted that several of the channel form parameters reported in Table 4.1 for Reach No. 1, Trans. No. 3 (TS13) appear to be significantly different from those for the other transects in Reach 1. An analysis is presented, therefore, in which the statistical significance of the observed differences is assessed.

5.1.1 Analysis of Data for Reach 1, Transect 3

Statistics derived from reach-averaged channel form data are presented in Table 5.1. In computing statistics for Reach 1, data for TS13 was excluded. The channel form data for TS13 (Table 4.1) was evaluated, instead, to determine if it is significantly different from the other transects in Reach 1. It was found that several of the form parameters for TS13 were outside of the 95% confidence bounds calculated for the averaged Reach 1 data, i.e., A, W, WP, W/d_{max}, W/D, and d_{max}/D. It is concluded from this analysis that the geomorphic processes acting at TS13 are anomalous to Reach 1. The channel form data for TS13, therefore, will not be used in any of the analyses performed herein.

Table 5.1 – Descriptive Statistics for Channel Size and Shape Parameters

Reach No.	Parameter	Mean	Std. Dev.	Confidence Limits -90%	+90%	-95%	+95%
1	Max. Depth, d_{max} [m]	3.70	0.26	3.40	4.00	3.30	4.11
	Area, A [m^2]	73.70	9.23	62.84	84.56	59.02	88.39
	Width, W [m]	30.70	1.64	28.77	32.62	28.09	33.30
	Wetted Perim., P [m]	32.62	1.88	30.41	34.84	29.63	35.62
	Hydr. Radius, R [m]	2.25	0.16	2.07	2.44	2.01	2.50
	Hydr. Depth, D [m]	2.39	0.18	2.19	2.60	2.11	2.67
	W/d_{max}	8.31	0.54	7.67	8.95	7.45	9.17
	W/D	12.84	0.30	12.48	13.19	12.35	13.32
	d_{max}/D	1.55	0.11	1.42	1.67	1.38	1.72
2	Max. Depth, d_{max} [m]	3.79	0.50	3.20	4.38	3.00	4.59
	Area, A [m^2]	74.23	8.03	64.78	83.67	61.45	87.00
	Width, W [m]	31.38	3.22	27.59	35.16	26.26	36.50
	Wetted Perim., P [m]	33.25	3.46	29.18	37.33	27.74	38.76
	Hydr. Radius, R [m]	2.23	0.14	2.07	2.40	2.01	2.46
	Hydr. Depth, D [m]	2.37	0.16	2.18	2.56	2.11	2.63
	W/d_{max}	8.30	0.37	7.86	8.74	7.71	8.89
	W/D	13.31	1.80	11.20	15.42	10.45	16.17
	d_{max}/D	1.61	0.23	1.34	1.88	1.24	1.97
3	Max. Depth, d_{max} [m]	3.94	0.34	3.61	4.26	3.51	4.36
	Area, A [m^2]	70.20	8.10	62.48	77.92	60.14	80.26
	Width, W [m]	28.29	1.57	26.79	29.78	26.34	30.24
	Wetted Perim., P [m]	30.20	1.23	29.02	31.37	28.67	31.72
	Hydr. Radius, R [m]	2.33	0.26	2.07	2.58	2.00	2.65
	Hydr. Depth, D [m]	2.49	0.32	2.18	2.79	2.09	2.89
	W/d_{max}	7.25	0.90	6.38	8.11	6.12	8.37
	W/D	11.54	1.79	9.84	13.25	9.32	13.76
	d_{max}/D	1.60	0.08	1.52	1.67	1.49	1.70

5.1.2 Comparison of Reach-Averaged Data

To assess similarities and differences in channel size and shape among the study reaches, reach-averaged values of the channel form parameters for Reaches 1, 2, and 3 are compared in this section. To facilitate this analysis, statistics have been calculated (Table 5.1) corresponding to the channel form parameters presented in Table 4.1.

Mean values for Reaches 1 and 2 are evaluated in relation to the confidence bounds for the Reach 3 data in the following analysis. Since Reach 3 is the control reach (i.e., no willows are present) it is expected that there will be some differences in the channel form. The following observations are noted:

1) the width-to-d_{max} ratio for Reaches 1 and 2 (W/d_{max} = 8.31 and 8.30, respectively) are significantly larger than W/d_{max} for Reach 3 (W/d_{max} = 7.25) at the 90% confidence level;
2) the width-to-depth ratio for Reach 2 (W/D = 13.31) is significantly larger than W/D for Reach 1 and Reach 3 (W/D = 12.84 and 11.54, respectively) at the 90% confidence level; and
3) the width and wetted perimeter for Reaches 1 and 2 (W = 30.70 and 31.38, WP = 32.62 and 33.25, respectively) are larger than for Reach 3 (W = 28.29 and WP = 30.20) at the 95% confidence level.

Among the remaining channel form parameters (d_{max}, A, R, D, and d_{max}/D) there is no statistical evidence that Reach 1 or Reach 2 values are significantly different from Reach 3 values.

Mean values for Reach 1 were evaluated in relation to the confidence bounds for Reach 2 data but no significant differences were observed between any of the parameters at the 90% confidence level. In contrast, when Reach 2 mean values were evaluated in relation to the confidence bounds for Reach 1 data, it was observed that W/D for Reach 2 (W/D = 13.31) is significantly larger than for Reach 1 (W/D = 12.84) at the 90% confidence level.

With reference to the channel evolution model developed by Schumm et al. (1984) for channels in northern Mississippi, the width and the width-to-d_{max} ratio for

Reaches 1 and 2 being larger than for Reach 3 suggests that Reach 1 and Reach 2 transects are further along the evolutionary sequence.

Schumm et al. classify channels with $W/d_{max} > 6.0$ as Type IV and channels with $W/d_{max} > 8.0$ as Type V. Type IV channels are actively widening, but at a reduced rate. Also, sediment accumulation is increasing, and a low-water sinuous thalweg has formed in the channel. This condition marks the beginning of quasi-equilibrium in the channel evolution. The final quasi-equilibrium channel is Type V. Alternate bars, stabilizing vegetal effects at the toe of bank and on point bars, and reclining bank slopes characterize this channel type.

The channel evolution model developed by Schumm et al. (1984) accurately describes what the writer has observed on Harland Creek except that at the toe of bank where the willow posts systems have been constructed, there is pronounced toe scour. If, as suggested by the W/d_{max} ratio, Reach 1 and Reach 2 are in different evolutionary stages in comparison to Reach 3, this difference must be considered in interpreting the results of the study, i.e., care must be taken in attributing differences in Reach 3 to the presence of willow posts in Reach 1 and Reach 2.

5.2 Bank Erosion, Deposition, and Maximum Scour Depth Gages

Erosion pins were emplaced in each transect selected for observation during this study. Horizontal erosion pins were used to detect bank erosion and vertically driven pins were used to monitor changes in the cross-section ground line. The locations within each transect where the erosion pins were placed and the dimensions of the erosion pins are described in Section 3.2.2. Maximum scour depth gages (washers) were emplaced in several transects for the purpose of detecting the maximum amount of scour occurring along the banks as described in Section 3.2.3. The data collected by monitoring the erosion pins was presented in Section 4.3. Presented in the following sections is an analysis of the collected data and a discussion about noted observations.

5.2.1 Analysis of Erosion Pin Data

Significant variability in the measured heights of the erosion pins was observed. Most of the variability is attributed to the location of the pin height measurement (i.e., on the upstream or downstream side of the erosion pin or up- or down-bank of the erosion pin). When significant differences in the four height measurements noted above were observed, all four measurements were recorded and the average value was reported as the height of the erosion pin.

Because of the variability in the pin height measurements, it was decided that only calculated differences of 5.0 cm (0.164 ft) or greater would be considered as significant in analyzing the erosion pin data. Presented in Table 5.2 to Table 5.4 are the calculated differences in the measured pin length relative to the initial length of the pin. If the measured pin length at time t_i, $PinLength(t_i)$, is greater than the initial pin length, $PinLength(t_0)$, then the elevation of the ground has been lowered (or, in the case of the horizontal pins, the ground line has retreated). If $PinLength(t_i)$ is less than $PinLength(t_0)$ then the ground elevation has increased or advanced.

It is not always clear from the calculated values presented in Table 5.2 to Table 5.4 whether the ground line is aggrading, degrading, or both. Three terms are used, therefore, to describe the observed trends at each erosion pin: A = aggradation noted, D = degradation noted, and B = both aggradation and degradation noted. For every erosion pin where a net change in the pin height of 5.0 cm (0.164 ft) or more was observed, a note is recorded in the tables to describe the observed trend. A summary of findings from the data presented in Table 5.2 to Table 5.4 follows:

1) Regarding the horizontally driven pins, aggradation was observed at EP11-3, EP12-3, EP21-3, and EP23-3. Degradation (or bank retreat) was observed

Table 5.2 – Reach 1 Net Bank Aggradation (+) and/or Degradation (-) [cm]

Transect No.	Point No.	Date					Notes
		7 Aug 97	30 Oct 97	9 Jan 98	8 Mar 98	8 Aug 98	
1	1	0.0	-1.3	0.8	1.7	0.8	
	2	0.0	-1.3	-0.1	-0.4	0.2	
	3	0.0	4.6	7.0	6.7	6.1	A
	4						
	5	0.0	4.4	3.5[1]	3.8[2]	5.9	A
	6	0.0	-2.4	0.3[1]	1.2[3]	2.8	B
2	1	0.0	0.8	0.5	0.8	-0.4	
	2	0.0	-0.2	0.2	1.1	0.2	
	3	0.0	1.5	5.2	4.0	6.1	A
	4	0.0	-0.5	0.1	0.7	-0.8	
	5	0.0	-1.3	-0.4	-0.1	-1.0	
	6	0.0	-3.7	5.5	-4.9	0.9	B
3	1	0.0	-2.1	-0.3	0.3	-0.3	
	2	0.0	0.9	0.3	-1.5	-0.9	
	3	0.0	0.0	4.0	-1.2	-1.5	B
	4	0.0	-4.6	-4.9	-4.6	-1.2	
	5	0.0	-0.1	-0.1	-0.1	1.1	B
	6	0.0	-2.4	Erosion pin missing			D
4	1	0.0	0.9	0.3	1.3	0.6	
	2	0.0	-2.5	-2.5	0.6	-0.1	
	3	0.0	-1.2	0.3	2.4	-1.5	
	4	0.0	-2.6	-3.2	-2.0	-2.0	
	5	0.0	0.6	1.5	0.0	0.6	
	6	0.0	-3.1	Erosion pin missing			D
5	1	0.0	-0.6	-0.6	-0.3	-0.3	
	2	0.0	0.0	-0.7	-0.3	0.6	
	3	0.0	-1.5	-9.4	-12.2	-9.8	D
	4						
	5	0.0	2.8	13.5	15.2[4]		A
	6	0.0	0.1	17.5	27.5[4]		A

A = aggradation noted
D = degradation noted
B = both aggradation and degradation noted
[1]Maximum scour depth gage found 1.3 cm (0.5 in.) below ground surface.
[2]Maximum scour depth gage found 0.3 cm (0.12 in.) below ground surface.
[3]The maximum scour depth gage at this location was not observable on this date - because it was below the water surface.
[4]On 8 Mar 98 this erosion pin was disturbed while looking for the maximum scour depth gage that had been placed over the pin. The gage was never found and the pin was not reset.

Table 5.3 – Reach 2 Net Bank Aggradation (+) and/or Degradation (-) [cm]

Transect No.	Point No.	Date 7 Aug 97	30 Oct 97	9 Jan 98	9 Mar 98	8 Aug 98	Notes
1	1	0.0	0.3	0.6	0.0	0.6	
	2	0.0	-4.8	-1.7	-1.1	-2.0	
	3	0.0	3.0	4.6	4.6	8.2	A
	4	0.0	-2.5	-2.5	-2.8	-3.1	
	5	0.0	0.3	1.2	1.2	3.1	
	6	0.0	-0.4	10.0	8.1	11.5	A
2	1	0.0	0.0	0.6	-0.7	0.9	
	2	0.0	-6.1	-5.1	-3.0	-4.8	D
	3	0.0	-2.4	0.6	0.6	0.3	
	4	0.0	1.1	1.7	1.1	2.3	
	5	0.0	-5.5	-6.7	-7.0	-7.3	D
	6	0.0	-4.3	-2.8[1]	2.1	2.1	B
3	1	0.0	-0.7	0.8	-0.5	-0.7	
	2	0.0	-0.2	1.3	1.3	-0.5	
	3	0.0	-3.0	3.0	3.4	6.1	A
	4	0.0	-7.7	-7.1	-7.7	-10.1	D
	5	0.0	-1.6	-2.2	-3.1	-3.1	
	6	0.0	-4.6	0.5	-7.1	-0.4	B
4	1	0.0	-1.1	-1.1	-1.7	-2.1	
	2	0.0	0.0	0.3	3.3	1.2	
	3	0.0	0.0	-0.6	-0.6	0.0	
	4	0.0	-0.7	-0.4	-1.0	-1.0	
	5	0.0	-0.1	-1.3	-3.2	-2.6	
	6	0.0	-4.1	-1.0	-0.1	1.4	B

A = aggradation noted
D = degradation noted
B = both aggradation and degradation noted
[1]Maximum scour depth gage found 0.6 cm (0.25 in.) below ground surface.

Table 5.4 – Reach 3 Net Bank Aggradation (+) and/or Degradation (-) [cm]

Transect No.	Point No.	Date					Notes
		8 Aug 97	6 Dec 97	8 Jan 98	8 Mar 98	8 Aug 98	
1	1	0.0	-1.2	-0.9	-0.6	-0.3	
	2	0.0	-0.1		-0.4	-0.1	
	3						
	4						
	5						
	6						
2	1	0.0	-0.6		-0.6	-0.6	
	2	0.0	0.8	0.5	0.8	0.5	
	3	0.0	-3.0	-3.0	-3.0	2.7	B
	4	0.0	1.7	0.7	-1.1	0.4	
	5	0.0	-0.4	-0.7	-0.7	0.5	
	6	0.0	-2.0	-2.0	-3.2	-2.0	
3	1	0.0	-0.7		-1.3	-1.0	
	2	0.0	-0.1	0.2	-0.4	-0.7	
	3	0.0	-2.4	-1.5	-0.3	-2.1	
	4	0.0	-2.7	-3.0	2.4	-2.7	B
	5	0.0	-2.6	-2.6	1.1	-2.6	
	6	0.0	-6.3	-8.4	-5.1	-8.1	D
4	1	0.0	-1.5		-1.5	-1.2	
	2	0.0	0.5	0.8	0.8	0.5	
	3	0.0	0.0	-1.8	-1.8	-0.3	
	4	0.0	-2.5	-0.1	-4.4	-0.1	
	5	0.0	-1.9	-1.3	-4.0	-0.4	
	6	0.0	-2.4	-0.8	-6.3	-1.5	B
5	1			0.0	-0.3	-0.6	
	2			0.0	3.0	0.0	
	3			0.0	1.1	0.3	
	4			0.0	-0.6	-0.6	
	5			0.0	0.0	0.3	
	6			0.0	-2.4	-2.1	

A = aggradation noted
D = degradation noted
B = both aggradation and degradation noted

only at EP15-3 and both aggradation and degradation were observed at EP13-3.

2) Among the vertically driven pins, aggradation was observed at EP11-5, EP15-5, EP15-6, and EP21-6. Degradation was observed at EP13-6, EP14-6, and EP22-1, EP22-5, EP23-4, and EP33-6. Both aggradation and degradation were observed at EP11-6, EP12-6, EP13-5, EP22-6, EP23-6, EP24-6, EP33-4, and EP34-6.
3) The data do not provide any conclusive evidence regarding seasonal trends in bank erosion.

It is interesting that aggradation occurred at three of the horizontal erosion pins and that significant degradation occurred at only one of the horizontal pins. Taking all three study reaches into consideration, it is noted that no significant aggradation and/or degradation occurred at eight of the fourteen sections evaluated.

If Reaches 1 and 2, where the willow posts are planted, are considered separately from Reach 3, then aggradation and degradation at the horizontal pins can be interpreted in another light. First, it is noted that none of the horizontal pins where aggradation and/or degradation occurred are in Reach 3. Second, regarding Reaches 1 and 2, aggradation occurred at four of the nine transects and aggradation and/or degradation occurred at six of the nine transects.

There are two possible explanations as to why aggradation might be occurring at the horizontal erosion pins. One possible explanation is that shallow rotational or translational slides are occurring near the top of the bank and partly covering the erosion pins with failed bank material. The other possibility is that sediment aggrading on the horizontal erosion pins is being fluvially deposited.

Among the vertical pins where significant aggradation and/or degradation was observed, the following is noted:

1) Of the eighteen pins, eleven are EP*wx*-6 pins, four are EP*wx*-5 pins, two are EP*wx*-4 pins, and one is an EP*wx*-1 pin. In other words, among the eighteen pins where erosion and degradation was noted, 61% were at the lower (basal) part of the bank, 22% were at the middle part of the bank, and 10% were on the upper part of the bank.
2) Among the eighteen pins, four were noted as aggrading (22%), six were noted as degrading (33%), and eight were noted as both aggrading and degrading (50%).
3) Only three of the eighteen noted pins (17%) are in Reach 3. Of the fifteen remaining pins, eight are in Reach 1 and seven are in Reach 2.
4) Significant aggradation and/or degradation were observed at all nine of the EP*wx*-6 pins (100%) in Reaches 1 and 2 and at two of the four EP*wx*-6 pins (50%) in Reach 3.
5) Significant aggradation and/or degradation were observed at four of nine EP*wx*-5 pins (44%) in Reaches 1 and 2 and none of the four EP*wx*-5 pins (0%) in Reach 3.
6) Significant aggradation and/or degradation were observed at one of nine EP*wx*-4 pins (11%) in Reaches 1 and 2 and one of four EP*wx*-4 pins (25%) in Reach 3.

The observation that significant aggradation and/or degradation were observed 100% of the EP*wx*-6 pins in Reaches 1 and 2 indicate that there is a great deal of basal activity along Harland Creek. Watson et al. (1995) noted a similar observation after comparing bank-lines in four sets of aerial photographs taken between 1955 and 1991. Watson et al. estimated that the average bank migration is 4.3 m (14 ft) per year or about 15% of the bendway channel width annually. Judging from the number of EP*wx*-6 pins significantly affected by aggradation and/or degradation, there is more basal activity in Reaches 1 and 2 than in Reach 3.

5.2.2 Analysis of Maximum Scour Depth Gage Data

Maximum depth scour gages (washers) were placed over erosion pins in Reach 1 at transects 1, 2, 3, and 5; in Reach 2 at transects 1 and 2; and in Reach 3 at transects 1, 4, and 5. Any observed displacement of the washers was noted and measured in the field. A summary of noted observations is presented in the following paragraphs.

In only a few cases were washers found below the ground surface. On January 9, 1998, the washers at EP11-5 and EP11-6 were found 1.3 cm (0.5 in.) below the ground surface. On March 8, 1998, the washer at EP11-5 was found 0.3 cm (.12 in.) below the ground and the washer at EP11-6 could not be observed because it was below the water surface. The reason why the washers at erosion pins EP11-5 and EP11-6 were below the ground surface was because of the accumulated debris immediately downstream of the erosion pins. Figure 5.1 is a photograph of EP11-6 and the accumulated debris just downstream of EP11-6.

The only other documented observations involving the erosion pins occurred on January 9, 1998. The washer at EP22-6 was observed 0.6 cm (0.25 in.) below the ground surface. Also, after measuring the height of EP15-5 and EP15-6, an attempt was made to recover the washers that had been placed over the erosion pins but the washers were never found.

Because of the meager number of documented comments involving the maximum scour depth gages, it is concluded that along the banks of Harland Creek, general scour, i.e., scour in a channel or floodplain that is not localized at a pier, abutment, or other obstruction to flow (Richardson et al., 1990) is not a prevalent problem.

5.3 Analysis of Soil Grain-Size Data

Presented in this section is an analysis of the bank material grain-size data reported in Table 4.6. This analysis is directly addresses the working hypothesis for this study (Section 1.2), which states that willow posts planted along an eroding bank will

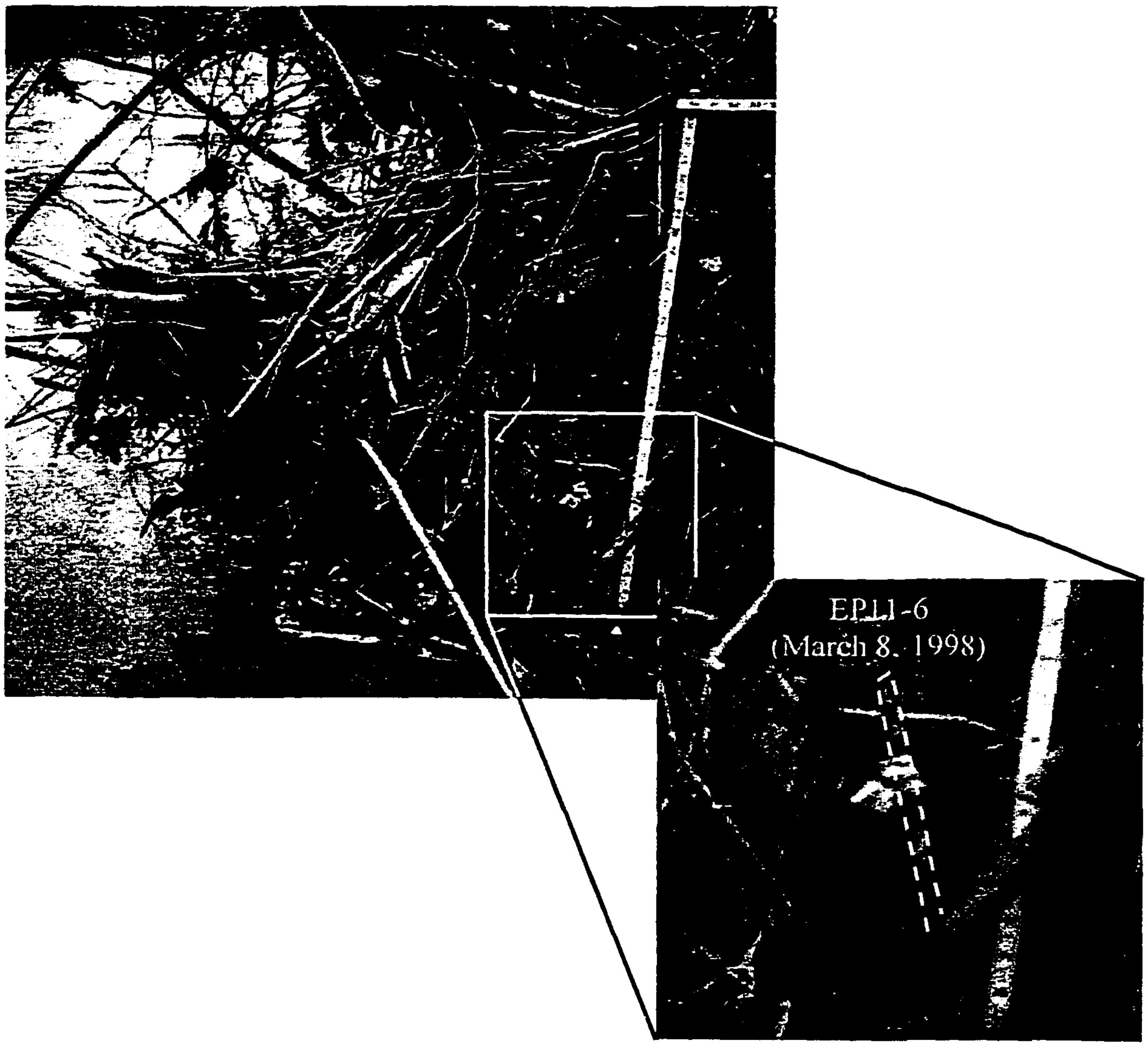

Figure 5.1 – Photograph of EP11-6. Note the accumulated debris just behind the erosion pin. This photograph was taken looking downstream.

thrive only if the posts are able to induce net sediment deposition. If sediment on the surface of the bank were found to be finer than sediment from the subsurface, then it would be reasonable to assume that the surface material is finer because the willows have reduced flow velocity and sediment transport capacity atop the bank.

The specific objective of this analysis is to ascertain whether the grain-size of the surface soil is smaller than that of the subsurface soil. The Wilcoxon matched-pairs signed-ranks test, described in Section 3.3.3, was used to assess trends in the soil grain size with respect to depth. Results from the test are summarized in Table 5.5.

Table 5.5 – Statistical Analysis of Variations in Soil Median Grain-Size with Depth below the Ground Surface*

Reach No.	Depth Increment Being Compared**	n	$T_{n:\alpha=0.05}$	T_+	Conclusion
1	2	13	21	72	Fail to reject H_0
	3	11	13	62	"
	4	8	5	25	"
2	2	11	13	21	"
	3	12	17	56	"
	4	12	17	74	"
3	2	12	17	53	"
	3	12	17	32	"
	4	10	10	32	"

H_o: the median value of the differences in the surface soil d_{50} versus the subsurface soil d_{50} is greater than or equal to zero (i.e., there is no difference in the d_{50} for the surface soil versus the subsurface soil).

H_a: the median value of the difference in the subsurface soil d_{50} is less than zero (i.e., the d_{50} for the surface soil is smaller than the d_{50} for the subsurface soil).

*This analysis uses the Wilcoxon matched-pairs signed-rank test.

**Soil samples from depth increment 1 are being compared to samples from depth increments 2, 3, and 4.

The results in Table 5.5 are for a comparison between soil samples from depth increment 1 and soil samples from depth increments 2, 3, and 4. None of the comparisons yielded sufficient evidence to reject the null hypothesis (H_o: there is no difference in the

d_{50} for the surface soil versus the subsurface soil) in favor of the alternative hypothesis (H_a: the surface soil is smaller than the d_{50} for the subsurface soil). That is, the calculated T_{+} values are not less than the corresponding test statistics $T_{n,\alpha}$.

Figure 5.2, Figure 5.3, and Figure 5.4 show, for each study reach, how the median grain-size varies with depth below the surface for soil sampling points 2, 4, 5, and 6. Each point shown on the plot is the average value of all d_{50} data observed for that reach and point number. The whiskers attached to each point show the minimum and maximum d_{50} values observed. As noted from the Wilcoxon matched-pairs signed-ranks test, the patterns in the plots show no indication that the surface soil material is finer than the subsurface material.

It is concluded from this analysis of the soil grain size data that the willow posts have not resulted in net sediment deposition during the three-year period between when they were planted (March 1994) and when soil samples for this study were derived (August 1997).

5.4 Analysis of Vegetation Density Data

Presented in the following paragraphs is an analysis of the vegetation density data presented in Section 4.5. The objective in evaluating the data is to assess and compare the vegetal characteristics of the three reaches selected for evaluation.

Three VDIs are used herein to quantify vegetation density (Section 3.4.3): Veg_d, $VDI(h_{50})$, and $VDI(h_{mean})$. In the analyses presented in this section, separate results are derived for each VDI. Results derived from different VDIs are compared to determine which is most advantageous in differentiating the vegetal characteristics of the study reaches.

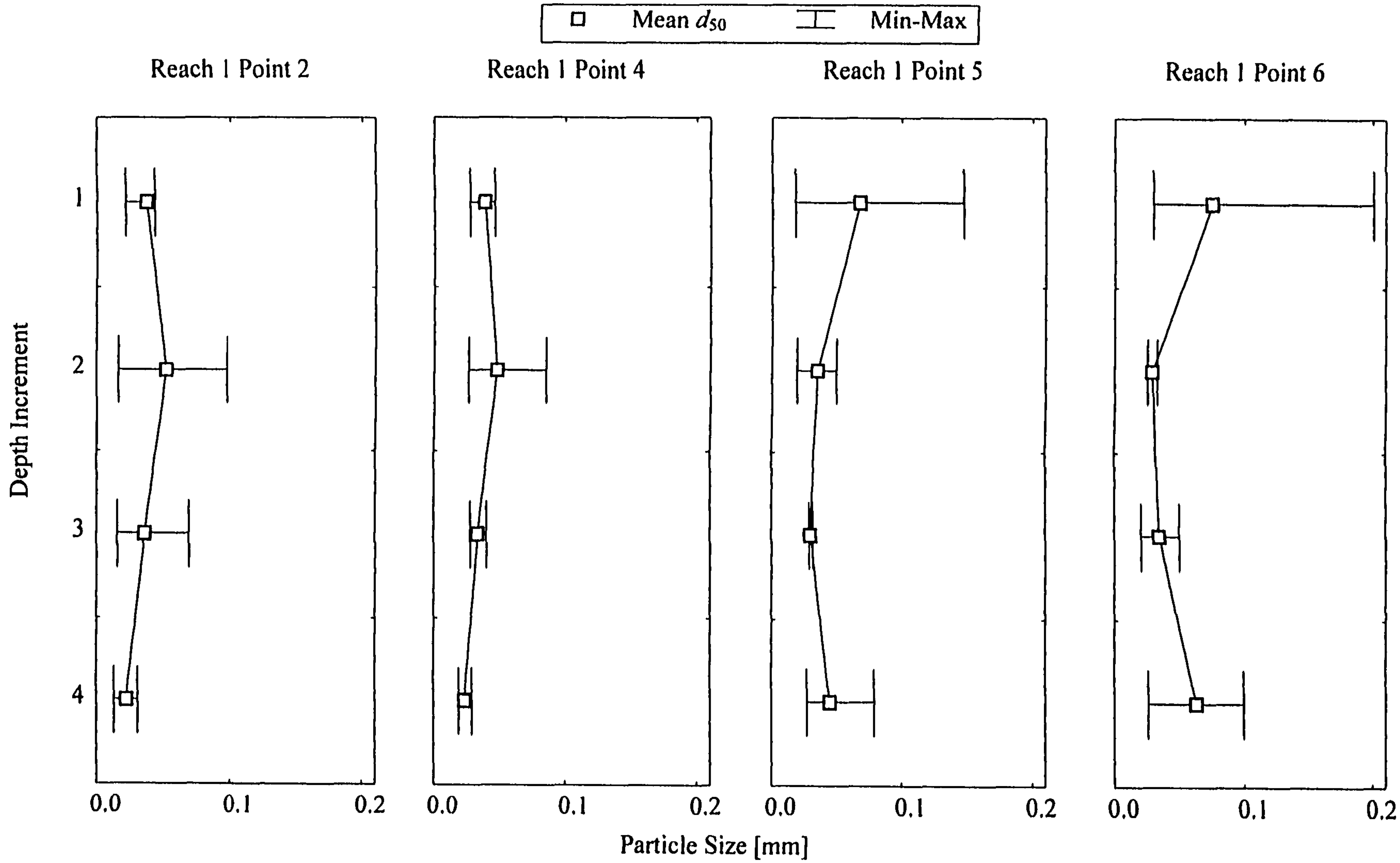

Figure 5.2 – Variation in median grain size (d_{50}) with depth below the surface for Reach 1, Point Nos. 2, 4, 5, 6. See Figure 3.3 for key to point locations.

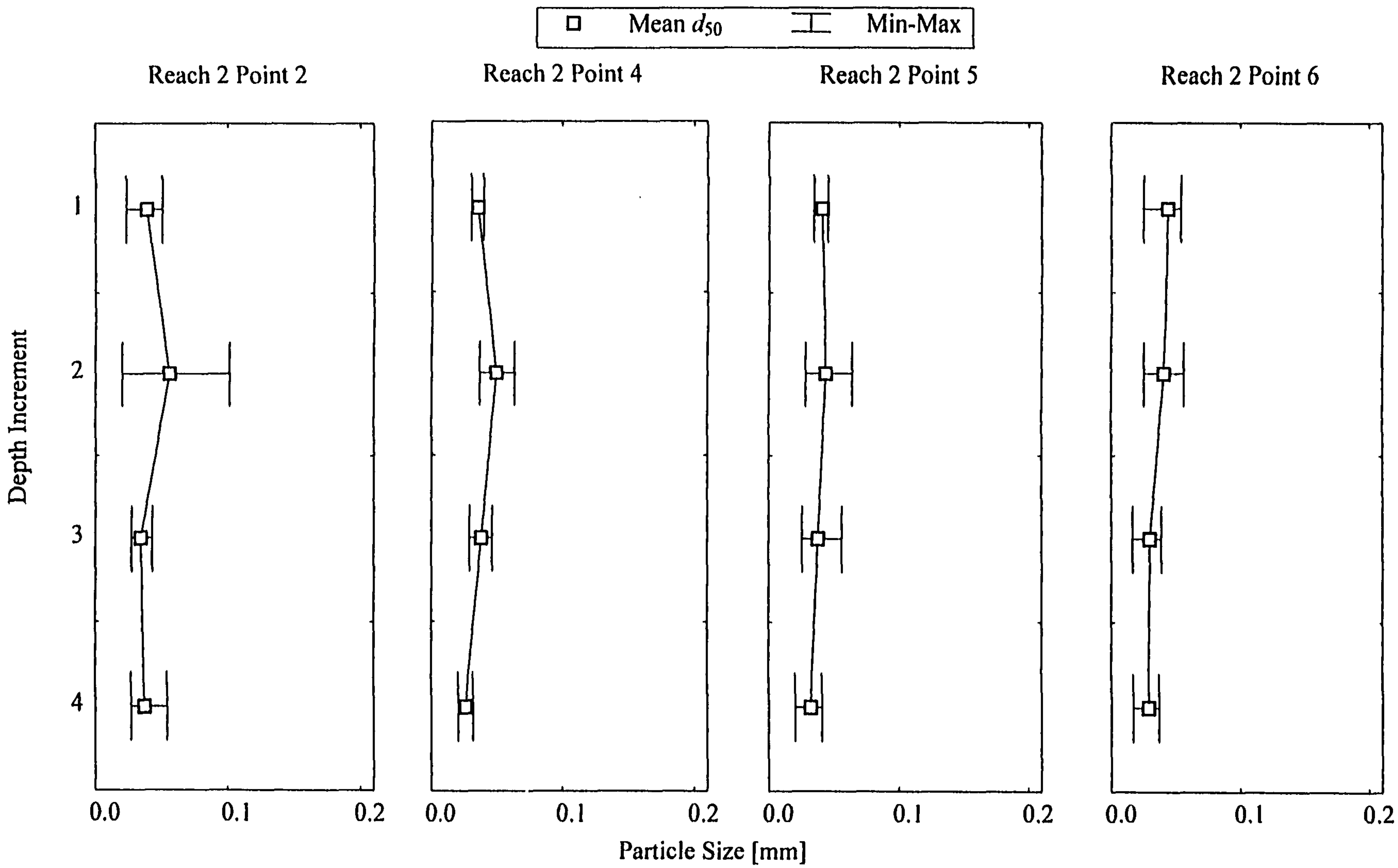

Figure 5.3 – Variation in median grain size (d_{50}) with depth below the surface for Reach 2, Point Nos. 2, 4, 5, 6. See Figure 3.3 for key to point locations.

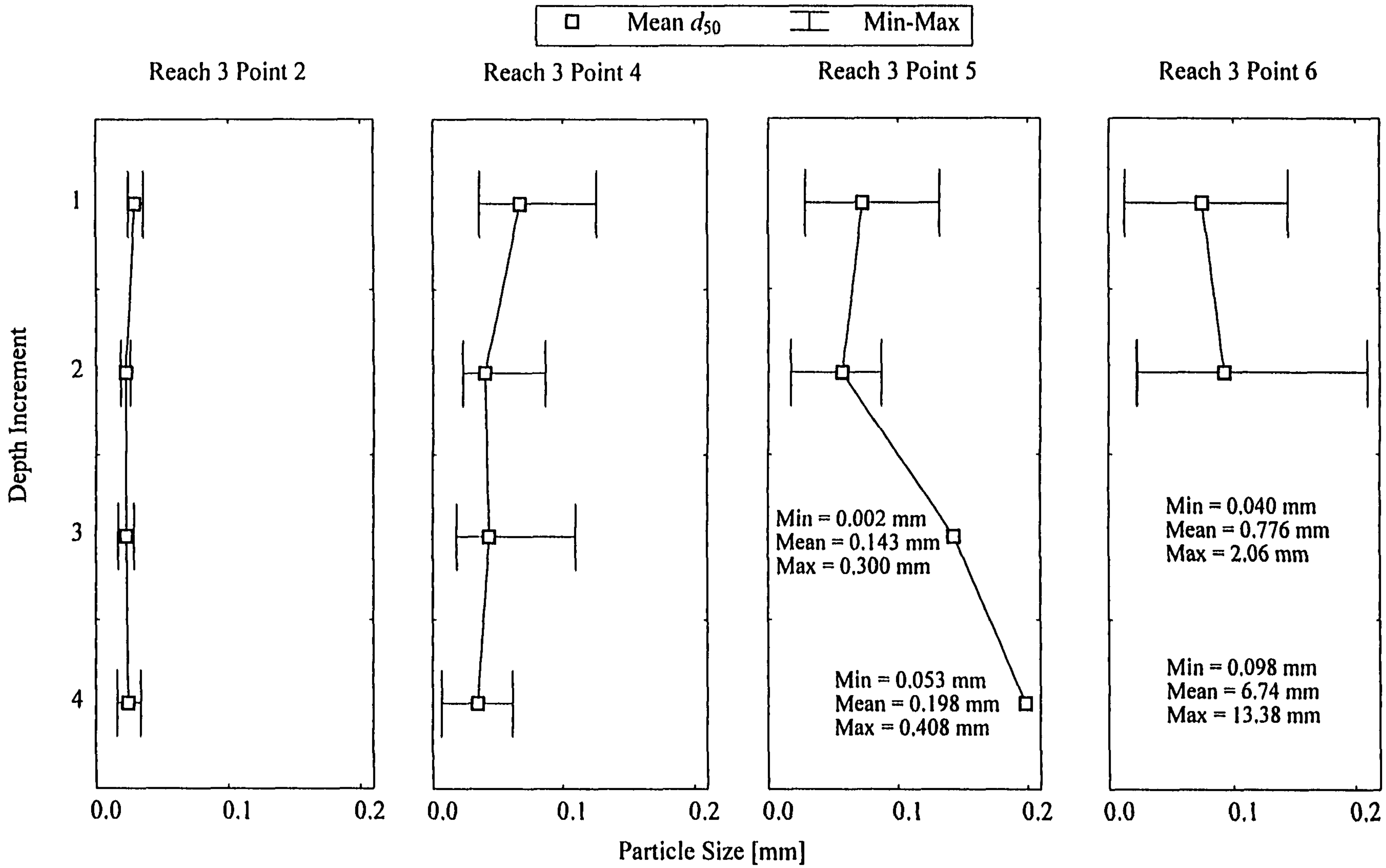

Figure 5.4 – Variation in median grain size (d_{50}) with depth below the surface for Reach 3, Point Nos. 2, 4, 5, 6. See Figure 3.3 for key to point locations.

5.4.1 Vegetation Density Comparison By Transect

VDIs were calculated for each of the study transects. Furthermore, at each transect, vegetation density measurements were taken in three different seasons. Plots of the calculated VDIs are presented in Figure 5.5 to Figure 5.7. Shown in each plot are results derived by using a particular VDI. Three lines are shown on each plot; each line represents results for a particular season. Each point shown in Figure 5.5 to Figure 5.7 was calculated by (1) calculating the VDI of interest for each setup established in the transect, and (2) calculating an average VDI from the VDIs calculated for each setup.

It is clear from Figure 5.5, Figure 5.6, and Figure 5.7 that the vegetation density along Harland Creek was substantially greater in August 1997 than in either January 1998 or March 1998. In contrast, differences between the January 1998 and March 1998 data are not apparent.

Intuitively it is expected that the vegetation density would be related from season to season. On this basis, it is argued that the representativeness of a given VDI can be evaluated by how well it measures correlation among vegetation density measurements taken in different seasons. The lines plotted within Figure 5.5, Figure 5.6, and Figure 5.7, appear to be cross-correlated, that is, there is interdependence among the three lines shown on each plot. The correlation coefficient, $r_{X,Y}$, can be used to determine quantitatively the degree of linear interrelationship between the lines plotted for each season. The equation for calculating $r_{X,Y}$ is (Mood et al., 1974)

$$r_{X,Y} = \frac{s_{X,Y}}{s_X s_Y} \tag{5.1}$$

where

$$s_{X,Y} = \frac{1}{n}\sum_{j=1}^{n}\left(x_j - \bar{x}\right)\left(y_j - \bar{y}\right) \tag{5.2}$$

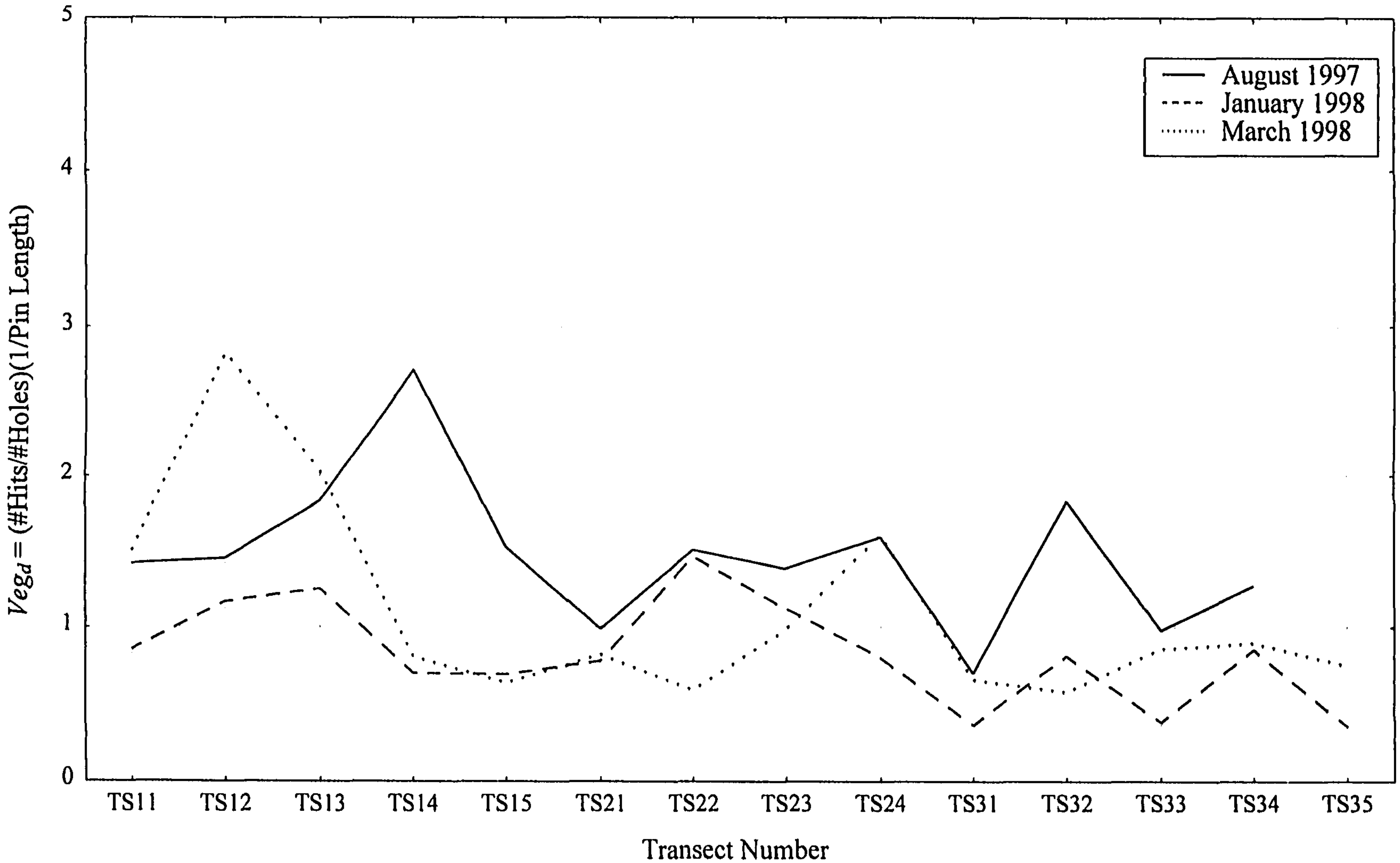

Figure 5.5 – Seasonal comparison of Veg_d by transect.

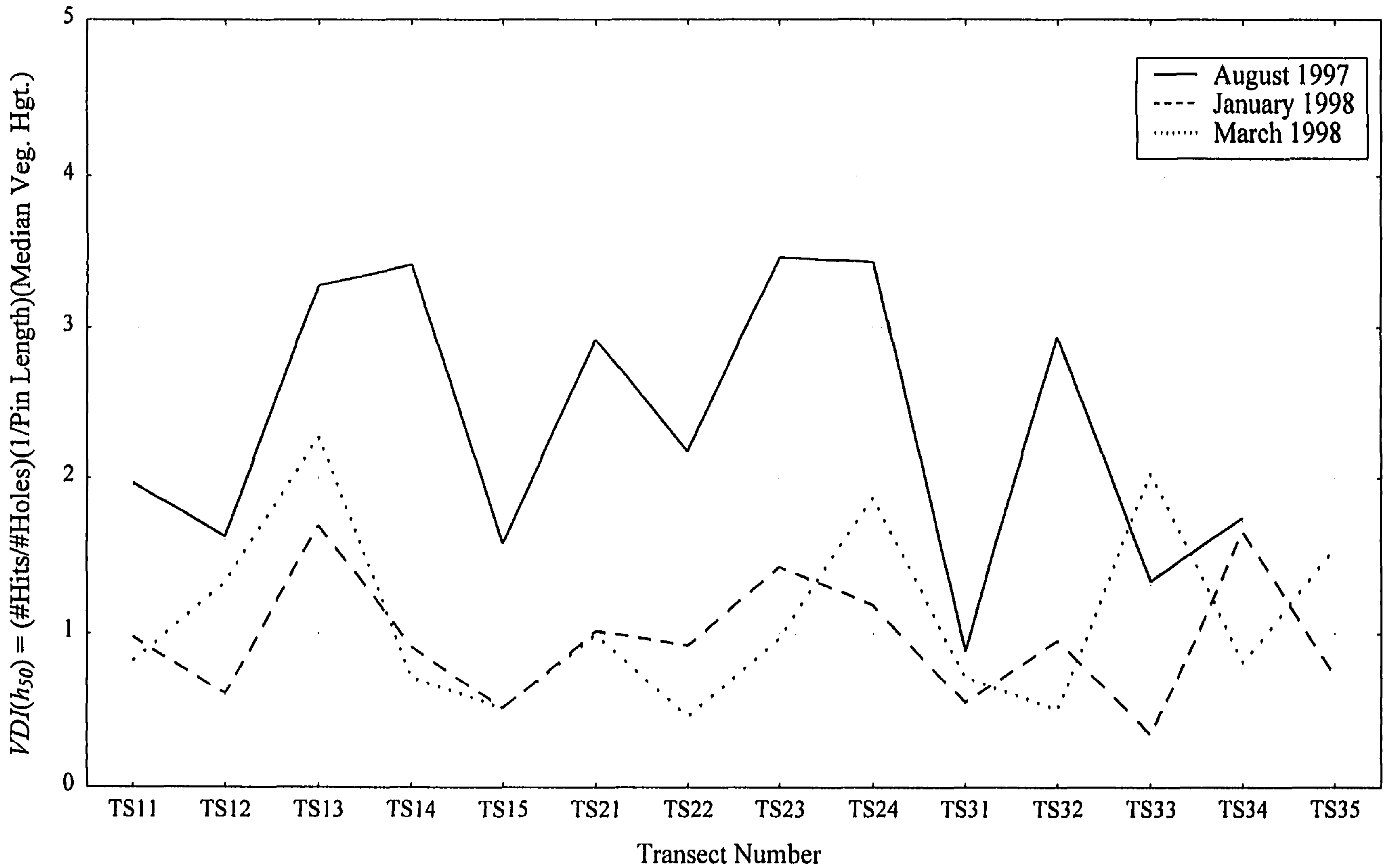

Figure 5.6 – Seasonal comparison of $VDI(h_{50})$ by transect.

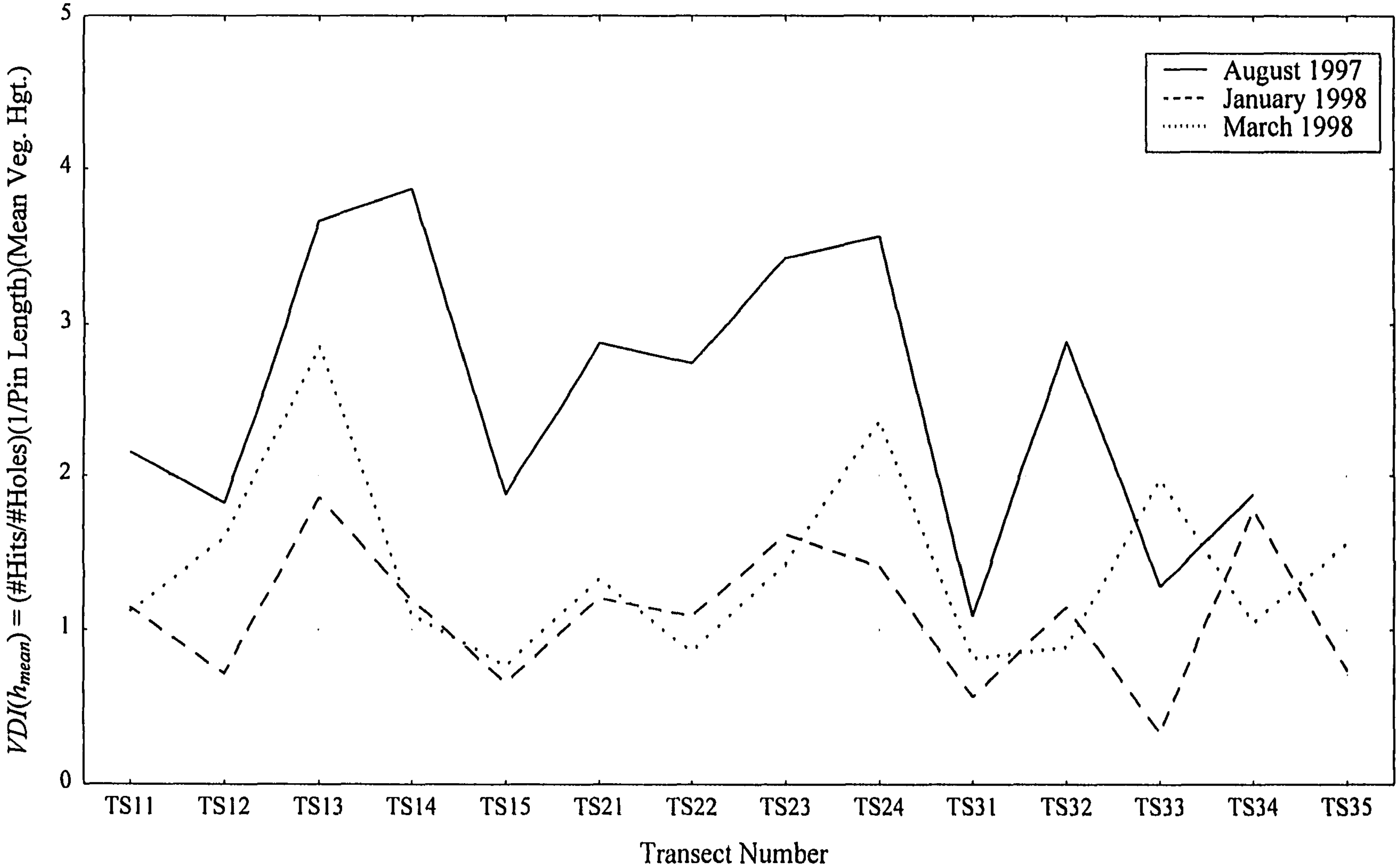

Figure 5.7 – Seasonal comparison of $VDI(h_{mean})$ by transect.

and $\bar{x}$ and $\bar{y}$ are sample mean values; s_X and s_Y are sample standard deviations; x_i and y_i are variable values; s_{XY} is the sample covariance of X and Y; and X and Y are the names of the variables being evaluated. The range of r_{XY} is from –1 to 1. A coefficient of 1 means a perfect positive correlation, -1 means a perfect negative correlation, and zero (0) means no correlation (Porkess, 1991).

For each of the VDIs established for this study, Table 5.6 shows correlation coefficients between data derived in different seasons. The correlation coefficients are generally highest for the August 1997 versus January 1998 data. Also, the coefficients for $VDI(h_{mean})$ are higher overall, than those for either Veg_d or $VDI(h_{50})$. It is concluded from these results that among the three indices evaluated, $VDI(h_{mean})$ yields the most consistent results from season to season.

Table 5.6 – Correlation Coefficients between VDI's for Different Seasons

	Veg_d	$VDI(h_{50})$	$VDI(h_{mean})$
$r_{Aug97,Jan98}$	0.30	0.61	0.70
$r_{Aug97,Mar98}$	0.10	0.19	0.37
$r_{Jan98,Mar98}$	0.42	0.14	0.31

5.4.2 Vegetation Density Comparison By Reaches

To assess the possibility that the willow post systems in Reach 1 and Reach 2 promote bank stability, in the following analysis the density of vegetation in Reach 1 and Reach 2 are compared to the density of vegetation in Reach 3. Also evaluated in this analysis is how well the three VDIs used herein distinguish seasonal vegetation density.

To compare vegetation density among different reaches, an average VDI was calculated for each reach and season. The mean VDI, standard error, and standard deviation for each reach are plotted in Figure 5.8, Figure 5.9, and Figure 5.10. A particular VDI is featured in each plot.

Comparing a particular VDI for a particular season, it can be seen in either Figure 5.8, Figure 5.9, or Figure 5.10, that Reach 1 and Reach 2 values are higher than Reach 3 values. These results suggest that the willow post systems in Reach 1 and Reach 2 enhance bank stability by fostering an environment that is more conducive to the establishment of volunteer vegetation.

Also noted in Figure 5.8 to Figure 5.10 is that the reach-averaged VDI values vary seasonally. The VDI values for August 1997 are clearly higher than the VDI's for either January 1998 or March 1998. In Figure 5.8 and Figure 5.9 the calculated VDI's for January 1998 and March 1998 data are not noticeably different at Reach 2. In contrast, in Figure 5.10 where $VDI(h_{mean})$ is plotted, greater vegetation density is apparent for March 1998 compared to January 1998. These observations indicate that all of the VDIs considered in this study do a fair job of representing vegetation density but suggest that $VDI(h_{mean})$ is a more robust index.

To assess the generality of the patterns observed in Figure 5.8 to Figure 5.10 (i.e., vegetation density highest in August 1997 and lowest in January 1998) VDIs were calculated using season-averaged VDIs. Season-averaged VDIs, were computed by averaging the VDIs for every setup in all three reaches for a particular season. A box plot with the computed values is shown in Figure 5.11.

It can be seen in Figure 5.11 that all of the seasoned-averaged VDI's follow the same patterns observed in Figure 5.8 to Figure 5.10. This result supports the claim made above, that each of the VDI's does a fair job of representing vegetation density. One final observation about the data plotted in Figure 5.11 is that the greatest spread in index values is yielded by values for $VDI(h_{mean})$.

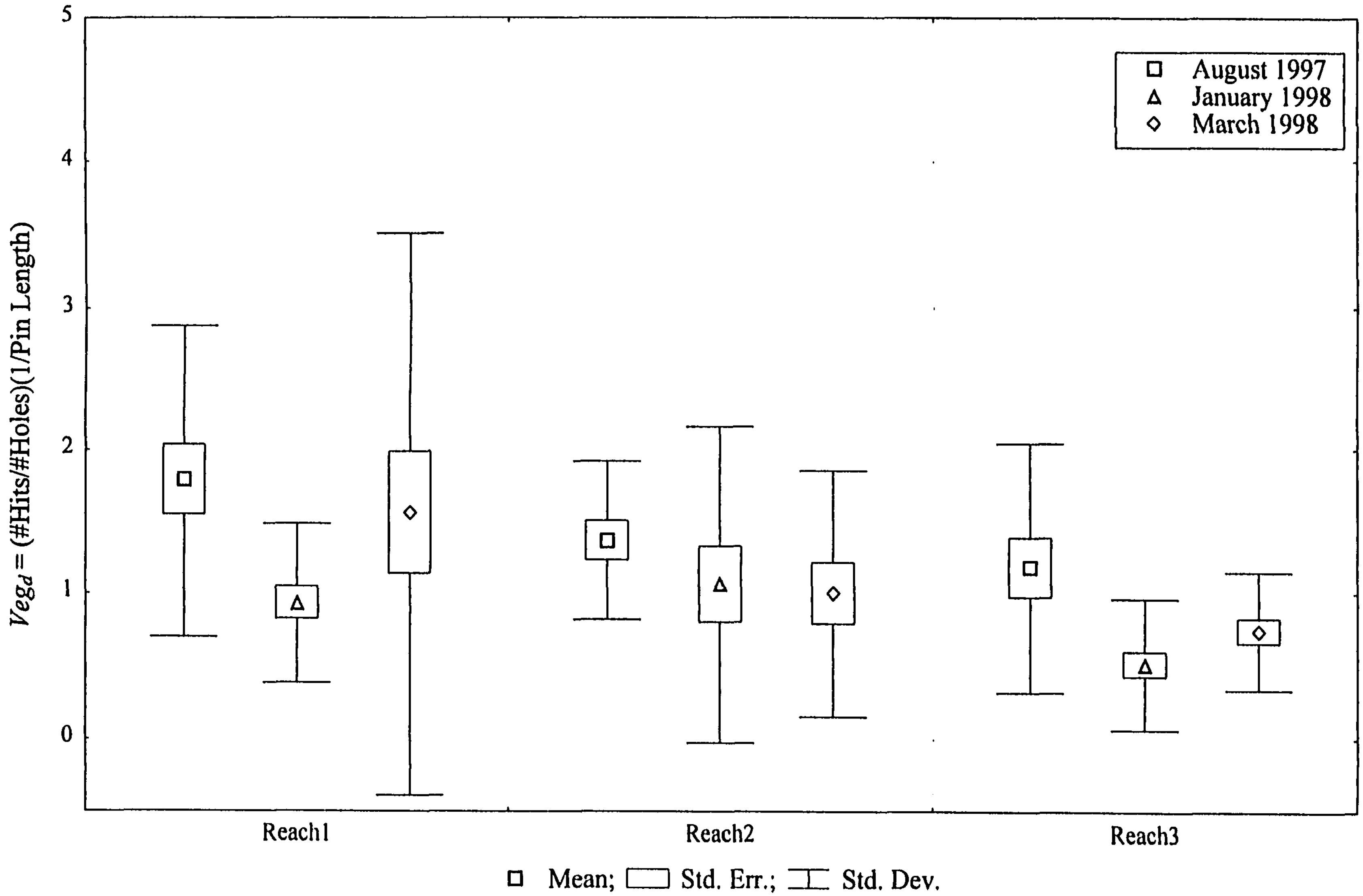

Figure 5.8 – Seasonal comparison of Veg_d by reach.

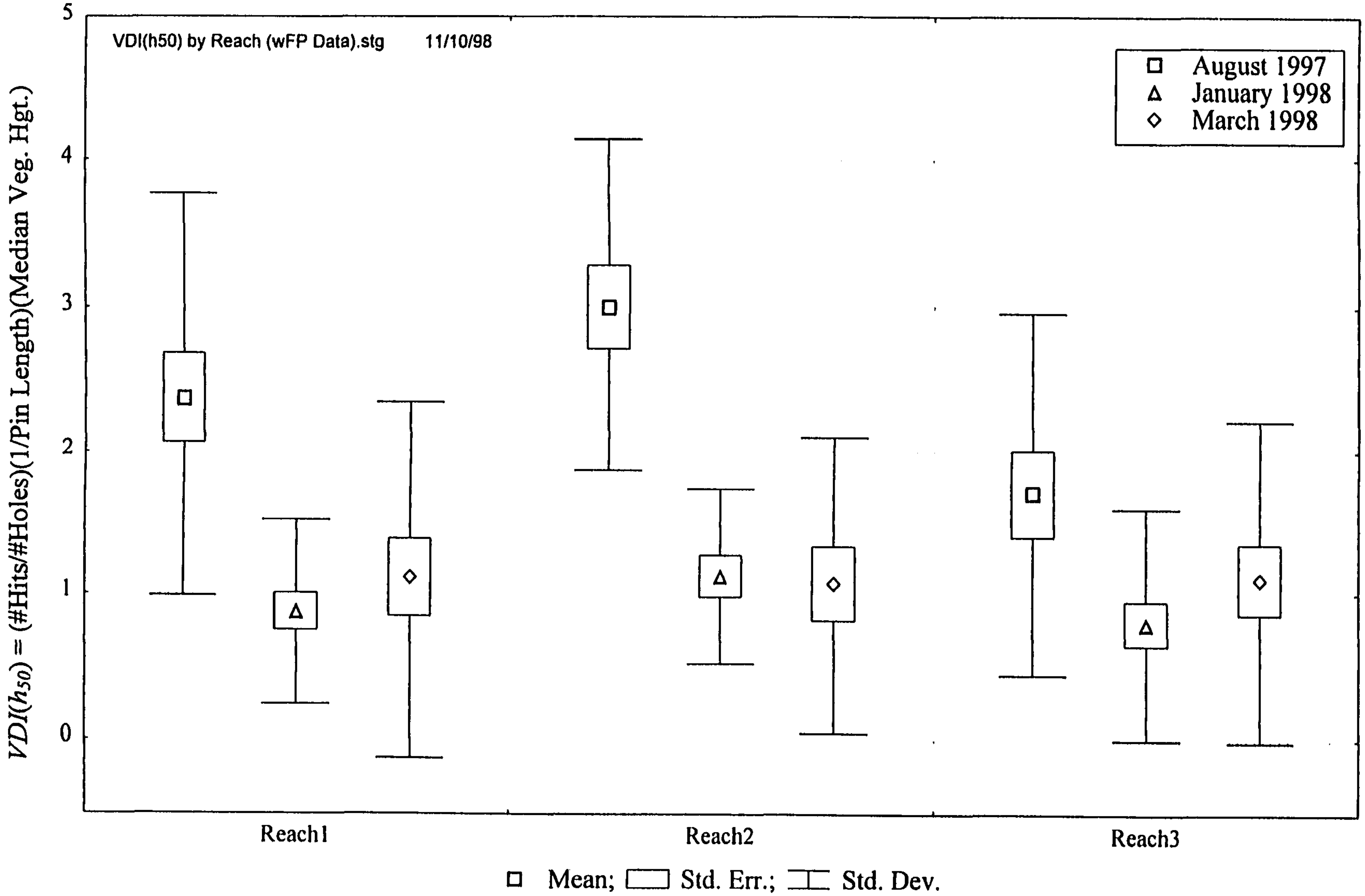

Figure 5.9 – Seasonal comparison of $VDI(h_{50})$ by reach.

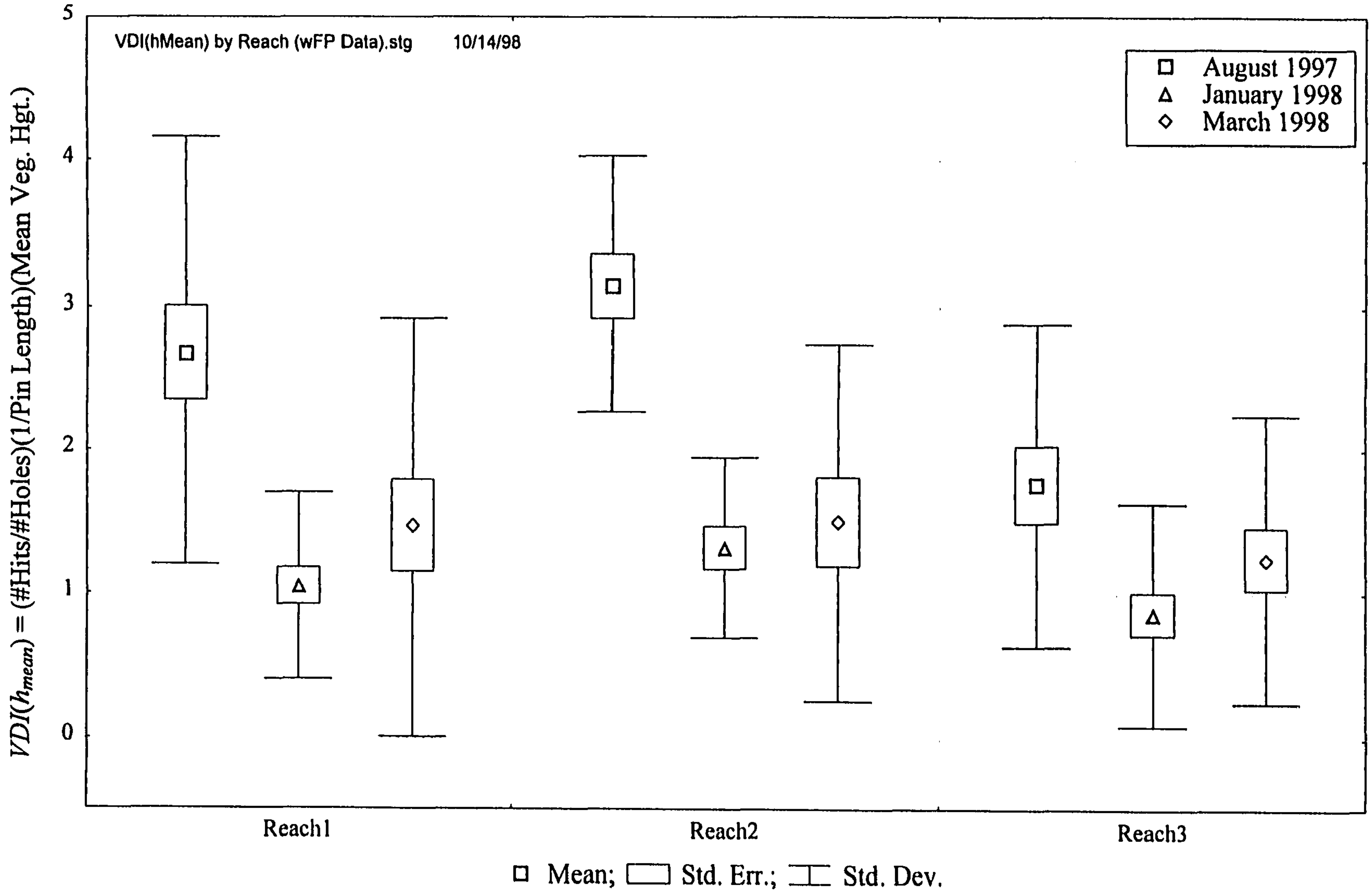

Figure 5.10 – Seasonal comparison of $VDI(h_{mean})$ by reach.

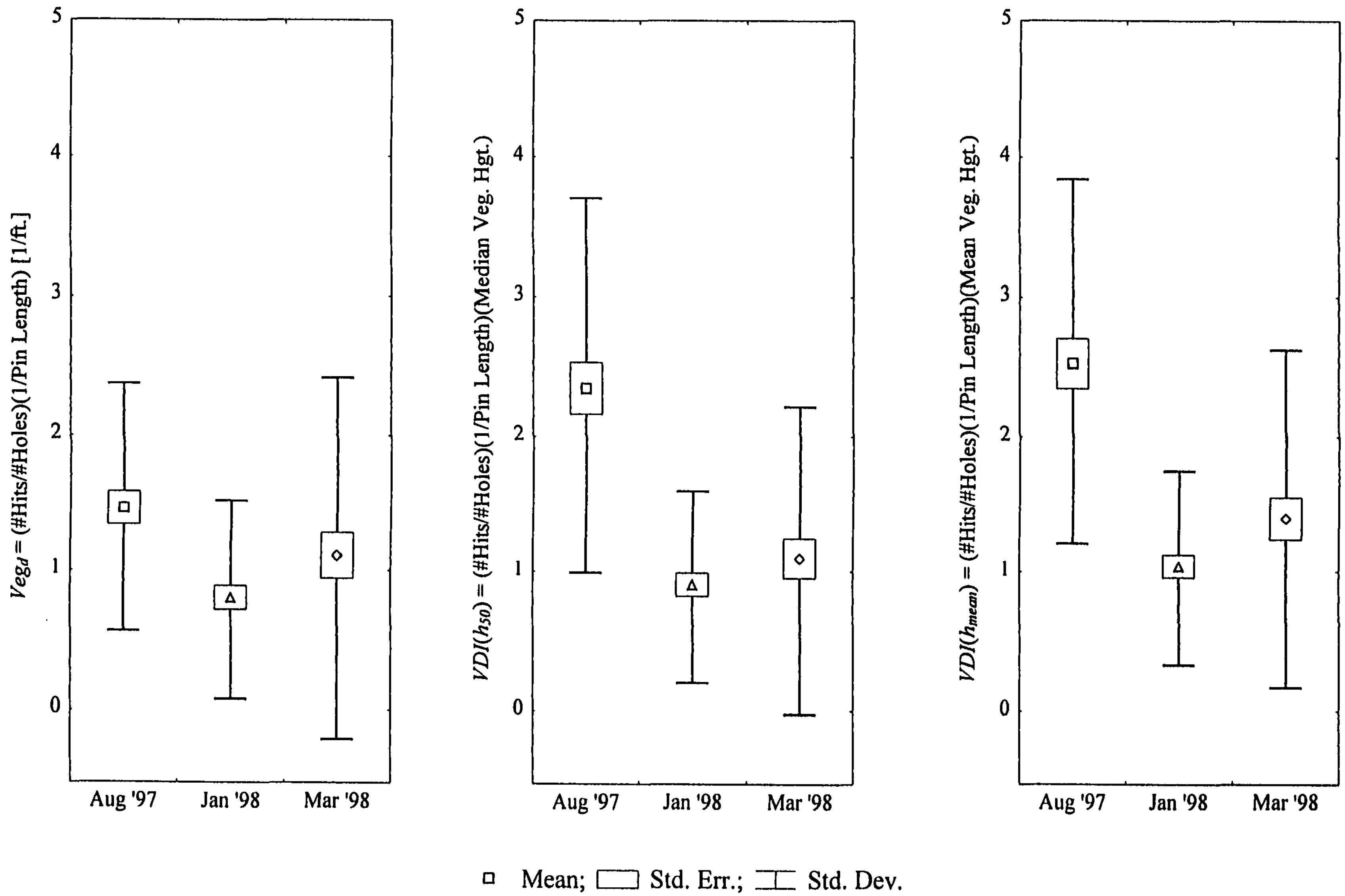

Figure 5.11 – Comparison of season-averaged *VDI's*.

5.5 Results and Analysis from Physical Model (Flume) Study

Detailed descriptions of the flume, the tests that were performed, and the data derived from the model study were presented in Section 3.6. Presented in the following paragraphs are the results and an analysis of the data derived from the model study.

Three flow conditions, each with a particular discharge and depth, were targeted for use in the flume (Section 3.6.5). For each of the targeted flow conditions, different dowel configurations were tested and the results were compared. To facilitate making comparisons among tests performed under the same targeted flow conditions, calculated depth-averaged velocities, $U_x(z)$, were divided by the depth-averaged velocity at the toe of slope, $U_x(z_{toe})$, where z is the distance from the left edge of the flume to the vertical line at which the depth-averaged velocity was computed. Computed values of $U_x(z)/U_x(z_{toe})$ are referred to herein as relative velocities. Plots of $U_x(z)/U_x(z_{toe})$ versus z are presented throughout this section. The dashed lines in each plot indicate areas where the depth-averaged velocity was interpolated or assumed in accordance with procedures described in Appendix B.

5.5.1 Test to Verify Uniformity of Flow

Two model study tests were performed for the purpose of verifying that approximately uniform flow was occurring at the test section of the flume (Flume Sect. 2 in Figure 3.7). This was necessary to verify that the velocity data being recorded would have general value, i.e., to verify that the data did not reflect only local conditions in the flume. To test for uniformity, point velocity measurements were made at Flume Sect. 1 and Flume Sect. 2 under similar hydraulic conditions and with no dowels present. From the recorded measurements, relative velocities were computed and results for both flume sections were plotted together for comparison (Figure 5.12). The relative velocities are within 13% of each other and it is concluded, therefore, that flow at Flume Sect. 2 can be considered uniform.

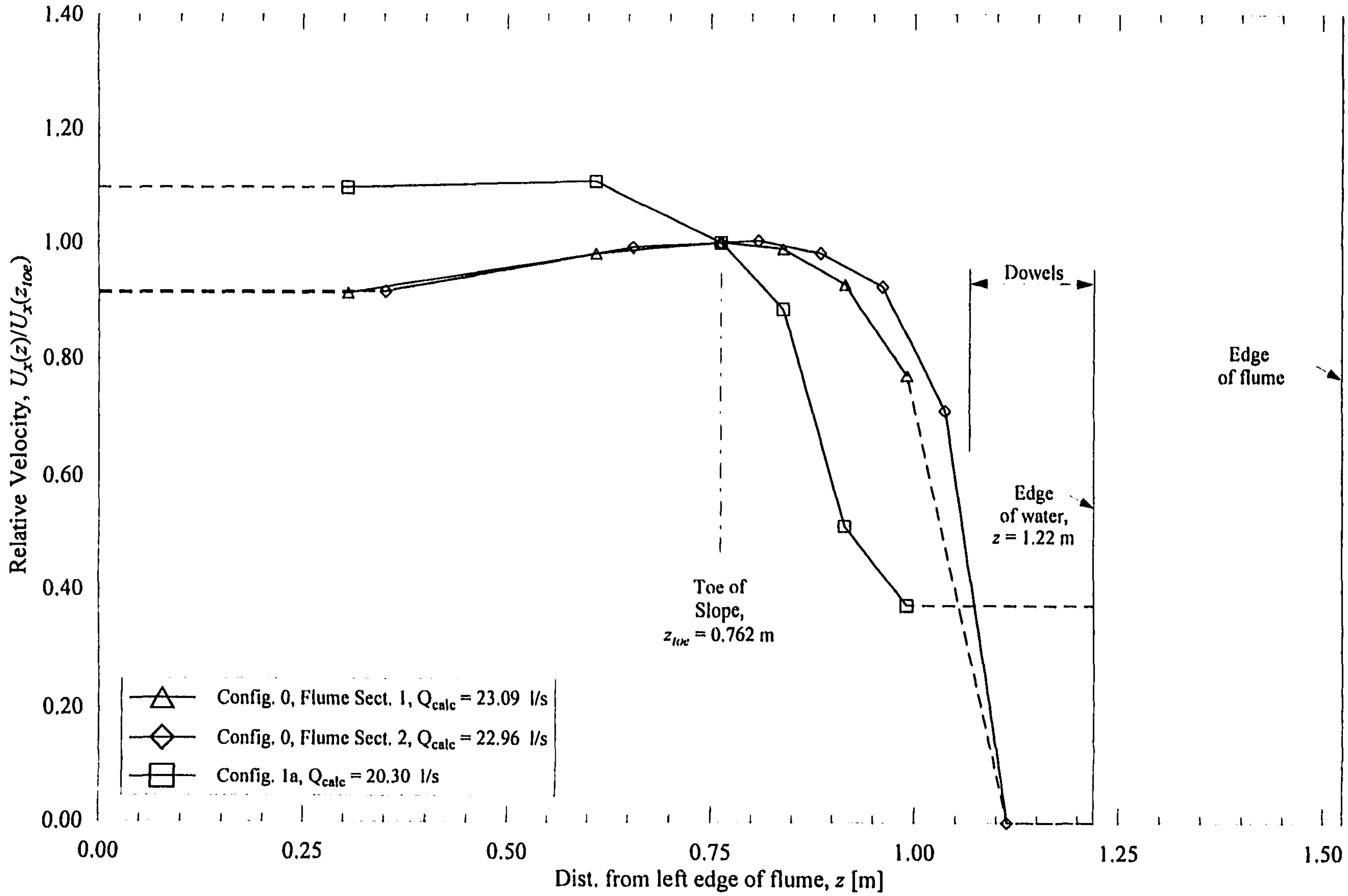

Figure 5.12 – Plot of depth-averaged velocity for base flow conditions (Configuration 0) and dowel Configuration 1a. Nominal depth = 22.9 cm (0.75 ft).

5.5.2 Impact of Dowels on Depth-Averaged Velocity Distribution

Figure 5.12 to Figure 5.14 show that the presence of dowels in the flume significantly alters flow patterns therein. Compared to the no-dowels condition (Configuration 0), velocities atop the bank are much smaller when dowels are present. The effect that dowels have on velocities over the bed of the flume is less clear.

Referring to Figure 5.14, a comparison of relative velocities for Configuration 1b, three rows of 10.16-cm- (4.0-in.-) tall dowels, not staggered, and Configuration 3, three rows of 10.16-cm- (4.0-in.-) tall dowels, staggered, indicates that staggering the dowels does not significantly reduce velocities over the bank as suggested in previous studies, i.e., Schiechtl and Stern (1997), Petryk (1969), and Li and Shen (1973). On the contrary, the rectangular configuration resulted in a 16% lower relative velocity at the center row of dowels, compared to the staggered configuration.

In Figure 5.14 the relative velocity profile for Configuration 1a, three rows of 24.13-cm- (9.5-in.-) tall dowels, not staggered, indicates that the height of the dowels greatly decreases depth-averaged velocities atop the bank. Among the tested configurations, Configuration 1a has the lowest relative velocity at the center row of dowels, which is 18% less than the second lowest velocity and 60% less than the Configuration 0 velocity.

If only differences in relative velocity of 20% or more are considered significant, then a comparison of the relative velocity profiles in Figure 5.14, at the row of dowels located 1.143 m (3.75 ft) from the left edge of flume indicates the following:

1) Configuration 1a yields a significantly lower relative velocity than Configuration 3 (32%).
2) The relative velocity yielded by Configuration 1a is not significantly less than the relative velocities yielded by either Configuration 1b (18%) or Configuration 2 (19%).

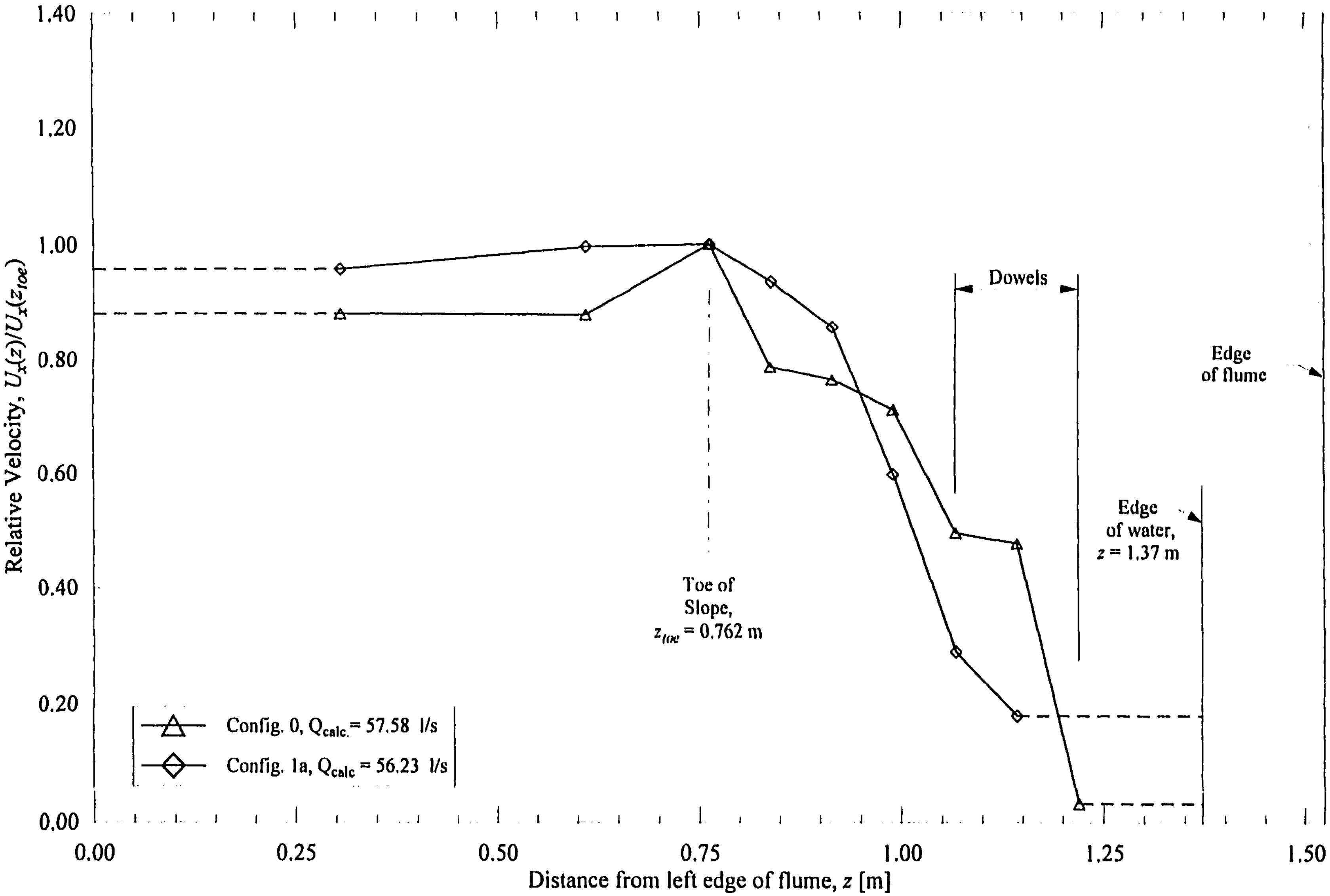

Figure 5.13 – Plot of depth-averaged velocity for base flow conditions (Configuration 0) and dowel Configuration 1a. Nominal depth = 30.5 cm (1.00 ft).

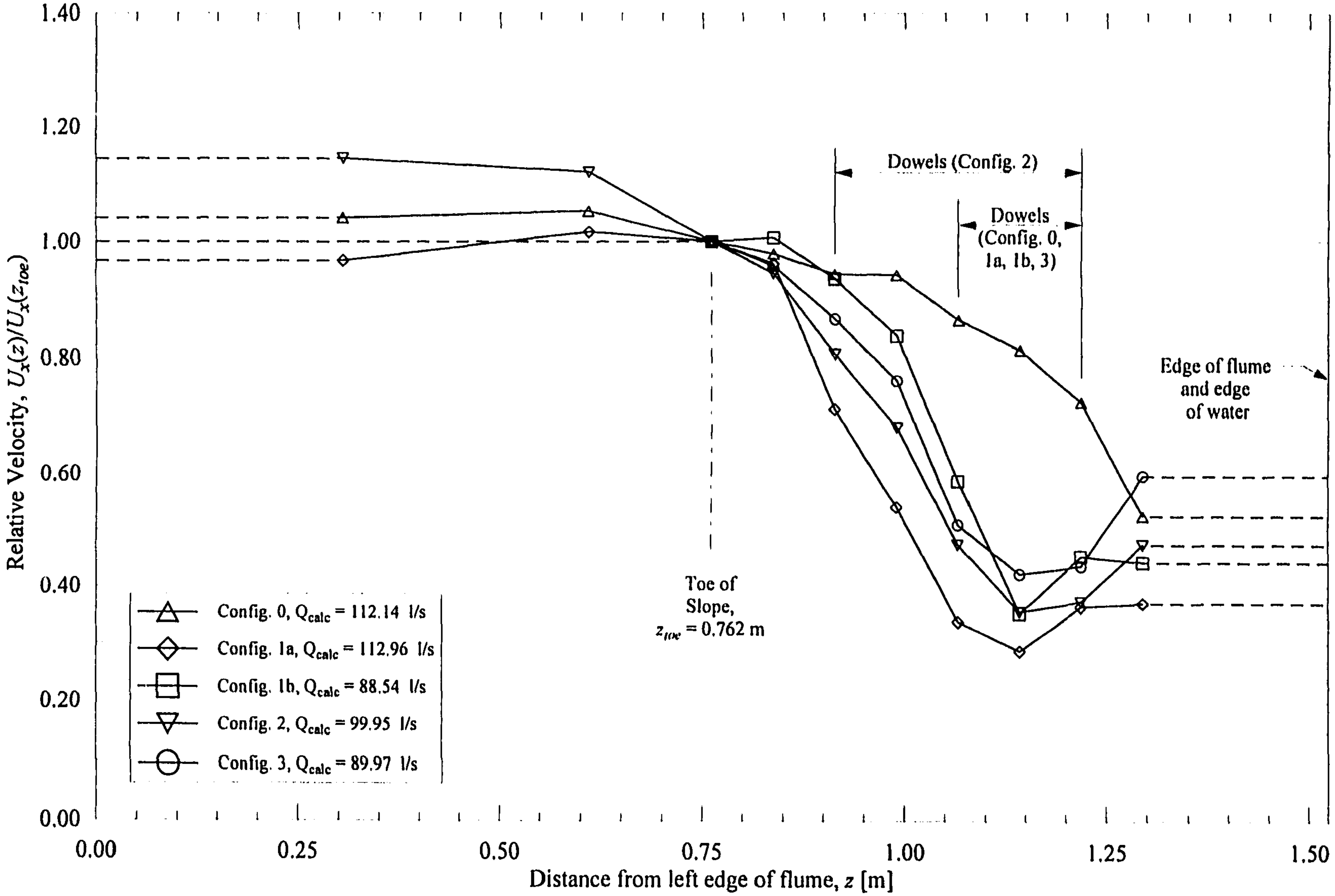

Figure 5.14 – Plot of depth-averaged velocity for base flow conditions (Configuration 0) and dowel Configurations 1a, 1b, 2, and 3. Nominal depth = 38.1 cm (1.25 ft).

3) The relative velocities yielded by Configurations 1b and 2 are not significantly lower than the relative velocity yielded by Configuration 3 (16% for both).

4) All of the dowel configurations yield significantly lower velocities than Configuration 0 (by 57% on average).

The high relative velocity in the flume bed for Configuration 2 is a result of blockage to flow (there are five rows of dowels in Configuration 2 compared to three rows for the other tests). Since the water surface elevation and discharge were controlled during the flume tests, an increase in blockage atop the bank necessarily results in an increase in velocity atop the bed.

From Figure 5.14 it can be seen that relative velocities over the bed of the flume are not directly related to relative velocities atop the bank. That is, an increase in velocity over the flume bed does not directly indicate how velocities atop the bank are affected by a particular dowel configuration. In Figure 5.14, note that Configuration 2 yields the greatest relative velocity in the main channel but not the smallest velocity atop the bank. In contrast, the relative velocities for Configuration 1a are smaller atop the bed and bank than any of the other relative velocities.

5.5.3 Distribution of Flow Over The Bed Versus The Bank

The calculated discharges (Q_{calc}) from the flume tests (Table 4.10 to Table 4.19) were divided into two parts: flow over the bed of the flume (Q_{bed}) and flow over the bank (Q_{bank}). Given a particular nominal flow depth, the percentage of the total flow passing over the bank can be used as a basis for comparing the influence of the different dowel configurations tested in the flume. Among the dowel configurations tested at a flow depth of 38.1 cm (1.25 ft) the following observations are noted:

1) Configuration 2 has the smallest value of Q_{bank} / Q_{calc} (23.0%)

2) Configuration 1a has the second smallest value of Q_{bank} / Q_{calc} (23.4%)

3) Configuration 3 has the third smallest value of Q_{bank} / Q_{calc} (26.6%)

4) Configuration 1b has the fourth smallest value of Q_{bank} / Q_{calc} (27.0%)

5) Configuration 0 yields the largest value of Q_{bank} / Q_{calc} (29.3%)

The results listed above indicate that Configurations 1a and 2 yield comparable values of Q_{bank} / Q_{calc}; likewise for Configurations 1b and 3.

5.5.4 Effect of Dowel Configuration on Roughness Coefficients

The geometry of the flume, measured water surface elevations, and calculated discharge values were used to calculate *n*-values for each test performed in the flume as described in Section 3.6.7. It was anticipated that the calculated *n*-values would vary, principally as a function of the dowel configuration since the bed and bank materials were the same for every test performed in the flume. What was observed instead was that the *n*-values vary inversely with the cross-section-averaged velocity, even for those tests in which there were no dowels in the flume (Figure 5.15). It is concluded from this analysis that grain resistance caused by the bed and bank material and/or form roughness due to the formation of ripples on the bank are primarily responsible for the total resistance to flow.

5.5.5 Transverse Velocity Gradients

The shear stress near a channel bed due to a viscous fluid is typically defined as (Julien, 1995):

$$\tau_{xy} = \mu \frac{du_x}{dy} \tag{5.3}$$

where μ is the dynamic viscosity of the fluid, the *x*-axis is parallel to the principal direction of flow, the *y*-axis is vertical, and u_x is the time averaged velocity at a fixed point in space (Figure 5.16). It follows that for the side slope in a channel or flume there

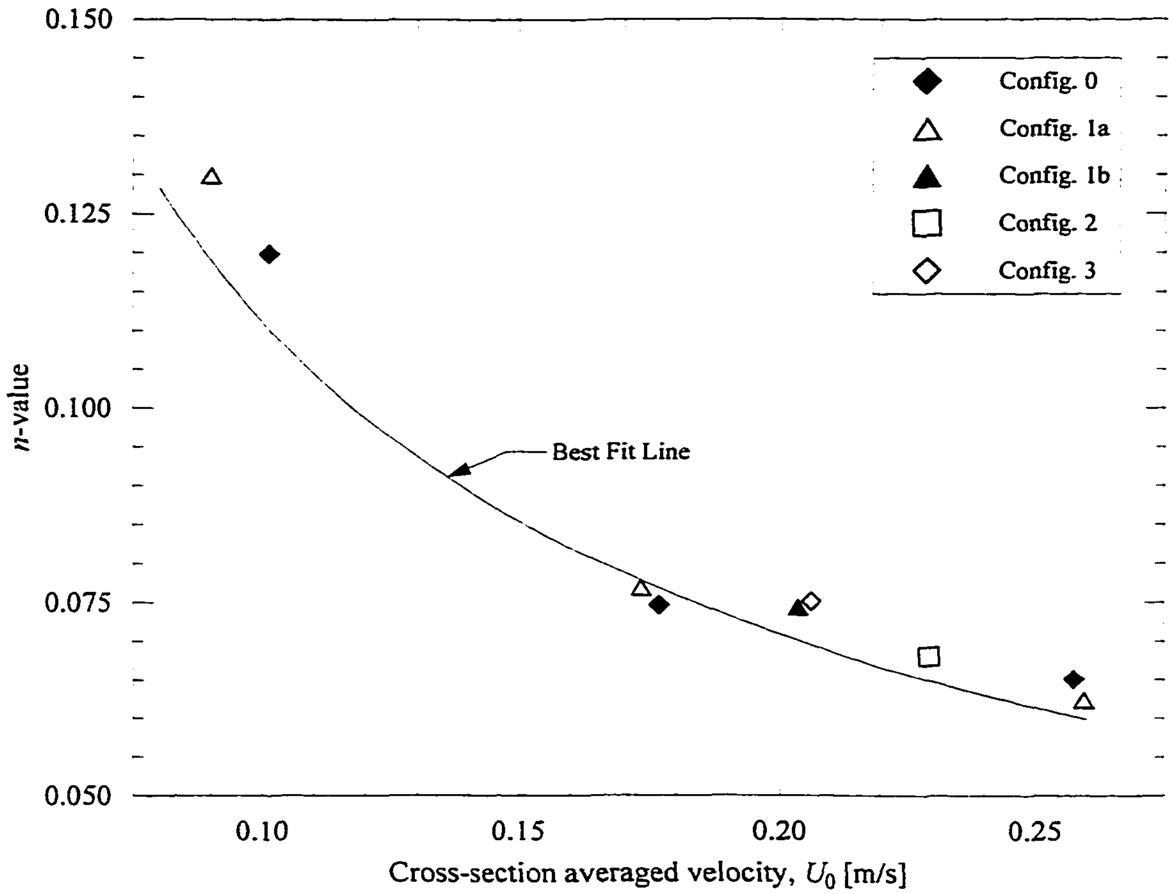

Figure 5.15 – Plot showing calculated n-value for different dowel configurations versus velocity.

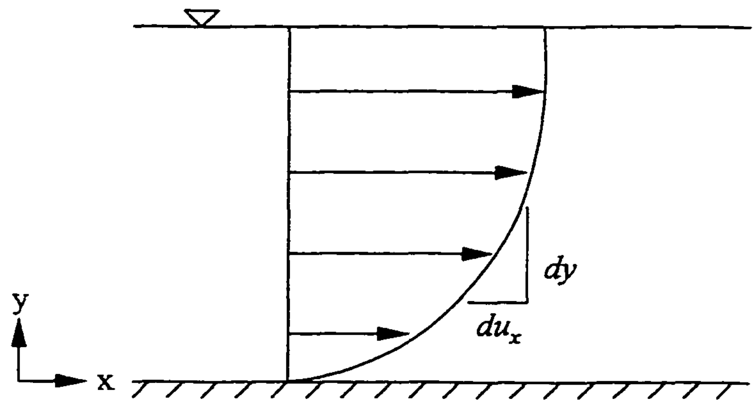

(a) Elevation View

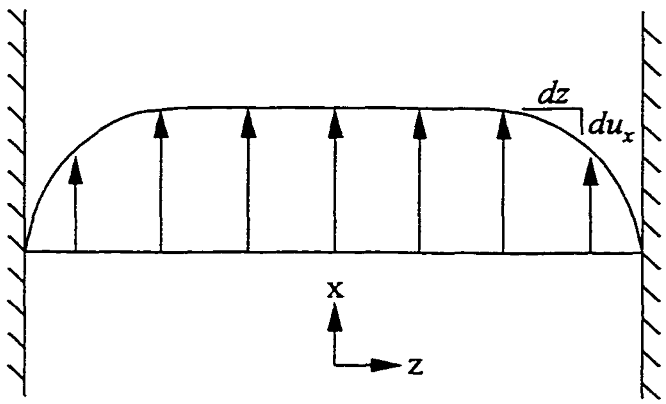

(b) Plan View

Figure 5.16 – Variable definition sketch for calculating longitudinal shear stress, τ_{xy}.

is a component of shear stress due to the distribution of velocity across the width of the channel. For the side slope in a channel or flume, (5.3) becomes

$$\tau_{xy} = \mu\left(\frac{du_x}{dy} + \frac{du_x}{dz}\right) \tag{5.4}$$

where the z-axis is horizontal and transverse to the principal direction of flow (Figure 5.16).

A noteworthy effect of the dowels on the flow field is to increase the magnitude of the transverse velocity gradient, du_x/dz, atop the bank. From (5.4) it can be deduced that increasing du_x/dz atop the bank means increased shear on the bank unless du_x/dy is proportionately reduced. This matter was not explored experimentally as part of this study but it is clear from Figure 5.12 through Figure 5.14 that the magnitude of du_x/dz is greater when dowels are present. It is implied from these observations that dowels increase the likelihood of toe-scour (i.e., scour at that portion of a stream cross-section where the lower bank terminates and the channel bottom or the opposite lower bank begins).

Figure 5.17 is a photograph of the flume, taken shortly after one of the flume tests (Configuration 1a). A carpenter's ruler was placed on the bank slope and a pencil was placed at that point on the bank exhibiting the greatest amount of general scour. The point is between the channel toe of slope and the row of dowels closest to the toe of slope. Figure 5.17 suggests that toe-scour may be an important process in the success or failure of willow post systems.

The photographs in Figure 5.18 and Figure 5.19 show ripples atop the bank in the flume. The photographs were taken after a test with Configuration 0 (no dowels) and Configuration 1b, respectively. Both tests were performed with a nominal flow depth of 38.1 cm (1.25 ft), and a discharge of about 112 l/s (3.96 cfs). When no dowels are present (Figure 5.18) the crest of each ripple is advance most rapidly about midway up the bank; near the bank toe, the crest is advancing at the slowest rate. The ripple patterns appear to

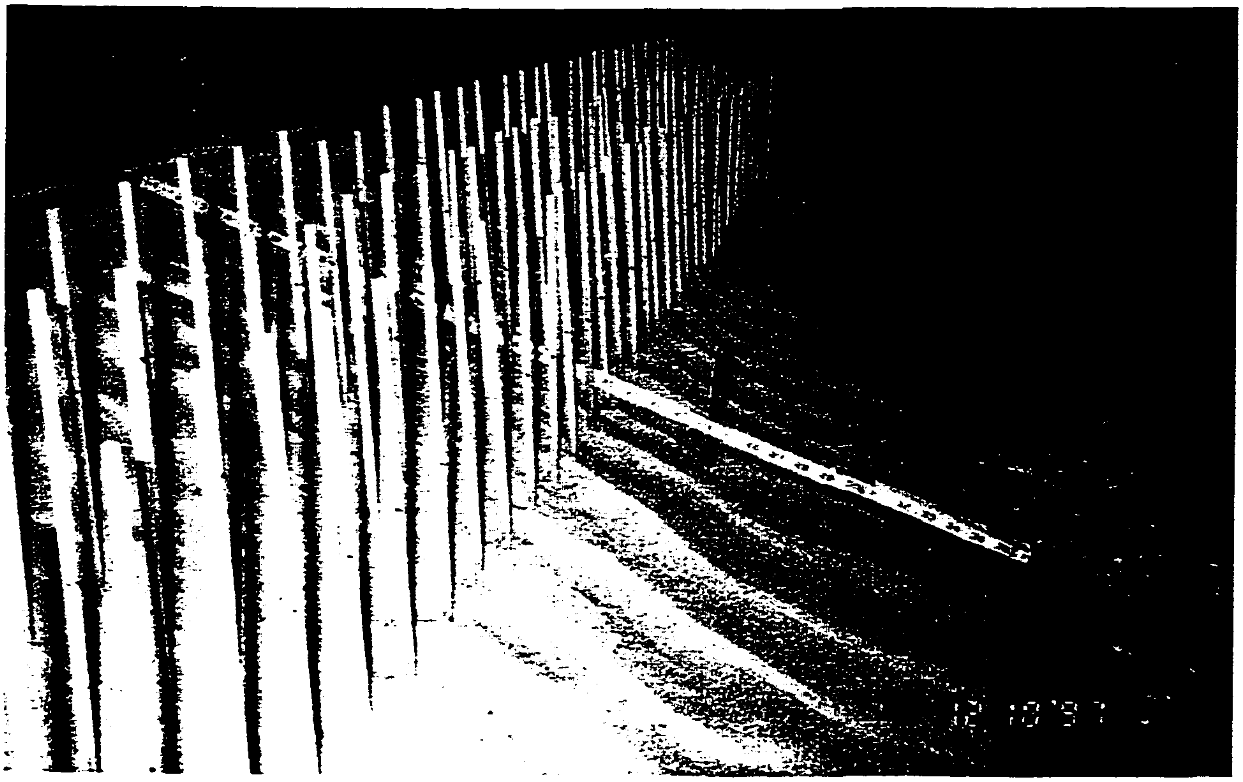

Figure 5.17 – Photograph taken after flume test (Configuration 1a, depth = 38.1 cm, discharge = 112.96 l/s). The pencil indicates the location of maximum scour along the bank.

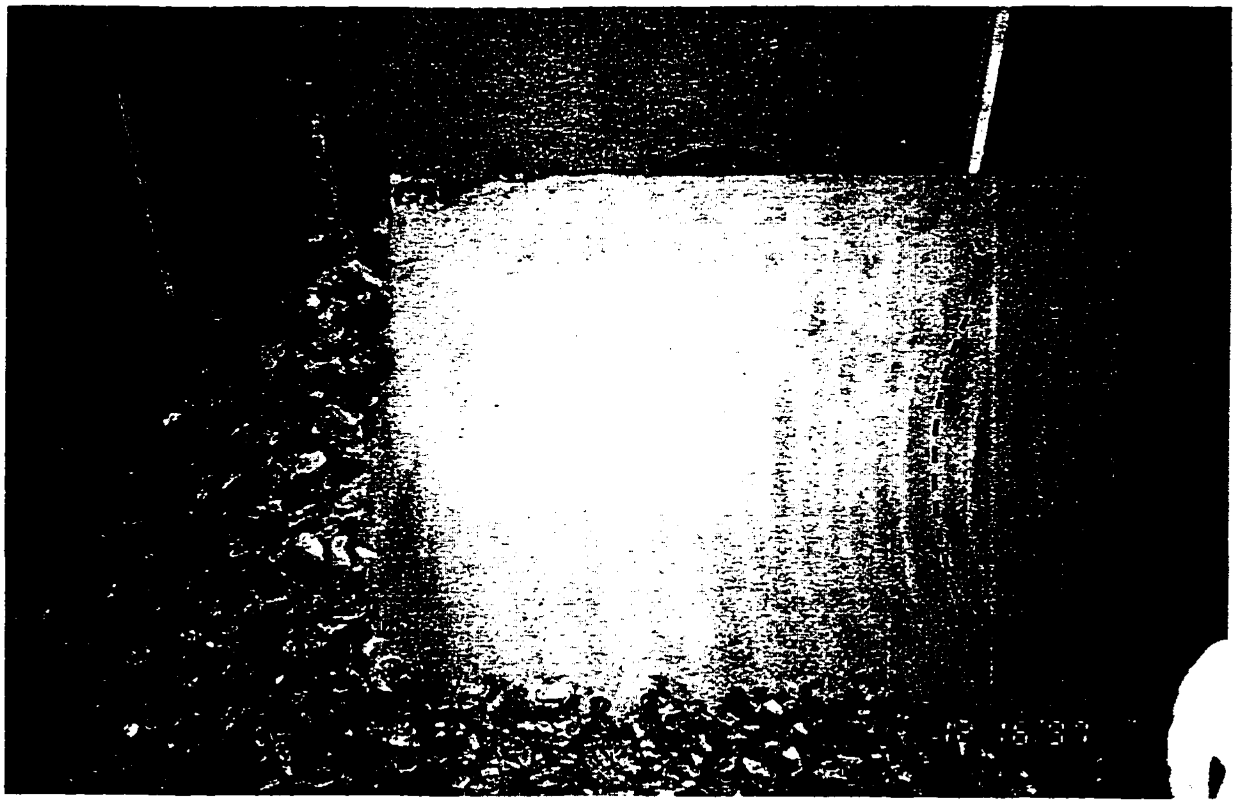

Figure 5.18 – Photograph taken after flume test (Configuration 0, depth = 38.1 cm, discharge = 112.14 l/s). Note that the crest of the ripples form smooth bows with an apex about midway up the bank.

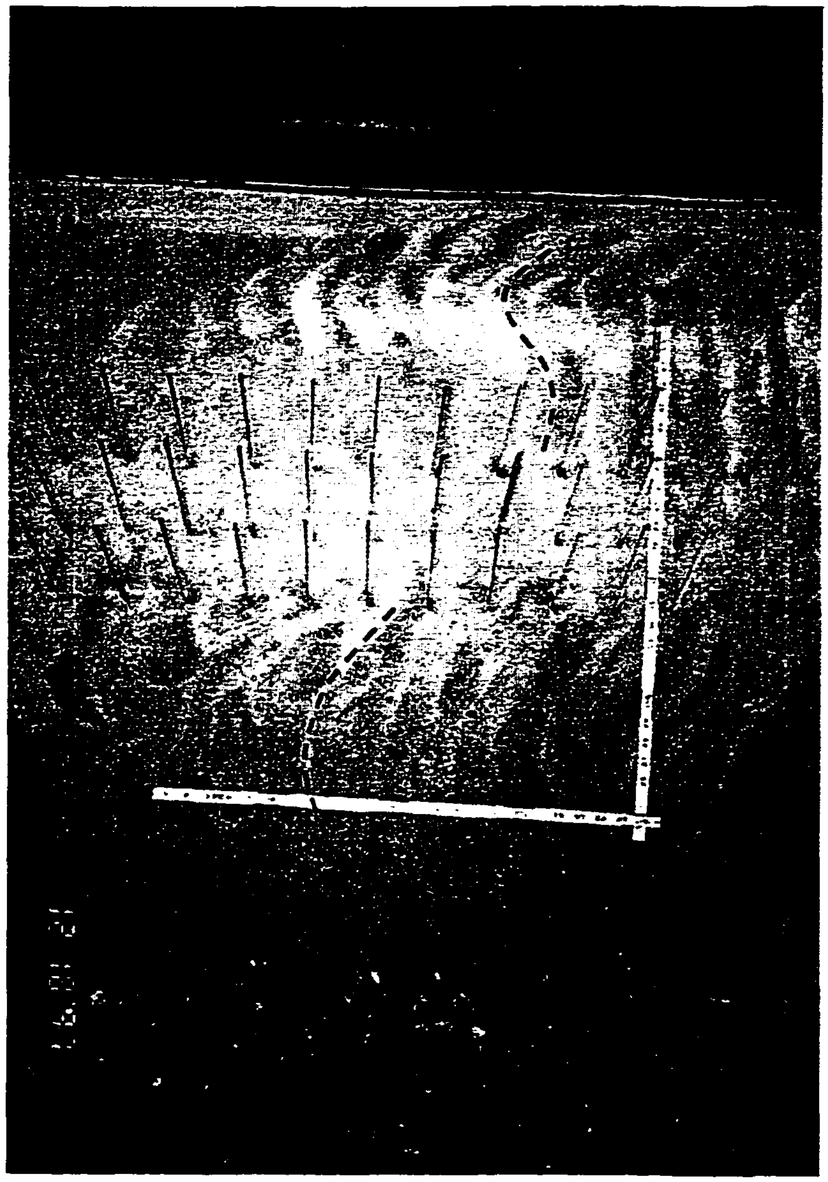

Figure 5.19 – Photograph taken after test flume (Configuration 1a, depth = 38.1 cm, discharge = 112.96 l/s). Note that the crest of the ripples form sharp bows with an apex about midway between the toe of slope and the row of dowels closest to the toe of slope.

move in unison over the entire bank. In contrast, when dowels are present (Figure 5.19) the crest of the ripples advance most rapidly about midway between the toe of slope and the row of dowels closest to the toe of slope. The ripple pattern seen in Figure 5.19 suggests, as does Figure 5.17, that toe-scour is an important process in the success or failure of willow post systems.

Using the pattern formed by the crest of the ripples as an indication of the shear stress over the bank, it is concluded that the presence of dowels significantly alters the distribution of stress on the bank. That is, when dowels are present, the point of maximum shear stress along the bank is shifted closer to the bank toe. Based on the observations noted above, it is recommended that consideration be given to the need for toe protection when willow posts are used to stabilize a bank.

5.6 Analytical Models for Flow Through Vegetation (Analysis and Results)

In this section, comparisons are made between computed and predicted depth-averaged velocities. The computed depth-averaged velocities (Section 4.6) were derived from point velocity measurements using procedures described in Appendix B. Predicted depth-averaged velocities were derived from two analytical models. The first model, referred to herein as Petryk's model, was originally developed by Petryk (1969) and Li and Shen (1973) but has been modified so that it can be used to predict velocities through vegetation in trapezoidal channels (Section 3.7.2). The second model was developed in the present research and is referred to as the proposed model (or Wilkerson's model). The proposed model was described in Section 3.7.3. A comparison of results obtained from the two analytical models is presented in Section 5.6.1. The results are discussed in Section 5.6.2.

For comparing the results yielded by Petryk's model and the proposed model, a statistical function called the multiple-partial coefficient of determination, denoted herein as $r^2_{P \cdot W}$ or $r^2_{W \cdot P}$, will be used. The multiple-partial coefficient of determination is the proportional reduction in the variance of prediction errors when one model is used relative to another model (Graybill and Iyer, 1994). Where Petryk's model (P) yields a reduction in the variance of prediction errors relative to Wilkerson's model (W) then $r^2_{P \cdot W}$ will be reported. Conversely, where Wilkerson's model yields a reduction in variance of prediction errors relative to Petryk's model then $r^2_{W \cdot P}$ will be reported.

5.6.1 Computed and Predicted Velocity Profiles

Computed and predicted velocity profiles are presented throughout this section for all flume tests in which the flow depth was either 30.5 cm (1.00 ft) or 38.1 cm (1.25 ft). Among tests for which no dowels were present, the depth-averaged velocity distribution for tests performed at a flow depth of 22.9 cm (0.75 ft) was observed to be markedly different from the velocity distribution yielded by tests performed at higher flow depths (Figure 3.13). Because such different velocity distributions were yielded, none of the tests conducted at a flow depth 22.9 cm (0.75 ft) were modeled analytically. It is noted that the likely reason that the velocity profiles deviate when the flow depth is 22.9 cm (0.75 ft) is because of the variable relationship between grain-size (d_{50}) resistance and flow depth (d) when the ratio d/d_{50} is less than 100 (Julien, 1995).

Except for flume tests performed with dowel Configuration 1a, the dowel configurations and flow conditions tested in the flume violate, to a greater or lesser extent, the analytical model assumption that each cylindrical element protrudes through the water surface (Section 3.7.5). Those flume tests in which there were submerged dowels are modeled herein, in spite of violating a model assumption, because the results yield information about the robustness of the models being used.

5.6.1.1 Configuration 1a, Depth = 38.1 cm, Discharge = 112.96 l/s

Plotted in Figure 5.20 are predicted velocity profiles that were derived using Petryk's model and the writer's model, for Configuration 1a [three rows of 24.1-cm- (9.5-

in.-) tall dowels]. Corresponding depth-averaged velocities, computed from flume test data, are also plotted in the figure. The predicted and computed velocities are for a nominal flow depth of 38.1 cm (1.25 ft) and a discharge of 112.96 l/s (3.99 cfs).

In the vicinity of the dowels, the velocity profile predicted by Petryk's model exhibits several interesting characteristics. Directly behind each row of dowels, the velocities predicted using Petryk's model are fairly close to velocities observed in the flume (1.5% difference on average). Between the dowels, Petryk's model predicts that the depth-averaged velocity is as much as 77% greater than the predicted velocity for points directly behind the dowels. Also, between the toe of slope and the first row of dowels, predictions derived from Petryk's model differ from the computed velocities by 22% on average.

Velocities predicted by the writer's model show fair agreement with the computed velocities. Directly behind the three rows of dowels, the average prediction error is 1.3% of the computed velocity. Between the toe of slope and the first row of dowels, the average prediction error is 8% of the computed velocities. The multiple-partial correlation coefficient for the two models, $r^2_{W|P}$, is 0.68.

Calculated depth-averaged velocities from this flume test were used to calibrate the writer's model. The concurrence between the computed and predicted velocities, thus, is biased. In the remaining comparisons between predicted and computed velocities, the predicted velocities are independent of the computed velocities and the results, therefore, are completely objective.

5.6.1.2 Configuration 1a, Depth = 30.5 cm, Discharge = 56.23 l/s

In Figure 5.21 depth-averaged velocity profiles predicted using Petryk's model and the writer's model with Configuration 1a [three rows of 24.1-cm- (9.5-in.-) tall dowels] are plotted. Computed velocities derived from the flume study are also

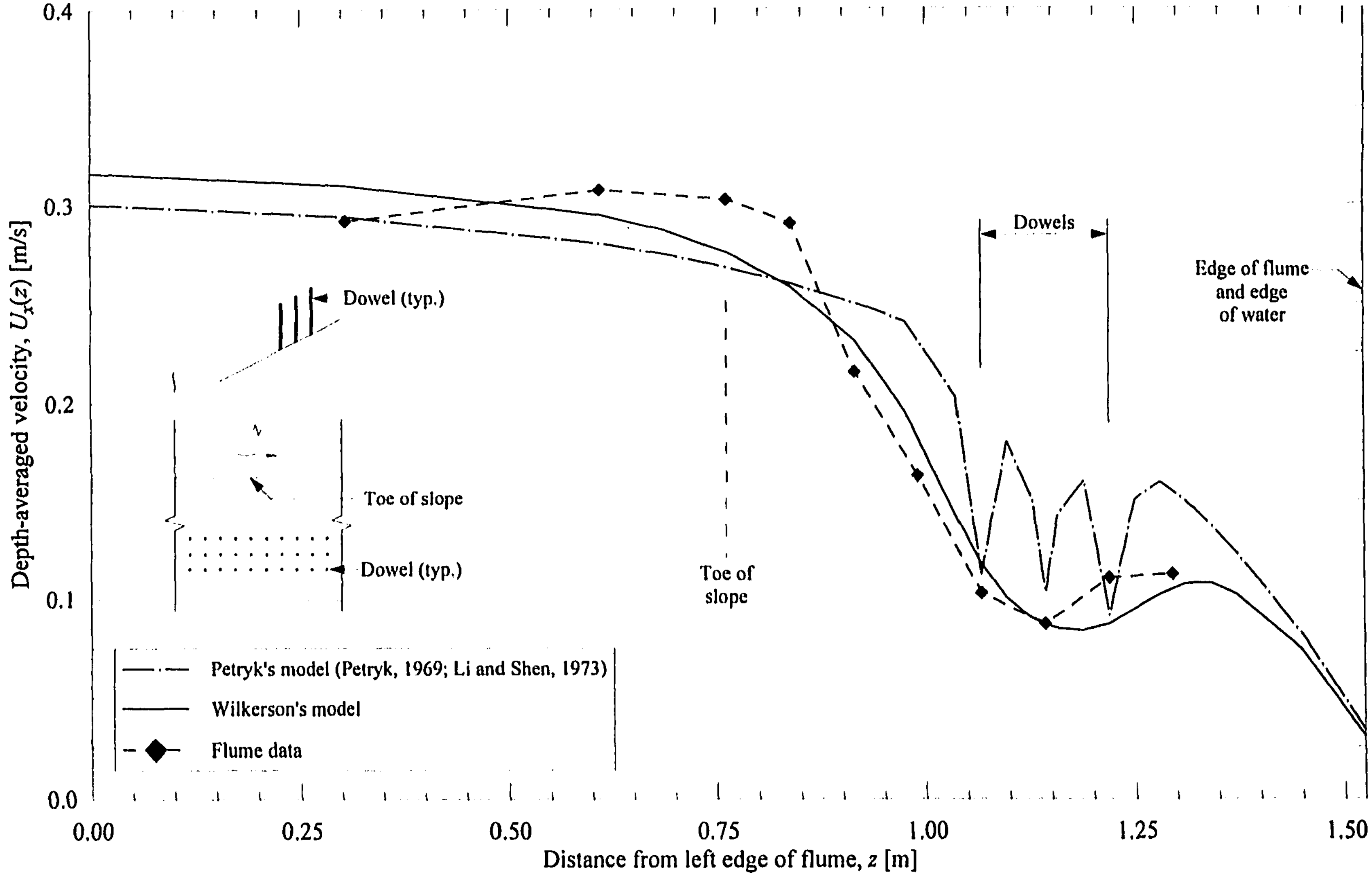

Figure 5.20 – Predicted and calculated depth-averaged velocity profiles for Configuration 1a (nominal depth = 38.1 cm, and discharge = 112.96 l/s).

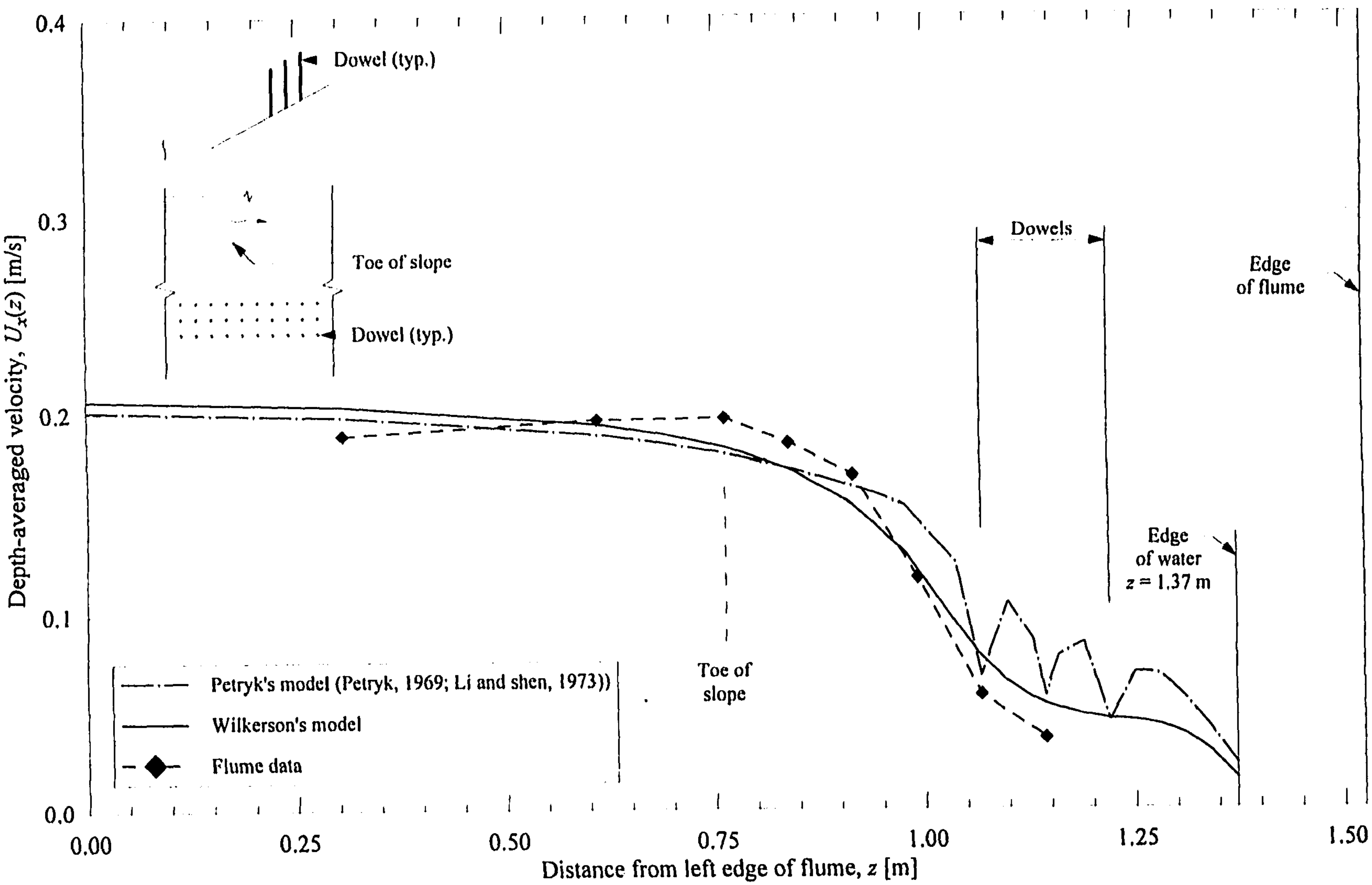

Figure 5.21 – Predicted and calculated depth-averaged velocity profiles for Configuration 1a (nominal depth = 30.5 cm, and discharge = 56.23 l/s).

plotted. The velocity profiles are for a nominal flow depth of 30.5 cm (0.75 ft) and a discharge of 56.23 l/s (1.99 cfs).

The velocity distribution predicted by Petryk's model indicates a substantial increase in velocity between rows of dowels (up to 86% greater than predicted velocities for points behind the dowels). Directly behind each row of cylinders, the velocity's yielded by Petryk's model follow the trend observed in the flume but the velocities defects behind the cylinder are underestimated by 1.5% on average. The velocity profile yielded by the writer's model is similar to the profile derived by using Petryk's model at points directly behind the dowels and over the channel bed. Directly behind the dowels the average prediction error yielded by the writer's model is 1.8%. Between the toe of slope and the nearest row of dowels, velocities predicted by the writer's model and Petryk's model are within 11% and 12% on average, respectively. A comparison of prediction errors for the models yields $r^2_{W|P} = 0.27$.

5.6.1.3 Configuration 1b, Depth = 38.1 cm, Discharge = 88.54 l/s

Presented in Figure 5.22 are predicted velocities from Petryk's model and the writer's model along with computed velocities from the flume study for Configuration 1b [three rows of 10.2-cm- (4.0-in.-) tall dowels in a rectangular grid; nominal depth = 38.1 cm (1.25 ft), discharge = 88.54 l/s (3.13 cfs)].

Directly behind the dowels Petryk's model and the writer's model yield average prediction errors of 22% and 24%, respectively, of the computed velocities; both models underestimated velocity behind the cylinders. Between rows of dowels, Petryk's model predicts velocity increases of up to 77%, relative to predicted velocities behind the dowels. Between the toe of slope and the first row of dowels, Petryk's model and the writer's model yield average prediction errors of 9.4% and 20%, respectively, of the computed velocities. The writer's model consistently underestimated velocities between

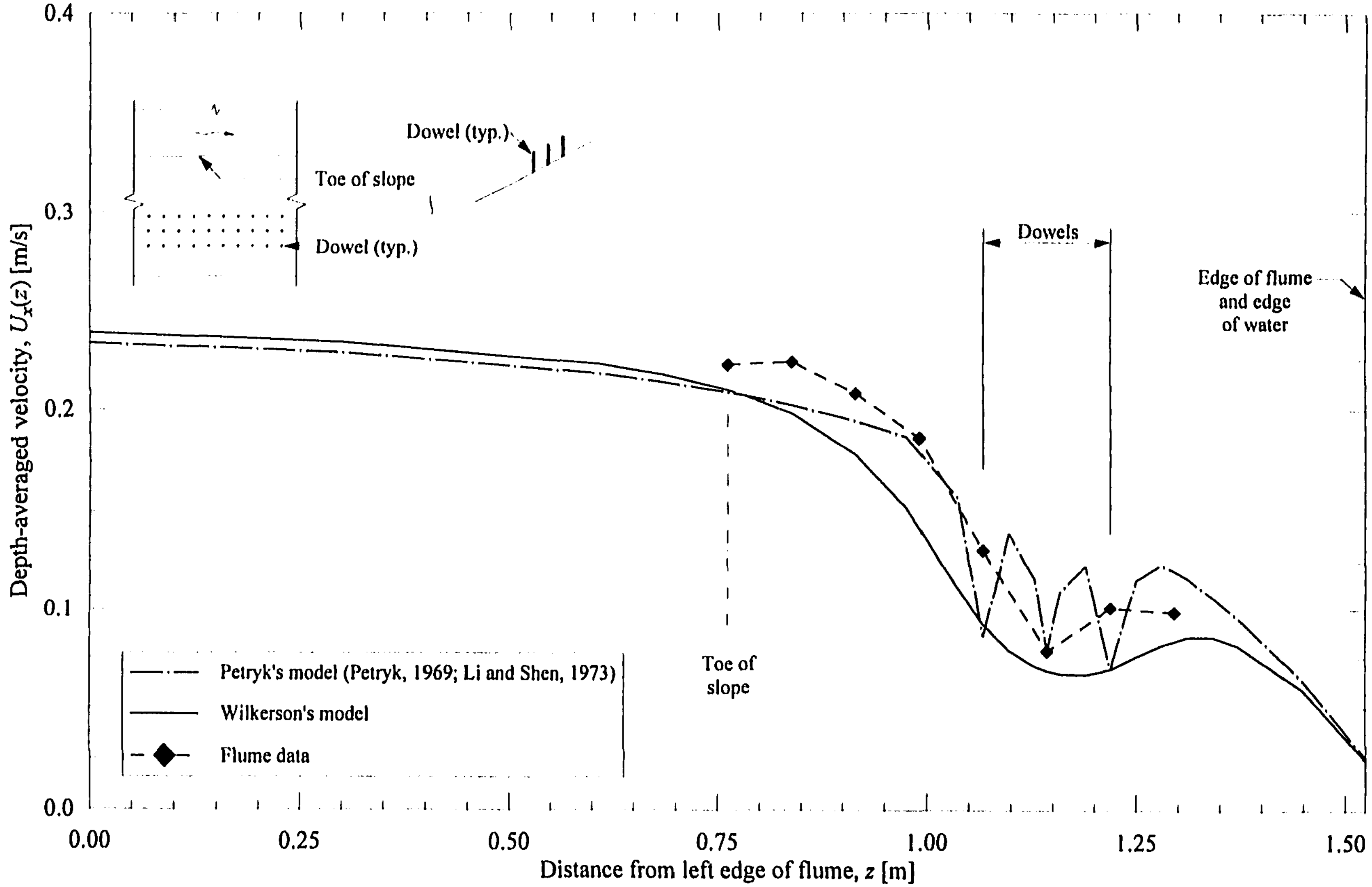

Figure 5.22 – Predicted and calculated depth-averaged velocity profiles for Configuration 1b (nominal depth = 38.1 cm, and discharge = 88.54 l/s).

the toe of slope and the first row of dowels. A comparison of prediction errors for the models yields $r^2_{P|W} = 0.33$.

All three rows of dowels were submerged for this test thus violating an assumption of the analytical models. Differences between the computed and predicted depth-averaged velocities are larger for this configuration in comparison to results for Configuration 1a. The larger prediction errors are presumed to be in response to the violated assumption.

5.6.1.4 Configuration 2, Depth = 38.1 cm, Discharge = 99.95 l/s

Presented in Figure 5.23 are predicted velocities from Petryk's model and the writer's model along with calculated depth-averaged velocities from the flume study for Configuration 2 [nominal depth = 38.1 cm (1.25 ft), discharge = 99.95 l/s (3.53 cfs)]. In Configuration 2, five rows of dowels were used. The two rows of dowels closest to the water were 5.08 cm (2.0 in.) in height and the remaining three rows were 10.16 cm (4.0 in.) in height.

Between rows of dowels, velocities predicted by Petryk's model show increases in velocity of up to 115%, relative to velocities predicted for points directly behind the dowels. Behind the taller dowels, velocities predicted by Petryk's model are within 13% of the calculated velocities, whereas behind the shorter dowels the predicted velocities are up to 46% smaller than the calculated velocities. The corresponding values for the writer's model are 49% and 68%, respectively. Prediction errors from the models were compared and yielded $r^2_{P|W} = 0.46$.

5.6.1.5 Configuration 3, Depth = 38.1 cm, Discharge = 89.87 l/s

Plotted in Figure 5.24 are predicted depth-averaged velocities from Petryk's model and the writer's model as well as calculated depth-averaged velocities from the flume study for Configuration 3 [nominal depth = 38.1 cm (1.25 ft), discharge = 89.87 l/s

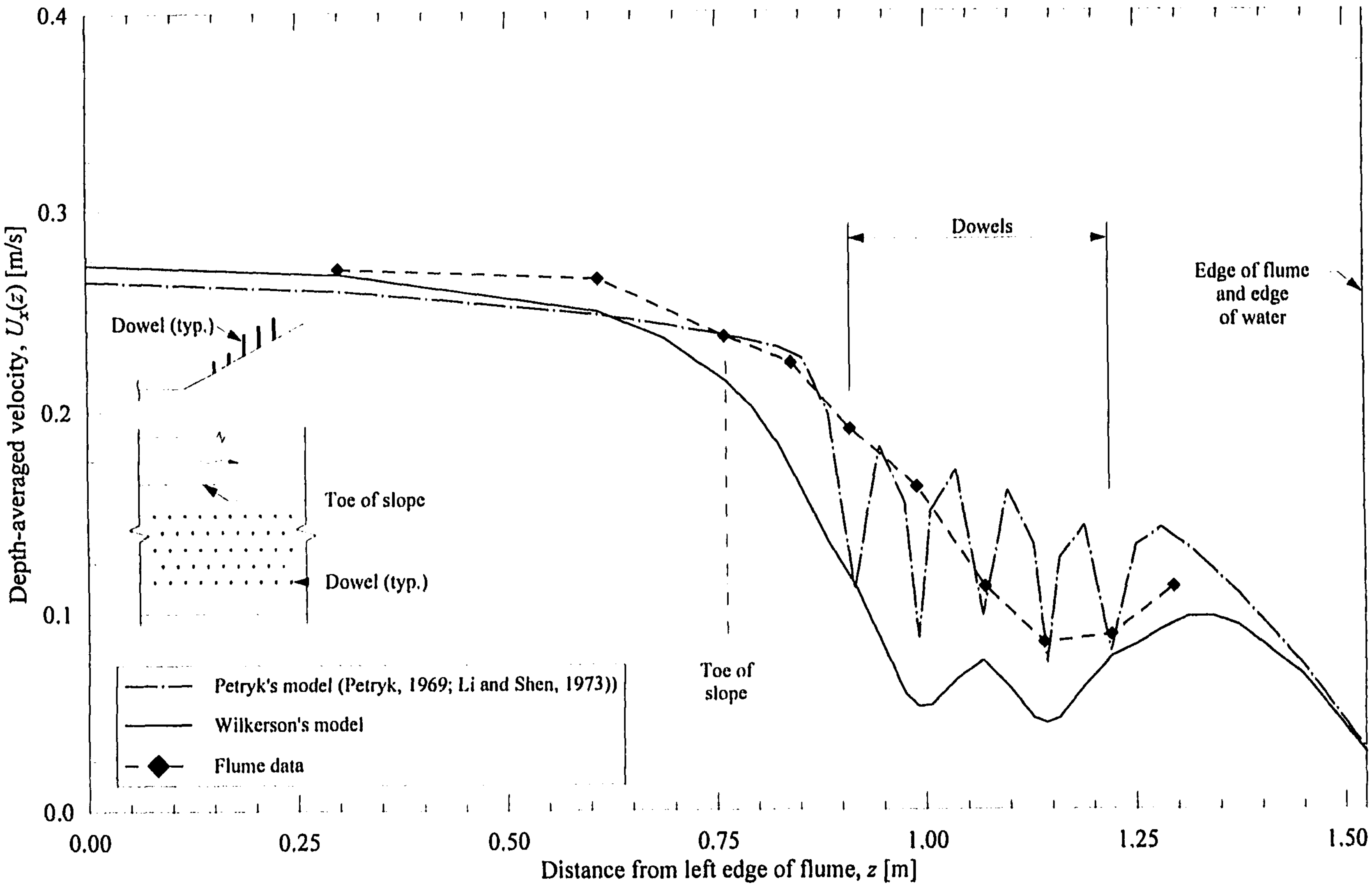

Figure 5.23 – Predicted and calculated depth-averaged velocity profiles for Configuration 2 (nominal depth = 38.1 cm, and discharge = 99.95 l/s).

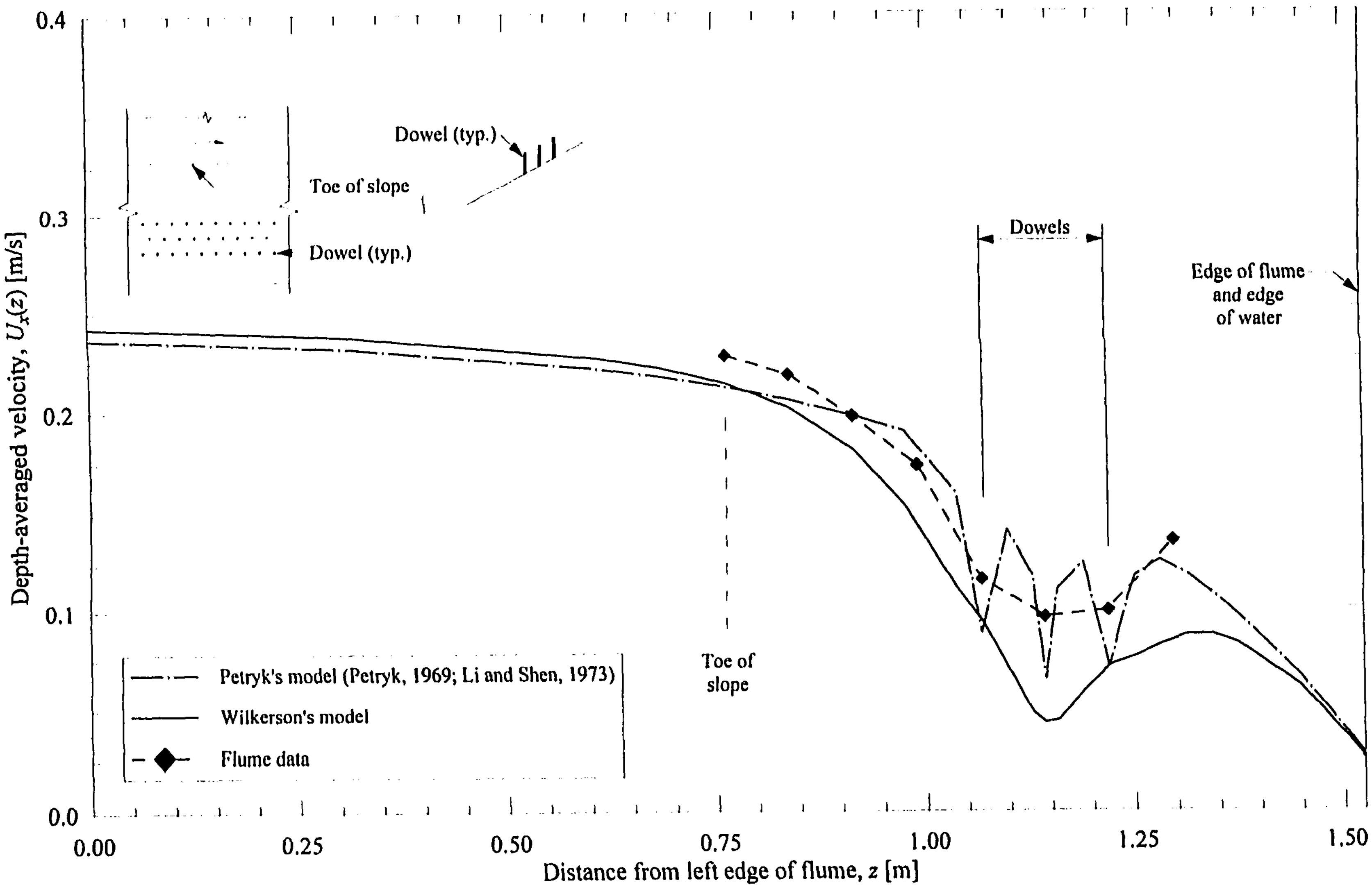

Figure 5.24 – Predicted and calculated depth-averaged velocity profiles for Configuration 3 (nominal depth = 38.1 cm, and discharge = 89.87 l/s).

(3.17 cfs)]. This dowel configuration is comprised of three rows of 10.2-cm- (4.0-in.-) tall dowels; the middle row of dowels is staggered with respect to the first and third rows of dowels (Figure 3.9).

At points directly behind the dowels, the velocities predicted by Petryk's model and the writer's model are smaller than the calculated velocities by 29% and 35% on average, respectively. Both models underestimate velocities behind the dowels. Between the toe of slope and the first row of dowels, the average prediction error for both models is 11%; the writer's model consistently underestimated velocities. Between rows of dowels, results from Petryk's model shows increases in velocities of up to 120% relative to predicted velocities for points directly behind the dowels. Comparing prediction errors from the models yielded $r_{PIW}^2 = 0.61$.

5.6.2 Discussion

In the comparisons presented in Section 5.6.1 it was noted that Petryk's model predicts large increases in depth-averaged velocity between rows of dowels. Results from the proposed model, in contrast, suggest that between rows of dowels, the depth-averaged velocity does not vary. To investigate this matter further, point velocity measurements made atop the bank, in a horizontal-plane located 6.10 cm (0.20 ft) below the water surface (Section 3.6.4.2) were examined. Vector plots of the horizontal-plane point velocity measurements are presented in Figure 5.25, Figure 5.26, and Figure 5.27 for dowel Configurations 1a, 1b, and 3, respectively. Each of the plotted vectors was derived from

$$\bar{u}_{xz} = u_x \mathbf{i} + u_z \mathbf{j} \tag{5.5}$$

and

$$|\bar{u}_{xz}| = \sqrt{u_x^2 + u_z^2} \tag{5.6}$$

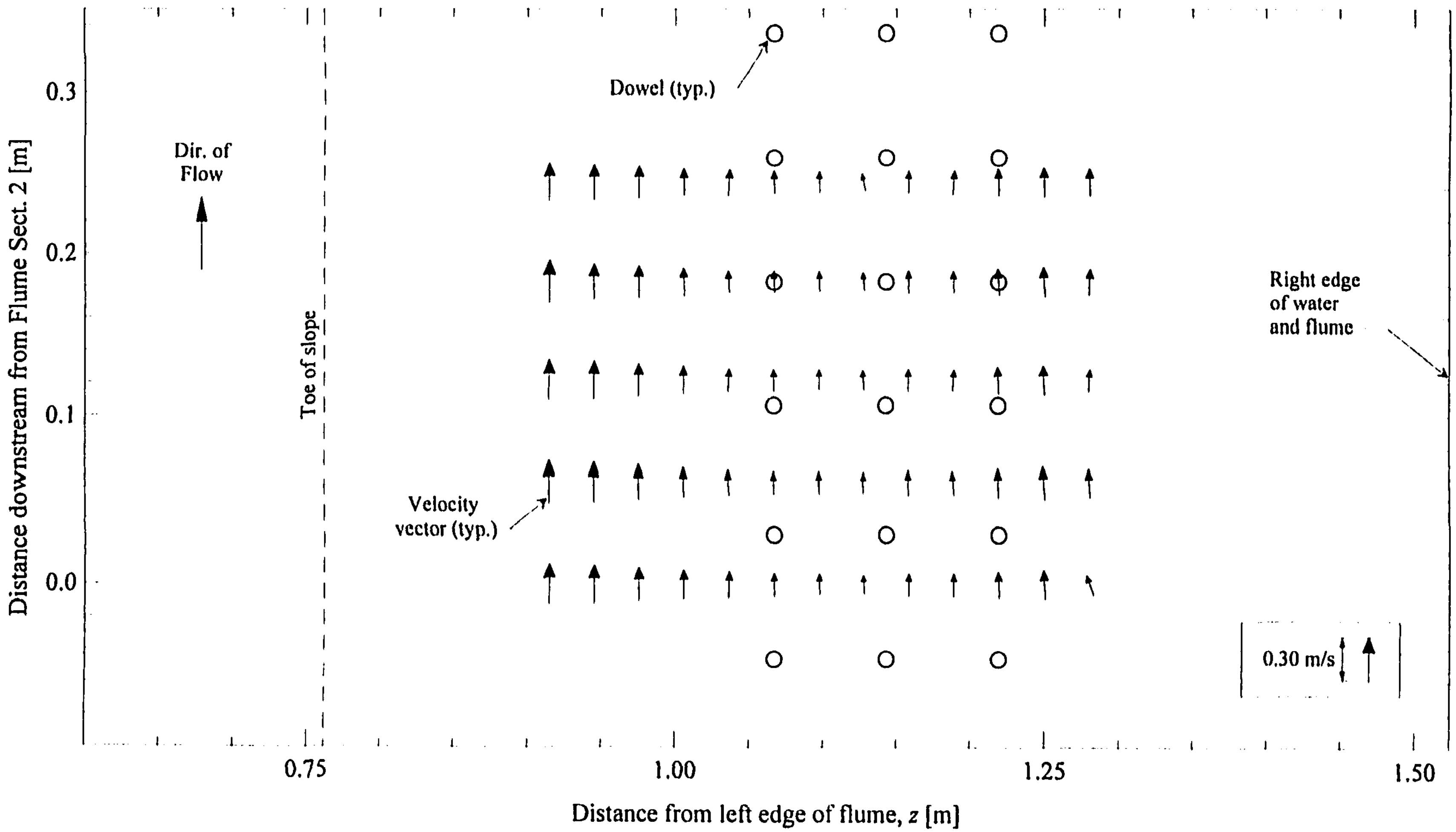

Figure 5.25 – Vector plot showing point velocity measurements taken in horizontal plane for Configuration 1a (nominal depth = 38.1 cm and discharge = 112.96 l/s).

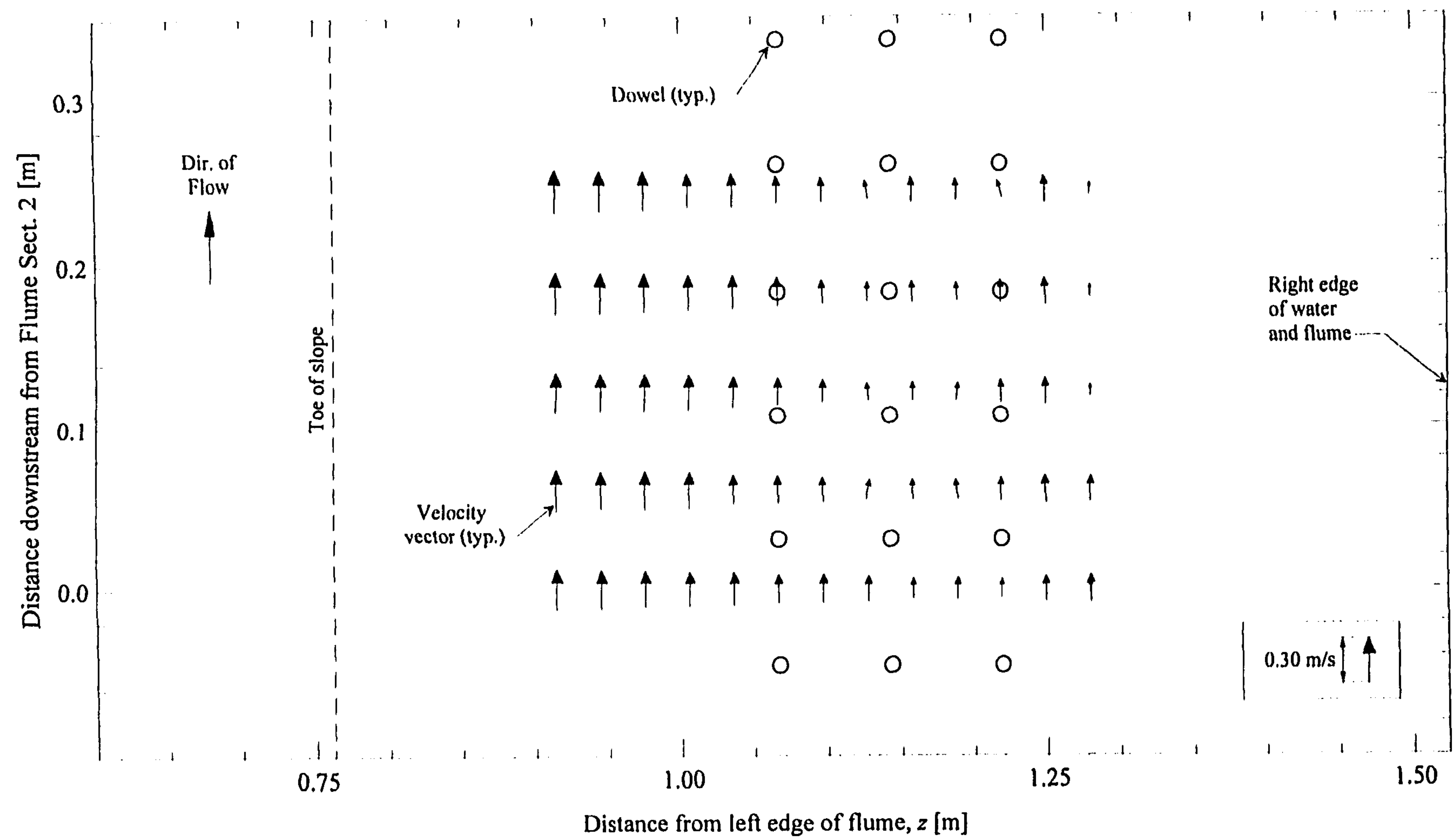

Figure 5.26 – Vector plot showing point velocity measurements taken in horizontal plane for Configuration 1b (nominal depth = 38.1 cm and discharge = 88.54 l/s).

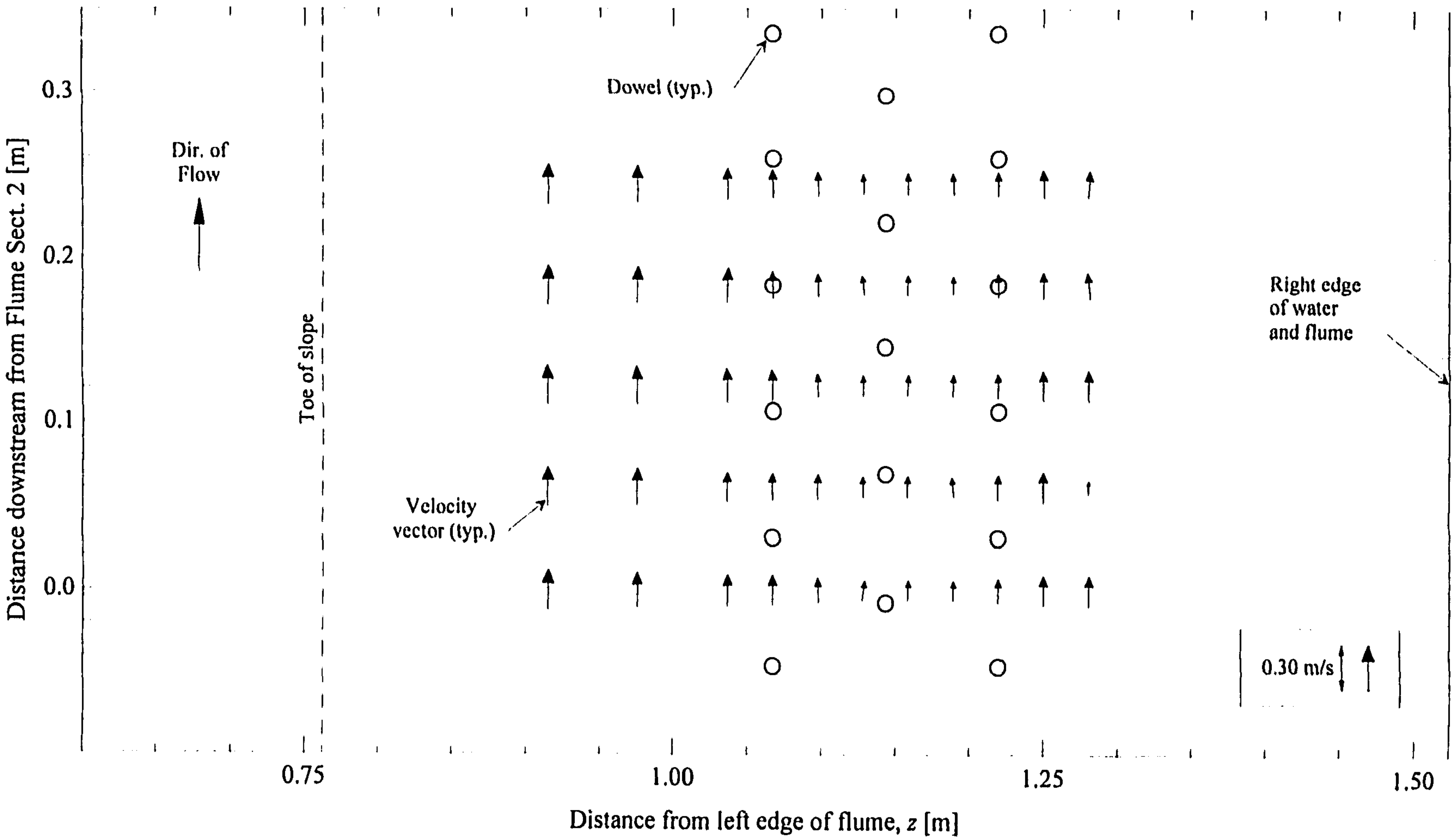

Figure 5.27 – Vector plot showing point velocity measurements taken in horizontal plane for Configuration 3 (nominal depth = 38.1 cm and discharge = 89.87 l/s).

where $\bar{u}_{xz}$ is a velocity in the horizontal plane, and u_x and u_z, respectively, are longitudinal and transverse components of velocity.

It is clear in Figure 5.25, Figure 5.26, and Figure 5.27 that there is no significant increase in velocity between rows of dowels. It can be concluded, thus, that the predicted velocity profiles that were developed using Petryk's model are in error in the region between rows of dowels.

Model predictions for Configuration 1a, the only configuration in which all dowels were emergent, were quite reasonable. Between the two models, the writer's model, yielded better results, i.e., resulted in smaller prediction errors. The multiple-partial coefficient of determination, $r^2_{W|P}$ was 0.68 and 0.27, respectively, for flow depths of 38.1 cm (1.25 ft) and 30.5 cm (1.00 ft).

It was noted in Section 5.6.1 that prediction errors from the models were larger for tests in which there were submerged dowels. For example, directly behind the dowels, average prediction errors were less than 2% for Configuration 1a (either flow depth) whereas for Configurations 1b and 3 the average error ranged between 22% and 35%.

The multiple-partial coefficient of determination yielded for Configurations 1b, 2, and 3 were $r^2_{P|W} = 0.33$, $r^2_{P|W} = 0.46$, and $r^2_{P|W} = 0.61$, respectively. These results indicate that Petryk's model yields smaller prediction errors when dowels are submerged. In light of the large errors that result, though, it is not recommended that either Petryk's model or the writer's model be used to predict depth-averaged velocity distributions when there are submerged cylinders. For submerged dowels, models such as those proposed by Fischenich (1997), Lopez and Garcia (1997), and Nepf (1998) should be investigated.

5.7 Application of Analytical Model to Harland Creek

In Section 5.6 an analytical model was proposed for evaluating flow through vegetation in trapezoidal channels. Furthermore, predictions from the model were shown to compare quite well to measurements recorded in a physical model with simulated willow posts. In this section the proposed model is used to hypothetically evaluate the effects of willow posts at Harland Creek.

The objectives of this exercise are twofold: to assess how well the model simulates prototype scale applications and to demonstrate how the model can be used to assist in the design of willow posts systems.

Plotted in Figure 5.28 is the existing ground line and low water elevation of a surveyed cross-section in Reach 1 (Watson, 1998). Superimposed on the existing ground line are the proposed ground line and three rows of planted willow posts. The bank slope on which the planted willow posts are shown is the concave (outer) bank. The slope of the proposed concave bank slope is 2H:1V. The height of the willow posts is 1.22 m (4 ft). The first row of willows is 0.30 m (1.0 ft) above the low water elevation and the remaining rows are spaced 0.91 m (3 ft) apart, horizontally. Along the direction of flow the willow posts are spaced 0.91 m (3 ft) apart. The positions of the planted willow posts in Figure 5.28 are representative of willow post systems constructed at Harland Creek.

The computer program HEC-RAS (USACE, 1997) was used to perform backwater calculations along Harland Creek and to develop the stage-discharge relation for the cross-section shown in Figure 5.28. Since results from the analytical model are most accurate when the vegetation is emergent, of interest is the lowest stage at which the willows are not submerged, that is 30.69 m (100.69 ft). The corresponding discharge, Q, is 32.58 cms (1,150 cfs), cross-section averaged velocity, U_0, is 0.98 m/s (3.23 fps), and the flow depth over the bed, Y, is 2.06 m (6.75 ft).

In order to use the proposed model, an equation for describing the depth-averaged velocity profile across the bed and bank of the channel, in the absence of willow posts must be prescribed. For a trapezoidal channel, the general form of such an equation is

$$\frac{U_x(r)}{U_0} = \beta_0 + \beta_1 \exp(r/Y) \tag{3.18}$$

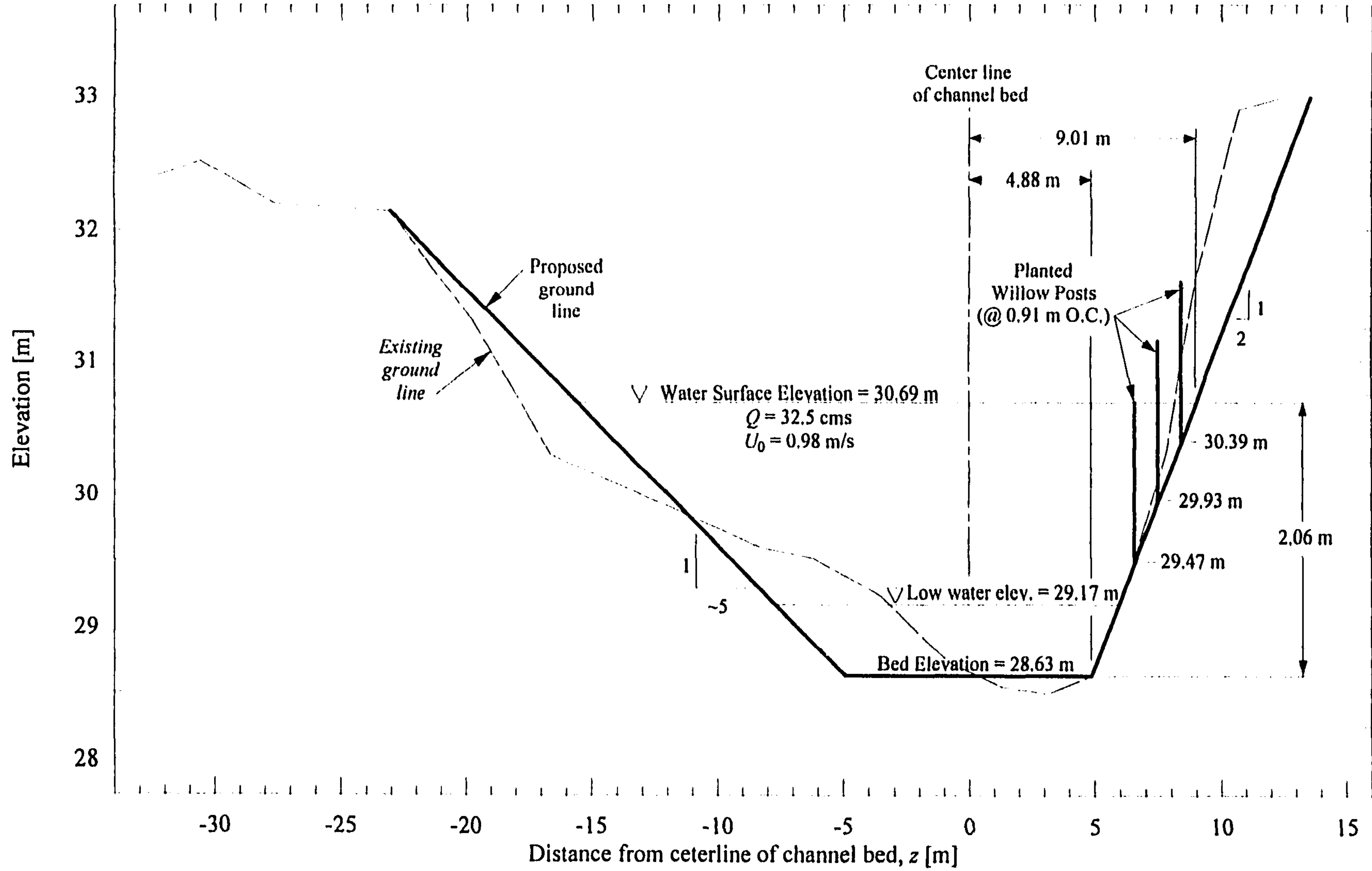

Figure 5.28 – Existing cross-section at Harland Creek with hypothetical proposed cross-section geometry.

Replacing r in (3.18) with $z - z_{toe}$ (z is the transverse distance from the center line of the channel to the point of interest and z_{toe} is the transverse distance from the channel center line to the toe of slope, equation becomes

$$\frac{U_x(z)}{U_0} = \beta_0 + \beta_1 \exp\left(\frac{z - z_{toe}}{Y}\right) \tag{5.7}$$

To establish values for β_0 and β_1 in (5.7), it is assumed that $U_x(z = 4.88 \text{ m}) = U_0$ $= 0.98$ m/s and $U_x(z = 9.01 \text{ m}) = 0$. The resulting equation is

$$\frac{U_x(z)}{U_0} = 1.157 - 0.157 \exp\left(\frac{z - z_{toe}}{Y}\right) \tag{5.8}$$

where $z_{toe} = 4.88$ m and the nominal flow depth, $Y = 2.06$ m (Figure 5.28). The depth-averaged velocity profile yielded by (5.8) is plotted in Figure 5.29. The depth-averaged velocity profile that results after imposing the willow post system designed for this exercise is also shown in Figure 5.29. The profile was computed by using (5.8) in (3.16) and by following the procedure outlined in Section 3.7.3.

At the center row of dowels in Figure 5.29, the predicted velocity is 0.22 m/s (0.731 fps). For the same location, with no dowels present, the predicted velocity, from (5.8), is 0.61 m/s (2.01 fps). At the center row of dowels, thus, the velocity is reduced by 64%. The dowel configuration and flow condition for Configuration 1a (nominal depth = 38.1 cm) are comparable to the hypothetical case evaluated above. In the model, a velocity reduction of 60% (Section 5.5.2) was observed at the center row of dowels. These results indicate that the proposed model is applicable to prototype scale problems.

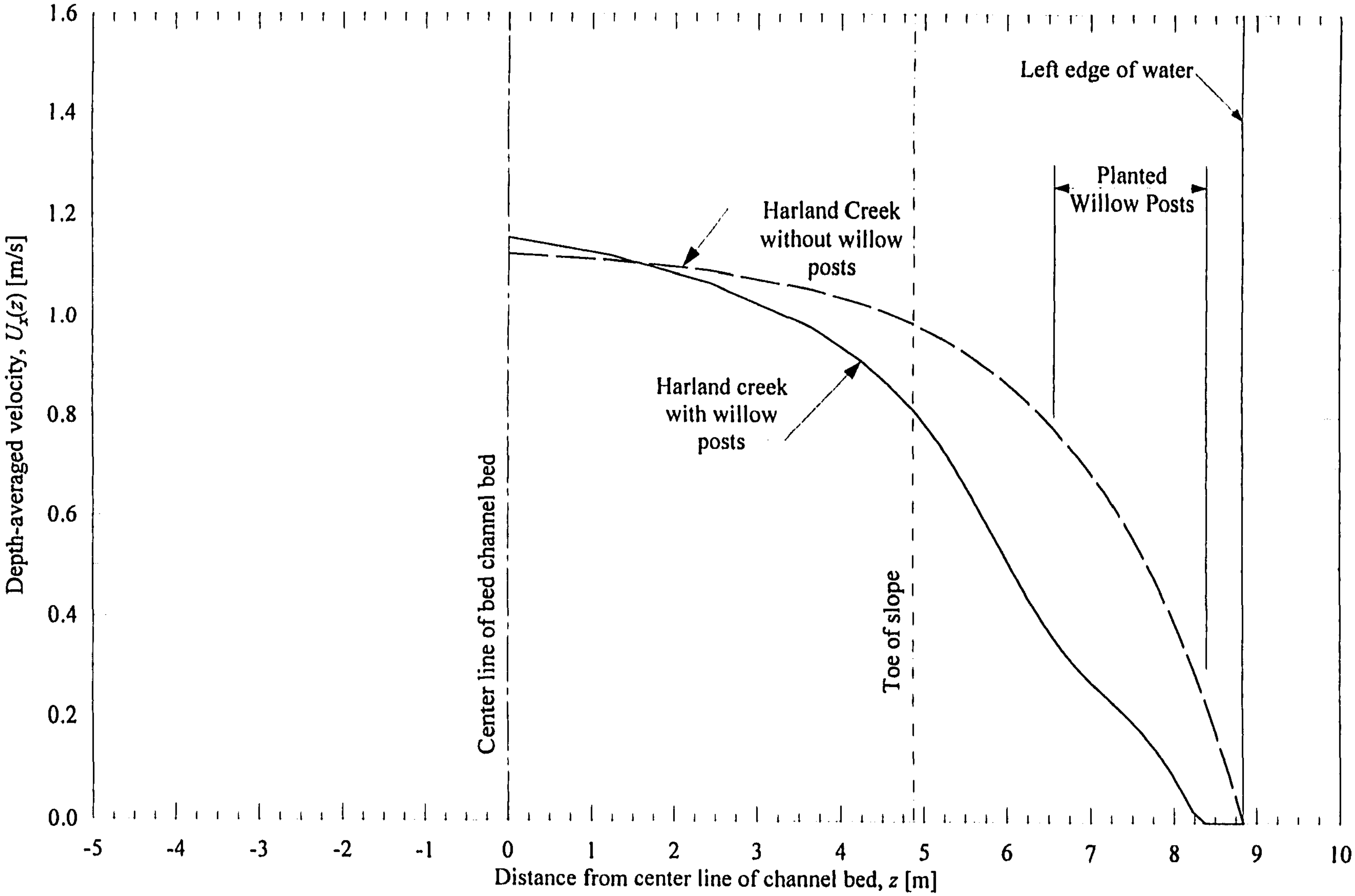

Figure 5.29 – Predicted depth-averaged velocity profiles in Harland Creek, Mississippi, with and without willow posts and with hypothetical proposed cross-section geometry.

6. Conclusions and Recommendations

Bioengineering has been shown to have great utility in regards to bank stabilization efforts by Schiechtl and Stern (1997) and Gray and Sotir (1995) among others, but many questions remain about how bioengineering systems work and how system reliability can be improved. By answering questions about near-bank processes and the influence of willow posts on near-bank processes, which are two of the primary objectives of this study, the current research contributes to the insight of engineers and others facing these issues.

The main conclusions developed in this study are presented in Section 6.1. Recommendations for improving willow post systems are presented in Section 6.2 and recommendations for future research are presented in Section 6.3.

6.1 Conclusions

Field, laboratory, and analytical studies were performed for this research in order that definitive conclusions could be drawn. Summarized in the following statements are the most important findings of this study.

1) Bank erosion pins placed on the banks of Harland Creek showed that scour and deposition occurred most frequently at the lower part of the bank and least frequently in the upper part of the bank. Of the eighteen erosion pins at which significant aggradation and/or degradation was observed, eleven (61%) were at the lower part of the bank, four (22 %) were at the middle part of the bank, and two (10%) were on the upper part of the bank.

2) A statistical analysis of variations in soil grain-size with depth below the ground was performed using the Wilcoxon matched-pairs signed-rank test. It is concluded from the test results that no deposition has occurred in the vicinity of the planted willow posts in Reach 1 or Reach 2; continued bank migration, therefore, is expected to undermine the constructed willow post systems.

3) Vegetation density was found to be greater in the reaches with planted willow posts than in the control reach. Using $VDI(h_{mean})$, for example, yields that vegetation density in Reach 1 and Reach 2, respectively, was 34% and 44% greater than in Reach 3 during August 1997. In January 1998, $VDI(h_{mean})$ for Reach 1 and Reach 2, respectively, was 18% and 35% greater than $VDI(h_{mean})$ for Reach 3. These results suggest that planted willow posts create an environment that is conducive to the establishment of volunteer vegetation.

4) Three vegetation indices were evaluated: Veg_d , $VDI(h_{50})$, and $VDI(h_{mean})$. Analyses of vegetation density data indicate that $VDI(h_{mean})$ yielded the most consistent results when measurements from different seasons were compared. Season-to-season cross-correlation was measured using Pearson's product moment correlation, $r_{X,Y}$. The computed correlation coefficients, $r_{Aug97,Jan98}$, $r_{Aug97,Mar98}$, and $r_{Jan98,Mar98}$ were 0.70, 0.37, and 0.31, respectively.

5) Results from the physical model study indicate that depth-averaged velocities are greatly reduced by the presence of any configuration of dowels. For the dowel configurations tested herein, velocities were reduced by an average of 57% at the center row of dowels. Emergent dowels were found to be most effective at reducing depth-averaged velocities, i.e., in comparison to when no dowels were present, the velocity at the center row of three rows of emergent dowels was 60% lower. It is also concluded that dowels increase the potential

for toe scour by increasing transverse shear stress, and that the tested dowel configurations do not affect Manning's roughness coefficients (*n*-values) differently.

6) Results from two analytical models for predicting flow through vegetation, one developed by Petryk (1969) and Li and Shen (1973), and the other developed herein, were compared to results from the physical model study. When no model assumptions are violated, both models yield reasonable results directly behind the dowels (i.e., within 2% on average) but Petryk's model overestimates velocities between rows of dowels by as much as 86%. When no model assumptions or limitations are violated, the model developed herein yielded a greater reduction in the variance of prediction errors in comparison to Petryk's model, i.e., $r^2_{W|P} = 0.48$ on average. Prediction errors were computed as the difference in velocities calculated from the physical model tests and velocities predicted by the analytical models.
7) Use of the proposed model for predicting flow through vegetation was demonstrated for a graded cross-section in Harland Creek. At the location of the center row of dowels, a 64 % reduction in the velocity was observed with dowels versus without dowels. Simulated willow posts, arranged in the same configuration and subjected to comparable flow conditions, yielded a 60% reduction in velocity at the center row of dowels. These results indicate that the model is applicable to prototype scale applications.

6.2 Recommendations for Improving Willow Post Systems

Following is a discussion about improving the implementation of willow post systems. Hopefully the recommendations presented in this discussion will provide useful information for practicing engineers and others that implement bioengineering techniques.

The model study data presented herein demonstrates how planted willow post systems increase the potential for toe scour, and field observations corroborate the assertion that toe scour is an important process in the success or failure of planted willow post systems. The first recommendation, thus, is that the need for toe protection must be given due consideration prior to the construction of willow post systems. It is quite possible that construction of a willow post systems without toe stabilization may lead to increased toe scour in areas that are normally prone to toe scour. Materials that can be used for constructing toe protection include rock riprap but bioengineering techniques for providing toe protection are also available as described in Schiechtl and Stern (1997) for example.

Criteria for planting woody vegetation for streambank protection are provided in Nunnally and Sotir (1997). Toe protection should extend up the bank to at least the elevation at which the vegetation will be planted.

The increased potential for toe scour that results from the construction of willow post systems must be taken into account in designing toe protection. If rock riprap is used for toe protection, for example, then increasing the size of the rock should be considered.

Removing material from point bars that are across from planted willow post systems is another way that toe scour induced by willow posts can be countered. Even though the point bar will eventually be rebuilt, the increased cross-section area that results from removing the point bar material will reduce stress on the outer bank while the planted vegetation becomes established. The excavated point bar material might serve well as backfill behind the toe protection or in the holes where the willow posts are planted.

6.3 Recommendations for Future Research

The following recommendations are derived from questions that have arisen during the course of the present research. These are presented with the intention of extending and verifying the results reported herein.

1) Additional analytical tools for evaluating traditional and bioengineered stream stabilization works should be developed.
2) In the flume study performed for this research, the water surface elevation at the test section was adjusted to a preselected elevation. In a natural stream system with downstream control, the water surface elevation at a section would vary in response to the introduction of roughness elements such as willow posts. Flume tests similar to those described herein should be performed to evaluate how bioengineered systems affect water surface elevations.
3) In this study, depth-averaged velocities were evaluated to compare different simulated willow post configurations. Bed and bank shear stress measurements should be recorded in flow with submerged and emergent simulated willow posts to assess the potential of willow post systems to enhance toe scour.

7. References

Abraham, D. and Derrick, D. (1993). Harland Creek bendway weir/willow post DEC Demonstration Project. Vicksburg, MS: U.S. Army Corps of Engineers, Waterways Experiment Station.

American Society for Testing and Materials (1993). Annual book of ASTM standards (Vol. 04.08). Philadelphia, PA: Author.

Ayres, Q. C. (1936). Soil erosion and its control. New York, NY: McGraw-Hill.

Barnes, H. H., Jr. (1967). Roughness characteristics of natural channels (U.S. Geological Survey, Water-supply paper 1849), Washington, D.C.: U.S. Government Printing Office.

Black, C. A. (1968). Soil-plant relationships (2nd ed.). New York, NY: Wiley.

Blackmarr, W. A. (Ed.). (1995). Documentation of hydrologic, geomorphic, and sediment transport measurements on the Goodwin Creek experimental watershed, northern Mississippi, for the period 1982-1993, Preliminary Release (Research Report No. 3). Oxford, MS: USDA-ARS, National Sedimentation Laboratory.

Bowles, J. E. (1992). Engineering properties of soils and their measurement (4th ed.). New York, NY: McGraw-Hill.

Brookes, A. and Shields, Jr., F. D. (1996). Perspectives on river channel restoration. In A. Brookes and Shields, Jr., F. D. (Eds.), River channel restoration: Guiding principles for sustainable projects (pp. 1-19). New York, NY: Wiley.

Buckingham, E. (1915). Model Experiments and the forms of empirical equations. *Transaction of the American Society of Mechanical Engineers*, *37*, 263.

Chow, V. T. (1959). Open-Channel Hydraulics. New York: McGraw-Hill.

Church, M. and Rood, K. (1983). Catalogue of alluvial river channel regime data. Vancouver, Canada: The University of British Columbia, The Department of Geography.

Colby, B. R. (1964). Scour and fill in sand-bed streams (U.S. Geological Survey Professional Paper 462-D). Washington, DC: U.S. Government Printing Office.

Coppin, N. J. and Richards, I. G. (Eds.). (1990). Use of vegetation in civil engineering. London, UK: Butterworths.

Daniel, W. W. (1990). Applied nonparametric statistics (2nd ed.). Boston, MA: PWS-Kent.

Derrick, D. L. (1997). Harland Creek bendway weir/willow post bank stabilization demonstration project. In Wang, S. Y., Langendoen, E. J., and Shields, Jr., F. D. (Eds.), Management of landscapes disturbed by channel incision (pp. 351-356). Oxford, MS: Univ. of Mississippi.

Eskinazi, S. (1959). Mixing of wakes in a turbulent shear flow. *NASA Technical Note D-83.*

Fenzl, R. N. and Davis, J. R. (1964). Hydraulic resistance relationships for surface flow in vegetated channels. *Transactions of the ASAE, 7*, 46-51, 55.

Ferguson, R. I. (1973). Channel pattern and sediment type. *Area, 5*, 38-41.

Fischenich, J. C. (1996). Velocity and resistance in densely vegetated floodways. Unpublished doctoral dissertation, Colorado State University, Fort Collins, CO.

Fischenich, J. C. (1997). Hydraulic impacts of riparian vegetation: Summary of literature (Technical Report No. EL-97-9). Vicksburg, MS: U.S. Army Corps of Engineers, Waterways Experiment Station.

Fisher, K. (1995). Modelling the hydraulic impact of vegetation in river channels (Report SR 346). Wallingford, UK: HR Wallingford.

Flippin-Dudley, S. J. (1997). Vegetation measurements for estimating flow resistance. Unpublished doctoral dissertation, Colorado State University, Fort Collins, CO.

Gray, D. H. and Leiser, A. T. (1982). Biotechnical slope protection and erosion control. New York, NY: Van Nostrand.

Gray, D. H. and Sotir, R. B. (1995). Biotechnical and soil bioengineering slope stabilization. New York, NY: Wiley.

Graybill, F. A., and Iyer, H. K. (1994). Regression analysis: concepts and applications. Belmont, CA: Duxbury.

Grissinger, E. H., Little, W. C., and Murphey, J. B. (1981). Erodibility of streambank materials of low cohesion. *Transactions of the ASAE, 24*, 624-630.

Gwinn, W. R. and Ree, W. O. (1980). Maintenance effects on the hydraulic properties of a vegetation-lined channel. *Transactions of the ASAE, 23(3)*, 636-642.

Happ, S. C., Rittenhouse, G., Dobson, G. C. (1940). Some principles of accelerated stream and valley sedimentation (U.S. Department of Agriculture Technical Bulletin No. 695). Washington, DC: U.S. Government Printing Office.

Henderson, F. M. (1966). Open channel flow. Upper Saddle River, NJ: Prentice Hall.

Hicks, D. M. and Mason, P. D. (1991). Roughness characteristics of New Zealand rivers. Wellington, New Zealand: Water Resources Survey, Dept. of Scientific and Industrial Research Marine and Freshwater.

Hill, P. G., Schaub, U. W., and Senoo, Y. (1963). Turbulent Wakes in Pressure Gradients. *Journal of Applied Mechanics*, *30*(Series E, No. 4), 518-524.

Hooke, J. M. (1979). An analysis of the processes of river bank erosion. *Journal of Hydrology*, *42*, 39-62.

Hsieh, T. (1964). Resistance of cylinder piers in open-channel flow. *Journal of the Hydraulics Division, Proc. of ASCE*, *90*(HY1), 161-173.

Isaacs, L. T. (1965). Hydrodynamic forces on surface piercing circular cylinders and flat plates. Unpublished master's thesis, University of Queensland, at St. Lucia, Brisbane, Australia.

Julien, P. Y. (1995). Erosion and sedimentation. Cambridge, UK: Cambridge University.

Kouwen, N. and Unny, T. E. (1973). Flexible roughness in open channels. *Journal of the Hydraulics Division, Proc. of ASCE*, *99*(HY5), 713-728.

Kouwen, N. (1988). Field estimation of the biomechanical properties of grass. *Journal of Hydraulic Research*, *26*(5), 559-568.

Li, R.-M. and Shen, H. W. (1973). Effect of tall vegetations on flow and sediment. *Journal of the Hydraulics Division, Proc. of ASCE*, *99*(HY5), 793-814.

Lopez, F. and Garcia, M. (1997). Open-channel flow through simulated vegetation: Turbulence modeling and sediment transport (Wetlands Research Program Tech. Rep. WRP-CP-10). Vicksburg, MS: U.S. Army Corps of Engineers, Waterways Experiment Station.

Maynord, S. T. (1992). Riprap stability: Studies in near-prototype size laboratory channel (Tech. Report HL-92-5). Vicksburg, MS: U.S. Army Corps of Engineers, Waterways Experiment Station.

Mood, A. M., Graybill, F. A., and Boes, D. C. (1974). Introduction to the theory of statistics. New York: McGraw-Hill.

National Research Council. (1992). Restoration of aquatic ecosystems—science, technology and public policy. Washington, DC: National Academy Press.

Nepf, H. (1998). Drag, turbulence and diffusion in flow through emergent vegetation. Cambridge, MA: Massachusetts Institute of Technology, Dept. of Civil and Environmental Engineering.

Nunnally, N. R., and Sotir, R. B. (1997). Criteria for selection and placement of woody vegetation in streambank protection. In Wang, S. Y., Langendoen, E. J., and Shields, Jr., F. D. (Eds.), Management of landscapes disturbed by channel incision (pp. 816-821). Oxford, MS: Univ. of Mississippi.

Petryk, S. (1969). Drag on cylinders in open channel flow. Unpublished doctoral dissertation, Colorado State University, Fort Collins, CO.

Petryk, S. and Bosmajian, G., III. (1975). Analysis of flow through vegetation. *Journal of the Hydraulics Division, Proc. of ASCE*, *101*(HY7), 871-884.

Porkess, R. (1991). The Harper Collins Dictionary of Statistics. New York: HarperCollins.

President's Commission on Americans Outdoors. (1986). Report and recommendations to the president of the United States. Washington, DC: U.S. Government Printing Office.

Rahmeyer, W., Werth, D., and Cleere, R. (1994). The study of resistance and stability of vegetation in flood channels (Utah State University Lab Report No. USU-376; Federal Contract No. DACW39-94-K-0009 for U.S. Army Corps of Engineers, Waterways Experiment Station, Vicksburg, MS). Logan, UT: Utah State University, Utah Water Research Lab.

Reichardt, H. (1943). New theory of free turbulence. *Royal Aeronautical Society Journal*, *47*, 167-176.

Rice, C. M. (1949). Dictionary of geological terms. Ann Arbor, MI: Edwards Bros.

Richardson, E. V., Simons, D. B., and Julien, P. Y. (1990). Highways in the river environment participant notebook (Report No. FHWA-HI-90-016). Washington, DC: Federal Highway Administration, National Highway Institute.

Riley, S. J. (1972). A comparison fo morphometric measures of bankfull. *Journal of Hydrology*, *17*, 23-31.

Roberson, J. A., and Crowe, C. T. (1985). Engineering Fluid Mechanics (3rd ed.). Boston, MA: Houghton Mifflin.

Roseboom, D. P. (1992). Streambank stabilization training. Peoria, IL: Illinois State Water Survey.

Schiechtl, H. M. (1973). Sicherungsarbeiten im Landschaftsbau. 244 S., Verl.G. D. W. Callwey, München. (Fundamental reference book. Control work in landscape construction).

Schiechtl, H. M. (1980). Bioengineering for land reclamation and conservation (N. K. Horstmann, Trans. Coord.). Edmonton, Canada: University of Alberta Press.

Schiechtl, H. M., and Stern, R. (1997). Water bioengineering techniques for watercourse bank and shoreline protection (L. Jaklitsch, Trans.; D. H. Barker, Ed.). Klosterneuburg, Austria: Blackwell Science.

Schlichting, H. (1979). Boundary-layer theory (7th ed.; J. Kestin, Trans.). New York: McGraw-Hill.

Schumm, S. A. (1960). The shape of alluvial channels in relation to sediment type (U.S. Geological Survey Professional Paper 352-B). Washington, DC: U.S. Government Printing Office.

Schumm, S. A. (1971). Fluvial geomorphology: The historical perspective. In H. W. Shen (Ed.), River mechanics (Vol. 1, pp. 4-1 to 4-30). Littleton, CO: Water Resources.

Schumm, S. A., Harvey, M. D., and Watson, C. C. (1984). Incised channels morphology, dynamics and control. Littleton, CO: Water Resources.

Shen, H. W., Schumm, S. A., Nelson, J. D., Doehring, D. O., Skinner, M. M., and Smith, G. L. (1981). Methods for assessment of stream-related hazards to highways and bridges (Report No. FHWA/RD-80/160). Washington, DC: Federal Highway Administration, Office of Research and Development, Environmental Division.

Shields, Jr., F. D. (1991). Woody vegetation and riprap stability along the Sacramento river mile 84.5-119. *Water Resources Bulletin, 27*(3), 527-536.

Simon, A. and Hupp, C. R. (1987). Geomorphic and vegetative recovery processes along modified Tennessee streams: an interdisciplinary approach to distributed fluvial systems. Forest hydrology and watershed management (Proceedings of the Vancouver Symposium, IAHS-AISH Publ. No. 167, 251-262).

Soil Survey Staff (1960). Soil classification: A comprehensive system (7th approximation). Washington, DC: USDA, Soil Conservation Service.

Sowers, G. F. (1979). Introductory soil mechanics and foundations: Geotechnical engineering. New York, NY: Macmillan.

Statsoft. (1995). Statistica (Volume I: General conventions and statistics I). Tulsa, OK: Author.

Temple, D. M. (1991). Changes in vegetal resistance during long-duration flows. *Transactions of the ASAE, 34*(4), 1769-1774.

Testa, III, S. and Lago, P. K. (1994). The aquatic hydrophilidae (Coleoptera) of Mississippi (Mississippi Agricultural and Forestry Experimental Station, Technical Bulletin 193, Mississippi Entomological Museum No. 5).

Thorne, C. R. (1990). Effects of vegetation on riverbank erosion and stability. In J. B. Thornes (Ed.), Vegetation and erosion (pp. 125-143). Chicaster, UK: Wiley.

Thorne, C. R., Chang, H. H., and Hey, R. D. (1988). Prediction of hydraulic geometry of gravel-bed streams using the minimum stream power concept. In W.R. White (Ed.), International conference on river regime (pp. 29-40). Chicaster, UK: Wiley.

Thorne, C. R. and Osman, A. M. (1988). The influence of bank stability on regime geometry of natural channels. In W.R. White (Ed.), International conference on river regime (pp. 135-147). Chicaster, UK: Wiley.

Wang, S. Y., Langendoen E. J., and Shields, Jr., F. D. (Eds.). (1997). Management of landscapes disturbed by channel incision (p. iv). Oxford, MS: Univ. of Mississippi.

Watson, C. C., Abt, S. R., and Thornton, C. I. (1994). Recommendations for bioengineering stabilization of five sites on Harland Creek, Mississippi (Contract Report No. DACW39-94-K-0015 for U.S. Army Corps of Engineers, Waterways Experiment Station, Vicksburg, MS). Fort Collins, CO: Colorado State University, Dept. of Civil Engineering.

Watson, C. C., Gessler, D., and Abt, S. R. (1995). Inspection of selected bank stabilization sites (Contract Report No. DACW39-94-K-0003 for U.S. Army Corps of Engineers, Waterways Experiment Station, Vicksburg, MS). Fort Collins, CO: Colorado State University, Dept. of Civil Engineering.

Watson, C. C., Abt, S. R., and Derrick, D. (1997). Willow posts bank stabilization. *Journal of the American Water Resources Association, 33*(2), 293-300.

Watson, C. C. (1998). [Demonstration erosion control survey data (1997)]. Unpublished raw data.

White, F. M. (1991). Viscous fluid flow (2nd ed.). New York, NY: McGraw-Hill.

Wilkerson, G. V. (1998). Evidence of willow post induced deposition. In S. R. Abt, J. Young-Pezeshk, and C. C. Watson (Eds.), Water Resources Engineering 98' (Vol. 1, pp. 435-440). Reston, VA: ASCE.

Williams, G. P. (1978). Bank-full discharge of rivers. *Water Resources Research, 14*(6), 1141-1154.

Wolman, M. G. (1959). Factors influencing erosion of a cohesive river bank. *American Journal of Science, 257*, 204-216.

Wolman, M. G. and Leopold, L. B. (1957). River flood plains: Some Observations on their formation (U.S. Geological Survey Professional Paper 282-C). Washington, DC: U.S. Government Printing Office.

Wu, T. H. (1995). Slope stabilization. In R. P. C. Morgan and Rickson, R. J. (Eds.), Slope stabilization and erosion control: A bioengineering approach, (pp. 221-264). London, UK: E & FN Spon.

U.S. Army Corps of Engineers. (1997). HEC-RAS (Version 2.0) [Computer Software]. Davis, CA: Author.

U.S. Army Corps of Engineers. (1981). The streambank erosion control evaluation and demonstration act of 1974, Section 32, Public Law 93-251. Main report of final report to congress. Washington, DC: U.S. Government Printing Office.

U.S. Army Corps of Engineers. (1970). Engineering and design; laboratory soils testing (Eng. Manual No. 1110-2-1906). Washington, DC: Author.

U.S. Geological Survey (1977). National Handbook of Recommended Methods for Water-Data Acquisition, Chapter 1 – Surface Water. Office of Water Data Coordination, Geological Survey, U.S. Dept. of the Interior. Reston, Virginia.

U.S. Geological Survey (1991). National Water Summary 1988-89: Hydrologic Events and Floods and Droughts (USGS Water Supply Paper 2375). Washington, DC: U.S. Government Printing Office.

Vanoni, V. A. (Ed.). (1975). Sedimentation engineering (ASCE-Manuals and Reports on Engineering Practice, No. 54). New York: ASCE

Yang, C. T. (1996). Sediment transport: Theory and practice. New York, NY: McGraw-Hill.

Yano, M. (1966). Turbulent diffusion in a simulated vegetative cover. Unpublished doctoral disseratation, Colorado State University, Fort Collins, CO.

Appendix A. Survey Data

The survey data in Table A.1 through Table A.14 were used to compute channel form (shape and size) parameters for transects in each study reach. Following is a list of abbreviations used in the tables.

LB	left bank
LS	left stake
LWE	left waters edge
RB	right bank
RS	right stake
RWE	right waters edg
WS	water surface

Table A.1 – Reach 1 Transect 1 Survey Data

Point	Northing	Easting	Dist.	Elev.	Desc.
August 1997					
116	8396.00	9077.12	-1.03	105.67	SS11-2
117	8383.25	9078.21	10.99	103.59	SS11-3
118	8379.14	9081.79	16.23	106.49	SS11-5
119	8374.81	9085.04	21.52	98.44	SS11-6
January 1998					
244	8396.40	9080.27	-0.03	105.41	RB
999			8.78	105.41	RB (Interpolated)
246	8385.53	9083.93	11.37	103.95	RB
248	8380.79	9085.54	16.34	101.16	RB
250	8375.71	9088.07	22.02	97.79	RB
251	8375.25	9088.79	22.74	97.17	RWE
252	8373.72	9089.82	24.56	95.70	WS
253	8372.73	9093.38	26.96	93.77	WS
254	8367.29	9095.45	32.77	93.49	Thalweg
255	8364.25	9095.78	35.66	93.53	WS
256	8345.54	9103.90	56.05	94.97	WS
257	8341.43	9106.50	60.88	95.68	WS
258	8339.55	9109.10	63.67	97.08	LWE
259	8325.05	9114.66	79.17	98.04	LB
260	8309.11	9121.53	96.52	99.99	LB
261	8301.89	9125.71	104.83	104.49	LB
242	8295.43	9127.48	111.43	104.85	LB
262	8291.17	9128.57	115.75	104.79	LB
243	8396.43	9080.42	0.00	106.43	RS
241	8295.67	9127.48	111.22	106.36	LS
March 1998					
5	8380.70	9085.68	16.46	101.22	RB
6	8376.80	9087.14	20.61	99.13	RB
7	8375.90	9087.94	21.76	98.41	RB
8	8375.84	9088.27	21.96	97.68	RB
20	8374.61	9088.99	23.38	96.90	RB
21	8373.78	9089.92	24.53	95.52	RB
22	8373.07	9090.23	25.29	94.12	RB
23	8371.90	9090.84	26.61	93.66	RB
14	8340.50	9102.28	59.91	94.79	WS
15	8334.93	9106.41	66.71	96.82	WS
16	8324.69	9110.77	77.82	96.96	LWE
17	8307.48	9121.24	97.85	100.30	LB
18	8301.68	9124.39	104.44	104.58	LB
19	8295.40	9127.49	111.44	104.93	LB

Table A.2 – Reach 1 Transect 2 Survey Data

Point	Northing	Easting	Dist.	Elev.	Desc.
August 1997					
41	8442.79	9190.51	-0.28	108.22	RB
39	8436.22	9192.20	6.51	107.77	RB
38	8433.63	9192.71	9.14	105.97	RB
37	8431.39	9192.98	11.39	105.50	RB
35	8429.25	9193.86	13.67	104.82	RB
34	8425.61	9194.37	17.34	102.53	RB
32	8422.65	9195.35	20.44	100.12	RB
31	8420.96	9195.37	22.09	97.36	RB
29	8419.04	9196.36	24.18	95.49	RWE
28	8413.55	9197.49	29.78	92.39	Thalweg
27	8402.52	9200.35	41.18	94.32	WS
26	8395.22	9201.64	48.58	94.74	WS
25	8389.70	9202.58	54.17	95.49	LWE
24	8365.87	9208.91	78.82	98.32	LB
23	8357.32	9210.64	87.53	99.08	LB
22	8354.34	9211.23	90.57	98.84	LB
21	8348.46	9212.59	96.61	100.94	LB
20	8342.31	9214.11	102.94	101.41	LB
19	8335.95	9215.67	109.49	105.39	LB
18	8331.70	9216.68	113.85	105.91	LB
17	8324.14	9218.05	121.53	106.18	LB
40	8442.54	9190.66	0.00	109.73	RS
16	8323.94	9218.16	121.75	107.15	LS
120	8441.59	9188.01	0.33	107.96	SS12-2
121	8432.63	9188.64	9.20	106.42	SS12-3
122	8429.76	9188.63	11.99	105.74	SS12-4
123	8424.52	9190.27	17.47	102.40	SS12-5
124	8419.59	9189.17	22.02	98.68	SS12-6
March 1998					
30	8382.02	9201.28	61.36	95.79	WS
29	8369.87	9203.21	73.63	96.99	WS
28	8355.56	9206.03	88.21	97.09	LWE
27	8351.31	9210.67	93.40	98.86	LB
26	8343.30	9214.81	102.14	101.41	LB
25	8336.64	9216.29	108.95	105.23	LB
24	8324.21	9218.24	121.50	106.20	LB

Table A.3 – Reach 1 Transect 3 Survey Data

Point	Northing	Easting	Dist.	Elev.	Desc.
August 1997					
68	8409.30	9422.77	-0.27	108.95	RB
62	8404.35	9417.34	7.07	108.27	RB
61	8404.34	9417.13	7.24	107.60	RB
60	8402.38	9415.17	10.00	106.07	RB
58	8393.99	9405.99	22.44	101.98	RB
54	8389.64	9401.38	28.78	100.05	RB
56	8389.88	9401.05	28.87	99.99	RB
53	8387.60	9398.72	32.12	95.35	RWE
52	8386.08	9396.41	34.86	93.78	Thalweg
51	8376.02	9386.21	49.17	95.47	LWE
50	8348.73	9356.00	89.88	97.80	LB
49	8335.80	9341.78	109.10	98.84	LB
48	8324.20	9328.91	126.42	100.16	LB
47	8317.84	9321.79	135.97	100.71	LB
46	8310.77	9314.44	146.16	102.53	LB
45	8306.89	9310.00	152.06	105.54	LB
44	8300.19	9302.46	162.15	106.90	LB
43	8295.72	9296.70	169.42	106.76	LB
67	8409.01	9422.67	0.00	110.37	RS
42	8295.93	9296.59	169.36	108.27	LS
125	8417.41	9417.64	-1.86	108.80	SS13-2
126	8413.83	9408.99	6.96	107.95	SS13-3
127	8404.57	9408.49	13.52	105.24	SS13-4
128	8402.70	9398.55	22.17	102.47	SS13-5
129	8398.01	9391.64	30.45	100.41	SS13-6
March 1998					
31	8394.25	9405.67	22.51	101.94	RB
32	8392.48	9403.36	25.41	101.07	RB
33	8391.82	9402.13	26.77	99.05	RB
34	8391.27	9401.05	27.93	98.08	RWE
35	8390.30	9400.09	29.30	95.51	WS
36	8389.13	9398.73	31.09	94.17	WS
47	8375.96	9383.93	50.91	96.24	WS
46	8342.35	9342.22	104.40	97.08	WS
45	8334.90	9333.82	115.62	97.87	LWE
39	8313.31	9313.45	145.20	106.92	LB
37	8295.57	9296.92	169.35	106.49	LB

Table A.4 – Reach 1 Transect 4 Survey Data

Point	Northing	Easting	Dist.	Elev.	Desc.
August 1997					
91	8264.73	9477.85	0.65	109.06	RB
89	8262.35	9475.36	3.74	108.90	RB
88	8262.26	9472.93	6.08	107.62	RB
87	8260.18	9467.48	11.90	105.66	RB
85	8259.19	9464.64	14.91	102.56	RB
84	8257.96	9460.02	19.68	101.38	RB
82	8256.74	9457.25	22.69	100.47	RB
81	8255.74	9454.18	25.92	98.61	RB
79	8255.42	9453.15	26.99	95.84	RWE
78	8253.92	9447.81	32.54	94.75	WS
77	8252.67	9443.21	37.31	94.47	Thalweg
76	8250.68	9436.19	44.61	96.02	LWE
75	8245.12	9416.16	65.38	97.08	LB
74	8240.19	9398.04	84.15	96.19	LB
73	8238.65	9392.14	90.24	96.73	LB
72	8237.25	9387.08	95.49	98.85	LB
71	8235.08	9380.30	102.60	103.81	LB
70	8231.69	9370.79	112.69	106.88	LB
90	8265.14	9478.41	0.00	110.03	RS
69	8231.97	9370.69	112.71	108.39	LS
130	8266.82	9479.11	-1.17	109.03	SS14-2
131	8267.08	9472.88	4.71	102.08	SS14-3
132	8267.44	9465.41	11.75	104.42	SS14-4
133	8266.02	9457.68	19.55	100.87	SS14-5
134	8264.96	9453.95	23.43	98.75	SS14-6
March 1998					
51	8258.36	9459.55	20.02	101.20	RB
52	8257.64	9457.30	22.37	99.83	RB
53	8257.49	9456.61	23.08	98.25	RB
69	8241.53	9387.90	93.44	97.99	LWE
68	8232.52	9370.71	112.52	106.95	LB

Table A.5 – Reach 1 Transect 5 Survey Data

Point	Northing	Easting	Dist.	Elev.	Desc.
August 1997 and March 1998					
67	8207.31	9526.53	-20.34	112.94	RB
113	8206.40	9526.36	-19.96	112.88	RB
112	8206.30	9526.32	-19.90	113.91	RB
66	8206.84	9524.03	-17.80	112.72	RB
65	8203.96	9516.99	-10.28	111.30	RB
64	8201.63	9507.35	-0.36	110.33	RB
111	8200.55	9507.32	-0.08	110.24	RB
63	8200.69	9505.26	1.89	110.10	RB
109	8199.33	9502.50	4.89	109.75	RB
62	8199.97	9498.32	8.81	109.31	RB
107	8198.43	9498.09	9.39	107.59	RB
61	8199.34	9497.74	9.52	105.55	RB
60	8198.70	9495.49	11.85	103.80	RB
59	8197.80	9492.10	15.36	102.28	RB
106	8197.17	9491.89	15.71	102.06	RB
58	8196.50	9488.52	19.14	100.62	RB
57	8196.09	9483.91	23.72	99.01	RB
104	8194.57	9481.81	26.12	98.03	RB
102	8192.09	9473.63	34.65	96.04	RWE
101	8190.50	9469.71	38.83	94.36	Thalweg
100	8189.88	9464.44	44.10	95.88	LWE
99	8184.14	9442.09	67.18	96.82	LB
98	8180.05	9423.28	86.42	97.08	LB
97	8178.83	9417.88	91.95	96.16	LB
96	8177.29	9411.20	98.81	96.32	LB
95	8175.06	9402.04	108.24	104.43	LB
94	8173.89	9395.31	115.05	106.49	LB
70	8174.05	9391.00	119.21	106.69	LB
93	8172.83	9390.40	120.08	106.76	LB
110	8200.71	9507.20	0.00	111.73	RS
92	8172.85	9390.51	119.97	108.14	LS
136	8209.03	9502.41	2.72	109.41	SS15-3
138	8204.78	9486.50	19.18	101.30	SS15-5
139	8201.89	9478.47	27.67	98.03	SS15-6
135	8224.20	9531.41	-29.01	112.69	SS15-7

Table A.6 – Reach 2 Transect 1 Survey Data

Point	Northing	Easting	Dist.	Elev.	Desc.
August 1997					
13	6549.19	8307.27	0.08	110.03	RB
15	6546.18	8307.19	3.01	110.18	RB
16	6543.82	8308.31	5.55	110.06	RB
17	6541.42	8309.59	8.16	108.97	RB
18	6540.36	8309.87	9.25	108.11	RB
20	6537.93	8310.15	11.69	106.55	RB
22	6535.85	8310.68	13.84	105.06	RB
25	6530.48	8311.26	19.20	102.06	RB
27	6526.56	8311.87	23.17	100.84	RB
28	6521.03	8312.66	28.74	99.51	RB
30	6517.98	8313.56	31.91	99.20	RB
32	6517.11	8314.06	32.87	98.95	RB
33	6515.24	8314.96	34.88	96.87	RB
34	6513.95	8315.32	36.22	96.48	RWE
35	6511.41	8316.24	38.89	96.39	WS
36	6506.86	8317.47	43.60	96.57	LWE
37	6502.71	8317.89	47.75	96.89	Bed
38	6493.05	8319.74	57.58	96.94	Bed
39	6482.50	8322.44	68.46	96.30	RWE
40	6475.88	8323.37	75.13	95.75	Thalweg
41	6468.17	8324.73	82.96	96.35	LWE
42	6464.95	8325.35	86.24	97.20	LB
43	6461.45	8326.35	89.87	97.92	LB
44	6457.77	8327.43	93.68	99.13	LB
45	6456.01	8327.41	95.40	101.43	LB
46	6452.49	8327.90	98.95	103.40	LB
47	6446.50	8328.98	105.04	107.24	LB
48	6444.29	8329.27	107.26	107.43	LB
50	6442.84	8329.53	108.73	107.70	LB
12	6549.26	8307.25	0.00	111.38	RS
49	6442.76	8329.53	108.81	108.80	LS
14	6546.81	8301.72	1.28	110.07	SS21-2
19	6538.12	8304.12	10.27	108.14	SS21-3
23	6534.33	8304.86	14.13	105.69	SS21-4
26	6529.51	8305.77	19.03	102.52	SS21-5
31	6516.49	8308.60	32.36	99.32	SS21-6

Table A.7 – Reach 2 Transect 2 Survey Data

Point	Northing	Easting	Dist.	Elev.	Desc.
August 1997					
86	6580.38	8423.41	-0.13	110.13	RB
87	6578.00	8424.36	2.43	110.04	RB
84	6574.79	8425.14	5.73	108.91	RB
83	6573.50	8425.15	6.97	107.79	RB
81	6570.76	8426.36	9.94	106.86	RB
79	6567.72	8427.00	13.03	105.51	RB
77	6564.77	8428.16	16.19	103.75	RB
75	6563.25	8428.42	17.72	102.55	RB
73	6560.34	8429.62	20.85	100.85	RB
71	6557.83	8429.93	23.35	99.79	RB
70	6555.21	8429.82	25.83	96.53	RWE
69	6553.98	8430.36	27.16	95.80	Thalweg
68	6546.60	8431.89	34.68	96.43	WS
67	6542.98	8432.39	38.29	96.24	WS
66	6535.40	8434.63	46.19	95.84	WS
65	6528.37	8436.89	53.58	95.96	WS
64	6524.43	8438.89	57.92	96.59	LWE
63	6521.09	8440.05	61.45	97.43	LB
62	6514.06	8442.62	68.92	98.59	LB
61	6505.05	8445.11	78.26	99.65	LB
60	6498.93	8446.77	84.61	100.19	LB
59	6495.17	8448.16	88.60	100.51	LB
58	6490.33	8449.41	93.60	102.39	LB
57	6484.86	8451.75	99.51	105.42	LB
56	6482.71	8452.10	101.68	106.46	LB
55	6480.18	8452.99	104.35	107.26	LB
85	6580.27	8423.47	0.00	111.47	RS
54	6480.02	8453.03	104.51	108.98	LS
88	6580.28	8421.36	-0.61	110.01	SS22-2
82	6570.02	8419.97	8.84	106.52	SS22-4
78	6562.46	8420.74	16.31	103.64	SS22-5
74	6559.01	8423.89	20.51	101.12	SS22-6

Table A.8 – Reach 2 Transect 3 Survey Data

Point	Northing	Easting	Dist.	Elev.	Desc.
		August 1997			
127	6615.72	8665.47	-0.14	110.16	RB
125	6614.20	8665.38	1.38	110.19	RB
124	6610.04	8664.91	5.56	110.17	RB
123	6608.19	8664.57	7.44	109.35	RB
121	6607.22	8664.25	8.44	109.13	RB
119	6605.47	8664.33	10.17	108.78	RB
118	6602.65	8663.71	13.04	107.65	RB
117	6600.52	8663.60	15.17	106.49	RB
115	6597.99	8663.01	17.76	105.18	RB
113	6596.53	8663.14	19.19	104.94	RB
112	6595.35	8663.07	20.36	103.45	RB
110	6592.41	8662.20	23.40	101.54	RB
108	6590.99	8662.36	24.78	100.26	RB
107	6586.43	8661.55	29.41	96.69	RWE
106	6585.15	8661.05	30.74	95.06	Thalweg
105	6581.84	8660.40	34.11	95.63	WS
104	6575.26	8658.53	40.88	96.30	WS
103	6568.09	8656.91	48.21	96.65	LWE
102	6564.57	8656.30	51.78	97.22	LB
101	6555.36	8653.84	61.25	97.39	LB
100	6547.42	8652.70	69.27	99.44	LB
99	6540.64	8651.71	76.12	99.60	LB
98	6529.51	8650.90	87.25	101.01	LB
97	6519.37	8650.39	97.37	101.23	LB
96	6512.15	8650.02	104.57	102.12	LB
95	6508.64	8651.17	107.89	103.53	LB
94	6503.11	8649.98	113.52	105.57	LB
93	6496.73	8649.04	119.98	107.37	LB
92	6489.28	8647.51	127.57	107.58	LB
91	6483.54	8646.99	133.32	108.12	LB
126	6615.57	8665.50	0.00	111.63	RS
90	6483.31	8646.89	133.56	109.55	LS
128	6618.04	8661.51	-1.89	110.06	SS23-2
122	6607.76	8661.13	8.34	109.69	SS23-4
116	6599.25	8658.22	17.18	105.69	SS23-5
111	6592.10	8659.65	24.05	100.80	SS23-6

Table A.9 – Reach 2 Transect 4 Survey Data

Point	Northing	Easting	Dist.	Elev.	Desc.
		August 1997			
163	6309.47	8946.01	0.05	111.34	RB
161	6309.20	8944.73	1.36	111.11	RB
160	6309.08	8943.76	2.33	110.53	RB
159	6308.96	8942.65	3.45	109.52	RB
158	6308.77	8941.57	4.55	106.87	RB
156	6308.64	8940.24	5.88	105.88	RB
153	6307.60	8933.82	12.37	104.03	RB
150	6307.00	8929.51	16.71	102.11	RB
148	6307.39	8927.90	18.28	99.65	RB
147	6307.31	8925.56	20.62	98.00	RWE
146	6307.43	8923.39	22.77	95.45	WS
145	6307.17	8920.33	25.84	94.08	WS
144	6306.37	8916.54	29.69	93.82	Thalweg
143	6306.76	8911.23	34.94	94.54	WS
142	6305.09	8901.69	44.60	97.26	WS
141	6304.40	8894.38	51.94	98.12	LWE
140	6304.25	8886.99	59.30	99.52	LB
139	6303.41	8874.92	71.40	100.99	LB
138	6301.64	8857.58	88.83	101.88	LB
137	6300.17	8846.69	99.81	101.69	LB
136	6300.13	8845.15	101.35	102.93	LB
135	6301.34	8842.34	104.03	104.30	LB
134	6300.50	8837.17	109.26	105.92	LB
133	6300.18	8832.73	113.71	107.57	LB
132	6297.05	8825.90	120.81	108.84	LB
131	6296.91	8821.48	125.21	108.71	LB
162	6308.98	8946.12	0.00	113.52	RS
130	6297.04	8821.48	125.21	110.08	LS
164	6311.13	8945.80	0.11	110.99	SS24-2
157	6316.81	8940.02	5.32	106.10	SS24-4
154	6312.35	8934.00	11.73	103.98	SS24-5
151	6310.42	8929.75	16.15	102.01	SS24-6

Table A.10 – Reach 3 Transect 1 Survey Data

Point	Northing	Easting	Dist.	Elev.	Desc.
August 1997					
11	9326.55	9921.85	-0.33	201.82	LB
13	9324.42	9921.67	1.77	201.80	LB
14	9321.94	9922.10	4.27	201.55	LB
15	9320.93	9922.22	5.30	201.08	LB
16	9320.47	9922.37	5.77	200.24	LB
17	9318.78	9922.73	7.49	198.68	LB
19	9318.01	9922.76	8.25	198.29	LB
20	9314.41	9923.33	11.89	197.28	LB
22	9311.27	9923.48	15.04	195.68	LB
25	9310.17	9923.31	16.11	194.93	LB
26	9309.17	9923.05	17.07	193.35	LB
27	9305.51	9924.02	20.82	193.73	LB
28	9303.02	9924.76	23.37	193.80	LB
29	9298.72	9925.32	27.71	192.11	LB
31	9295.64	9925.47	30.79	190.98	LB
33	9291.94	9926.35	34.56	189.95	LB
34	9286.26	9927.01	40.27	188.13	LWE
35	9280.23	9927.73	46.35	187.17	WS
36	9275.13	9928.58	51.51	186.48	Thalweg
37	9266.56	9929.55	60.14	187.21	WS
38	9259.34	9930.20	67.39	187.90	RWE
39	9254.93	9931.01	71.85	189.49	RB
40	9250.40	9931.48	76.41	191.11	RB
41	9245.18	9931.56	81.61	191.33	RB
42	9241.10	9932.63	85.77	190.95	RB
43	9240.39	9932.55	86.47	191.82	RB
44	9233.43	9932.84	93.43	194.89	RB
45	9227.78	9932.76	99.04	197.34	RB
46	9222.74	9932.92	104.06	199.26	RB
48	9219.58	9933.40	107.25	199.75	RB
10	9326.23	9921.98	0.00	203.31	LS
47	9219.69	9933.21	107.13	201.27	RS
12	9326.37	9921.13	-0.23	201.88	SS31-2
23	9318.95	9931.11	8.20	198.61	SS31-4
24	9312.24	9930.04	14.76	195.67	SS31-5
32	9296.55	9932.38	30.60	191.05	SS31-6

Table A.11 – Reach 3 Transect 2 Survey Data

Point	Northing	Easting	Dist.	Elev.	Desc.
August 1997					
83	9271.88	9780.90	0.01	206.18	LB
78	9264.70	9783.57	7.62	206.00	LB
74	9263.35	9784.58	9.28	203.59	LB
70	9261.32	9785.31	11.42	201.35	LB
53	9257.69	9786.91	15.38	197.68	LB
54	9254.72	9788.17	18.61	197.14	LB
55	9253.04	9789.00	20.48	197.06	LB
56	9249.44	9790.85	24.53	195.70	LB
57	9247.58	9791.56	26.51	194.50	LB
58	9245.98	9792.53	28.37	192.66	LB
59	9244.52	9793.12	29.95	189.13	LB
60	9242.08	9794.04	32.54	188.23	LWE
61	9236.76	9795.91	38.13	186.98	Thalweg
62	9230.55	9798.37	44.79	187.50	WS
63	9224.98	9801.86	51.33	188.07	RWE
64	9222.32	9803.31	54.36	189.24	RB
65	9216.69	9806.85	60.97	190.81	RB
66	9202.93	9814.43	76.68	192.92	RB
67	9193.23	9819.69	87.70	193.09	RB
68	9192.09	9820.42	89.05	194.43	RB
72	9188.42	9822.72	93.36	198.34	RB
76	9184.92	9824.33	97.21	200.41	RB
81	9178.87	9827.66	104.11	200.69	RB
80	9172.71	9831.02	111.12	201.24	RB
51	9169.89	9832.05	114.11	201.33	RB
82	9271.90	9780.93	0.00	207.81	LS
50	9169.55	9832.12	114.44	202.86	RS
79	9263.18	9787.07	10.55	201.82	SS32-4
75	9256.34	9792.45	19.08	197.02	SS32-5
71	9252.60	9794.25	23.22	195.98	SS32-6
52	9173.88	9838.08	113.24	200.99	SS32-1

Table A.12 – Reach 3 Transect 3 Survey Data

Point	Northing	Easting	Dist.	Elev.	Desc.
August 1997					
119	8842.16	9818.75	0.12	202.92	RB
117	8844.61	9813.09	6.27	202.62	RB
116	8846.67	9808.58	11.22	201.27	RB
115	8847.02	9806.64	13.15	199.71	RB
114	8846.95	9806.53	13.23	198.04	RB
113	8848.10	9803.32	16.64	196.59	RB
111	8848.60	9800.89	19.09	195.66	RB
110	8849.55	9798.93	21.26	194.76	RB
108	8850.26	9796.78	23.52	193.46	RB
104	8850.86	9795.35	25.07	192.05	RB
102	8850.98	9792.79	27.52	190.11	RB
101	8853.04	9789.26	31.55	189.22	RB
100	8853.48	9787.95	32.92	188.67	RWE
99	8854.01	9786.34	34.62	187.97	WS
98	8857.05	9777.41	44.05	186.65	Thalweg
97	8861.28	9767.56	54.75	187.04	WS
96	8864.14	9759.67	63.14	188.67	LWE
95	8867.02	9751.32	71.98	189.92	LB
94	8872.35	9740.03	84.41	192.26	LB
93	8872.99	9738.73	85.86	191.79	LB
92	8874.69	9737.09	88.00	192.16	LB
91	8874.88	9735.93	89.15	193.81	LB
90	8876.42	9729.86	95.37	197.66	LB
89	8877.88	9724.99	100.45	200.35	LB
88	8878.68	9722.24	103.30	201.76	LB
86	8878.93	9720.60	104.92	202.04	LB
118	8842.03	9818.82	0.00	204.35	RS
85	8879.02	9720.52	105.03	203.48	LS
120	8844.99	9818.98	0.89	203.44	SS33-2
107	8854.20	9804.31	17.87	196.81	SS33-4
106	8856.34	9800.82	21.89	195.02	SS33-5
87	8884.67	9721.92	105.71	201.45	SS33-1
105	8856.54	9796.71	25.81	192.13	SS33-6

Table A.13 – Reach 3 Transect 4 Survey Data

Point	Northing	Easting	Dist.	Elev.	Desc.
August 1997					
159	8839.42	9524.97	0.21	208.11	LB
157	8836.98	9525.73	2.76	208.07	LB
156	8832.11	9526.68	7.68	207.00	LB
155	8831.13	9526.66	8.62	205.29	LB
153	8829.96	9527.64	10.02	202.15	LB
151	8828.60	9527.69	11.34	201.03	LB
149	8825.14	9529.31	15.13	198.83	LB
147	8823.24	9530.46	17.29	197.48	LB
146	8820.50	9531.03	20.07	196.67	LB
144	8816.81	9531.98	23.87	195.83	LB
142	8814.70	9533.01	26.20	194.58	LB
141	8810.54	9535.08	30.80	192.86	LB
140	8805.74	9536.73	35.87	191.04	LB
139	8803.70	9537.36	38.01	189.41	LB
138	8801.68	9538.28	40.21	188.88	LWE
137	8799.66	9538.71	42.27	188.42	Thalweg
136	8796.26	9539.16	45.64	188.93	WS
135	8792.38	9539.74	49.51	189.06	RWE
134	8789.19	9541.13	52.97	189.27	RB
133	8786.18	9542.03	56.11	190.12	RB
132	8773.78	9545.94	69.12	190.90	RB
131	8764.12	9547.74	78.85	193.47	RB
130	8755.42	9549.77	87.75	194.81	RB
129	8743.46	9553.67	100.34	195.99	RB
128	8739.62	9554.79	104.33	198.33	RB
127	8735.68	9556.11	108.49	200.15	RB
126	8726.97	9560.28	118.07	201.74	RB
125	8717.09	9564.95	128.91	201.76	RB
158	8839.66	9525.03	0.00	209.58	LS
124	8716.93	9565.07	129.09	203.17	RS
160	8841.25	9526.75	0.98	208.21	SS34-2
154	8830.80	9534.02	11.21	200.92	SS34-4
150	8826.99	9534.00	14.83	198.31	SS34-5
145	8819.75	9538.90	23.23	195.26	SS34-6

Table A.14 – Reach 3 Transect 5 Survey Data

Point	Northing	Easting	Dist.	Elev.	Desc.
January 1998					
397	8263.92	11080.11	0.40	198.36	LB
312	8277.21	11070.48	16.40	197.46	LB
396	8281.37	11066.37	22.61	197.08	LB
313	8284.02	11064.81	25.26	196.71	LB
394	8284.72	11064.53	26.38	195.87	LB
314	8285.34	11063.57	27.06	194.74	LB
393	8285.43	11064.05	27.23	194.86	LB
392	8286.25	11062.99	28.53	194.20	LB
391	8287.52	11061.63	30.38	193.83	LB
390	8288.34	11061.12	31.34	193.73	LB
389	8290.15	11059.63	33.68	193.35	LB
387	8291.31	11059.06	34.94	192.92	LB
315	8292.04	11058.94	35.19	192.77	LB
386	8291.79	11058.43	35.71	192.59	LB
316	8293.07	11058.23	36.44	190.42	LB
385	8292.89	11058.24	36.69	190.34	LB
384	8294.25	11057.17	38.42	190.00	LB
382	8295.15	11056.40	39.61	189.53	LB
317	8295.72	11055.81	40.02	189.35	LB
381	8295.52	11056.06	40.11	189.38	LB
380	8296.29	11055.47	41.08	188.17	LB
318	8296.77	11054.69	41.53	187.63	LWE
319	8298.78	11053.33	43.96	185.75	WS
320	8307.70	11044.14	56.66	184.71	Thalweg
321	8308.92	11042.93	58.36	185.23	WS
322	8324.07	11029.76	78.44	185.45	WS
323	8327.81	11016.34	90.27	187.47	RWE
324	8349.85	11006.95	112.85	194.03	RB
325	8363.32	11000.77	127.18	199.24	RB
399	8365.49	10999.87	129.84	199.49	RB
326	8375.10	10993.65	140.84	199.34	RB
398	8263.59	11080.33	0.00	199.96	LS
400	8365.67	10999.90	129.96	201.01	RS
399	8365.49	10999.87	129.84	199.49	SS35-1
401	8264.20	11053.92	16.83	197.93	SS35-2
402	8268.15	11049.30	22.79	197.22	SS35-3
403	8279.57	11048.62	32.18	194.10	SS35-4
404	8281.16	11046.75	34.59	193.83	SS35-5

Appendix B. Supplemental Model Data and Analyses

Point velocity measurements, recorded in conjunction with the physical model (flume) study performed for this research, were taken along vertical axes in planes oriented normal to the direction of flow and in a horizontal planes located 6.10 cm (0.20 ft) below the water surface (Section 3.6). In this appendix, point velocities measured along vertical axes are reported. The measured values were used herein to calculate depth-averaged velocities and discharge rates through the flume, and results from the calculations are used throughout this study. The procedures followed to calculate depth-averaged velocities and discharge rates are described in Section B.1 and Section B.2, respectively.

Manning's roughness coefficients (*n*-values) were calculated for each test performed in the physical model as described in Section 3.6.7. The detailed calculations that were required to determine the *n*-values are presented in Section B.3.

B.1 Calculation of Depth-Averaged Velocities

Measurements taken in a plane oriented normal to the direction of flow are presented in Tables D.1 to D.10. In addition to the coordinates and longitudinal velocity for each point, the tables include values for secondary velocities, i.e., horizontal (u_z) and vertical (u_y) velocities in the plane of flow. It is noted that values of u_z and u_y are typically one or two orders of magnitude smaller than velocities normal to the plane of flow, u_x. Secondary velocities, u_z and u_y, consequently, were not considered in this analysis.

At every location in the flume where point velocity measurements were taken along a vertical axis, the depth-averaged velocity, U_x, was calculated. For calculating U_x, the velocity at the bed of the flume was assumed equal to zero and the velocity at the water surface was assumed equal to the velocity measurement taken closest to the water surface. The equation used to calculate U_x is

$$U_x = \frac{\sum_{i=1}^{n}\left(\frac{(u_x)_{i+1}+(u_x)_i}{2}\right)(y_{i+1}-y_i)}{\sum_{i=1}^{n}(y_{i+1}-y_i)} = \frac{1}{d}\cdot\sum_{i=1}^{n}\left(\frac{(u_x)_{i+1}+(u_x)_i}{2}\right)(y_{i+1}-y_i) \qquad \text{(B.1)}$$

where n is the total number of point velocities (recorded and assumed) along the current vertical axis, $(u_x)_i$ is the ith point velocity along the vertical axis, y_i is the height above an arbitrary datum to the ith point, and d is the total flow depth at the vertical axis where the velocity measurements were recorded. The calculated depth-averaged velocities for each test are summarized in Section 4.6.

B.2 Calculated Flow Rates in Flume

The target flow rates established for this study (Section 3.6.5) were compared to calculated flow rates to verify that the target flow rates had been attained (Section 3.6.6).

The equation used to calculate flow rates through the flume, Q_{calc}, is

$$Q_{calc} = \sum_{j=1}^{m-1} Q_j = \sum_{j=1}^{m-1}\left(\frac{(U_x)_j+(U_x)_{j+1}}{2}\right)\left(\frac{d_j+d_{j+1}}{2}\right)(z_{j+1}-z_j) \qquad \text{(B.2)}$$

where m is the number of locations in the cross-section at which U_x values were calculated or assumed, $(U_x)_j$ is the depth-averaged velocity (Section B.1) corresponding to the jth location in the cross-section, d_j is the flow depth at the jth location in the cross section, and z_j is the horizontal distance from the left edge of the flume to the jth location in the cross-section. Along the edges of the flume, U_x was assumed equal to the most proximate calculated value of U_x.

B.3 Calculation of Manning's Roughness Coefficients

Manning's roughness coefficients (*n*-values) were calculated for each test performed in the physical model. The procedure followed herein to calculate the *n*-values is described in Section 3.6.7. Results from the detailed calculations that were performed in order to determine *n*-values are presented in Table B.11 through Table B.19. These results are summarized in Table 4.23.

Table B.1 – Point Velocity Measurements for Dowel Configuration 0 (No Dowels). Nominal Depth = 22.9 cm. Measurements taken at Flume Sect. 1.

Point No.	z [m]	y [m]	u_x [m/s]	u_y [m/s]	u_z [m/s]
9	0.30	0.17	0.1407	0.0011	-0.0036
10	0.30	0.14	0.1363	-0.0019	-0.0037
11	0.30	0.11	0.1098	0.0005	-0.0010
12	0.30	0.08	0.0903	-0.0026	-0.0007
13	0.30	0.05	0.0701	0.0009	-0.0039
15	0.61	0.17	0.1337	-0.0008	-0.0009
16	0.61	0.14	0.1394	0.0000	-0.0015
17	0.61	0.11	0.1285	0.0012	-0.0033
18	0.61	0.08	0.1170	0.0023	-0.0039
19	0.61	0.06	0.1142	0.0008	-0.0016
20	0.76	0.17	0.1425	-0.0013	-0.0022
21	0.76	0.14	0.1501	0.0005	-0.0046
22	0.76	0.11	0.1309	0.0034	-0.0031
23	0.76	0.08	0.1205	0.0040	-0.0026
24	0.76	0.06	0.0963	0.0045	-0.0028
25	0.84	0.15	0.1431	-0.0017	-0.0025
26	0.84	0.12	0.1306	-0.0005	-0.0018
27	0.84	0.09	0.1173	-0.0029	-0.0012
28	0.84	0.06	0.0254	-0.0173	-0.0007
30	0.91	0.17	0.1338	-0.0020	-0.0020
31	0.91	0.14	0.1240	-0.0026	-0.0016
32	0.91	0.11	0.0668	-0.0185	-0.0009
34	0.99	0.17	0.1186	-0.0016	-0.0010
36	0.99	0.12	0.0005	0.0002	-0.0001

Table B.2 – Point Velocity Measurements for Dowel Configuration 0 (No Dowels). Nominal Depth = 22.9 cm. Measurements taken at Flume Sect. 2.

Point No.	z [m]	y [m]	u_x [m/s]	u_y [m/s]	u_z [m/s]
40	0.35	0.17	0.1347	0.0018	-0.0006
41	0.35	0.14	0.1265	-0.0002	0.0005
42	0.35	0.11	0.1180	-0.0026	-0.0011
43	0.35	0.08	0.1027	-0.0038	-0.0044
44	0.35	0.05	0.0643	-0.0044	-0.0022
45	0.66	0.17	0.1481	-0.0017	-0.0030
46	0.66	0.14	0.1504	-0.0002	-0.0047
47	0.66	0.11	0.1203	-0.0027	-0.0013
48	0.66	0.08	0.1069	0.0005	-0.0017
49	0.66	0.05	0.0648	0.0006	-0.0012
50	0.81	0.17	0.1489	-0.0010	-0.0037
51	0.81	0.14	0.1444	-0.0001	-0.0056
52	0.81	0.11	0.1471	0.0022	-0.0074
53	0.81	0.08	0.1089	-0.0009	-0.0029
54	0.81	0.05	0.0462	-0.0011	-0.0025
55	0.88	0.16	0.1459	-0.0024	-0.0033
56	0.88	0.11	0.1104	-0.0013	0.0001
57	0.88	0.08	0.0610	-0.0200	0.0007
58	0.96	0.17	0.1326	-0.0023	-0.0016
59	0.96	0.14	0.1105	-0.0060	0.0002
60	0.96	0.11	0.0803	-0.0240	0.0016
61	1.04	0.17	0.1053	-0.0041	-0.0025
62	1.04	0.15	0.0594	-0.0233	-0.0011
63	1.11	0.17	0.0000	0.0003	-0.0001

Table B.3 – Point Velocity Measurements for Dowel Configuration 0 (No Dowels). Nominal Depth = 30.5 cm. Measurements taken at Flume Sect. 2.

Point No.	z [m]	y [m]	u_x [m/s]	u_y [m/s]	u_z [m/s]
1	0.30	0.24	0.2467	-0.0020	-0.0021
2	0.30	0.18	0.2385	-0.0025	-0.0010
3b	0.30	0.12	0.2189	0.0010	-0.0008
4	0.30	0.06	0.1586	0.0028	-0.0029
5	0.30	0.03	0.0008	0.0003	-0.0001
6	0.61	0.24	0.2530	-0.0114	-0.0094
7	0.61	0.18	0.2270	0.0049	0.0056
8	0.61	0.12	0.2306	0.0105	-0.0033
9	0.61	0.06	0.1427	0.0027	-0.0008
10	0.61	0.03	0.0010	-0.0006	-0.0003
11	0.76	0.24	0.2501	-0.0075	-0.0025
12	0.76	0.21	0.2444	-0.0048	-0.0026
13	0.76	0.18	0.2407	0.0002	-0.0037
15	0.76	0.12	0.2439	-0.0006	-0.0038
16	0.76	0.09	0.2049	-0.0036	0.0000
17	0.76	0.06	0.1900	0.0053	-0.0031
18	0.76	0.03	0.1572	0.0133	-0.0056
19	0.84	0.24	0.2429	-0.0091	-0.0042
20	0.84	0.21	0.2437	-0.0011	0.0000
21	0.84	0.18	0.2194	-0.0066	0.0014
23	0.84	0.12	0.1951	-0.0018	0.0013
24	0.84	0.09	0.0032	-0.0034	-0.0005
25	0.91	0.24	0.2337	-0.0029	-0.0022
26	0.91	0.21	0.2290	-0.0030	-0.0007
27	0.91	0.18	0.2227	-0.0011	-0.0030
28	0.91	0.15	0.1932	-0.0001	-0.0011
29	0.91	0.12	0.0000	0.0018	-0.0002
30	0.99	0.24	0.2169	-0.0034	0.0009
31	0.99	0.21	0.2189	-0.0022	-0.0016
32	0.99	0.18	0.1928	-0.0068	-0.0031
33	0.99	0.15	-0.0002	0.0000	-0.0006
34	0.99	0.12	0.0000		
35	1.07	0.24	0.2038	-0.0016	-0.0019
36	1.07	0.21	0.0295	0.0003	-0.0004
37	1.07	0.20	0.0002	-0.0006	-0.0002
38	1.14	0.24	0.1536	0.0068	-0.0011
39	1.14	0.21	0.0001	0.0005	0.0004
40	1.22	0.24	0.0076	-0.0041	0.0006

Table B.4 – Point Velocity Measurements for Dowel Configuration 0 (No Dowels). Nominal Depth = 38.1 cm. Measurements taken at Flume Sect. 2.

Point No.	z [m]	y [m]	u_x [m/s]	u_y [m/s]	u_z [m/s]
1	0.30	0.32	0.3363	0.0013	0.0000
2	0.30	0.26	0.3384	-0.0020	0.0020
3	0.30	0.20	0.3355	0.0003	-0.0017
4	0.30	0.14	0.2886	0.0000	0.0018
5	0.30	0.08	0.2038	-0.0047	-0.0039
6	0.30	0.05	0.1408	-0.0048	-0.0065
7	0.61	0.32	0.3301	0.0021	0.0031
9	0.61	0.20	0.3285	-0.0009	0.0014
10	0.61	0.14	0.3232	-0.0037	-0.0045
11	0.61	0.08	0.2149	-0.0012	-0.0037
12	0.61	0.05	0.1530	-0.0001	-0.0001
13	0.76	0.32	0.3328	-0.0091	0.0005
14	0.76	0.29	0.3426	-0.0044	-0.0010
15	0.76	0.26	0.3312	-0.0021	-0.0058
16	0.76	0.23	0.3251	-0.0081	-0.0011
17	0.76	0.20	0.3222	-0.0003	-0.0074
18	0.76	0.17	0.2958	0.0021	-0.0013
19	0.76	0.14	0.2572	0.0035	-0.0047
20	0.76	0.11	0.2321	0.0035	-0.0033
21	0.76	0.08	0.1952	0.0173	0.0784
22	0.84	0.32	0.3344	-0.0079	-0.0027
23	0.84	0.29	0.3313	-0.0059	-0.0024
24	0.84	0.26	0.3256	-0.0034	-0.0036
25	0.84	0.23	0.3252	-0.0002	-0.0059
26	0.84	0.20	0.2940	-0.0006	0.0015
27	0.84	0.17	0.2752	-0.0066	0.0023
28	0.84	0.14	0.2339	0.0016	-0.0049
29	0.84	0.11	0.1635	-0.0111	-0.0158
30	0.91	0.32	0.3260	-0.0034	0.0020
31	0.91	0.29	0.3328	-0.0042	-0.0069

Table B.4 – (cont.)

Point No.	z [m]	y [m]	u_x [m/s]	u_y [m/s]	u_z [m/s]
32	0.91	0.26	0.3053	-0.0029	-0.0003
33	0.91	0.23	0.2980	-0.0058	-0.0005
34	0.91	0.20	0.2695	0.0013	-0.0018
35	0.91	0.17	0.2267	0.0099	-0.0054
36	0.99	0.32	0.3128	-0.0022	-0.0001
37	0.99	0.29	0.3231	-0.0037	-0.0004
38	0.99	0.26	0.2940	-0.0015	0.0002
39	0.99	0.23	0.2983	-0.0067	-0.0024
40	0.99	0.20	0.2459	0.0057	-0.0034
41	0.99	0.18	0.2033	0.0011	0.0038
42	1.07	0.32	0.3002	-0.0043	-0.0004
43	1.07	0.29	0.3044	0.0007	-0.0027
44	1.07	0.26	0.2487	-0.0012	0.0024
45	1.07	0.23	0.2282	0.0091	-0.0093
46	1.14	0.32	0.2925	-0.0016	-0.0048
47	1.14	0.29	0.2541	-0.0005	-0.0003
48	1.14	0.26	0.2148	0.0035	0.0041
49	1.22	0.32	0.2409	0.0024	-0.0013
50	1.22	0.29	0.2282	0.0026	-0.0099
51	1.22	0.27	0.1766	-0.0062	-0.0100
52	1.30	0.32	0.1793	0.0020	0.0062

Table B.5 – Point Velocity Measurements for Dowel Configuration 1a (Long Dowels). Nominal Depth = 22.9 cm. Measurements taken at Flume Sect. 2.

Point No.	z [m]	y [m]	u_x [m/s]	u_y [m/s]	u_z [m/s]
1	0.30	0.17	0.1354	-0.0006	0.0004
2	0.30	0.14	0.1131	0.0007	0.0043
3	0.30	0.11	0.1117	-0.0042	0.0016
4	0.30	0.08	0.0937	0.0045	0.0035
5	0.30	0.06	0.0905	-0.0017	0.0005
6	0.61	0.17	0.1333	0.0001	0.0009
7	0.61	0.14	0.1291	0.0000	0.0002
8	0.61	0.11	0.1135	-0.0012	0.0023
9	0.61	0.08	0.1069	-0.0005	-0.0007
10	0.61	0.06	0.0784	-0.0005	-0.0002
11	0.76	0.17	0.1339	-0.0016	0.0007
12	0.76	0.14	0.1326	-0.0021	-0.0006
13	0.76	0.11	0.1132	0.0003	0.0009
14	0.76	0.08	0.0856	-0.0094	0.0026
15	0.76	0.07	0.0398	-0.0067	-0.0015
16	0.84	0.17	0.1053	-0.0021	0.0048
17	0.84	0.14	0.1165	-0.0028	0.0019
18	0.84	0.12	0.0944	-0.0049	0.0036
19	0.91	0.17	0.0918	-0.0027	0.0047
20	0.91	0.15	0.0179	-0.0020	0.0006
21	0.99	0.18	0.0547	-0.0117	0.0006
22	0.99	0.18	0.0379	-0.0144	0.0013

Table B.6 – Point Velocity Measurements for Dowel Configuration 1a (Long Dowels). Nominal Depth = 30.5 cm. Measurements taken at Flume Sect. 2.

Point No.	z [m]	y [m]	u_x [m/s]	u_y [m/s]	u_z [m/s]
1	0.30	0.24	0.2460	-0.0035	0.0104
2	0.30	0.18	0.2397	-0.0021	0.0059
4	0.30	0.06	0.1462	-0.0015	0.0027
5	0.30	0.05	0.1032	-0.0135	0.0024
6	0.61	0.24	0.2462	-0.0110	0.0073
7	0.61	0.18	0.2420	-0.0041	0.0020
8	0.61	0.12	0.2309	0.0012	0.0014
9	0.61	0.06	0.1453	0.0129	0.0012
10	0.61	0.04	0.0758	0.0140	-0.0032
11	0.76	0.24	0.2435	-0.0057	0.0049
12	0.76	0.21	0.2544	-0.0087	0.0005
13	0.76	0.18	0.2378	-0.0022	0.0067
14	0.76	0.15	0.2426	-0.0054	0.0048
15	0.76	0.12	0.2050	0.0027	0.0073
16	0.76	0.09	0.2101	0.0086	-0.0012
17	0.76	0.07	0.1649	-0.0171	-0.0027
18	0.84	0.24	0.2442	-0.0102	0.0005
19	0.84	0.21	0.2409	-0.0088	0.0011
20	0.84	0.18	0.2276	-0.0043	0.0013
21	0.84	0.15	0.2278	-0.0009	0.0020
22	0.84	0.12	0.1769	0.0012	0.0045
23	0.84	0.11	0.1351	-0.0210	0.0045
24	0.91	0.24	0.2102	-0.0122	0.0021
25	0.91	0.21	0.2124	-0.0123	0.0040
26	0.91	0.18	0.2218	-0.0075	0.0008
27	0.91	0.15	0.1895	-0.0005	-0.0020
28	0.91	0.15	0.1512	-0.0268	0.0041
29	0.99	0.24	0.1430	-0.0044	0.0069
30	0.99	0.27	0.1453	-0.0034	0.0086
31	0.99	0.21	0.1631	-0.0074	0.0048
32	0.99	0.18	0.1239	-0.0173	0.0016
34	1.07	0.24	0.0885	-0.0047	0.0075
35	1.07	0.22	0.0462	-0.0131	0.0001
36	1.14	0.27	0.0469	0.0026	0.0017
37	1.14	0.26	0.0515	0.0014	0.0023

Table B.7 – Point Velocity Measurements for Dowel Configuration 1a (Long Dowels). Nominal Depth = 38.1 cm. Measurements taken at Flume Sect. 2.

Point No.	z [m]	y [m]	u_x [m/s]	u_y [m/s]	u_z [m/s]
1	0.30	0.32	0.3598	-0.0171	0.0144
2	0.30	0.26	0.3605	0.0021	0.0086
3	0.30	0.20	0.3287	0.0146	0.0137
4	0.30	0.17	0.3281	0.0106	0.0112
5	0.30	0.14	0.3357	0.0191	0.0014
6	0.30	0.08	0.2227	0.0045	-0.0012
7	0.30	0.05	0.1559	-0.0092	0.0001
8	0.61	0.32	0.3705	-0.0034	-0.0048
9	0.61	0.26	0.3632	-0.0061	-0.0033
10	0.61	0.20	0.3645	0.0032	0.0025
11	0.61	0.14	0.3316	0.0126	0.0021
12	0.61	0.08	0.2740	0.0224	-0.0116
14	0.76	0.35	0.3639	-0.0123	-0.0045
15	0.76	0.32	0.3631	-0.0076	-0.0016
16	0.76	0.29	0.3657	-0.0084	-0.0034
17	0.76	0.26	0.3625	-0.0010	-0.0048
18	0.76	0.23	0.3604	0.0013	0.0004
19	0.76	0.20	0.3546	0.0012	-0.0030
20	0.76	0.17	0.3502	0.0069	-0.0011
21	0.76	0.14	0.3224	0.0094	-0.0010
22	0.76	0.11	0.3144	0.0190	-0.0044
23	0.76	0.08	0.2587	0.0098	-0.0069
24	0.76	0.05	0.1575	0.0134	-0.0083
25	0.84	0.35	0.3585	-0.0109	-0.0078
26	0.84	0.32	0.3559	-0.0031	0.0023
27	0.84	0.29	0.3625	-0.0017	0.0000
28	0.84	0.26	0.3573	-0.0058	-0.0052
29	0.84	0.23	0.3525	-0.0065	-0.0019
30	0.84	0.20	0.3377	0.0001	-0.0016
31	0.84	0.17	0.3094	0.0034	0.0033
32	0.84	0.14	0.2912	0.0100	-0.0026
33	0.84	0.11	0.2242	0.0157	-0.0018
34	0.84	0.08	0.1461	0.0120	-0.0059
35	0.91	0.35	0.2789	-0.0059	0.0057
36	0.91	0.32	0.2977	-0.0086	0.0019
37	0.91	0.29	0.2959	-0.0110	0.0014
38	0.91	0.26	0.3020	-0.0099	-0.0034
40	0.91	0.23	0.2767	-0.0132	-0.0073
41	0.91	0.20	0.2472	-0.0054	-0.0069
42	0.91	0.17	0.1592	0.0125	-0.0163

Table B.7 – (cont.)

Point No.	z [m]	y [m]	u_x [m/s]	u_y [m/s]	u_z [m/s]
43	0.99	0.35	0.2142	-0.0034	0.0090
44	0.99	0.32	0.1797	0.0083	0.0012
45	0.99	0.29	0.1840	0.0013	0.0062
46	0.99	0.26	0.2078	-0.0021	0.0045
47	0.99	0.23	0.1928	-0.0020	-0.0042
49	0.99	0.17	0.1376	-0.0099	-0.0001
50	1.07	0.35	0.1208	0.0022	0.0020
51	1.07	0.32	0.1294	0.0056	0.0023
52	1.07	0.29	0.1146	0.0048	-0.0022
53	1.07	0.26	0.1181	0.0044	0.0020
55	1.07	0.21	0.1113	-0.0005	0.0068
56	1.14	0.35	0.1143	0.0014	0.0031
57	1.14	0.32	0.1122	0.0019	-0.0001
58	1.14	0.29	0.1071	0.0077	-0.0001
59	1.14	0.26	0.0935	0.0289	0.1343
60	1.22	0.35	0.1439	0.0037	0.0045
61	1.22	0.32	0.1523	0.0116	0.0009
62	1.22	0.29	0.1217	0.0182	-0.0010
63	1.30	0.35	0.1974	0.0129	-0.0009
64	1.30	0.32	0.0974	-0.0023	0.0061

Table B.8 – Point Velocity Measurements for Dowel Configuration 1b (Short Dowels). Nominal Depth = 38.1 cm. Measurements taken at Flume Sect. 2.

Point No.	z [m]	y [m]	u_x [m/s]	u_y [m/s]	u_z [m/s]
2	0.76	0.32	0.3078	-0.0036	0.0039
3	0.76	0.29	0.2942	-0.0023	0.0057
4	0.76	0.26	0.3014	-0.0034	0.0044
5	0.76	0.23	0.2673	-0.0045	0.0135
6	0.76	0.20	0.2924	-0.0036	0.0005
7	0.76	0.17	0.2311	0.0021	0.0091
8	0.76	0.14	0.2235	0.0109	0.0046
10	0.76	0.09	0.1492	0.0012	0.0001
11	0.84	0.35	0.3057	-0.0007	0.0028
12	0.84	0.32	0.2998	-0.0048	0.0048
13	0.84	0.29	0.2918	-0.0069	0.0062
14	0.84	0.26	0.2954	-0.0053	0.0058
15	0.84	0.23	0.2755	-0.0070	0.0042
16	0.84	0.20	0.2614	0.0047	0.0013
17	0.84	0.17	0.2301	0.0010	0.0044
18	0.84	0.14	0.1688	-0.0052	0.0046
19	0.84	0.12	0.1624	-0.0043	0.0033
20	0.91	0.35	0.2949	-0.0099	0.0003
21	0.91	0.32	0.2824	-0.0072	0.0024
22	0.91	0.29	0.2765	-0.0059	0.0024
23	0.91	0.26	0.2722	-0.0025	-0.0012
24	0.91	0.23	0.2407	-0.0039	0.0041
25	0.91	0.20	0.2264	-0.0069	-0.0026
26	0.91	0.17	0.2045	-0.0011	-0.0029
27	0.91	0.14	0.0914	0.0020	-0.0006
28	0.99	0.35	0.2651	-0.0048	-0.0003
29	0.99	0.32	0.2459	-0.0034	-0.0001
30	0.99	0.29	0.2328	-0.0019	0.0013
31	0.99	0.26	0.2055	0.0010	-0.0002
32	0.99	0.23	0.1928	-0.0002	-0.0046

Table B.8 – (cont.)

Point No.	z [m]	y [m]	u_x [m/s]	u_y [m/s]	u_z [m/s]
33	0.99	0.20	0.1932	-0.0123	-0.0067
34	0.99	0.17	0.1195	-0.0035	-0.0027
35	1.07	0.35	0.1998	-0.0004	0.0041
36	1.07	0.32	0.1707	0.0020	-0.0009
37	1.07	0.29	0.1462	0.0053	-0.0015
38	1.07	0.26	0.1430	0.0017	-0.0124
39	1.07	0.23	0.1054	0.0064	0.0005
40	1.07	0.21	0.1041	0.0007	-0.0002
41	1.14	0.35	0.1365	-0.0015	0.0020
42	1.14	0.32	0.1048	0.0050	0.0034
43	1.14	0.29	0.0931	0.0016	0.0033
45	1.14	0.25	0.0425	-0.0179	0.0030
46	1.22	0.35	0.1283	-0.0001	-0.0027
47	1.22	0.32	0.1263	0.0073	-0.0015
48	1.22	0.29	0.1232	0.0068	-0.0048
50	1.30	0.33	0.1355	0.0030	0.0015

Table B.9 – Point Velocity Measurements for Dowel Configuration 2 (5 Rows Staggered). Nominal Depth = 38.1 cm. Measurements taken at Flume Sect. 2.

Point No.	z [m]	y [m]	u_x [m/s]	u_y [m/s]	u_z [m/s]
1	0.30	0.32	0.3111	0.0042	0.0098
2	0.30	0.26	0.3164	0.0015	0.0045
3	0.30	0.20	0.3196	0.0040	0.0070
4	0.30	0.14	0.3074	0.0012	0.0019
5	0.30	0.08	0.2527	-0.0018	-0.0023
6	0.30	0.04	0.1328	-0.0115	-0.0059
7	0.61	0.32	0.3194	-0.0041	0.0041
8	0.61	0.26	0.3226	-0.0025	0.0027
9	0.61	0.20	0.3236	-0.0037	0.0041
10	0.61	0.14	0.2833	0.0067	0.0027
11	0.61	0.08	0.2180	-0.0016	-0.0046
12	0.61	0.06	0.1658	0.0000	-0.0054
13	0.76	0.35	0.3205	-0.0004	0.0042
14	0.76	0.32	0.3239	-0.0053	0.0059
15	0.76	0.29	0.3054	-0.0066	0.0079
16	0.76	0.26	0.3156	0.0004	0.0055
17	0.76	0.23	0.2973	-0.0002	0.0046
18	0.76	0.20	0.2784	0.0020	0.0062
19	0.76	0.17	0.2600	-0.0093	0.0081
20	0.76	0.14	0.2339	0.0017	0.0040
21	0.76	0.11	0.2109	0.0058	0.0037
22	0.76	0.09	0.1693	0.0069	0.0007
23	0.84	0.35	0.3266	-0.0042	0.0057
24	0.84	0.32	0.3168	-0.0027	0.0080
25	0.84	0.29	0.2941	-0.0049	0.0113
26	0.84	0.26	0.2952	-0.0052	0.0069
27	0.84	0.23	0.2861	-0.0075	-0.0005
28	0.84	0.20	0.2490	-0.0002	-0.0022
29	0.84	0.17	0.2140	-0.0017	0.0016
30	0.84	0.14	0.1769	-0.0009	-0.0061
31	0.84	0.12	0.1410	-0.0089	-0.0123
32	0.91	0.35	0.2947	-0.0011	0.0037
33	0.91	0.32	0.2887	-0.0053	0.0034
34	0.91	0.29	0.2642	-0.0015	0.0003
35	0.91	0.26	0.2552	-0.0054	0.0028
36	0.91	0.23	0.2270	-0.0024	-0.0045
37	0.91	0.20	0.1882	0.0007	0.0011
38	0.91	0.17	0.1568	0.0064	-0.0016
39	0.91	0.15	0.0810	-0.0055	0.0006
40	0.99	0.35	0.2552	-0.0032	0.0014

Table B.9 – (cont.)

Point No.	z [m]	y [m]	u_x [m/s]	u_y [m/s]	u_z [m/s]
41	0.99	0.32	0.2275	-0.0039	0.0059
42	0.99	0.29	0.2106	0.0050	0.0029
43	0.99	0.26	0.1826	0.0066	-0.0021
44	0.99	0.23	0.1629	-0.0054	0.0011
45	0.99	0.20	0.1583	-0.0107	-0.0056
46	0.99	0.19	0.1058	-0.0045	0.1251
47	1.07	0.35	0.1977	0.0007	0.0036
48	1.07	0.32	0.1442	0.0053	0.0034
49	1.07	0.29	0.1290	0.0052	-0.0032
50	1.07	0.26	0.1224	-0.0012	-0.0002
51	1.07	0.23	0.0831	-0.0051	0.0049
52	1.14	0.35	0.1273	0.0024	0.0042
53	1.14	0.32	0.1143	-0.0006	-0.0026
54	1.14	0.29	0.0924	0.0024	-0.0018
55	1.14	0.27	0.0831	-0.0044	-0.0014
56	1.22	0.35	0.1235	-0.0025	-0.0012
57	1.22	0.32	0.1381	0.0049	0.0021
58	1.22	0.30	0.0963	-0.0168	-0.0014
59	1.30	0.35	0.1759	0.0005	0.0000
60	1.30	0.34	0.1508	-0.0130	0.0004
61	1.37	0.35	0.0003	-0.0002	-0.0002

Table B.10 – Point Velocity Measurements for Dowel Configuration 3 (3 Rows Staggered). Nominal Depth = 38.1 cm. Measurements taken at Flume Sect. 2.

Point No.	z [m]	y [m]	u_x [m/s]	u_y [m/s]	u_z [m/s]
1	0.76	0.32	0.2990	-0.0016	0.0077
2	0.76	0.26	0.2951	-0.0026	0.0068
3	0.76	0.20	0.2800	-0.0087	0.0097
4	0.76	0.14	0.2329	0.0027	-0.0010
5	0.76	0.08	0.1451	-0.0042	-0.0075
6	0.84	0.32	0.3016	-0.0055	0.0050
7	0.84	0.26	0.2825	-0.0031	0.0034
8	0.84	0.20	0.2514	-0.0063	0.0043
9	0.84	0.14	0.1807	-0.0013	0.0025
10	0.91	0.32	0.2775	-0.0026	0.0014
11	0.91	0.26	0.2509	-0.0027	0.0045
12	0.91	0.20	0.2280	-0.0048	-0.0034
13	0.91	0.14	0.0897	-0.0098	0.0021
14	0.99	0.35	0.2331	-0.0022	0.0031
15	0.99	0.32	0.2444	0.0030	0.0012
16	0.99	0.29	0.2018	0.0048	0.0020
17	0.99	0.26	0.2030	-0.0003	-0.0017
18	0.99	0.23	0.1766	0.0006	-0.0005
19	0.99	0.20	0.1805	-0.0043	-0.0041
20	1.07	0.35	0.2049	0.0021	0.0005
21	1.07	0.32	0.1579	0.0068	0.0048
22	1.07	0.29	0.1465	0.0033	-0.0017
23	1.07	0.26	0.1348	-0.0073	-0.0006
24	1.07	0.23	0.1191	-0.0080	0.0067
25	1.07	0.20	0.0002	-0.0004	-0.0002
26	1.14	0.35	0.1443	-0.0011	0.0073
27	1.14	0.32	0.1070	-0.0045	0.0048
28	1.14	0.29	0.1028	-0.0048	0.0074
29	1.14	0.26	0.1058	-0.0023	0.0025
30	1.22	0.35	0.1303	-0.0038	0.0009
31	1.22	0.32	0.1408	0.0017	0.0031
32	1.22	0.29	0.1055	-0.0106	-0.0036
33	1.30	0.35	0.1893	-0.0019	-0.0003
34	1.30	0.34	0.1968	-0.0019	0.0005

Table B.11 – Calculation of n-value for Dowel Configuration 0 (No Dowels). Nominal Depth = 22.9 cm. Discharge = 22.94 l/s.

Flume Sect. No., i	$y_{i,act}$ [m]	$\Delta y_{i,act}$ [m]	y_{est} [m]	A_i [m^2]	$V_i^2/2g$ [m]	$H_i'=y_i+V_i^2/2g$ [m]	P_i [m]	R_i [m]	$S_{f,i}$	$S_{f,avg}$	Δx [m]	h_f [m]	$H_i''=H_{i-1}''+h_f$ [m]	$(H_i'-H_i'')^2$ [m^2]	$(y_{i,act}-y_{est})^2$ [m^2]
1	0.2249		0.225	0.222	0.001	0.226	1.490	0.149	0.0019				*0.226*		1.16E-08
		0.0030								0.0019	1.303	0.0025			
2	0.2280		0.228	0.225	0.001	0.228	1.499	0.150	0.0018				0.228	5.41E-08	5.35E-08
		0.0015								0.0018	1.219	0.0022			
3	0.2295		0.230	0.228	0.001	0.230	1.505	0.151	0.0018				0.230	1.50E-08	1.53E-08

Calculated n-value : <u>0.1199</u> Total SSE, $\Sigma(H_i'-H_i'')^2+\Sigma(y_{i,act}-y_{est})^2$ = 1.49E-07

Table B.12 – Calculation of n-value for Dowel Configuration 1a (Tall Dowels). Nominal Depth = 22.9 cm. Discharge = 20.39 l/s.

Flume Sect. No., i	$y_{i,act}$ [m]	$\Delta y_{i,act}$ [m]	y_{est} [m]	A_i [m^2]	$V_i^2/2g$ [m]	$H_i'=y_i+V_i^2/2g$ [m]	P_i [m]	R_i [m]	$S_{f,i}$	$S_{f,avg}$	Δx [m]	h_f [m]	$H_i''=H_{i-1}''+h_f$ [m]	$(H_i'-H_i'')^2$ [m^2]	$(y_{i,act}-y_{est})^2$ [m^2]
1	0.2262		0.226	0.224	0.000	0.227	1.494	0.150	0.0018				*0.227*		1.10E-09
		0.0024								0.0017	1.303	0.0023			
2	0.2286		0.229	0.226	0.000	0.229	1.502	0.151	0.0017				0.229	5.15E-09	5.13E-09
		0.0018								0.0017	1.219	0.0020			
3	0.2304		0.230	0.229	0.000	0.231	1.508	0.152	0.0016				0.231	1.43E-09	1.44E-09

Calculated n-value : <u>0.1299</u> Total SSE, $\Sigma(H_i'-H_i'')^2+\Sigma(y_{i,act}-y_{est})^2$ = 1.43E-08

Table B.13 – Calculation of n-value for Dowel Configuration 0 (No Dowels). Nominal Depth = 30.5 cm. Discharge = 57.49 l/s.

Flume Sect. No., i	$y_{i,act}$ [m]	$\Delta y_{i,act}$ [m]	y_{est} [m]	A_i [m^2]	$V_i^2/2g$ [m]	$H_i'=y_i+V_i^2/2g$ [m]	P_i [m]	R_i [m]	$S_{f,i}$	$S_{f,avg}$	Δx [m]	h_f [m]	$H_i''=H_{i-1}''+h_f$ [m]	$(H_i'-H_i'')^2$ [m^2]	$(y_{i,act}-y_{est})^2$ [m^2]
1	0.3054		0.305	0.326	0.002	0.307	1.751	0.186	0.0016				*0.307*		3.82E-09
		0.0024								0.0016	1.303	0.0021			
2	0.3078		0.308	0.329	0.002	0.309	1.758	0.187	0.0016				0.309	1.77E-08	1.72E-08
		0.0015								0.0016	1.219	0.0019			
3	0.3094		0.309	0.332	0.002	0.311	1.763	0.188	0.0015				0.311	4.80E-09	4.80E-09

Calculated n-value : <u>0.0575</u> Total SSE, $\Sigma(H_i'-H_i'')^2+\Sigma(y_{i,act}-y_{est})^2$ = 4.84E-08

Table B.14 – Calculation of n-value for Dowel Configuration 1a (Tall Dowels). Nominal Depth = 30.5 cm. Discharge = 56.35 l/s.

Flume Sect. No., i	$y_{i,act}$ [m]	$\Delta y_{i,act}$ [m]	y_{est} [m]	A_i [m^2]	$V_i^2/2g$ [m]	$H_i'=y_i+V_i^2/2g$ [m]	P_i [m]	R_i [m]	$S_{f,i}$	$S_{f,avg}$	Δx [m]	h_f [m]	$H_i''=H_{i-1}''+h_f$ [m]	$(H_i'-H_i'')^2$ [m^2]	$(y_{i,act}-y_{est})^2$ [m^2]
1	0.3014		0.301	0.321	0.002	0.303	1.738	0.185	0.0017				*0.303*		1.20E-09
		0.0024								0.0017	1.303	0.0022			
2	0.3039		0.304	0.324	0.002	0.305	1.745	0.186	0.0017				0.305	5.58E-09	5.43E-09
		0.0018								0.0017	1.219	0.0020			
3	0.3057		0.306	0.326	0.002	0.307	1.751	0.186	0.0016				0.307	1.53E-09	1.52E-09

Calculated n-value : 0.0769 Total SSE, $\Sigma(H_i'-H_i'')^2+\Sigma(y_{i,act}-y_{est})^2$ = 1.53E-08

Table B.15 – Calculation of n-value for Dowel Configuration 0 (No Dowels). Nominal Depth = 38.1 cm. Discharge = 112.14 l/s.

Flume Sect. No., i	$y_{i,act}$ [m]	$\Delta y_{i,act}$ [m]	y_{est} [m]	A_i [m^2]	$V_i^2/2g$ [m]	$H_i'=y_i+V_i^2/2g$ [m]	P_i [m]	R_i [m]	$S_{f,i}$	$S_{f,avg}$	Δx [m]	h_f [m]	$H_i''=H_{i-1}''+h_f$ [m]	$(H_i'-H_i'')^2$ [m^2]	$(y_{i,act}-y_{est})^2$ [m^2]
1	0.3789		0.379	0.432	0.003	0.382	1.988	0.217	0.0022				*0.382*		4.53E-10
		0.0027								0.0021	1.303	0.0028			
2	0.3816		0.382	0.436	0.003	0.385	1.997	0.219	0.0021				0.385	2.13E-09	2.02E-09
		0.0027								0.0021	1.219	0.0025			
3	0.3844		0.384	0.441	0.003	0.388	2.006	0.220	0.0021				0.388	5.71E-10	5.69E-10

Calculated n-value : 0.0651 Total SSE, $\Sigma(H_i'-H_i'')^2+\Sigma(y_{i,act}-y_{est})^2$ = 5.74E-09

Table B.16 – Calculation of n-value for Dowel Configuration 1a (Tall Dowels). Nominal Depth = 38.1 cm. Discharge = 112.99 l/s.

Flume Sect. No., i	$y_{i,act}$ [m]	$\Delta y_{i,act}$ [m]	y_{est} [m]	A_i [m^2]	$V_i^2/2g$ [m]	$H_i'=y_i+V_i^2/2g$ [m]	P_i [m]	R_i [m]	$S_{f,i}$	$S_{f,avg}$	Δx [m]	h_f [m]	$H_i''=H_{i-1}''+h_f$ [m]	$(H_i'-H_i'')^2$ [m^2]	$(y_{i,act}-y_{est})^2$ [m^2]
1	0.3770		0.377	0.429	0.004	0.381	1.982	0.217	0.0021				*0.381*		2.93E-11
		0.0027								0.0020	1.303	0.0026			
2	0.3798		0.380	0.434	0.003	0.383	1.991	0.218	0.0020				0.383	1.47E-10	1.39E-10
		0.0024								0.0020	1.219	0.0024			
3	0.3822		0.382	0.437	0.003	0.386	1.999	0.219	0.0020				0.386	4.20E-11	3.97E-11

Calculated n-value : 0.0624 Total SSE, $\Sigma(H_i'-H_i'')^2+\Sigma(y_{i,act}-y_{est})^2$ = 3.97E-10

Table B.17 – Calculation of n-value for Dowel Configuration 1b (Short Dowels). Nominal Depth = 38.1 cm. Discharge = 88.64 l/s.

Flume Sect. No., i	$y_{i,act}$ [m]	$\Delta y_{i,act}$ [m]	y_{est} [m]	A_i [m²]	$V_i^2/2g$ [m]	$H_i'=y_i+V_i^2/2g$ [m]	P_i [m]	R_i [m]	$S_{f,i}$	$S_{f,avg}$	Δx [m]	h_f [m]	$H_i''=H_{i-1}''+h_f$ [m]	$(H_i'-H_i'')^2$ [m²]	$(y_{i,act}-y_{est})^2$ [m²]
1	0.3786		0.379	0.432	0.002	0.381	1.987	0.217	0.0018				*0.381*		4.85E-10
		0.0024								0.0018	1.303	0.0023			
2	0.3810		0.381	0.435	0.002	0.383	1.995	0.218	0.0017				0.383	2.26E-09	2.19E-09
		0.0020								0.0017	1.219	0.0021			
3	0.3830		0.383	0.439	0.002	0.385	2.001	0.219	0.0017				0.385	6.22E-10	6.10E-10

Calculated n-value : **0.0744**

Total SSE, $\Sigma(H_i'-H_i'')^2+\Sigma(y_{i,act}-y_{est})^2$ = 6.16E-09

Table B.18 – Calculation of n-value for Dowel Configuration 2 (5 Rows Staggered). Nominal Depth = 38.1 cm. Discharge = 99.96 l/s.

Flume Sect. No., i	$y_{i,act}$ [m]	$\Delta y_{i,act}$ [m]	y_{est} [m]	A_i [m²]	$V_i^2/2g$ [m]	$H_i'=y_i+V_i^2/2g$ [m]	P_i [m]	R_i [m]	$S_{f,i}$	$S_{f,avg}$	Δx [m]	h_f [m]	$H_i''=H_{i-1}''+h_f$ [m]	$(H_i'-H_i'')^2$ [m²]	$(y_{i,act}-y_{est})^2$ [m²]
1	0.3642		0.364	0.410	0.003	0.367	1.941	0.211	0.0022				*0.367*		4.63E-10
		0.0027								0.0021	1.303	0.0028			
2	0.3670		0.367	0.414	0.003	0.370	1.950	0.213	0.0021				0.370	2.17E-09	2.07E-09
		0.0027								0.0021	1.219	0.0025			
3	0.3697		0.370	0.418	0.003	0.373	1.958	0.214	0.0021				0.373	5.81E-10	5.84E-10

Calculated n-value : **0.0681**

Total SSE, $\Sigma(H_i'-H_i'')^2+\Sigma(y_{i,act}-y_{est})^2$ = 5.86E-09

Table B.19 – Calculation of n-value for Dowel Configuration 3 (3 Rows Staggered). Nominal Depth = 38.1 cm. Discharge = 89.77 l/s.

Flume Sect. No., i	$y_{i,act}$ [m]	$\Delta y_{i,act}$ [m]	y_{est} [m]	A_i [m²]	$V_i^2/2g$ [m]	$H_i'=y_i+V_i^2/2g$ [m]	P_i [m]	R_i [m]	$S_{f,i}$	$S_{f,avg}$	Δx [m]	h_f [m]	$H_i''=H_{i-1}''+h_f$ [m]	$(H_i'-H_i'')^2$ [m²]	$(y_{i,act}-y_{est})^2$ [m²]
1	0.3795		0.380	0.433	0.002	0.382	1.990	0.218	0.0018				*0.382*		1.16E-09
		0.0026								0.0018	1.303	0.0024			
2	0.3821		0.382	0.437	0.002	0.384	1.998	0.219	0.0018				0.384	5.40E-09	5.24E-09
		0.0020								0.0018	1.219	0.0022			
3	0.3840		0.384	0.440	0.002	0.386	2.005	0.220	0.0018				0.386	1.49E-09	1.45E-09

Calculated n-value : **0.0752**

Total SSE, $\Sigma(H_i'-H_i'')^2+\Sigma(y_{i,act}-y_{est})^2$ = 1.47E-08

Appendix C. Depth-Averaged Velocity Distribution in Trapezoidal Channel (Maynord's Data)

A model for predicting the depth-averaged velocity in a trapezoidal channel with a single or multiple cylinders was described in Section 3.7. In (3.12) the term $U_x(z)$ was introduced and defined as the free-stream depth-averaged velocity at any point across the width of a trapezoidal channel in the absence of any wakes. The following equation was given for $U_x(z)$:

$$\frac{U_x(z)}{U_0} = 1.152 - 0.139 \exp[r(z)/Y] \tag{3.19}$$

where U_0 is the mean velocity based on flow area, $r(z)$ is the distance from the toe of slope to the point of interest, z [$r(z)$ is positive atop the bank and negative over the channel bed], and Y is the flow depth over the channel bed. Although (3.19) is applicable only to the physical model used in this study, the approach taken to derive (3.19) can be applied to derive a similar expression for any trapezoidal channel. Presented in the following sections is the analysis from which (3.19) was developed.

Data from Maynord (1992) is used herein to examine depth-averaged velocity distributions in trapezoidal channels. Maynord worked to establish criteria for selecting a stable riprap size for open-channel flows and performed several tests in a trapezoidal channel with a bottom width of 3.66 m (12 ft) and 2:1 side slopes. Maynord recorded point velocities at numerous sections in the channel. Two of the sections were upstream of any bends in the channel; only data recorded in those bends is used.

Maynord (1992) calculated depth averaged velocities from point velocity measurements taken along vertical lines. The depth-averaged velocities reported by Maynord, $U_x(r)$, were divided by the cross-section-averaged velocity ($U_0 = Q/A$) to arrive at a dimensionless measure of the depth-averaged velocity at different locations across the width of the channel. The variable r is the perpendicular distance from the toe of slope to the vertical line for which the depth averaged velocity was calculated; r is positive atop the bank and negative atop the channel bed. Figure C.1 is a plot of $U_x(r)/U_0$ versus r/Y (Y is the channel flow depth atop the bed).

An equation of the form

$$\frac{U_x(r)}{U_0} = \beta_0 + \beta_1 \exp(r/Y) \tag{C.1}$$

was found to suitably fit the data reported by Maynord. Parameters were estimated for (C.1) using the method of least squares and Maynord's data; the resulting equation is

$$\frac{U_x(r)}{U_0} = 1.127 + 0.152 \exp(r/Y) \tag{C.2}$$

The applicability of (C.2) is limited to straight reaches in trapezoidal channels with 2:1 side slopes, and bed and bank materials similar to those used by Maynord (1992). The grain size distribution of the bed and bank materials used by Maynord is shown in Figure C.2.

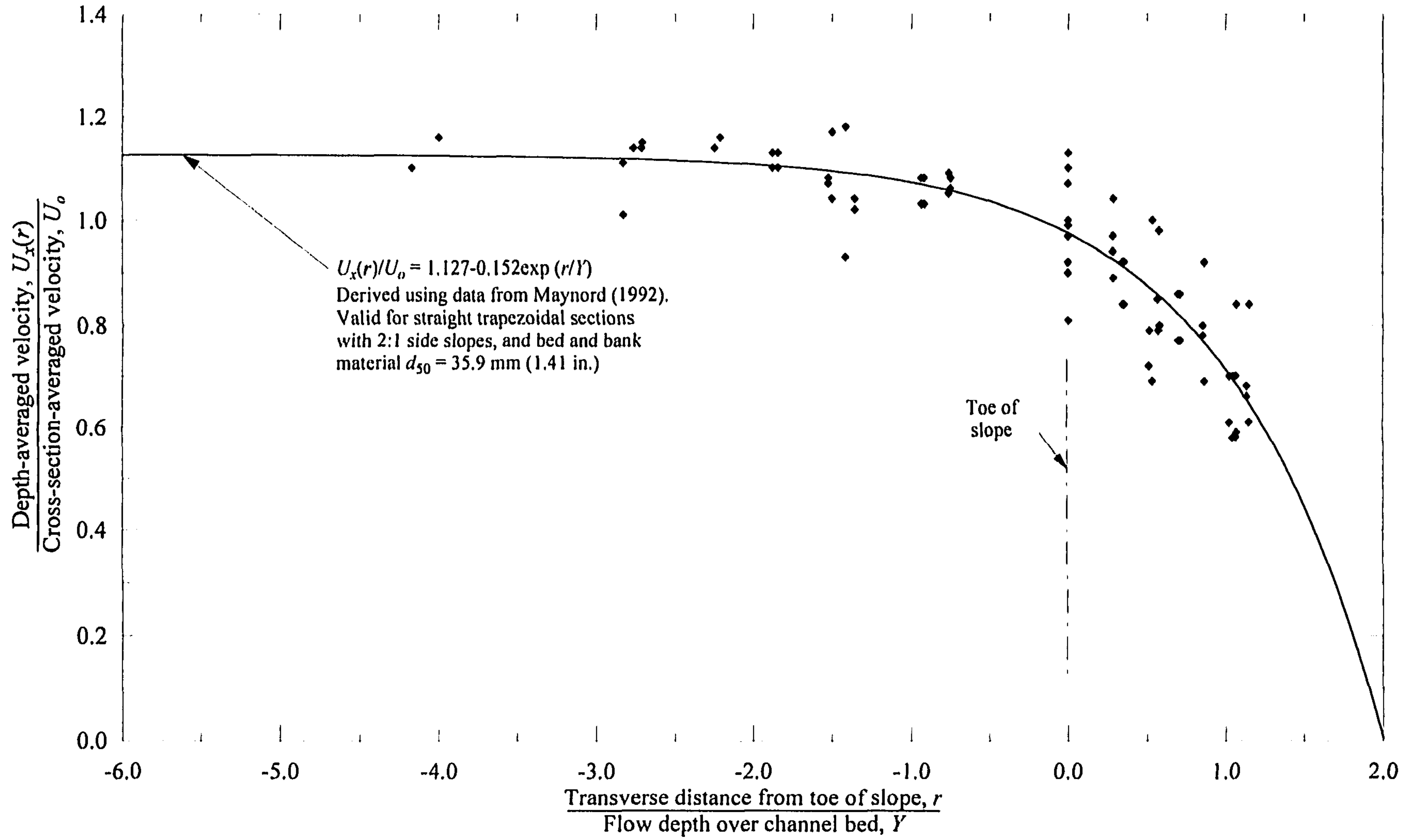

Figure C.1 – Depth-averaged velocity distribution in trapezoidal channel based on data from Maynord (1992).

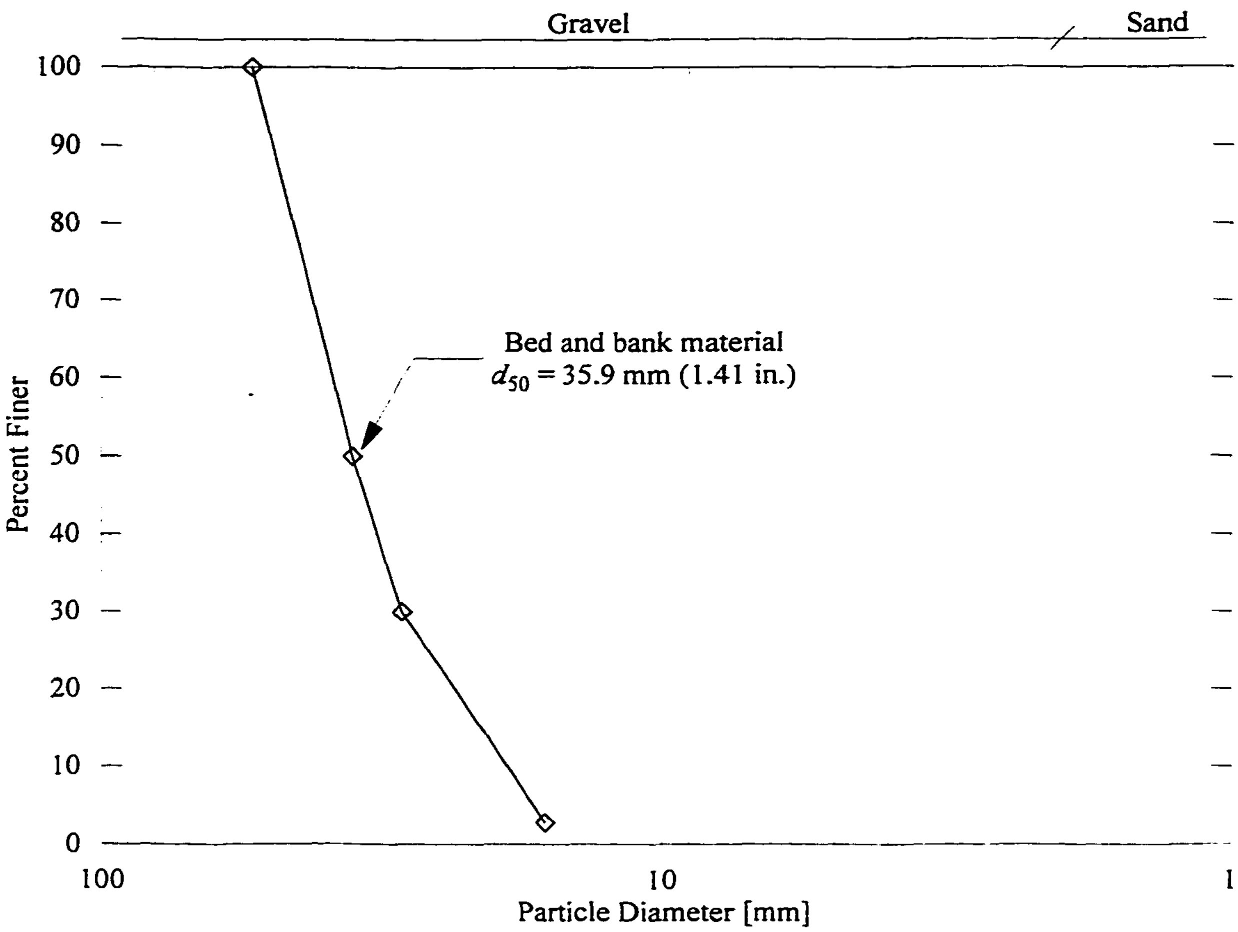

Figure C.2 – Grain size distribution of bed and bank material in trapezoidal channel by used by Maynord (1992).

Appendix D. Supplementary Soil Data

Table D.1 – Sixteenth Percentile Grain Size (d_{16}) of Soil Samples [mm]

Reach No.	Transect No.	Soil Sampling Point Number* 2				3	4				5				6				*Bed*	*Bar*
		Depth Increment* 1	2	3	4	1	1	2	3	4	1	2	3	4	1	2	3	4	1	1
1	1	0.014		0.016		0.012					0.016	0.010	0.009		0.012	0.007	0.011		0.491	4.06
	2	0.014	0.016	0.010	0.008	0.014	0.016	0.013	0.012	0.005	0.013	0.010	0.011	0.011	0.012	0.010	0.004		0.158	0.361
	3	0.015	0.018	0.014	0.011	0.012	0.016	0.022	0.015	0.012	0.022	0.016	0.011	0.017	0.021	0.012	0.016	0.025	0.388	0.235
	4	0.014	0.012	0.010	0.009	0.010	0.010	0.010	0.008	0.005	0.026	0.010	0.010	0.005	0.013	0.010	0.013	0.008	7.30	0.572
	5	0.003				0.003					0.005	0.004			0.097	0.004			16.34	2.19
2	1	0.017	0.022	0.016	0.013	0.018	0.015	0.017	0.016	0.010	0.016	0.013	0.012	0.012	0.019	0.016	0.016	0.014	0.188	0.395
	2	0.016	0.017	0.016	0.009	0.017	0.015	0.017	0.016	0.010	0.012	0.018	0.018	0.012	0.015	0.009	0.009	0.009	0.285	0.264
	3	0.014	0.018	0.009	0.013	0.015	0.012	0.013	0.010	0.010	0.016	0.019	0.014	0.011	0.005	0.007	0.002		0.403	0.375
	4	0.004		0.004	0.021	0.017	0.016		0.011		0.017	0.010	0.006	0.004	0.019	0.019	0.014	0.008	2.52	0.351
3	1	0.012	0.009	0.010	0.014	0.015	0.019	0.011	0.011	0.012									0.007	
	2	0.008	0.005	0.004	0.005	0.006	0.010	0.009	0.009	0.009	0.024	0.020	0.035	0.026	0.028	0.077	0.102	0.021	0.008	0.987
	3	0.007	0.004			0.009	0.010	0.002	0.002		0.009						0.004		0.040	0.301
	4	0.014	0.004	0.005	0.005	0.005	0.011	0.010	0.009	0.010	0.009	0.013	0.051	0.261	0.011	0.014		5.45	0.280	0.280
	5	0.011	0.008	0.009	0.006	0.017	0.022	0.017	0.022	0.017	0.022	0.020	0.022	0.016	0.025				0.359	

*See Figure 3.2 for a definition of this term.

Table D.2 – Twenty-fifth Percentile Grain Size (d_{25}) of Soil Samples [mm]

Reach No.	Transect No.	Soil Sampling Point Number*																		
		2				3	4				5				6				*Bed*	*Bar*
		Depth Increment*																		
		1	2	3	4	1	1	2	3	4	1	2	3	4	1	2	3	4	1	1
1	1	0.020		0.023		0.020					0.023	0.018	0.016		0.019	0.015	0.017		0.790	7.58
	2	0.021	0.022	0.016	0.012	0.021	0.022	0.019	0.018	0.010	0.019	0.021	0.017	0.017	0.016	0.016	0.010		0.218	0.421
	3	0.021	0.026	0.020	0.017	0.018	0.020	0.030	0.020	0.018	0.031	0.023	0.018	0.025	0.032	0.019	0.022	0.034	1.39	0.418
	4	0.020	0.018	0.015	0.015	0.016	0.016	0.016	0.015	0.010	0.046	0.017	0.017	0.013	0.019	0.016	0.019	0.012	8.35	0.989
	5	0.009	0.004			0.009					0.009	0.009			0.137	0.010			17.98	3.906
2	1	0.024	0.033	0.021	0.018	0.025	0.022	0.023	0.021	0.016	0.021	0.017	0.019	0.018	0.026	0.024	0.023	0.021	0.210	0.505
	2	0.021	0.023	0.022	0.016	0.020	0.020	0.025	0.024	0.015	0.019	0.025	0.026	0.020	0.024	0.016	0.016	0.016	0.426	0.308
	3	0.020	0.025	0.016	0.019	0.021	0.018	0.019	0.017	0.017	0.021	0.027	0.019	0.018	0.010	0.013	0.008	0.008	0.723	0.436
	4	0.010	0.008	0.012	0.030	0.024	0.021		0.019	0.009	0.023	0.018	0.013	0.010	0.027	0.026	0.021	0.016	4.87	0.394
3	1	0.019	0.016	0.017	0.019	0.021	0.027	0.017	0.018	0.019									0.019	
	2	0.015	0.011	0.009	0.012	0.011	0.018	0.016	0.015	0.015	0.037	0.030	0.060	0.040	0.049	0.131	0.152	0.031	0.015	1.657
	3	0.012	0.008	0.007	0.003	0.015	0.018	0.010	0.008		0.016	0.004			0.001	0.003	0.012		0.069	0.420
	4	0.019	0.010	0.009	0.011	0.010	0.018	0.018	0.019	0.017	0.016	0.021	0.135	0.301	0.018	0.020	0.203	8.22	0.355	0.329
	5	0.017	0.014	0.014	0.012	0.026	0.035	0.028	0.033	0.026	0.039	0.030	0.033	0.023	0.053				0.424	

*See Figure 3.2 for a definition of this term.

Table D.3 – Seventy-fifth Percentile Grain Size (d_{75}) of Soil Samples [mm]

		Soil Sampling Point Number*																		
		2				3	4				5				6				*Bed*	*Bar*
		Depth Increment*																		
Reach No.	Transect No.	1	2	3	4	1	1	2	3	4	1	2	3	4	1	2	3	4	1	1
1	1	0.091		0.222		0.112					0.185	0.089	0.071		0.113	0.070	0.058		9.50	20.30
	2	0.115	0.196	0.071	0.035	0.124	0.095	0.089	0.067	0.032	0.097	0.122	0.055	0.054	0.092	0.042	0.032		0.725	7.40
	3	0.097	0.189	0.113	0.067	0.060	0.100	0.187	0.103	0.068	0.125	0.131	0.062	0.174	0.147	0.062	0.127	0.187	15.75	6.84
	4	0.094	0.070	0.064	0.045	0.049	0.047	0.045	0.061	0.037	0.212	0.055	0.056	0.075	0.087	0.106	0.133	0.057	14.22	10.65
	5	0.037	0.029	0.028	0.026	0.037					0.037	0.034			0.239	0.100			30.60	16.24
2	1	0.126	0.192	0.108	0.064	0.121	0.088	0.112	0.090	0.051	0.090	0.053	0.077	0.092	0.103	0.134	0.084	0.103	0.351	11.01
	2	0.099	0.114	0.093	0.056	0.094	0.070	0.139	0.102	0.054	0.062	0.105	0.119	0.107	0.078	0.052	0.048	0.086	6.34	5.66
	3	0.069	0.122	0.057	0.070	0.085	0.068	0.098	0.064	0.051	0.123	0.150	0.089	0.073	0.053	0.046	0.026	0.027	10.18	8.16
	4	0.050	0.047	0.098	0.074	0.096	0.077		0.129	0.036	0.099	0.058	0.053	0.034	0.122	0.136	0.079	0.071	15.37	0.928
3	1	0.097	0.046	0.053	0.082	0.148	0.233	0.060	0.060	0.147									0.102	
	2	0.039	0.034	0.033	0.051	0.038	0.137	0.069	0.075	0.065	0.197	0.160	0.235	0.224	0.198	0.293	0.304	0.222	0.091	10.43
	3	0.072	0.034	0.029	0.027	0.078	0.153	0.048	0.030	0.029	0.130	0.044	0.010		0.047	0.063	0.079		0.300	9.06
	4	0.054	0.035	0.035	0.041	0.034	0.160	0.073	0.069	0.127	0.068	0.239	0.439	0.556	0.068	0.199	8.88		10.33	7.39
	5	0.052	0.042	0.041	0.035	0.170	0.191	0.168	0.200	0.159	0.196	0.164	0.195	0.142	0.207				8.82	

*See Figure 3.2 for a definition of this term.

Table D.4 – Eighty-fourth Percentile Grain Size (d_{84}) of Soil Samples [mm]

Reach No.	Transect No.	Soil Sampling Point Number* / Depth Increment*																		
		2				3	4				5				6				*Bed*	*Bar*
		1	2	3	4	1	1	2	3	4	1	2	3	4	1	2	3	4	1	1
1	1	0.124		0.286		0.148					0.219	0.127	0.103		0.160	0.123	0.081		12.69	22.02
	2	0.172	0.240	0.116	0.048	0.174	0.129	0.107	0.092	0.045	0.132	0.160	0.086	0.074	0.137	0.063	0.055		0.920	11.97
	3	0.139	0.213	0.162	0.105	0.086	0.146	0.215	0.157	0.115	0.172	0.164	0.087	0.205	0.184	0.088	0.185	0.215	19.23	9.63
	4	0.132	0.102	0.107	0.063	0.065	0.062	0.067	0.092	0.083	0.229	0.073	0.072	0.116	0.135	0.163	0.189	0.101	15.65	14.14
	5	0.051	0.040	0.038	0.033	0.055					0.056	0.053			0.270	0.206				29.53
2	1	0.171	0.214	0.148	0.094	0.169	0.126	0.170	0.125	0.066	0.124	0.071	0.108	0.134	0.159	0.182	0.120	0.137	0.433	14.24
	2	0.142	0.150	0.130	0.073	0.119	0.101	0.190	0.134	0.090	0.082	0.140	0.183	0.146	0.102	0.086	0.068	0.126		11.42
	3	0.093	0.157	0.082	0.103	0.113	0.091	0.128	0.105	0.067	0.162	0.180	0.135	0.127	0.067	0.065	0.034	0.036		19.02
	4	0.110	0.102	0.150	0.130	0.135	0.125		0.158	0.055	0.138	0.089	0.074	0.049	0.154	0.168	0.128	0.128		1.59
3	1	0.174	0.099	0.073	0.167	0.212	0.302	0.106	0.097	0.198									0.133	
	2	0.058	0.047	0.045	0.072	0.057	0.195	0.129	0.152	0.130	0.243	0.197	0.280	0.270	0.234	0.328	0.335	0.270	0.133	12.56
	3	0.154	0.052	0.039	0.036	0.133	0.205	0.072	0.040	0.049	0.186	0.071	0.016		0.068	0.088	0.104		0.372	12.23
	4	0.066	0.052	0.048	0.062	0.049	0.207	0.146	0.140	0.178	0.141	0.295	0.520	0.726	0.136	0.273	11.88		12.73	10.55
	5	0.070	0.058	0.055	0.046	0.212	0.218	0.203	0.237	0.199	0.222	0.194	0.226	0.179	0.230				11.56	

*See Figure 3.2 for a definition of this term.

Table D.5 – Geometric Mean Grain Size (d_g) of Soil Samples [mm]

Reach No.	Transect No.	Soil Sampling Point Number* 2				3	4				5				6				Bed	Bar
		Depth Increment* 1	2	3	4	1	1	2	3	4	1	2	3	4	1	2	3	4	1	1
1	1	0.041		0.067		0.042					0.060	0.036	0.030		0.044	0.030	0.030		2.50	9.45
	2	0.049	0.062	0.034	0.020	0.050	0.045	0.037	0.033	0.015	0.042	0.040	0.030	0.029	0.041	0.026	0.015		0.381	2.08
	3	0.046	0.062	0.047	0.034	0.032	0.048	0.069	0.048	0.037	0.061	0.052	0.031	0.059	0.062	0.033	0.055	0.074	2.73	1.50
	4	0.043	0.035	0.033	0.024	0.025	0.025	0.025	0.028	0.020	0.077	0.027	0.027	0.024	0.042	0.039	0.049	0.029	10.69	2.84
	5	0.012				0.012					0.017	0.015			0.162	0.028				8.05
2	1	0.054	0.068	0.048	0.034	0.055	0.043	0.053	0.045	0.025	0.044	0.031	0.036	0.040	0.054	0.054	0.043	0.044	0.286	2.37
	2	0.047	0.051	0.045	0.026	0.045	0.039	0.056	0.046	0.029	0.031	0.050	0.058	0.043	0.039	0.028	0.025	0.034		1.74
	3	0.037	0.053	0.028	0.037	0.041	0.033	0.041	0.032	0.026	0.051	0.059	0.044	0.037	0.018	0.022	0.009			2.67
	4	0.020		0.025	0.052	0.048	0.044		0.042		0.049	0.030	0.021	0.015	0.054	0.056	0.043	0.032		0.747
3	1	0.046	0.030	0.027	0.048	0.057	0.075	0.035	0.032	0.048									0.031	
	2	0.022	0.015	0.013	0.019	0.018	0.044	0.035	0.036	0.033	0.076	0.063	0.099	0.083	0.081	0.159	0.185	0.074	0.032	3.52
	3	0.032	0.015			0.034	0.045	0.013	0.009		0.041						0.020		0.123	1.92
	4	0.031	0.015	0.015	0.018	0.015	0.047	0.039	0.036	0.041	0.036	0.063	0.163	0.435	0.039	0.062			1.89	1.72
	5	0.028	0.022	0.022	0.017	0.061	0.069	0.059	0.071	0.059	0.070	0.062	0.070	0.053	0.076				2.04	

*See Figure 3.2 for a definition of this term.

Table D.6 – Standard Deviation (σ) of Soil Samples [mm]

Reach No.	Transect No.	Soil Sampling Point Number* 2				3	4				5				6				*Bed*	*Bar*
		Depth Increment* 1	2	3	4	1	1	2	3	4	1	2	3	4	1	2	3	4	1	1
1	1	3.01		4.23		3.53					3.66	3.54	3.40		3.65	4.06	2.69		5.08	2.33
	2	3.49	3.88	3.42	2.39	3.48	2.85	2.90	2.75	2.94	3.18	4.04	2.81	2.60	3.35	2.46	3.65		2.42	5.76
	3	3.05	3.41	3.42	3.13	2.69	3.04	3.12	3.26	3.08	2.81	3.16	2.78	3.48	2.95	2.71	3.36	2.91	7.04	6.41
	4	3.12	2.88	3.27	2.63	2.57	2.44	2.64	3.33	4.10	2.98	2.73	2.69	4.90	3.17	4.13	3.83	3.45	1.46	4.97
	5	4.31				4.56					3.40	3.50			1.67	7.31				3.67
2	1	3.20	3.13	3.08	2.73	3.09	2.90	3.20	2.77	2.62	2.79	2.30	2.96	3.33	2.93	3.34	2.77	3.12	1.52	6.00
	2	3.00	2.96	2.90	2.82	2.67	2.59	3.37	2.94	3.08	2.66	2.83	3.15	3.44	2.62	3.04	2.70	3.69		6.57
	3	2.54	2.96	2.94	2.81	2.75	2.75	3.13	3.27	2.55	3.16	3.05	3.09	3.41	3.69	3.01	3.95			7.12
	4	5.52		5.90	2.52	2.84	2.83		3.78		2.84	2.95	3.56	3.30	2.83	3.01	2.98	3.96		2.13
3	1	3.77	3.30	2.66	3.50	3.75	4.03	3.06	3.00	4.14									4.31	
	2	2.61	3.08	3.37	3.68	3.15	4.44	3.70	4.23	3.91	3.17	3.13	2.83	3.25	2.88	2.06	1.81	3.63	4.12	3.57
	3	4.87	3.50			3.88	4.50	5.56	4.22		4.51						5.08		3.03	6.37
	4	2.16	3.42	3.13	3.47	3.31	4.41	3.74	3.86	4.32	3.91	4.71	3.19	1.67	3.50	4.41			6.74	6.13
	5	2.55	2.66	2.53	2.68	3.48	3.13	3.46	3.32	3.38	3.15	3.13	3.22	3.35	3.05				5.68	

*See Figure 3.2 for a definition of this term.

Table D.7 – Skewness (γ) of Soil Samples

		Soil Sampling Point Number*																		
		2				3	4				5				6				*Bed*	*Bar*
		Depth Increment*																		
Reach No.	Transect No.	1	2	3	4	1	1	2	3	4	1	2	3	4	1	2	3	4	1	1
1	1	-0.043		-0.016		-0.031					-0.213	0.046	0.018		0.122	0.076	0.025		-0.208	-0.637
	2	0.173	0.023	0.087	0.028	0.186	-0.015	0.139	0.045	-0.208	0.086	-0.080	0.037	0.031	0.262	-0.052	-0.248		-0.117	0.553
	3	0.083	-0.362	0.214	0.071	0.068	0.134	-0.186	0.154	0.222	0.069	0.040	-0.021	-0.238	-0.168	0.015	0.077	-0.280	-0.584	-0.243
	4	0.073	0.042	0.151	-0.039	-0.063	-0.075	-0.036	-0.001	-0.051	-0.590	-0.059	-0.077	-0.093	0.242	0.132	0.204	0.094	-0.051	-0.281
	5	-0.409				-0.384					-0.063	-0.195			-0.420	0.051				-0.057
2	1	0.050	-0.344	0.095	0.056	0.110	0.077	0.072	0.201	-0.065	0.140	0.104	0.092	0.141	0.034	0.024	0.154	0.159	0.070	-0.125
	2	0.095	0.073	0.147	-0.053	0.191	0.104	-0.103	-0.019	0.104	-0.107	-0.055	0.032	0.032	-0.096	0.025	-0.030	0.059		0.551
	3	-0.038	-0.045	0.012	0.079	0.056	0.075	0.080	0.071	-0.216	0.126	-0.071	0.158	0.091	-0.245	-0.147	-0.477			0.394
	4	-0.088		-0.058	-0.056	0.044	0.180		0.017		0.075	0.019	-0.168	-0.282	0.011	-0.004	0.097	0.069		0.376
3	1	0.194	0.131	-0.041	0.278	0.225	-0.091	0.156	0.065	0.098									-0.340	
	2	-0.106	-0.304	-0.362	-0.204	-0.195	0.135	0.117	0.150	0.109	-0.210	-0.087	-0.386	-0.407	-0.299	-0.384	-0.365	-0.213	-0.205	-0.340
	3	0.116	-0.185			0.129	-0.026	-0.338	-0.467		0.124						-0.414		-0.402	0.372
	4	0.019	-0.268	-0.272	-0.208	-0.267	0.084	0.184	0.140	0.126	0.168	0.087	-0.525	0.129	0.199	0.198			0.068	0.511
	5	-0.035	-0.092	-0.195	-0.275	-0.094	-0.523	-0.317	-0.360	-0.037	-0.549	-0.299	-0.475	0.007	-0.586				0.451	

*See Figure 3.2 for a definition of this term.

Table D.8 – Gradient Coefficient of Soil Samples

Reach No.	Transect No.	Soil Sampling Point Number* 2				3	4				5				6				*Bed*	*Bar*
		Depth Increment* 1	2	3	4	1	1	2	3	4	1	2	3	4	1	2	3	4	1	1
1	1	3.01		4.23		3.54					3.80	3.54	3.40		3.70	4.08	2.69		5.38	2.67
	2	3.58	3.88	3.44	2.39	3.58	2.85	2.94	2.76	3.01	3.19	4.06	2.81	2.60	3.52	2.46	3.84		2.43	8.67
	3	3.06	3.75	3.54	3.14	2.70	3.07	3.19	3.32	3.17	2.81	3.16	2.78	3.63	3.00	2.71	3.38	3.05	12.12	7.07
	4	3.13	2.89	3.33	2.63	2.57	2.44	2.64	3.33	4.11	3.61	2.73	2.69	4.96	3.30	4.20	3.97	3.48	1.46	5.49
	5	5.09				5.36					3.41	3.61			1.71	7.35				3.68
2	1	3.20	3.37	3.10	2.73	3.11	2.91	3.21	2.83	2.63	2.82	2.30	2.97	3.37	2.93	3.34	2.80	3.18	1.52	6.15
	2	3.02	2.97	2.93	2.83	2.72	2.60	3.39	2.94	3.10	2.67	2.83	3.15	3.44	2.63	3.04	2.70	3.70		10.44
	3	2.54	2.97	2.94	2.82	2.75	2.76	3.14	3.28	2.60	3.19	3.06	3.14	3.43	3.88	3.05	4.84			9.36
	4	5.58		5.93	2.52	2.84	2.88		3.78		2.85	2.95	3.64	3.49	2.83	3.01	3.00	3.98		2.22
3	1	3.89	3.34	2.66	3.72	3.92	4.06	3.11	3.01	4.19									4.85	
	2	2.63	3.26	3.71	3.81	3.23	4.53	3.74	4.33	3.96	3.27	3.14	3.06	3.63	3.02	2.14	1.86	3.77	4.30	3.90
	3	4.95	3.59			3.94	4.50	6.52	5.21		4.59						6.28		3.34	7.94
	4	2.16	3.61	3.29	3.58	3.48	4.44	3.85	3.93	4.40	4.02	4.76	3.79	1.67	3.60	4.60			6.79	8.96
	5	2.55	2.67	2.57	2.77	3.51	3.71	3.73	3.63	3.38	3.79	3.31	3.73	3.35	3.72				7.51	

*See Figure 3.2 for a definition of this term.

Appendix E. Horizontal Point Frame Data

Table E.1 – Reach 1 Horizontal Point Frame Data (August 1997)

Guide Hole No.	Transect 1				Transect 2				Transect 3				Transect 4				Transect 5			
	Setup No.																			
	1	2	3	4	1	2	3	4	1	2	3	4	1	2	3	4	1	2	3	4
1												na	na	na	na	na		na	na	
2			1																	
3			1							1										
4										1							3			
5			1							2							3			
6															1		2			
7															1		1			
8																				
9										1										
10										1										
11			1														3			
12																	1			
13			1														1			
14			2							1						1				
15	1		2							3						2				
16										2						2				
17										2	2				1	2	1			
18										1	5					3	1			
19			1						1	1	2				2	1	1			
20			1							3	2	na			1		2			
21										5	na		na		na	na	na	na	na	
22									2	3	1									
23										3	3				2		1			
24									1		3				2					
25				3					2		2				2		1			
26			1	5					3	1	3				1					
27			1	5					1	2	4				1		3			
28			2	1					1	5	1				3	3	2			
29										1					3	2	1			
30	2		2							2				1	1	1	2			
31														2	1	1				
32										6	3			3	1	2				
33	2		1	3					1		2	1		4	1	2				
34			1	1					1					5	2	1				3
35				1					1	1		1		2	1		2			
36						3			3	1	1	2			2	1				
37				2		1	1		2	1	2	2			2					
38						4	2		1	3	1	2		1	2					3
39						5	2		2	2	1	3			1		1			
40						na	na		1	5	na	na	na	na	na	na	na	na	na	
41				4		2			1		5	2		3	2	3	5			
42				4		6				2	3	3		2	3	3	4			
43		1		3			2			2	3			na	3	4	3		2	
44		1		5		1	3			1				2	4	2	1		1	
45		2		2		2				3	2			2	4	3	1			
46		2		4		4		3		1	1		2	4	3	2				
47		3		5		3	1			2	3			2	4	2				1
48		4		3						4	5		2	1	3	3	1	2		1
49		2	2	1	1	2		3	3	4	4	1	2	4	2	1	2			2
50		1	2	2	1	3			2	3	3	5	3	3		1	2			3
51		3		1	2	1			4	4	1	3	10	6	3	2	2			1
52		2		1		2			3	2	3	7	8	7	3	3	1	1		2
53	3	2		2	1	6	2		3	3	5	1	5	3		3		6		2
54	2	4		1		4	3		1	3	3	5	5	7	1	2	1	4		4
55		7		1	1	4	4		2	1	4	5	5	6	1	5	1	5		7
56		5	1	3	2	2	4		2	1	7	4	7	2	3	5	3	5		3
57	1	4	2	5		2	3		2	2	2	2	6	4	1	na	5	5		4
58	1	4	na	1	2	na	7			1	2	2	5	6	2	na	3	4	1	3
59	3	5	na	1	3	na	na			1	1	6	na	5	1	na	4	2	2	3
60			na	na		na	na				na	na	na	na	na	na	na	na	na	na
Sum	15	52	26	70	13	57	34	6	46	100	95	57	60	87	77	68	71	40	6	42

na = Inaccessible guide hole

Table E.2 – Reach 1 Horizontal Point Frame Data (January 1998)

Guide Hole No.	Transect 1				Transect 2						Transect 3				Transect 4				Transect 5					
	Setup No.																							
	1	2	3	4	1	2	3	4	5	6	1	2	3	4	1	2	3	4	1	2	3	4	5	6
1	na	na					na		na	na				na	na			na	na	na	na	na	na	na
2														1			2							1
3																								
4														1			1							
5																	1							
6													1	1										
7		1											5											
8													3											
9																								
10																								1
11		1																						
12		2																						
13																1								
14																1	1							
15		1														1	1							
16																								
17																2								
18													1											
19		1																						
20	na	na					na		na	na		1		na	na	1	na	na	na	na	na	na	na	na
21	na	na			1		na		na	na				na	na		na	na	na	na	na	na	na	na
22		1													1						1			
23														1	1						1		1	
24														2	1									
25														1										
26	1	1																						
27												1	1	1										
28	1																							
29													1	1										
30																								
31		1											1											
32		1											1		1	1								
33													1			3								
34				2											1	2							1	
35		1		1								1			2								3	
36		1										2	1		3								3	
37		1										2			2								1	
38	1											1												
39												6				1		1						
40	na	na					na		na	na		5		na	na	2		na	na	na	na	na	na	na
41	na	na	na	na	na		na	na	na	na	na	na	na	na	na	na	na	na	na	na	na	na	na	na
42	1	1		1								3	6	2		3					1			
43		4										5	3	1	2	4					1			
44	2	1	1									3	5			2			1		1			
45	1	2				2					1		1	2		3		1			1			
46	1	2					1		1			1	4	3	1	2			2					
47	3	1			1							1	3	2	1	2			1					
48	4	1									1	1	1	1	1	2			1					1
49	2	1									2	1	1		2				1					
50	3			1				1			1	2	2	3		1			2		1			3
51	1	2			1			1			1	1				1			1	1	1			5
52	3	1	1								2	2	1			2		1						
53	3	1			1						2	2	1	1	1	2		1	2					3
54	3	1	4		1	1	1		2	2	1	4	3	1	1	2		3	2				2	3
55	3		1				3	1	1	2	2	3	2	1	2	3	3	1	3	1	3		2	3
56	3	3	2	1		2	2	2	3	3	2	3	4		1		4	1			2		2	4
57	na	1	5		2	1	2		3	4	4	2	5	3	3		2	1			3		1	2
58	na	1	2	2		3	3	na	2	6	3	5	na	3	5		4						1	4
59	na	3	na		3	7	4	na	4		3	2	na	4	3		na			1	4	1	3	8
60	na	na	na	na	na		na	na	na	na	na	na	na	na	na	na	na	na	na	na	na	na	na	na
Sum	36	39	16	8	10	16	16	5	16	17	25	60	58	36	35	44	19	26	16	3	20	1	20	38

na = Inaccessible guide hole

Table E.3 – Reach 1 Horizontal Point Frame Data (March 1998)

Guide Hole No.	Transect 1					Transect 2				Transect 3				Transect 4				Transect 5			
	Setup No.																				
	1	2	3	4	5	1	2	3	4	1	2	3	4	1	2	3	4	1	2	3	4
1																					
2																					
3						1															
4										1											
5							1			1									1		
6										1											
7							1														
8										2											2
9										1									1		
10										1						1					
11										1			1								
12										1						1	1				
13										1			1				1				1
14										2											
15							1														
16																					
17							1														
18							1														
19				1						1											
20				na			na					1									
21				na			na			na						na					
22					1					3						2	1				
23				1						3							1		1		1
24				1						3					1	1					
25				1						2					1				1		
26										2							2				
27										2							1				
28							1			1					1				1		
29							1								1		1	1			1
30							1			1			2				1				
31										2			1						1		
32							1														
33													1								
34	1														1						1
35	2									1			4								
36	2					1				1			3		1						
37						1			2	3			2						2		
38				2			1			2			5				2				2
39						1	1			2			2		1		1	1			
40	na	na		na		na				na			na		na		na	na			
41	na	na		na		na			na	8		1			1		3	na			
42				1			1			6		1	2		1	1	3		1		1
43	1			2						7			3								1
44	1			2		1				6			1	1	1		1	1			2
45					2	1				9			5				2				1
46					1	1				10		3	2			1			4		2
47					1					8		3	4		1						1
48	1			1		1	1			4		2	1		2	1		1	1		
49	3			2	1	4				9		3	4		1				1		
50					1					5		4	3		3			1	1		1
51	3								2	3		5	4		3		3		3		2
52	1	1					1			11		3	10		4		2				2
53		2		3		1	1			9		7	16		2	2	3		2		5
54		4		2		5	1			6		10	10		5		2	1	3		10
55	1	6		2					1	5		12	5		5	3	3		2		5
56	2	5		1	1	3	4	2	1	7		na	4		5	4	8	2	2		10
57	2	3			2	4	2	3	9	11	1	na	8		5	na	3	3	na		8
58	6	9			1	12		20	12	11		na	4		7	na	6	4			9
59	13	15		2	2	9	3	na	12	na	2	na	na		4	na	5	7			
60					na		na	na		na	na	na	na		na	na	na	na			
Sum	39	45	0	24	13	46	25	25	39	176	3	55	108	1	57	17	56	22	28	0	68

na = Inaccessible guide hole

Table E.4 – Reach 2 Horizontal Point Frame Data (August 1997)

Guide Hole No.	Transect 1				Transect 2				Transect 3				Transect 4			
	Setup No.															
	1	2	3	4	1	2	3	4	1	2	3	4	1	2	3	4
1	na	na	na	na	na				na	na	na		3		na	na
2	1			1							2	1	1			
3		2	1	1							2	3			1	
4	2	1	1	1							1					
5	3	2	2	1				1					1		1	
6	2	3	3	1				1				1			1	
7	1	2	1									1	2			
8		1	3					1			2	2	1		2	
9	1	1										2			3	
10	1										1	3			3	
11	1			1							2				2	
12	1			2							2	1			3	
13				1							1				2	
14			1	1				2	1						3	
15			3	4					3		3					
16	1		4	1					1		4				1	
17			3	3				2	1		4		1		2	
18	1		na	2				3			2		1		2	
19			2	1				2	1		1	2		1	1	
20			4	2				1			2	1	1	2		
21	na	na	na	na	na	1	1		na	na	na				1	1
22	1					1	4			1	1				1	
23	2					2	4	4		1	1					
24							2	1		2		1				
25								3	4	2						
26				1		1			5					2		
27						3			3		2	1	1	2		
28		2				6			5		1	1	1	3		1
29				1		3			3		2	4		4	2	
30				1		4	1		2		2	1	1	4	2	1
31	1	3		3		1			3		1	1		5	4	1
32		1		2		1	2		3		2			6	4	2
33	2		2	1		2			3	1	2				2	2
34		1	na	2					1	1	1			4	2	4
35		1	3	2		2	1		1	2				1		4
36			1	1	2	1		1	1	3	2		2	2		4
37	1	5			1			2	1	3			1	2		
38	1		1	1	1			1	4	2	1		1	3		1
39		2		3	2	1		1	2	2			3	3	2	2
40	na	na	na	na	na			2	na	na	na	1	4	2	na	na
41	1	1				1	1	1		1				3	1	3
42		2				2		1		2				2	1	4
43		1	2			1				2				2		2
44						2	3		1	2	2			5		3
45			1			2		3		3	3			3		2
46	2	1	1		1	4		2	1	2	5			3		3
47		2	1		3	2				1	1			4	2	3
48	1	3	na		1	2	2		2	4	3			3		2
49		3	na		1	2			3	5			1	2	1	2
50	4	2	2		2	3		1	1	2	2		2	1		4
51	2	2			1	2	1	1		4	2				1	4
52	1	3			3	3	4	1		3	1		1	1	3	6
53	2	2			8	2	5		3	2	3			1	na	4
54	1	2		2	4	4	4	4	2	4	2	2		2	3	5
55	3	4	1		5	2	3	3	1	4	2	3	4	3	4	5
56	na	2	1	3	2	3	4	3	1	5		na	na	2	3	3
57	na	3	3	6	5	na	1	na		3	1	2	na	2	2	3
58	na	na	4	4	na	na	2	na	2	4	3	1	na	1	4	4
59	na	na	na	2	na	na	5	na	1	2	na		na	1	2	3
60	na	na	na	na	na	na	na	na	na	na	na	na	na	na	na	na
Sum	40	60	51	58	42	66	50	48	66	75	77	35	33	87	74	88

na = Inaccessible guide hole

Table E.5 – Reach 2 Horizontal Point Frame Data (January 1998)

Guide	Transect 1				Transect 2					Transect 3				Transect 4			
Hole	Setup No.																
No.	1	2	3	4	1	2	3	4	5	1	2	3	4	1	2	3	4
1				na		na	na					na	2	na	na	na	na
2		1													1		
3	1	2											1	1	1		
4															1		
5							1								1		
6															1		
7			1												1		
8		1													1		
9		1	1			3	1										
10															1		
11		1															
12		1					1										
13																	
14		1				2											
15						1											
16																1	
17																2	
18																3	
19						1											
20			1	na		na	1					na		na	na	na	1
21				na		na	na					na	1	na	na	na	na
22			1												1		
23	1						1										1
24		1															
25	1	2	1														
26	1	1	1														1
27		2	1														
28	1	1								2							
29		1								1							
30										1							
31						1				1							1
32										1						1	1
33	2				1					2			1			2	2
34										1	1	1				1	1
35					1									1		2	1
36				1		1	1			4	1					1	
37				1													
38										1	1	1		2			
39	1					1				2		1					2
40				na		na	na			1	1	na		na	na	na	
41	na	na	na	na	na	na	na	1		na	na	na	na	na	na	na	na
42			1		1					2		3				3	1
43		1								1		1	1			3	
44	1		1							1		1	1	1	1	1	3
45	1				1					1		1	1			1	2
46				1	2					1		3	2			2	2
47	1		1	1	2	1				1			3			3	
48	4		2	1	1								2			1	2
49	5		3	1	3	1					2		5	1		2	4
50	1	1	2		1	1				1	1		2			6	1
51	2	2		3	3					1	1		2			4	3
52	3		1		2	1	1			3	2	na	1			3	1
53	1	4	3	2	4					1	4	na	2			1	1
54	2		2	1	4	2					5	na	3			3	1
55	1	1	2	2	3	2	2				5	na	5			2	3
56	2		2	7	6	2	1		2	1	6	na	5	1		3	3
57	2		2	5	4	2			3		6	na	5	1	na	1	7
58	3		na	4	3	1			5	2	3	na	7	2	na	2	5
59	na		na	na	4	3	1		9	2	na	na	5	1	na	1	4
60	na	na	na	na	na	na			na	na	na	na	na	na	na	na	na
Sum	37	25	29	30	46	26	11	1	19	35	39	12	57	11	10	55	54

na = Inaccessible guide hole

Table E.6 – Reach 2 Horizontal Point Frame Data (March 1998)

Guide Hole No.	Transect 1				Transect 2				Transect 3				Transect 4			
	Setup No.															
	1	2	3	4	1	2	3	4	1	2	3	4	1	2	3	4
1	1											1				
2																
3								1	1							
4																
5		1														2
6								1								
7								1								2
8																1
9		1														
10						1			1		1					
11				1		1		1			1					
12		1									1					1
13	1								1		2					
14											1				2	
15											1				1	
16											1				1	
17			1			2							1			
18			2										1			
19			1						1	1			1			
20											1		1			
21					2											
22		2			1		1									2
23		2				1		1								1
24			2			1					1		1			1
25	1		2			1							2			
26	1		1						1				5			
27						1		1	1		1		5			
28					1							1	4			
29													5			1
30						1		1			1		2			
31		1		1					1	1	1					
32			1							1	1					1
33			4					2	1	1	1				1	
34			1						1	2	1		1			
35	1	2								1						
36		1		1							3					
37		1		1						1	1		2			
38		2	2			2				1	1		2			
39		2	2			1			1	2	1					
40			1						na				2			
41			1			1				2			1			
42	1	2				1			1	1			2		2	1
43			2			2			4	2	1		2		1	1
44		1	1						2	1			3		3	2
45		1				2	2						3		4	1
46		1				2				1	2		4		9	1
47		3	2			1	1	1	3	1			5		7	
48											3		9		7	2
49		3		1			1	1		1	4	1	8		9	1
50			4	2			1	2		2	1	1	2		4	1
51		1	3	2	1		1			6		2			5	2
52			4	4			2	2		4	2	2			4	4
53		2	3	6			1	2		5	5	3	6		6	3
54		4	6	5		2		1			2	3	7		8	5
55		2	6	10	2	3		1		3	8	1	13		10	3
56				7	4	3				5	10	1	15		13	3
57	1	2	3	5	3	3	3			4	12	1	12		10	3
58		3	2	4	4	4	11		2	6	14	1	11		6	3
59	1	na	na	na	5	7			5	4	2	2			2	
60	na	na	na	na					na							
Sum	8	41	57	50	23	43	24	19	27	59	88	20	138	0	115	48

na = Inaccessible guide hole

Table E.7 – Reach 3 Horizontal Point Frame Data (August 1997)

Guide	Transect 1				Transect 2				Transect 3					Transect 4			
Hole	Setup No.																
No.	1	2	3	4	1	2	3	4	1	2	3	4	5	1	2	3	4
1	na	na	na	na	na		na	na		na	na	na	na			na	na
2							2				2					2	3
3	1						4				1					1	1
4	1						2	2									
5											1					3	
6							1				1					1	
7							2									2	
8							3									1	
9							3										
10		1					1										2
11		2					2										1
12							1										2
13	2						3										
14	2						2										
15							2			2							
16							1			2							
17							2										
18							3										2
19		1					1										2
20		1					3										1
21	na	na	na	na	na		na	na		na	na	na	na			na	na
22		3					1										
23		2					1										
24	1	2					3	1									
25		1					1	1									
26							2	1									
27							1										
28		2					1			1							
29										2							
30		1					2			2				1			
31							1						1				
32		1	1				1			1							
33		3	2							4							
34			1	1													
35		2											1				
36		1		1									1			2	
37				1												1	
38		na															
39										5					1		
40	na	na	na	na	na		na	na		na	na	na	na			na	na
41					2		2	1		1						1	
42					4		3	1		4				1	2		
43					2		1	2		1				3	3	2	
44										4		1			1	1	
45					1	1				1		2	2	2	1	3	
46					4	1				2		3		3	1	2	
47					3	3	1			3		4		7		3	
48	1				5	2		2		1		4	1	8		1	
49	1				4	2		3						3	2	3	
50	1		1		4	4	1	1	1	1				2	2	2	
51	2	1	1		4	5			2	1				3	1	8	
52	na	2			5	2	1	2	3	1				8	1	3	
53	3		1		4	2	1	2	1				1	7	3	4	
54	3	1	3		3	3	2	1	4	1	2		1	6		1	2
55	4	1	5		4	1	2	1	2						2	2	3
56	3	2	3		3		2		2					3	4	4	3
57	2		6		2	8	1	1	2	1				2	3	2	2
58	4	1	4	2	2	3	1		4			2		3		3	1
59	2	5	3	2	3	na	1	4	2	2		3		3	1	4	2
60	na	na	na		na		na	na	na	na	na	na	na	na	na	na	na
Sum	33	36	31	7	59	37	71	26	23	43	7	19	8	65	28	62	27

na = Inaccessible guide hole

Table E.8 – Reach 3 Horizontal Point Frame Data (January 1998)

Guide Hole No.	Transect 1 Setup No. 1	2	3	4	5	6	7	8	Transect 2 Setup No. 1	2	3	4	5
1	na	na	na	na	1	na		na	na	na			
2	1				1					1			
3	3				1								
4					1							1	
5					1								
6					1								
7					1								
8					1								
9					1								
10					1								
11					1								
12					1								
13												1	
14													
15	1												
16	1												
17													
18													
19													
20		na	na	na		na		na	na	na			
21		na	na	na		na		na	na	na		1	
22					1							1	
23					1								
24					1				2			2	
25					1				1			2	
26					1							1	
27					1								1
28					1								
29					1								
30					1							1	
31					1							2	
32					1							1	
33	1												
34									1				
35				1						1			
36	1	1		1									
37				2								1	
38									2				
39									1				
40		na	na	na	na	na		na		na			
41		na	na	na	na	na		na	na	na	2	2	1
42	1										3	1	
43					1			1				2	3
44												1	
45											1	1	1
46											1	4	2
47		1	1								2	5	
48		1				1					2	3	1
49					1						1	4	
50					2				2		3	1	3
51					1						1	1	1
52		1	1		1				1		3	1	1
53					1						1	2	
54					2							2	1
55	1	1	1		5						4	6	1
56	1		2						1		3	6	1
57	2	2	1		1				1		na	8	1
58	1	3	2	1		2					2	7	
59	2			1	1	3			na	na	1	9	1
60	na	na	na	na	na	na		na	na	na	na	na	na
Sum	16	10	8	6	39	6	0	1	12	2	30	80	19

na = Inaccessible guide hole

Table E.8 – (cont)

Guide Hole No.	Transect 3				Transect 4				Transect 5					
	Setup No.													
	1	2	3	4	1	2	3	4	1	2	3	4	5	6
1		na	na	na	na		na		na					na
2														
3														
4										1				
5									1					
6					1					1				1
7														1
8							1							
9														
10					1		1							1
11					1									1
12												1		1
13					1									1
14							1		1					
15							2					2		
16							3							
17					1		4							
18					1		3		1			2		
19							3		2					
20		na	na	na	na				na			1	1	
21		na	na	na	na		na		na					na
22														2
23					1		1							1
24					1		3							1
25						1	4							
26						3	2							
27						2	1							
28						3	2							
29					1	1	1							1
30						2								
31					1	1								
32														
33														
34														
35									2	2				
36									2	1				
37									1					
38								2	1					
39						1		1						
40		na	na	na	na		na		na			1		na
41	na	na	na	na	na	na	na	na	na	na	na	na	na	na
42					1						3			
43				2	4					1				
44					1						1			
45					2						2			
46										1				2
47										2	1			1
48				1		2		1		2	1			1
49				2		3	1	1		2				
50				1		2		1		3			2	
51				1	1	4	1			2				
52					2	4	1			1	1			
53			2	1	2	5	2			1	1			
54					2	3				1	1			
55				1	1	3				1				
56				1	1	4	1						2	
57				na		6	2			1			1	
58		1		na		2				2			1	
59				na		4	6		1				5	2
60	na	na	na	na	na	na	na	na	na	na	na	na	na	na
Sum	0	1	2	10	83	56	46	6	12	25	11	7	12	17

na = Inaccessible guide hole

Table E.9 – Reach 3 Horizontal Point Frame Data (March 1998)

Guide Hole No.	Transect 1					Transect 2				Transect 3				Transect 4				Transect 5			
Setup No.	1	2	3	4	5	1	2	3	4	1	2	3	4	1	2	3	4	1	2	3	4
1										na	na		na			na	na		1		
2										1											
3																			2		
4																			1		
5																					
6										1											
7										1									2		
8										1									3		
9										2									3		
10							1			1									1		
11							1			1						1					
12										1								1			
13						1	1			2											
14						1	1												1		
15						1													1		
16								1		2									2		
17										1											
18								1											1		
19		1						1											1	1	
20											na		na				na				
21									1		na		na	1			na		1		
22			1			1															
23						1														1	
24			1			1								1							
25							1				1	4									
26								1				1								1	
27						1	1	2			1	1		2			1			1	
28			1			1		1				3		1			2		1	1	
29		1										3		2					1		
30		1								1		2		1			1		2	2	
31		2						1				2						1		2	
32		1								1		5								3	
33												4							1	3	1
34	1	1										5							1	3	
35								1		1		3							1	2	
36										3		4						1	2	2	
37												3				2				2	
38												4								3	
39				2						1		2	2							4	
40										na	na		na				na				
41					1	2	2				na		na				na				
42		2					2								1						
43		1						1				1								1	
44		3												2							
45		1			2							2	1	2			2	1	1		
46					1								1	2			2		2		
47		2				1					1	1	2				2		1	3	
48		2	1			1				2		3	1	1			1	2		2	
49	2		2		2	2				1		2	1		1	3	1	3		3	
50			3		1	1				2		3	2	4			2	4		2	
51	2	3	2		1	1		1	2	1		2		1	1		2	1	2		
52	2	2	2	2	1	1		2		1			na	5	1		1	1	2	2	
53			3	2	1	2	1	2	1	2		1	na	5	2	1	1	3	1		
54	1	3	3	3	1	2	1	3	3	1			na	3	2	1		1	1		
55	3	1	3	1		1	4	na	3			1	na	3	3	1			1	2	1
56	1	1	3	1		1	4	4	3			2	na	2	3	3		3	1	2	
57	1	1	4	2		3	2	1	3	1			na	5	2	2		4		na	2
58		3	na	1		2	na	1	4	1		1	na	na	6	na	2	4		na	4
59			na	1		2	na	na	6			2	na	na	3	na	3	5	1	na	na
60			na				na	na		na			na	na	na	na	na	na		na	na
Sum	13	32	29	15	11	30	22	24	26	33	3	67	10	43	25	14	23	77	42	48	8

na = Inaccessible guide hole